DIURNAL AND SEASONAL VARIATIONS OF THE F2 REGION OF THE ANTARCTIC IONOSPHERE

A thesis submitted for the degree of Doctor of Philosophy of Rhodes University

by

Morgan Howard Williams

December, 1971.

Except where it is clear from the text that I am describing the work of others, the work described in this thesis is my own.

ACKNOWLEDGEMENTS

The task of thanking all those who assist in the preparation of a thesis such as this, is always a difficult one. There are usually so many people to whom one is indebted, directly or indirectly, that the problem is where to begin.

I must first thank Professor J.A. Gledhill, my research director, whose unfailing interest and enthusiasm were a constant source of encouragement to me. In our many fruitful discussions he offered countless ideas without which I would have been unable to complete this project.

I would also like to thank Dr. A.D.M. Walker who acted as my supervisor for a year during Professor Gledhill's absence, and who provided me with considerable assistance, advice and support.

For advice on numerical techniques I am indebted to Professor R.N. Braae, who has always been prepared to lend a sympathetic ear in time of need.

I also owe thanks to my many helpful friends in the Physics Department at Rhodes University. In particular Mr. A.J. Fletcher with whom I worked in the early stages of my research; Miss A.M. Wulff who cheerfully assisted me in plotting graphs, and Mr. A.W.V. Poole who is working on a similar research project.

My thanks are also due to Rhodes University for the award of a Research Scholarship during the first part of the work. I am also grateful to the Department of Transport of the Republic of South Africa for providing me with the opportunity of spending a year in the "great white south".

I would like to express my gratitude to all those who assisted in typing this work.

Finally, I wish to thank my wife and my parents for their encouragement and patience over the years.

CORRIGENDA

1) Figure 44 (copy of figure from Torr and Torr[160]) has been omitted, as it was not available when this thesis was presented.
2) On lines 18-22 on page 70 replace $F_{10.7}$ by $S_{10.7}$ and $\bar{F}_{10.7}$ by $\bar{S}_{10.7}$.

CONTENTS

'What is the use of a book' thought
Alice, 'without pictures or conversations?'
(Lewis Carroll)

The ice-shelf near SANAE, Antarctica

INTRODUCTION

INTRODUCTION

The F2 region of the ionosphere is in many ways more interesting than either the F1 or the E region. This may be due partly to the fact that an F2 layer is usually present and its critical frequency (f_0F2) can be measured at any hour of the day and any season of the year, which is not the case for the E and F1 layers, and partly to the fact that its behaviour is more complex and has many anomalies which need to be explained; for example, the variation of f_0F2 over Antarctica.

Over the southern polar regions one might expect the ionosphere to vary in a different manner from that observed over middle or low latitude stations since during summer the sun remains above the horizon for all hours of the day for stations within the Antarctic Circle. Likewise in winter the sun remains below the horizon (as seen from the Earth's surface) throughout the day.

However, the behaviour which is observed in Antarctic regions cannot be accounted for in terms of this simple solar explanation. At SANAE, the maximum value of the F2 critical frequency during the day occurs just after noon (local mean time) for eight months of the year but for the four months during summer it occurs at about 07 hours local time (= 07 hours Universal Time). At Byrd the maximum value occurs just after noon for nine months of the year but for the three winter months it occurs at 23 hours LMT (= 07 hours UT). At the south geographic pole, where there is negligible diurnal variation of the solar zenith angle, one would not expect any regular daily pattern in the F2 critical frequencies. However, even here a regular diurnal variation is present

with/...

with its maximum at about 06-07 UT (local time is of no significance since the longitude here is indeterminate) during the six winter months and at about 00 UT during the six summer months. Several mechanisms have been proposed but there is no general agreement concerning the cause of this anomalous behaviour.

In 1966 I began doing research on this phenomenon and in 1968 spent a year at the South African base in Antarctica (SANAE) as ionosphericist of the ninth South African expedition.

The first chapter of this thesis deals with an analysis of F2 critical frequency data first for SANAE and then for eleven other Antarctic and sub-Antarctic stations covering the period 1957 to 1969. This shows certain aspects of the F2 behaviour. Some of the results of this chapter have been reported in a paper by Gledhill and Williams[54].

The two most important mechanisms thought to be responsible for the Antarctic f_0F2 behaviour are incoming corpuscular radiation and horizontal neutral winds. These two mechanisms together with two others (the temperature theory of Torr and Torr[160] and the semi-annual variation of neutral atmospheric density) are discussed in detail in part 2 (Chapters 2 to 4) with a view to discovering which aspects of the f_0F2 behaviour over Antarctica can be explained by each theory.

An attempt is made in Part 3 (Chapters 5 and 6) to explain the observed behaviour by solving the continuity equation of the ionosphere for high-latitude stations.

Finally, besides the critical frequency, another parameter of importance in explaining the behaviour in

the/...

the F2 region is the height at which the F2 maximum occurs. This quantity cannot be read directly from an ionogram and it is not an easy quantity to determine. In fact the way in which it is usually obtained is by "scaling" the ionogram in question and converting the virtual heights obtained into real heights. In Part 4 (Chapter 7 and 8) an outline is given of the two computer programs which were written to perform this conversion.

PART I

HARMONIC ANALYSIS

"Like harmony ... there is a dark
Inscrutable workmanship that reconciles
discordant elements"

(Wordsworth)

CHAPTER I

AN HARMONIC ANALYSIS OF ANTARCTIC F2 CRITICAL FREQUENCIES.

1.1 INTRODUCTION

1.1.1 A REVIEW OF THE THEORIES OF THE ANTARCTIC ANOMALY

Since the first analyses of polar F2 data, there has been much dissension as to the mechanisms which give rise to the peculiar variation of f_0F2 at high latitudes. Coroniti and Penndorf[29] included two Antarctic stations (Port Lockroy and Decepcion Island) in an analysis of the variation of f_0F2 at a number of high-latitude stations during different seasons. Although during winter and the equinoctial months the behaviour at the Antarctic stations did not appear to be very different from that observed at those in the Arctic, they found that during the summer months, particularly at Port Lockroy, it was very different. In the same year Knecht[90] analysed 20 months of data from the South Pole station taken near sunspot maximum. He found that the critical frequency of the F2 region remains high even in winter; it seldom drops below about 5 MHz (at sunspot maximum), even though in the middle of winter the ionosphere is not directly illuminated below about 575 km. In addition he observed that the average f_0F2 varied considerably during the day reaching a maximum at about 06 UT for six months of the year during winter; this is surprising since the solar zenith angle exhibits negligible daily variation at the pole.

Rastogi[116, 117] attempted to explain the

anomalous/...

anomalous behaviour of f_0F2 at Antarctic stations on the basis of horizontal movement of ionization. Hill[64] showed quantitatively that the behaviour might be explained on the basis of a wind shear of the order of 25 to 50 m/s per 100 km in the F2 region, provided that the wind had the right directions at the right times. He also ascribed the difference between Arctic and Antarctic behaviour to the factor sin I cos I (where I = geomagnetic dip angle) in the wind term of the continuity equation (see equation 5.23).

In 1962 Duncan[37] put forward the theory that the electron densities in the F2 region vary with universal time, reaching a maximum near 07 hours UT in the southern polar region. This peak, although most noticeable in winter at the majority of stations (those stations in the Ross Sea area), is present throughout the year at some stations. Duncan suggested that it might be caused by the dumping of trapped particles into the F-region, and that this in turn may be caused by oscillations set up by the transport of the eccentric geomagnetic field through the interplanetary plasma. In the same year Piggott and Shapley[114] also showed that the F2 critical frequencies display a universal time dependence, and noted further that the transition between UT and LMT dependence was sometimes very sudden. They considered winds and diffusion from one hemisphere to the other along magnetic lines of force as possible causes, but decided that these could not explain the UT phenomenon. They mentioned precipitated particles as another possible mechanism, but drew no conclusions about this. Particles have also been proposed (Oguti and Marubashi[110]) as an important mechanism in explaining

another/...

another peak in f_0F2 observed at about 21 hours UT at Cape Hallett, 20 hours UT at Little America and 16 hours UT at South Pole. In this case it was suggested that particles enter the ionosphere via the magnetic neutral points.

The possibility of winds as the underlying mechanism behind the anomalous f_0F2 behaviour was revived by King et al[84], who suggested that the wind system calculated by Kohl and King[92] could explain the observed phenomena. In particular they considered the case of Port Lockroy. In reply to their article, Duncan[38] showed that their wind system could not account for the observed behaviour at several Antarctic stations. Challinor[19], who had himself previously written several papers on horizontal neutral winds in the F-region, also doubted whether winds were the chief cause of the UT behaviour. He felt that the term cos I sin I was not the sole factor responsible for the difference between Arctic and Antarctic behaviour. He suggested that the solution may lie in a combination of vertical drifts due to atmospheric winds and dumping of particles. This conclusion was also reached by King et al[82] who solved the continuity equation and the equation of motion of the neutral atmosphere simultaneously for several Antarctic stations in summer.

Torr and Torr[160] suggested that the 06 UT maximum observed at SANAE in summer may be due to the temperature dependence of recombination processes and production due to solar EUV at any height. Using the CIRA model atmosphere 3, they showed that N_mF2 reaches a maximum at about 08 LMT and a minimum at about 16 LMT for stations at a latitude 70^oS during summer, and

suggested/...

suggested that this may explain the behaviour of f_0F2 at SANAE.

Another mechanism which has been proposed by Hill[65] and by Sato and Rourke[132] is that of electromagnetic drifts. However, this theory has not received much support as it cannot account successfully for the peak in f_0F2 at 06 UT and at present the wind theory and the particle theory (or a combination of both) are generally accepted as being the most likely explanations of the anomalous Antarctic behaviour.

1.1.2 THE HARMONIC ANALYSIS

In 1959 Knecht[90] performed an harmonic analysis on the monthly median f_0F2 of the ionosphere over the south geographic pole. From the analysis of twenty months of data, he drew certain conclusions about the coefficients of the 24-hour and 12-hour components but did not comment on the mean value or "constant" term in the harmonic analysis. This chapter outlines the results of a similar analysis of f_0F2 data from SANAE and a further extension of the analysis to include data from eleven other stations in the Antarctic region. However, instead of using the monthly median values of the F2 critical frequencies as Knecht did, the mean geomagnetically quiet-day values were used. It was hoped that such an analysis might give further insight into the anomalous seasonal variation of the Antarctic ionosphere under quiet conditions.

1.2 THE/...

1.2 THE ANALYSIS OF SANAE DATA

The initial analysis was conducted on 69 months of f_0F2 data from SANAE for the period June 1962 to September 1969 (excluding the year 1965 when very few usable records were obtained). Means were taken of the hourly values of f_0F2 on the ten magnetically quiet days (Lincoln[96]) of each month and these hourly means were used in an harmonic analysis in terms of the function

$$f_0F2(\theta) = A_0 + A_1\sin(\theta+\phi_1) + A_2\sin(2\theta+\phi_2) + A_3\sin(3\theta+\phi_3) \qquad (1.1)$$

where $\theta = 360t/24$

and t = local standard time in hours (To within the accuracy of the results, LST ≈ LT). In the case of SANAE, LST = UT.

Some of the coefficients obtained from this analysis are shown in Fig. 1. The amplitudes of the first three terms (A_0, A_1 and A_2) and the phase angle of the 24-hour term (ϕ_1) are plotted against time in months.

The main part of this analysis is centred around the behaviour of the constant term, A_0, which is simply the mean of the hourly quiet-day values of f_0F2 for a given month. The 24-hour component is also of interest, as this gives an indication of the average diurnal range of f_0F2 for a particular month, the amplitude A_1 showing the magnitude of this range and the phase ϕ_1 the time of day of the maximum value of f_0F2 from this simple approximation. The higher order harmonics - the 12-hour and 8-hour components - are of less interest, partly because it is not possible to find, as for the first two terms, a single physical attribute of the f_0F2 behaviour pattern with which to associate them and partly because their amplitudes are small and of less significance than A_0 and A_1. The amplitude of the 12-hour component, A_2, is

usually /...

Figure 1

Coefficients of the Harmonic Analysis of f_oF2 at SANAE.

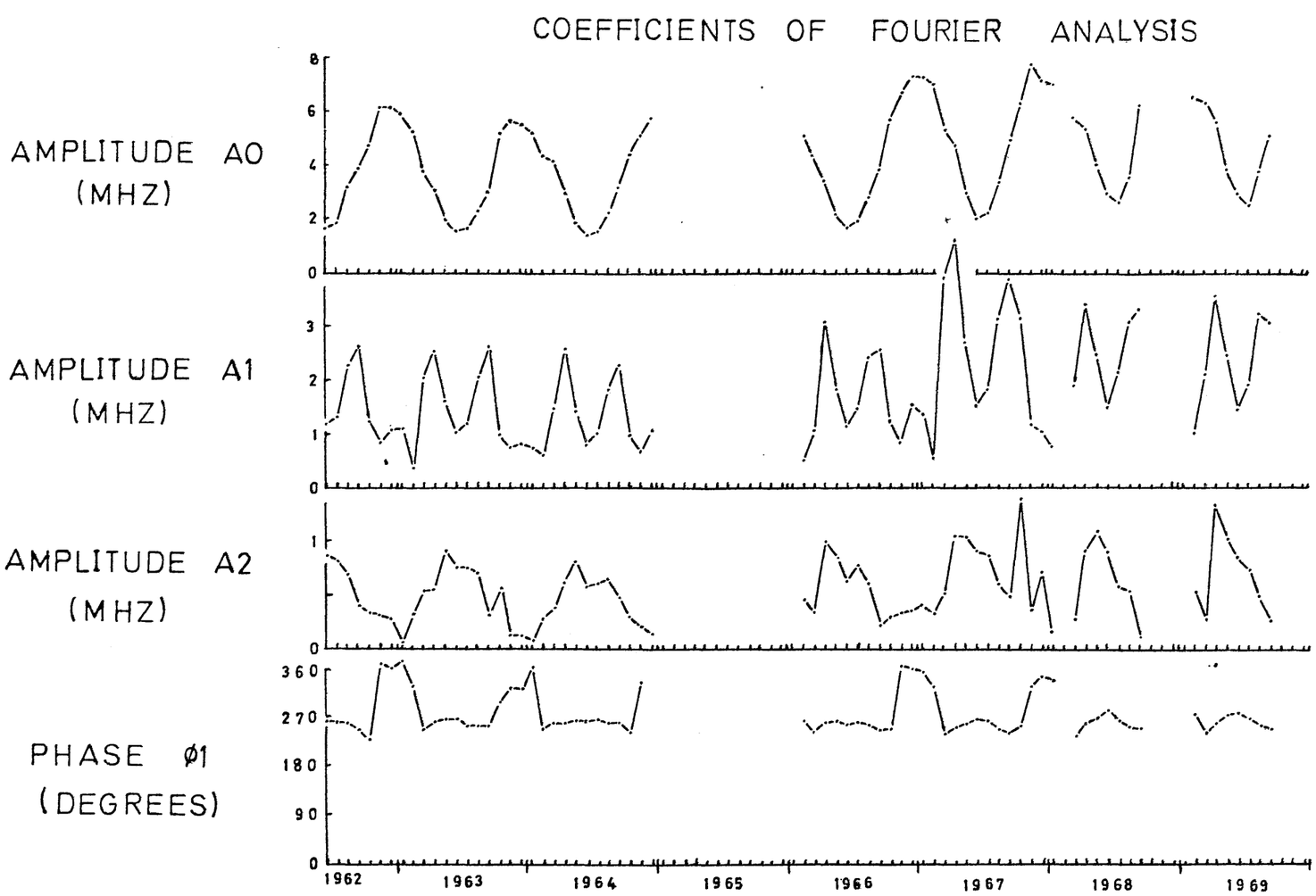
COEFFICIENTS OF FOURIER ANALYSIS
AMPLITUDE A0
(MHZ)
8
6
4
2
0
AMPLITUDE A1
(MHZ)
3
2
1
0
AMPLITUDE A2
(MHZ)
1
0
PHASE ø1
(DEGREES)
360
270
180
90
0
1962
1963
1964
1965
1966
1967
1968
1969

usually less than 0.5 MHz and the values of A_3 are even smaller. This means that A_2 is of the same order of magnitude as the standard deviation from the mean of a single quiet-day value at any hour (also about 0.5 MHz). These higher harmonics are therefore not considered further.

THE CONSTANT TERM, A_0

This is seen to have a regular annual variation which is almost sinusoidal with its maximum in summer, coupled with a long-term variation in which the value of A_0 for any particular month in 1964 (around sunspot minimum), say, is smaller than the value of A_0 for the same month in 1968 (near sunspot maximum). The regular annual variation might be expected, since the amount of solar EUV reaching the level of the F_2 maximum varies throughout the year with its peak in December, i.e. one might expect some dependence on some effective mean value of the cosine of the zenith angle of the sun. The long-term trend suggests a dependence on the sunspot number or 10.7 cm solar flux. Figure 2 which compares the constant term, A_0, with the sunspot number, the 10.7 cm solar flux and the average value of $\cos\chi$, $\overline{\cos\chi}$, (see below) tends to confirm these views.

For these reasons it was decided to fit a function of the form

$$G = A + BS + Cf(\cos\chi) + DSf(\cos\chi) \qquad (1.2)$$

to the monthly values of A_0 using the method of least squares (see Appendix 1). In this relation

S = average Zurich sunspot number, R_z, or average 10.7 cm solar flux, $S_{10.7}$, for the month, and

$f(\cos\chi)$ = an appropriate mean function of the cosine of

the/...

Figure 2

Comparison of constant term A_0(MHz) of the harmonic analysis with related quantities (SANAE data).

CONST. TERM
(MHZ)

SUNSPOT NO.

SOLAR FLUX

$\overline{\cos \chi}$

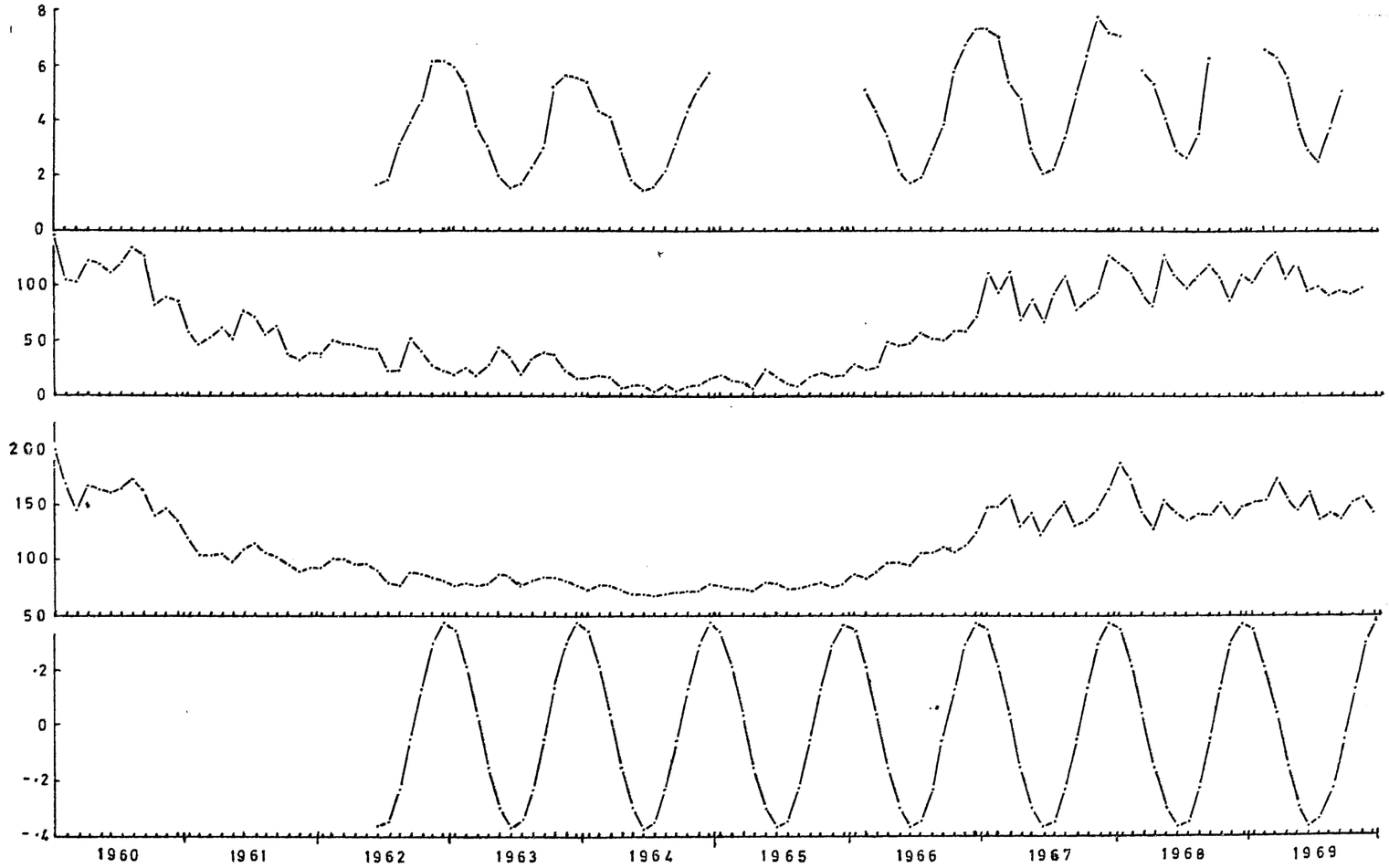

the solar zenith angle.

Several forms of $f(\cos\chi)$ were used. They are

(i) $\overline{\cos\chi_m}$: the average midday value of the cosine of the solar zenith angle, including negative values when the sun was below the horizon;

(ii) $\overline{\cos_o\chi_m}$: as (i) but with negative values replaced by zeroes since the effect of solar EUV may be expected to cease when the sun is below the horizon;

(iii) $\overline{\cos\chi}$: the average value (taken over the whole day) of $\cos\chi$, including negative values as in (i);

(iv) $\overline{\cos_o\chi}$: as (iii) but with negative values replaced by zeroes as in (ii);

(v) $\overline{\cos^{\frac{1}{4}}\chi}$: the average value of $\cos^{\frac{1}{4}}\chi$ for the whole month with zeroes when $\cos\chi$ was negative (The reason for choosing $\cos^{\frac{1}{4}}\chi$ will be explained in Section 1.4).

To estimate the goodness of fit of this function for various combinations of variables, the mean square residual $\sum_i (\Delta A_0)_i^2/n$ was calculated. Here $(\Delta A_0)_i$ is the difference between the observed value of A_0 for the i^{th} month and the value of the function G from the least squares fit for that month. n is the total number of months used in the least squares fit.

The mean square residuals for a number of cases are contained in Table 1. In analyzing the data from other Antarctic stations (section 1.3), it was found that equation (1.2) did not represent data well during a sunspot maximum period (1957 to 1960 or 1967 to 1969); for this reason the least squares analysis was conducted, first on

all/...

Table 1. Mean square residuals for various least squares fits to SANAE data

	WHOLE PERIOD		1962-1966	
	SUNSPOT NO.	SOLAR FLUX	SUNSPOT NO.	SOLAR FLUX
$\overline{\cos\chi_m}$	0.187	0.199	0.053	0.054
$\overline{\cos_\sigma \chi_m}$	0.213	0.226	0.057	0.060
$\overline{\cos\chi}$	0.204	0.217	0.052	0.056
$\overline{\cos_\sigma \chi}$	0.451	0.458	0.200	0.212
$\overline{\cos^{\frac{1}{2}}\chi}$	0.242	0.257	0.081	0.089

all the values of A_0, then using only values for the period 1962 to 1966 when sunspot activity was low. The mean square residuals for the sunspot minimum period are significantly smaller (generally by a factor of three to four) than those obtained using all the data. However, the number of values of A_0 fitted (n) is not so different - 42 in the sunspot minimum period and 69 when all the data are included. This confirms that equation (1.2) describes the A_0 data better when the solar activity is low than when it is high.

One unexpected result which arises from Table 1 is that a better fit is obtained when negative values are included in the $\cos\chi$ function than when they are replaced by zeroes. This applies to both midday and average daily values. Of the five $\cos\chi$ functions, $\overline{\cos\chi}_m$ almost always gives the best fit to the observed data.

It is also evident that in all cases the fits obtained using sunspot number are not very different from those derived from the 10.7 cm solar flux. Since the intensity of solar EUV reaching the ionosphere (and causing photoionization) ~~depends on~~ correlates with the magnitude of the 10.7 cm solar flux[175], this latter quantity is of more direct significance to ionospheric processes than the sunspot number; and hence only results of the least squares analyses using $S_{10.7}$ will be considered in the remainder of this analysis.

THE AMPLITUDE OF THE 24-HOUR COMPONENT, A_1

This too has a regular behaviour, but with maxima twice a year - in April and September. There are also indications of an additional much smaller maximum around December (Fig. 1).

THE/...

THE PHASE ANGLE OF THE 24-HOUR COMPONENT, ϕ_1

The maximum value of $\sin(\theta + \phi_1)$ in the second term of equation (1.1) occurs when $\theta + \phi_1 = 90^\circ$. From Fig. 1 it can be seen that for eight months of each year, ϕ_1 has a value just less than 270°, while for the remaining four months (during summer), it is close to 360°. When ϕ_1 has a value of 270°, the maximum in f_oF2 occurs at $\theta = 180^\circ$, i.e. about midday; a value of 360° for ϕ_1 signifies a maximum at 06 LMT. Thus the well-known morning maximum observed at stations in this region of Antarctica (Piggott and Shapley[114]) is clearly demonstrated.

1.3 ANALYSIS OF DATA FROM OTHER ANTARCTIC STATIONS

For comparison, values of f_oF2 from eleven other stations (Fig. 3) were subjected to the same analysis. Altogether about 840 station-months of data were used.

Fig. 4 shows the value of A_0 for the twelve stations including SANAE plotted against time. In Fig. 4(a) two distinct patterns of behaviour can be seen for each station. From July 1957 to about the end of 1960, A_0 exhibits a semiannual variation - reaching a maximum in March/April and in September/October of each year - and from about the end of 1960 onwards, it follows an annual variation more simply related to the position of the sun in the sky (similar to that observed at SANAE). The transition between these two types of behaviour appears to be fairly sharp, taking place over a period of a few months. An important point to notice is that the behaviour of A_0 follows a similar pattern at each station.

Values of A_0 for Vostok, Terre Adelie, Campbell Island and Byrd are plotted in Fig. 4(b). The same patterns of behaviour are observed for three of these

stations/...

Figure 3

Map of Antarctica showing stations considered in this analysis.

MAP OF ANTARCTICA SHOWING STATIONS

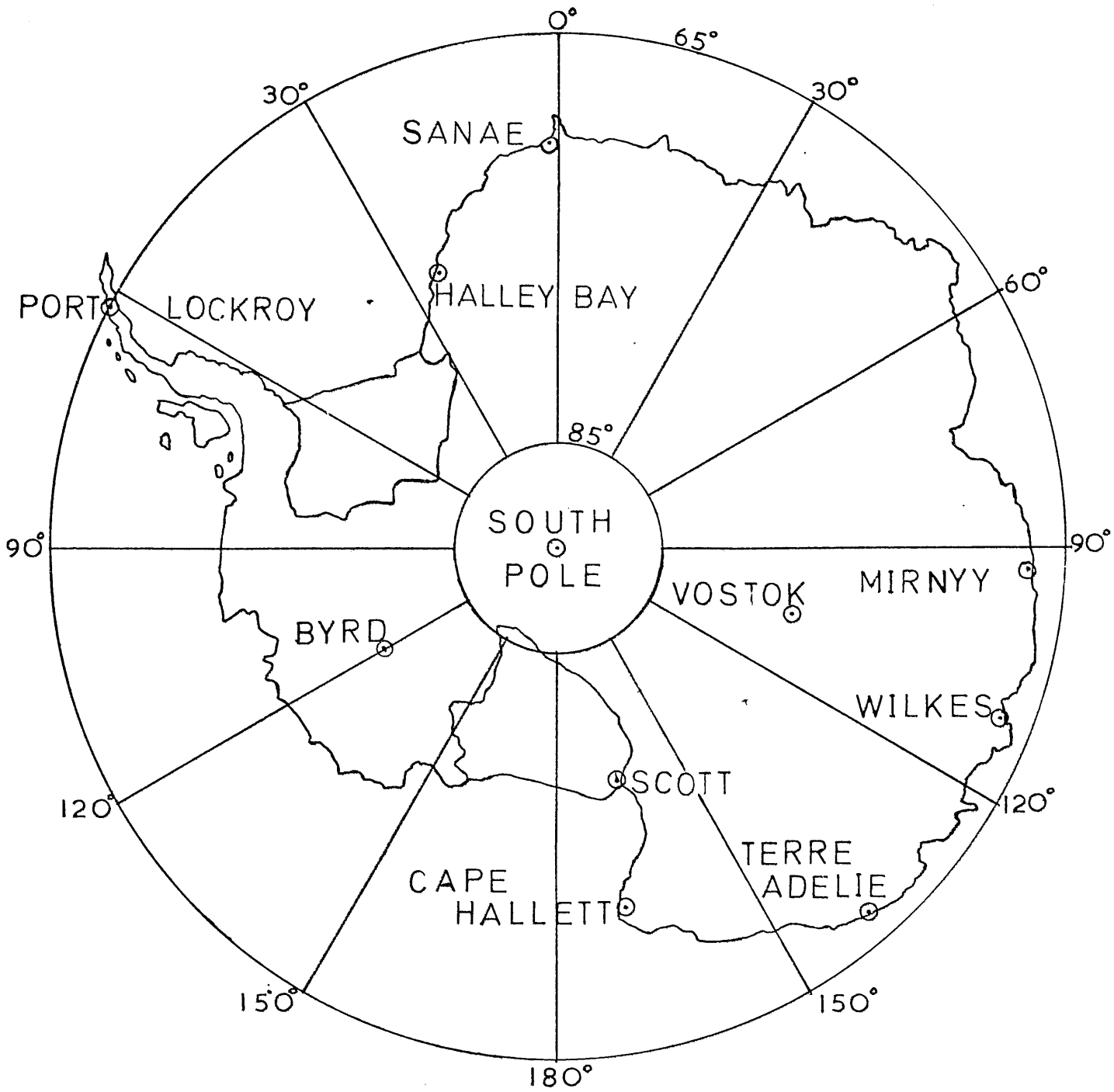

CAMPBELL ISLAND

Figure 4(a)

Amplitude of constant term A_0(MHz), at Scott, South Pole, Wilkes and Cape Hallett.

AMPLITUDE OF CONSTANT TERM (MHZ)

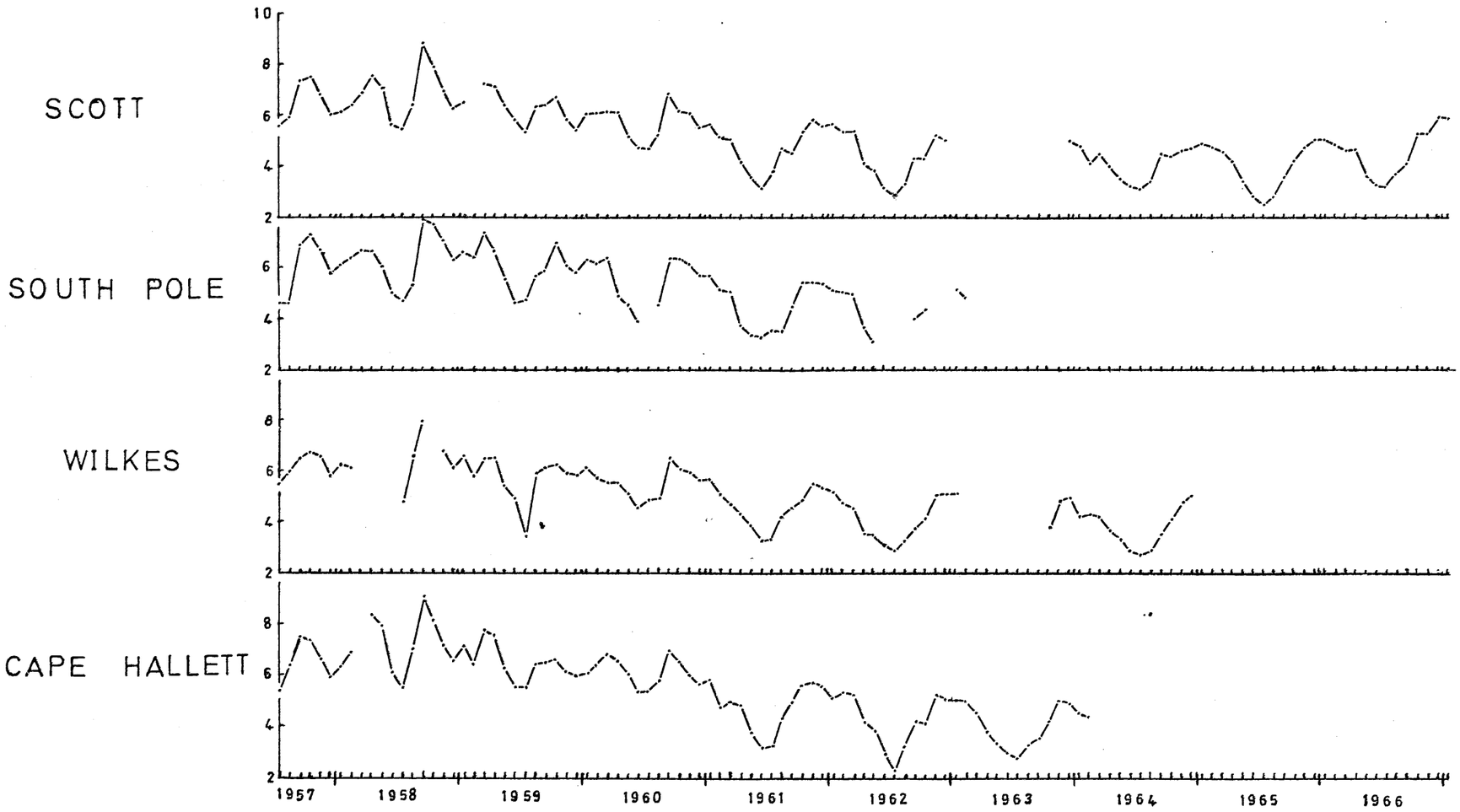

Figure 4(b)

Amplitude of constant term A_0 (MHz), at Vostok, Terre Adelie, Campbell Island and Byrd.

AMPLITUDE OF CONSTANT TERM (MHZ)

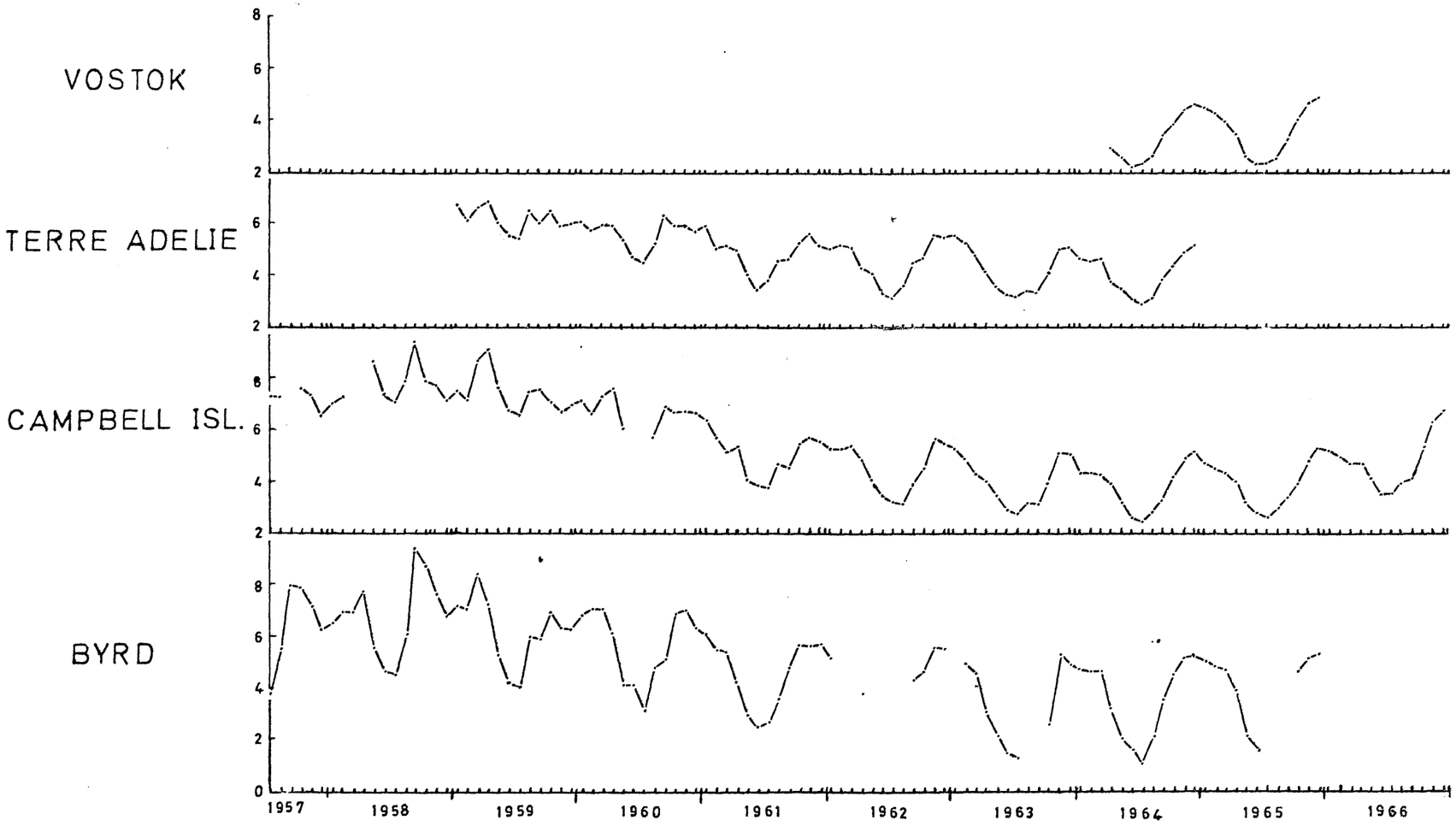

Figure 4(c)

Amplitude of constant term A_0(MHz), at Port Lockroy, Halley Bay, SANAE and Mirnyy.

AMPLITUDE OF CONSTANT TERM (MHZ)

PORT LOCKROY

HALLEY BAY

SANAE

MIRNYY

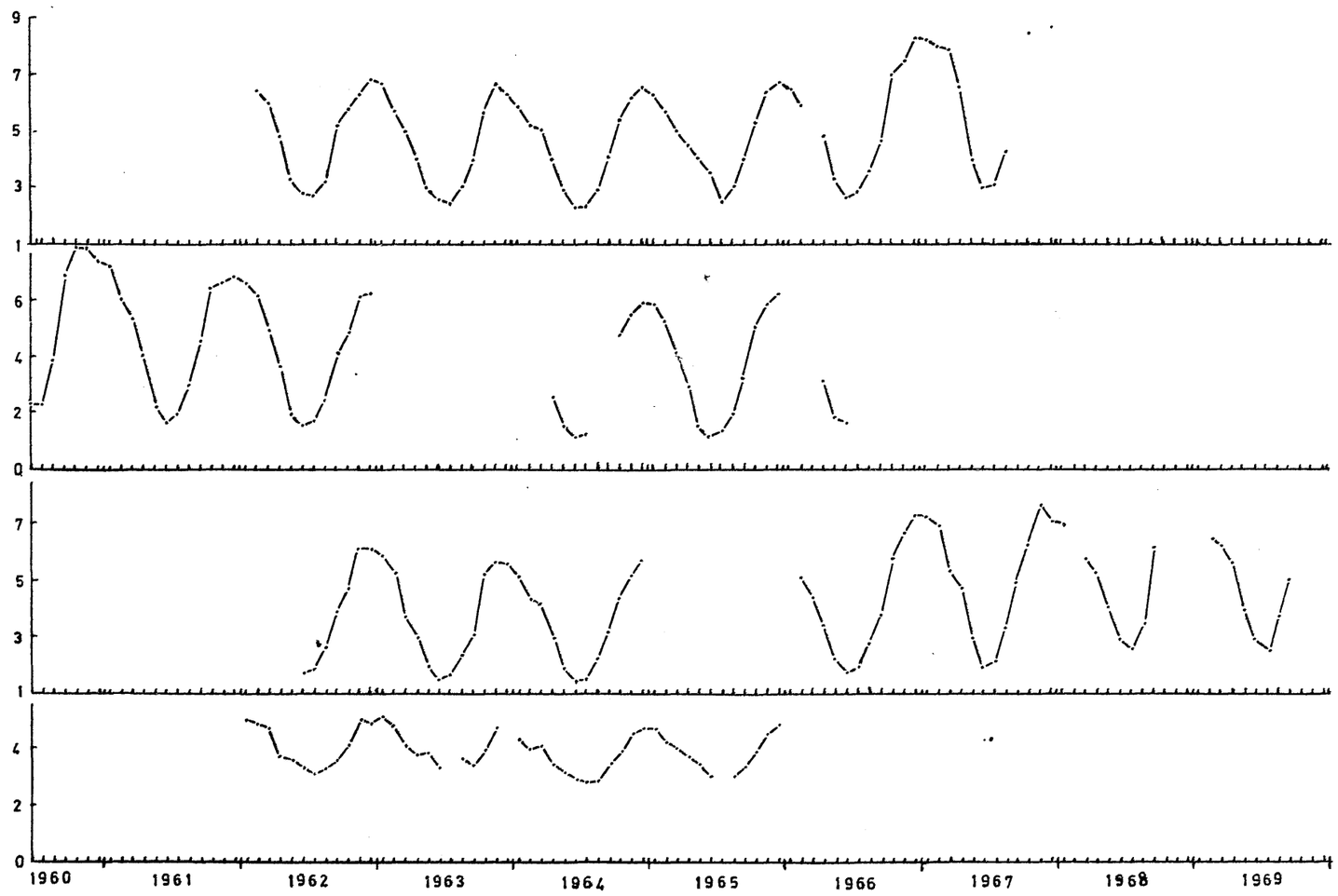

Table 2. June values of constant term A_0

Station \ Year	1958	1959	1960	1961	1962	1963	1964	1965	1966	1967	1968	1969
SOUTH POLE	4.96	4.61	3.91	3.25								
BYRD	4.63	4.16	4.06	2.52	1.66	1.46	1.59	1.69				
VOSTOK							2.16	2.32				
SCOTT	5.62	5.83	4.67		3.16		3.18	2.83	3.25			
HALLEY BAY			2.43	1.63	1.53		1.14	1.18				
CAPE HALLETT	6.12	5.51	5.29	3.11	2.92	2.88						
SANAE					1.71	1.53	1.42		1.71	1.98	2.89	2.89
TERRE ADELIE		5.54	4.66	3.43	3.33	3.18	3.09					
MIRNYY					3.29	3.36	2.93	3.02				
WILKES			4.63	3.26	3.02		2.88					
PORT LOCKROY					2.83	2.59	2.33	2.46	2.74	3.02		
CAMPBELL ISL.	7.33	6.71		3.81	3.48	2.93	2.57	2.76	3.46			
SOLAR FLUX	220	217	162	110	91	83	69	77	96	120	142	162

stations but for Vostok, for which very little data was available, the pre-1961 behaviour could not be verified. Likewise for the four stations shown in Fig. 4(c), the pattern of behaviour in years after 1960 is almost sinusoidal with its maximum in summer, but, owing to the unavailability of data, the pattern before 1960 could not be established. From figures given by Bellchambers et al[11], it seems that during the period 1957 to 1960 a pattern similar to that of Fig. 4(a) was present at Halley Bay while from the work of Penndorf[113] the same is true for Vostok and Port Lockroy. These other analyses were, however, not confined to quiet days.

Table 2 contains the values of A_0 for June of each year. This table shows clearly the strong dependence of A_0 on solar activity even when the sun is below the horizon. In particular, at the South Pole, where in June the sun remains below the horizon for all heights below about 575 km, the average value of f_0F2 is surprisingly high and shows a definite dependence on solar flux. All the other stations show a similar variation.

Since the pattern of behaviour of A_0 during the sunspot maximum period 1957 to 1960 is different from that observed during the period of low solar activity from 1961 to 1966, equation (1.2) was fitted first to all the data for each station and then only to values of A_0 for the period 1961 to 1966. In addition the analysis was repeated, leaving out the values of A_0 obtained during March, April, September and October to see the effect on the fit, since the behaviour pattern during the period 1957 to 1960 shows sharp maxima in these months for each station.

Table 3, which contains the mean square residuals

obtained/...

Table 3. Mean square residuals for fit of equation (2) under various conditions. M A S O = March, April, September and October; (a) $\overline{\cos \chi_m}$; (b) $\overline{\cos_o \chi_m}$; (c) $\overline{\cos \chi}$; (d) $\overline{\cos_o \chi}$; (e) $\overline{\cos^{\frac{1}{4}} \chi}$.

	WHOLE PERIOD										1961 to 1966									
	WITH M A S O					WITHOUT M A S O					WITH M A S O					WITHOUT M A S O				
	a	b	c	d	e	a	b	c	d	e	a	b	c	d	e	a	b	c	d	e
SPO	.380	.572	.379	.572	.441	.151	.207	.151	.208	.147	.072	.223	.072	.222	.107	.035	.071	.036	.072	.031
BYR	.569	.823	.586	1.03	.779	.217	.299	.224	.381	.257	.174	.440	.189	.679	.395	.070	.143	.075	.228	.106
VOS											.025	.066	.025	.129	.061	.009	.018	.008	.031	.016
SCO	.260	.291	.263	.326	.290	.125	.138	.126	.150	.136	.114	.155	.116	.208	.153	.084	.102	.084	.119	.100
HLB	.132	.295	.154	.709	.297	.053	.143	.058	.270	.134	.081	.201	.095	.547	.205	.044	.113	.048	.233	.108
ADR	.386	.399	.390	.437	.405	.213	.225	.214	.244	.226	.125	.153	.132	.231	.159	.084	.109	.087	.144	.107
SAN	.199	.226	.217	.458	.257	.128	.148	.133	.244	.176	.054	.060	.056	.212	.089	.041	.050	.042	.124	.066
PTG		.117	.121	.149	.123		.059	.064	.073	.063		.090	.092	.117	.093		.061	.062	.078	.065
MIR												.057	.051	.046	.051		.033	.031	.033	.033
WIL		.183	.184	.198	.184		.112	.113	.123	.114		.065	.062	.073	.060		.055	.056	.068	.055
PLO		.173	.198	.330	.202		.047	.045	.075	.060		.087	.097	.184	.097		.038	.033	.051	.041
CMP		.357	.355	.356	.347		.170	.161	.160	.160		.126	.122	.124	.108		.059	.060	.060	.057

SPO = South Pole
BYR = Byrd
VOS = Vostok
SCO = Scott
HLB = Halley Bay
ADR = Cape Hallett
SAN = SANAE
PTG = Terre Adelie
MIR = Mirnyy
WIL = Wilkes
PLO = Port Lockroy
CMP = Campbell Island

obtained on fitting equation (1.2) to the values of A_0 for all the stations, is subdivided into four quarters depending on whether

(a) all values of A_0 were used;

(b) all values of A_0 except those obtained in March, April, September and October were used;

(c) only values of A_0 obtained near sunspot minimum were used;

(d) values of A_0 near sunspot minimum excluding values obtained in March, April, September and October were used.

One result which is evident from this table is that if either the values of A_0 obtained during the solar maximum periods 1957 to 1960 and 1967 to 1969 or those obtained in March, April, September and October are omitted from the least squares analysis, the fit is noticeably improved, while it is at its best if both are omitted. Once again better agreement is obtained using $\cos\chi$ functions which include negative values of $\cos\chi$.

THE AMPLITUDE OF THE 24-HOUR TERM, A_1

Figure 5 contains the values of A_1 plotted for each station. In Fig. 5(a) a very distinct pattern of behaviour is evident for three of the stations - Port Lockroy, Halley Bay and SANAE, the three stations in the Weddell Sea anomaly (Penndorf[113]). For these stations A_1 attains peaks in March/April and September/October of each year and a third maximum is observed in December. The pattern is less well-defined for the fourth station, Mirnyy, but even so, peaks can be seen around the equinoxes.

For the remaining eight stations shown in

Figures/...

Figure 5(a)

Amplitude of 24-hour component, A_1(MHz), at Port Lockroy, Halley Bay, SANAE and Mirnyy.

AMPLITUDE OF 24-HOUR COMPONENT (MHZ)

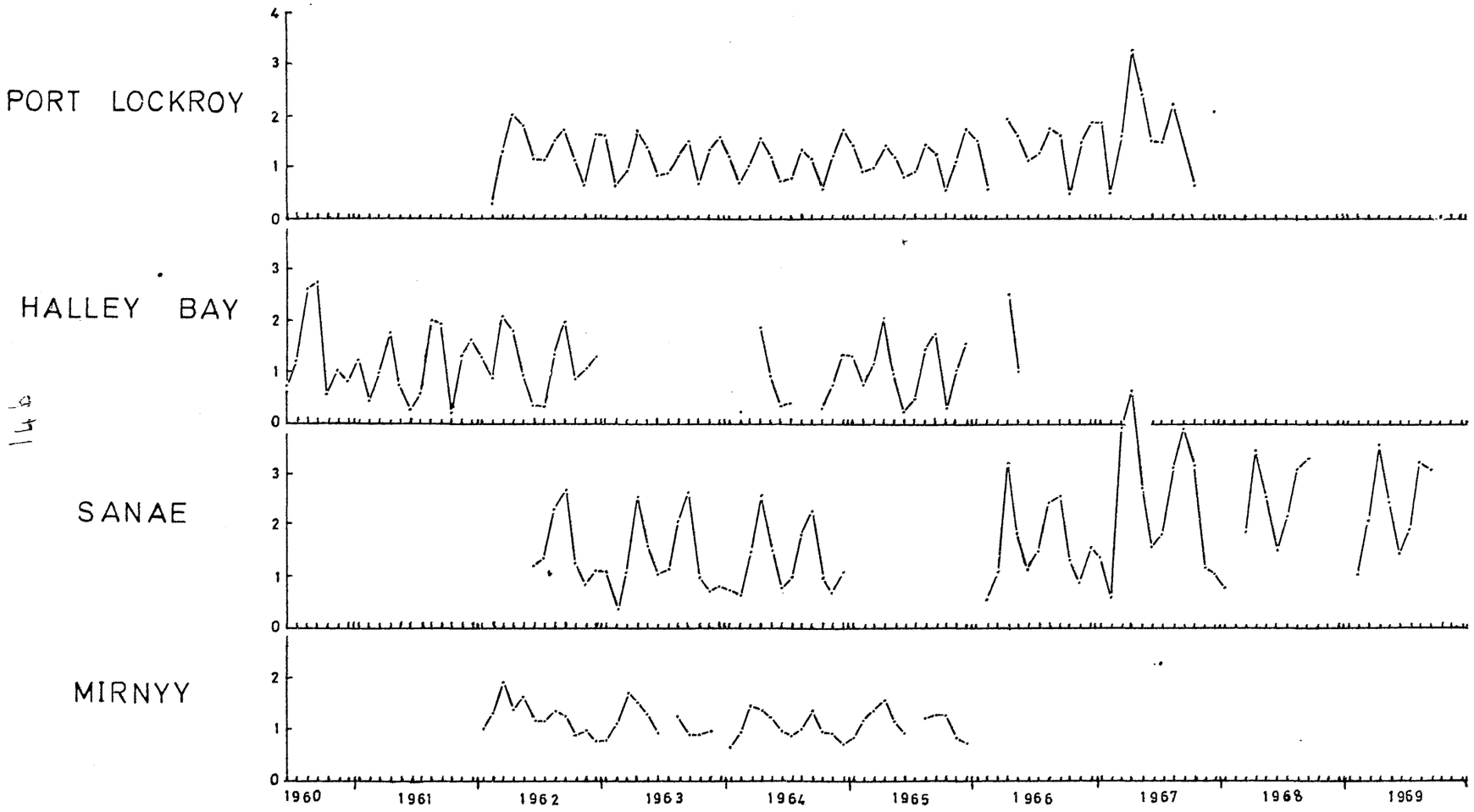

Figure 5(b)

Amplitude of 24-hour component, A_1(MHz), at Scott, South Pole, Wilkes and Cape Hallett.

AMPLITUDE OF 24-HOUR COMPONENT (MHZ)

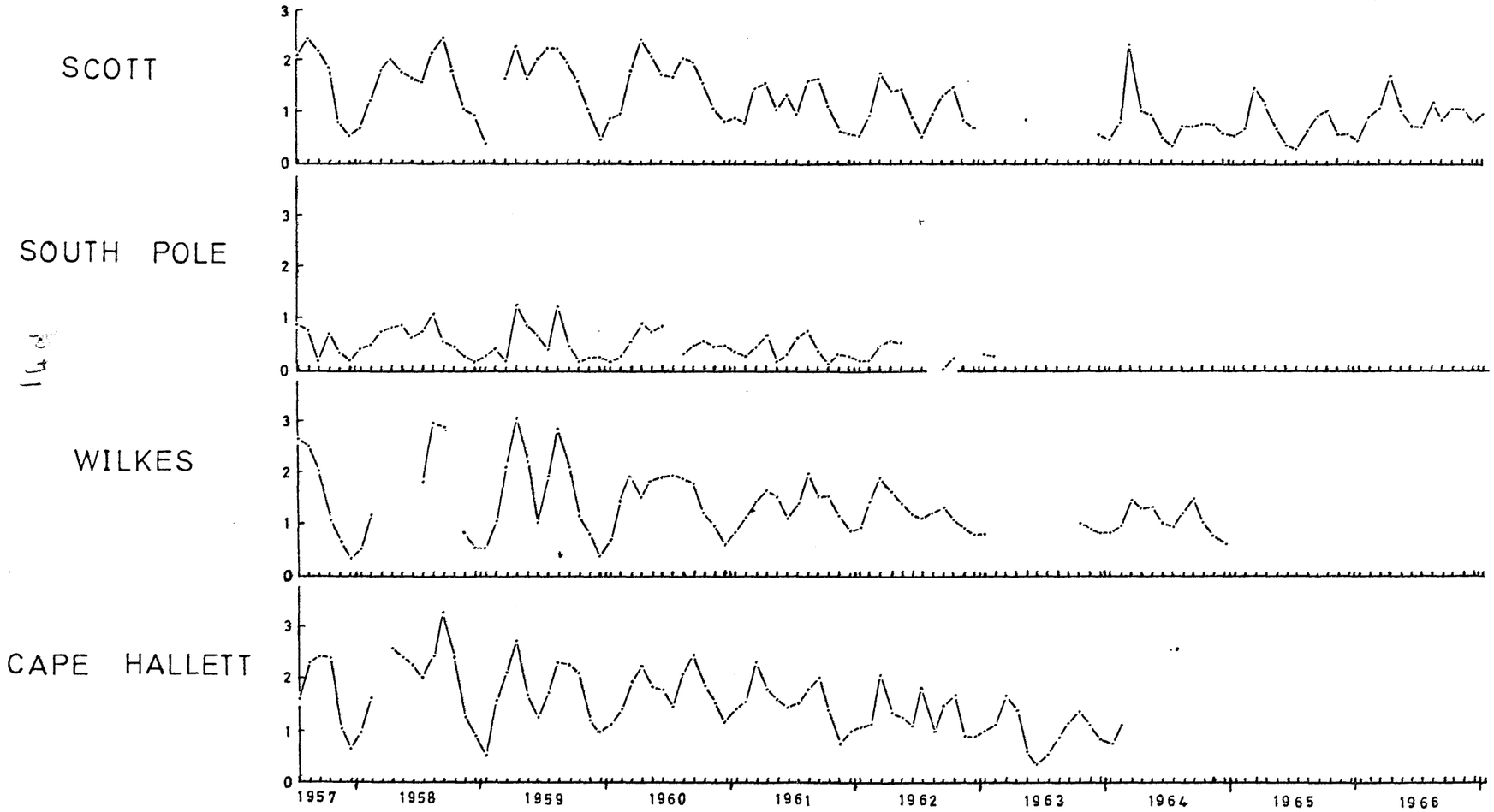

Figure 5(c)

Amplitude of 24-hour component, A_1(MHz), at Vostok, Terre Adelie, Campbell Island and Byrd.

AMPLITUDE OF 24-HOUR COMPONENT (MHZ)

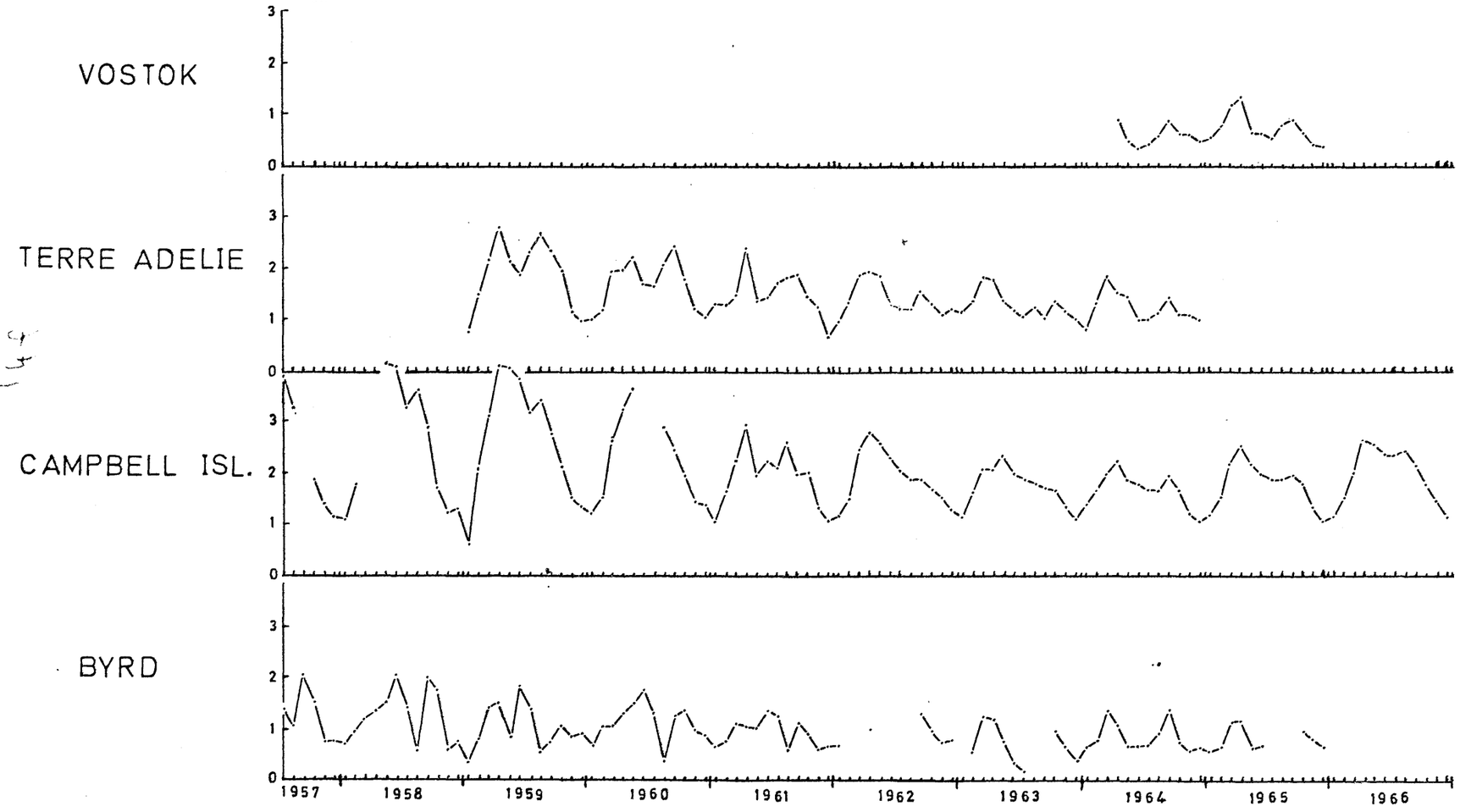

Figures 5(b) and 5(c) no clear pattern is discernible. However, for all stations except Campbell Island, A_1 does attain maximum values at the equinoxes, and even at Campbell Island the pattern (which has a large maximum in winter) does give some slight evidence of peaking at the equinoxes. Furthermore the magnitudes of these maxima are larger around sunspot maximum which suggests a dependence on solar activity.

The fact that Campbell Island is much further north than any other station at which the universal time behaviour of f_0F2 is observed, may account for the different behaviour observed at this station.

PHASE ANGLE OF THE 24-HOUR COMPONENT, ϕ_1

This is shown in Fig. 6. From the variation of ϕ_1 at SANAE, Halley Bay and Port Lockroy (Fig. 6(a)) it appears that for eight months of the year f_0F2 has its maximum slightly after noon, that is, the normal f_0F2 peak at about 13 to 14 hours LMT produced by the balance of production of ions and electrons due to solar EUV and loss due to recombination. However, for the four months during summer, the maximum occurs at about 06 to 08 hours UT.

At Byrd (Fig. 6(c)) the maximum in f_0F2 occurs at about 06 UT for three months during winter and for the remainder of the year it occurs soon after local noon. At South Pole (Fig. 6(b)) on the other hand, f_0F2 has its maximum at about 06 UT for the six winter months and at about 00 UT for the six months during summer. This latter result is in agreement with Knecht's[90] findings.

The rest of the stations used in this analysis lie in the vicinity of the 120°E longitude (at which 06 UT = 14 LMT) and hence it is difficult to distinguish between

UT/...

Figure 6(a)

Phase angle of 24-hour component, ϕ_1,(degrees),
at Port Lockroy, Halley Bay, SANAE and Mirnyy.

PHASE ANGLE OF 24-HOUR COMPONENT (IN DEGREES)

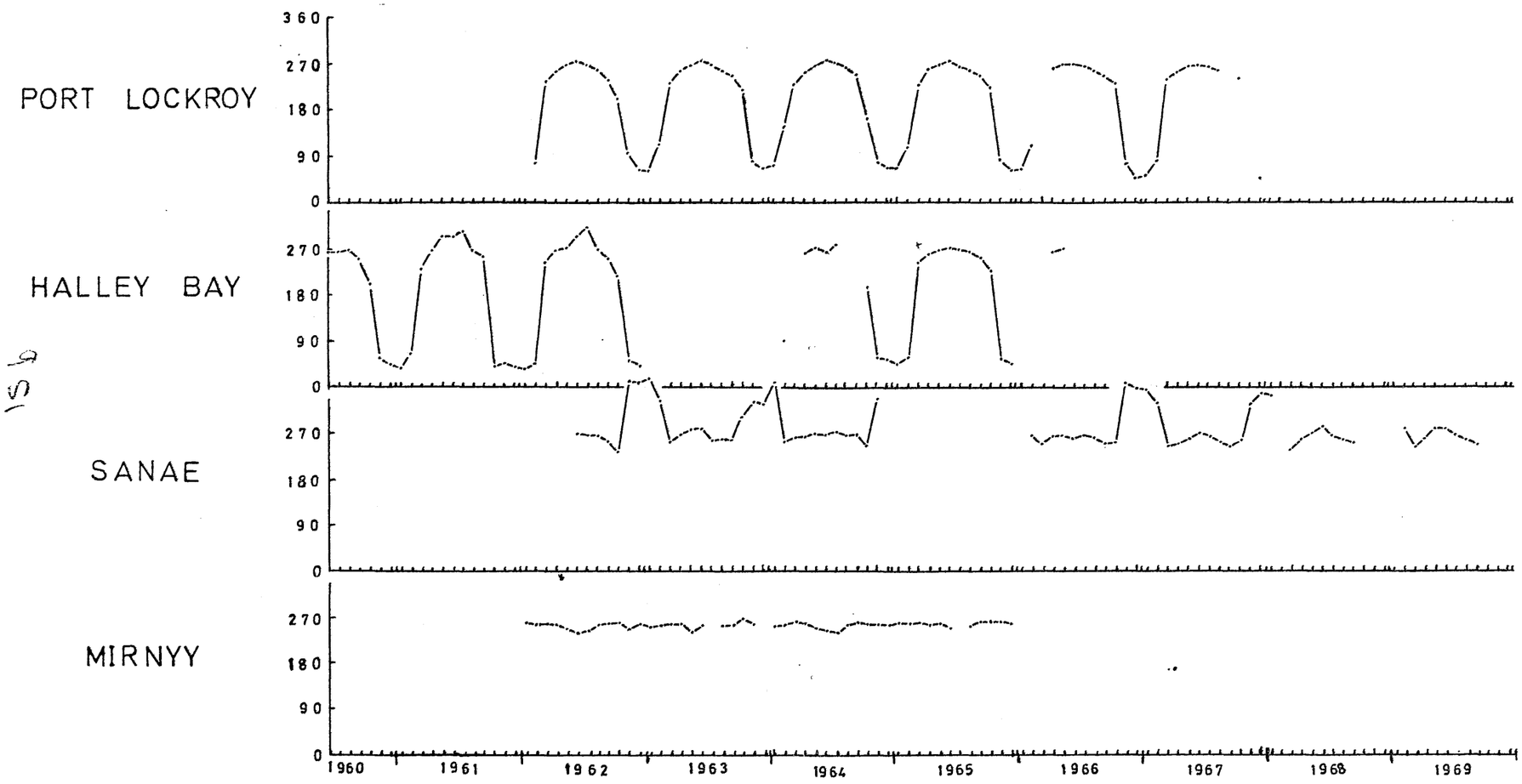

Figure 6(b)

Phase angle of 24-hour component, ϕ_1 (degrees), at Scott, South Pole, Wilkes and Cape Hallett.

PHASE ANGLE OF 24-HOUR COMPONENT (IN DEGREES)

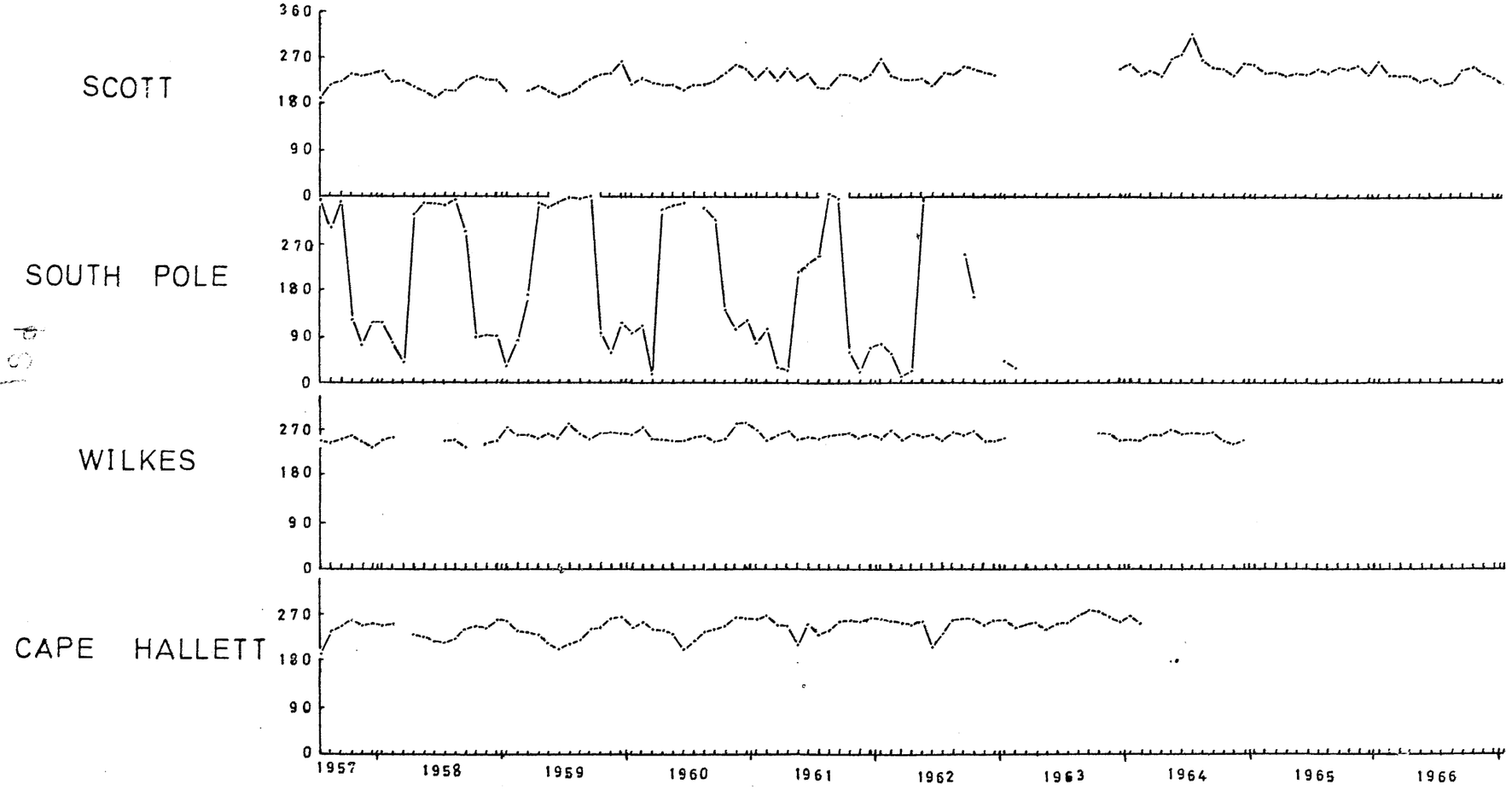

Figure 6(c)

Phase angle of 24-hour component, ϕ_1 (degrees), at Vostok, Terre Adelie, Campbell Island and Byrd.

PHASE ANGLE OF 24-HOUR COMPONENT (IN DEGREES)

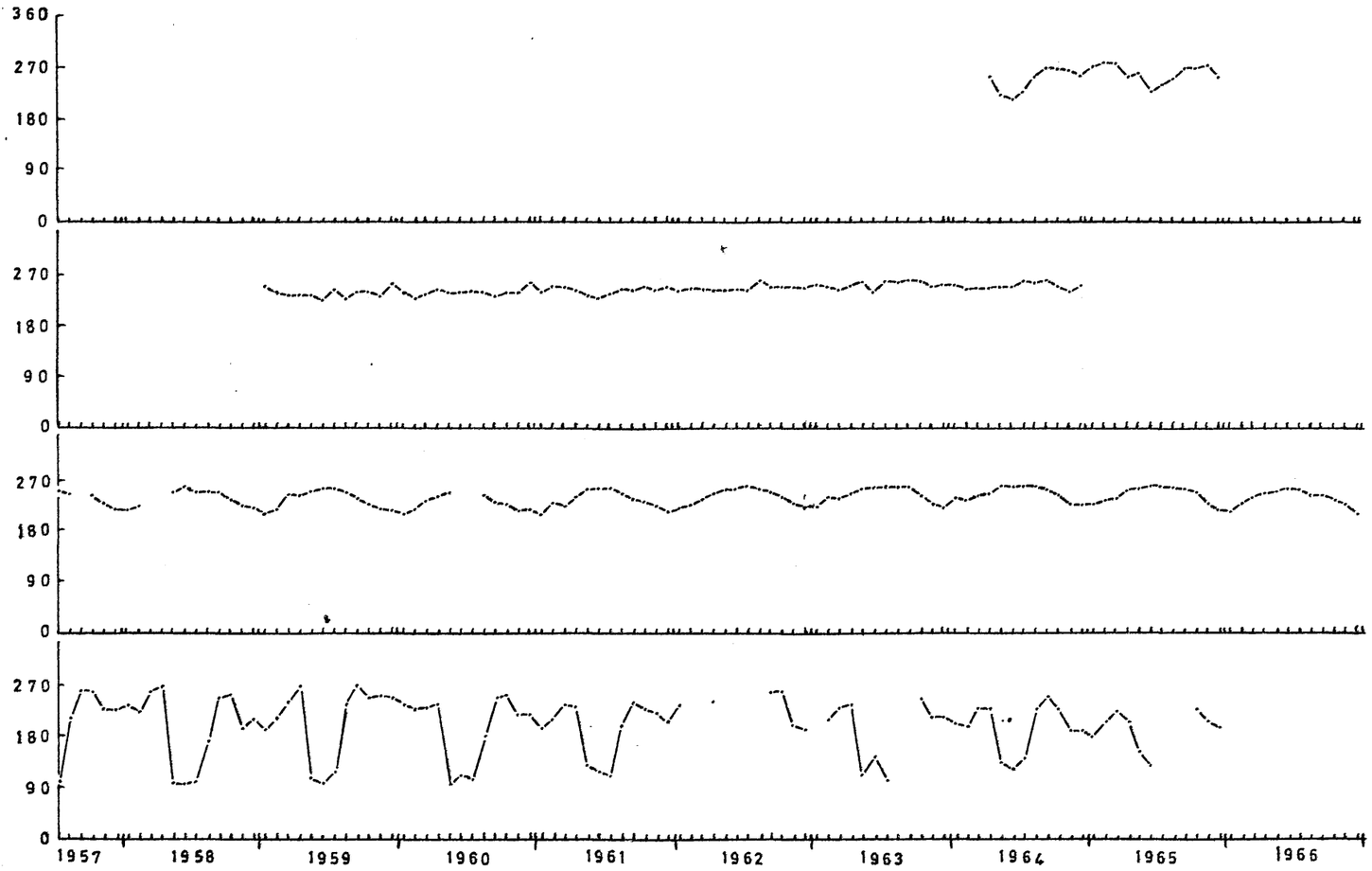

TABLE 4

The optimum value of n obtained when fitting equation (2) with $f(\cos\chi) = \overline{\cos^n\chi}$ to the A_o data for several stations. For comparison the mean square residuals obtained from this optimum fit are compared with those obtained on fitting equation (2) with $\overline{\cos\chi_m}$.

STATION	OPTIMUM VALUE OF n	MEAN SQUARE RESIDUALS USING $\overline{\cos^n\chi}$ WITH OPTIMUM n	MEAN SQUARE RESIDUALS USING $\overline{\cos\chi_m}$
SOUTH POLE	0.27	0.031	0.035
BYRD	0.12	0.102	0.070
VOSTOK	0.23	0.016	0.009
SCOTT	0.27	0.100	0.084
HALLEY BAY	0.03	0.091	0.044
CAPE HALLETT	0.00	0.090	0.084
SANAE	0.08	0.060	0.041
TERRE ADELIE	0.27	0.065	0.061
MIRNYY	0.55	0.031	0.033
WILKES	0.21	0.055	0.055
PORT LOCKROY	0.49	0.039	0.038
CAMPBELL ISLAND	0.40	0.056	0.059

UT control and local time control of f_0F2 values in these cases.

1.4 AN OPTIMUM $\cos^n\chi$

From Chapman's theory of layer formation (Ratcliffe[120]), the critical frequency of an α-Chapman layer is proportional to $\cos^{\frac{1}{4}}\chi$ while that of a β-Chapman layer depends on $\cos^{\frac{1}{2}}\chi$. Since the F2-layer has a β-type loss, one might expect f_0F2 to vary as $\cos^{\frac{1}{2}}\chi$ and hence A_0 to follow $\overline{\cos^{\frac{1}{2}}\chi}$. To investigate this possibility, least squares fits of equation (1.2) using the function $\overline{\cos^n\chi}$ were performed on the A_0 data; here n assumed values between 0 and 1 in steps of 0.01. The results for A_0 data near sunspot minimum and excluding values obtained in March, April, September and October are shown in Table 4..

The values of n obtained for SANAE, Cape Hallett and Halley Bay seem surprisingly low. The reason for this appears to be that the function (which is defined to be zero when $\cos\chi$ is negative), i.e.

is a poor approximation to the observations which appear to vary sinusoidally. Some average value of $\cos\chi$ which includes negative values is a much better approximation as can be seen from Table 4.

Further it would appear that the average value of n for which $\overline{\cos^n\chi}$ gives the best fit, is about 0.25. Thus the choice of the power $\frac{1}{4}$ in $\overline{\cos^{\frac{1}{4}}\chi}$ which may have seemed a rather arbitrary choice, does have some justification. Furthermore it is clear that the function $\overline{\cos\chi_m}$ still gives the best overall fit to the A_0 data.

1.5 INCLUSION/...

1.5 INCLUSION OF A SEMI-ANNUAL TERM

If the residuals $(\Delta A_0)_i$ obtained on fitting equation (1.2) to all the A_0 data for a particular station, are plotted against time, a semi-annual variation is evident, particularly during years of high solar activity. The residuals obtained using $\overline{\cos\chi_m}$ for four stations are shown in Fig. 7; a similar pattern is present at the other Antarctic stations.

This semi-annual effect is very noticeable when the residuals for the equinoctial months (March, April, September and October) are summed and compared with the sums of the residuals for the remaining months for each station. This is shown in Table 5 for the function $\overline{\cos\chi_m}$. Here the residuals are subdivided according to whether they fall in a period of low solar activity (1961 to 1966) or one of high solar activity (1957 to 1960 and 1967 to 1969). It is clear that the sum of the residuals for the equinoctial months is almost always positive. This is significant since the sum of all the residuals for each station is obviously zero. One cannot draw comparisons between these sums for different stations as a different number of months was used for each station. However, it is very clear from the table that the values of A_0 for equinoctial months obtained from the least squares fit of equation (1.2) are consistently smaller than the observed values during these months. For this reason the analysis was repeated for all stations, this time fitting a function of the form

$$G=A + BS + Cf(\cos\chi) + DSf(\cos\chi) + Eg(\cos\delta) + FSg(\cos\delta) \qquad (1.3)$$

where $g(\cos\delta)$ is a function with a semi-annual peak in March and September. The function selected was

$$g(\cos\delta) = \cos(60i^{\circ} + 180^{\circ})$$

where/...

Figure 7

Residuals from the fit of equation (2) to A_0 data for Scott, Byrd, South Pole and Cape Hallett.

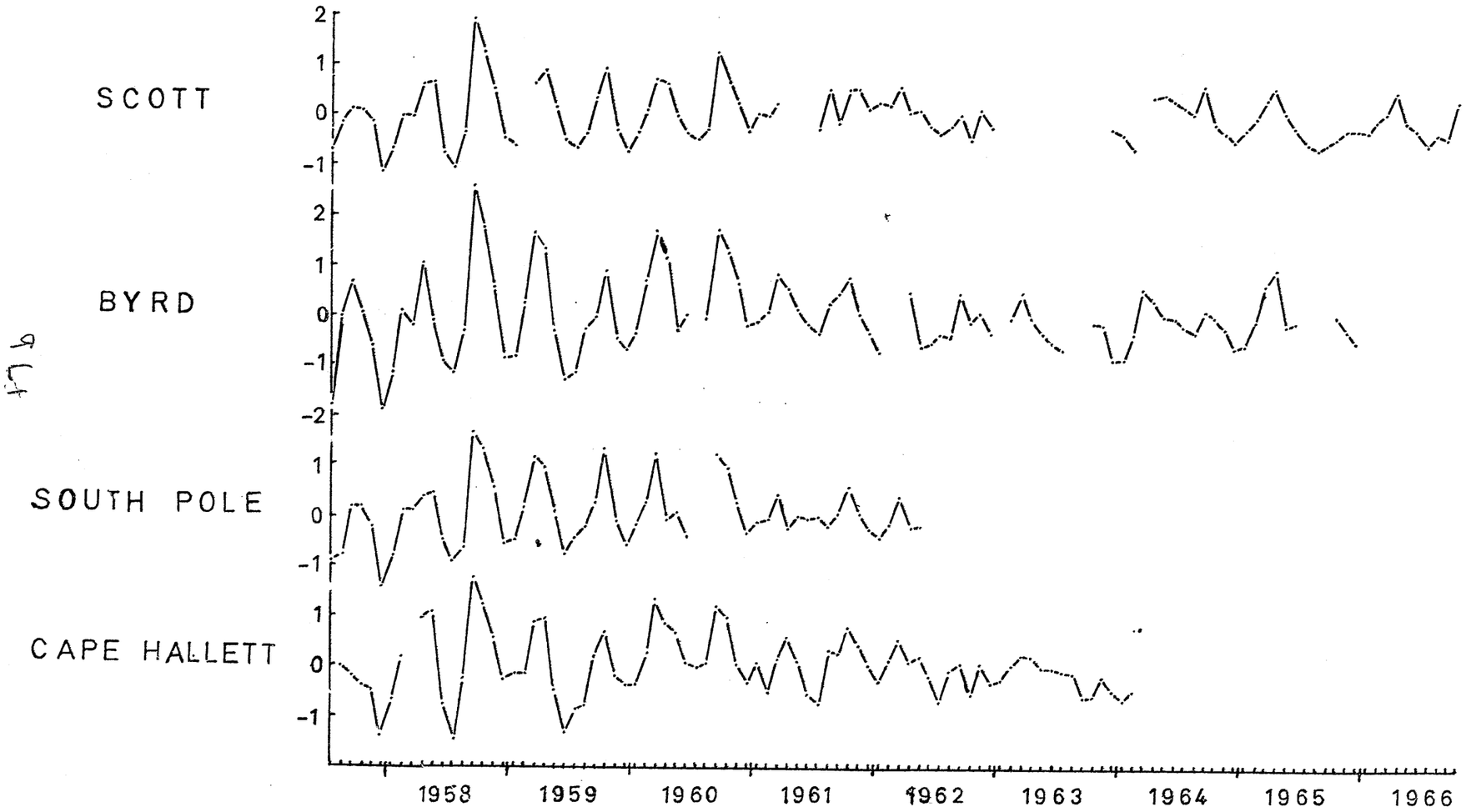
SCOTT
BYRD
SOUTH POLE
CAPE HALLETT
2
1
0
-1
-2
1958
1959
1960
1961
1962
1963
1964
1965
1966

Table 5. Residuals after fitting equation (2) with $\overline{\cos \chi_m}$ to all the A_0 data; for details see text.

	for M, A, S and O			for other months		
	SOLAR MAX	1961 - 1966	TOTAL	SOLAR MAX	1961 - 1966	TOTAL
SOUTH POLE	10.92	0.21	11.13	-8.43	-2.70	-11.13
BYRD	15.64	6.40	22.04	-12.05	-9.99	-22.04
SCOTT	10.13	2.12	12.25	-8.63	-3.62	-12.25
HALLEY BAY	1.29	3.13	4.42	-2.10	-2.32	-4.42
CAPE HALLETT	10.38	1.19	11.57	-7.30	-4.27	-11.57
SANAE	5.20	-0.26	4.94	-3.93	-1.01	-4.94
TERRE ADELIE	3.81	0.42	4.23	-3.17	-1.06	-4.23
WILKES	5.35	-1.78	3.57	-2.83	-0.74	-3.57
PORT LOCKROY	3.58	2.92	6.50	-3.09	-3.41	-6.50
CAMPBELL ISL.	7.44	-2.34	5.10	-3.07	-2.03	-5.10

Table 6. Mean square residuals obtained on fitting equation (3) to the A_0 data compared with those obtained using equation (2)
(a) using all the data (b) using only data from 1961 - 1966

	$\cos(30^o i)$				$\overline{\cos \chi_m}$			
	EQN. (2)		EQN. (3)		EQN. (2)		EQN. (3)	
	a	b	a	b	a	b	a	b
SOUTH POLE	0.377	0.080	0.235	0.075	0.380	0.072	0.232	0.063
BYRD	0.606	0.225	0.305	0.127	0.569	0.174	0.272	0.085
VOSTOK		0.051		0.050		0.025		0.024
SCOTT	0.277	0.139	0.197	0.133	0.260	0.114	0.181	0.108
HALLEY BAY	0.166	0.115	0.125	0.095	0.132	0.081	0.088	0.067
CAPE HALLETT	0.399	0.152	0.279	0.135	0.386	0.125	0.269	0.111
SANAE	0.256	0.087	0.228	0.086	0.199	0.054	0.180	0.053
TERRE ADELIE	0.141	0.119	0.118	0.114	0.117	0.090	0.098	0.086
MIRNYY		0.077		0.069		0.057		0.045
WILKES	0.192	0.079	0.153	0.073	0.183	0.065	0.146	0.057
PORT LOCKROY	0.270	0.162	0.226	0.159	0.173	0.087	0.145	0.087
CAMPBELL ISL.	0.379	0.168	0.362	0.167	0.361	0.126	0.337	0.119

Table 7. Values of the coefficients from the least squares fit of equation (3) using $\overline{\cos \chi_m}$

GEOGRAPHIC LATITUDE	STATION	A	B	C	D	E	F
90.0	SOUTH POLE	3.03(±.16)	.0138(±.0010)	4.15(±.22)	-0.0104(±.0038)	-0.170(±.088)	0.0039(±.0014)
80.0	BYRD	1.45(.14)	.0206(.0008)	6.02(.20)	-0.0147(.0030)	0.038(.078)	0.0048(.0011)
78.5	VOSTOK	2.49(.88)	.0057(.0104)	4.11(.13)	-0.0134(.0351)	0.586(.048)	-0.0075(.0152)
77.8	SCOTT	2.12(.12)	.0193(.0007)	3.97(.15)	-0.0158(.0024)	-0.199(.061)	0.0037(.0009)
75.5	HALLEY BAY	0.70(.19)	.0201(.0016)	4.50(.15)	0.0253(.0057)	-0.488(.058)	0.0073(.0021)
72.3	CAPE HALLETT	1.09(.22)	.0259(.0009)	5.08(.22)	-0.0229(.0035)	-0.161(.085)	0.0039(.0013)
70.3	SANAE	0.13(.25)	.0218(.0016)	6.02(.20)	-0.0004(.0058)	-0.401(.072)	0.0047(.0021)
66.7	TERRE ADELIE	1.46(.16)	.0213(.0007)	4.19(.15)	-0.0163(.0028)	-0.217(.054)	0.0030(.0011)
66.5	MIRNYY	1.64(.60)	.0174(.0037)	1.13(.12)	0.0151(.0167)	0.210(.046)	-0.0045(.0057)
66.3	WILKES	1.32(.20)	.0200(.0007)	4.08(.17)	-0.0143(.0028)	-0.383(.064)	0.0039(.0010)
65.3	PORT LOCKROY	1.24(.33)	.0144(.0019)	3.34(.18)	0.0299(.0073)	-0.652(.067)	0.0082(.0026)
52.5	CAMPBELL ISL.	-1.39(.36)	.0418(.0009)	6.39(.25)	-0.0320(.0040)	-0.334(.080)	0.0031(.0013)

where i is the number of the month, being 1 for January and 12 for December. This is a simple semi-annual sinusoidal variation with peaks in March and September.

Table 6 shows the mean square residuals obtained on fitting equation (1.3) to the A_0 data using only two $\cos\chi$ functions: a simple cosine function of the form $\cos(30i^0)$ and $\overline{\cos\chi_m}$. It is clear that equation (1.3) gives a rather better fit to the A_0 data than does equation (1.2), especially if data near sunspot maximum are used. Once again the average midday value of $\cos\chi$ fits the data best.

Table 7 contains the values of the coefficients A, B, C, D, E and F (together with their standard deviations) obtained from the least squares fit of equation (1.3) using $\overline{\cos\chi_m}$.

In Figures 8(a) and (b) the coefficients A and B are plotted against geographic latitude; A appears to increase with latitude and B to decrease. However, it is not immediately evident how A might be interpreted physically. It would represent the average value of f_oF2 for the whole period under consideration, under such conditions that both the 10.7cm flux from the sun and the noon value of $\cos\chi$ were zero. Since between July 1957 and October 1969 the average 10.7cm flux did not drop below 65 (units used are $10^{-22}Wm^{-2}Hz^{-1}$), the quantity A+65B may be a more realistic measure of the behaviour of the quiet F2 region. This is plotted in Fig. 8(c). From this figure it is apparent that under extremely quiet solar conditions if the sun were to reach the horizon at noon, the average value of f_oF2 would <u>increase</u> with increasing latitude. This surprising result adds weight to the conclusion that no simple theory based on

ionization/...

Figure 8

(a) Coefficient A (MHz) from equation (3) plotted against geographic latitude.

(b) Coefficient B (MHz/unit of solar flux) from equation (3) plotted against geographic latitude.

(c) The quantity A + 65 B (MHz) plotted against geographic latitude.

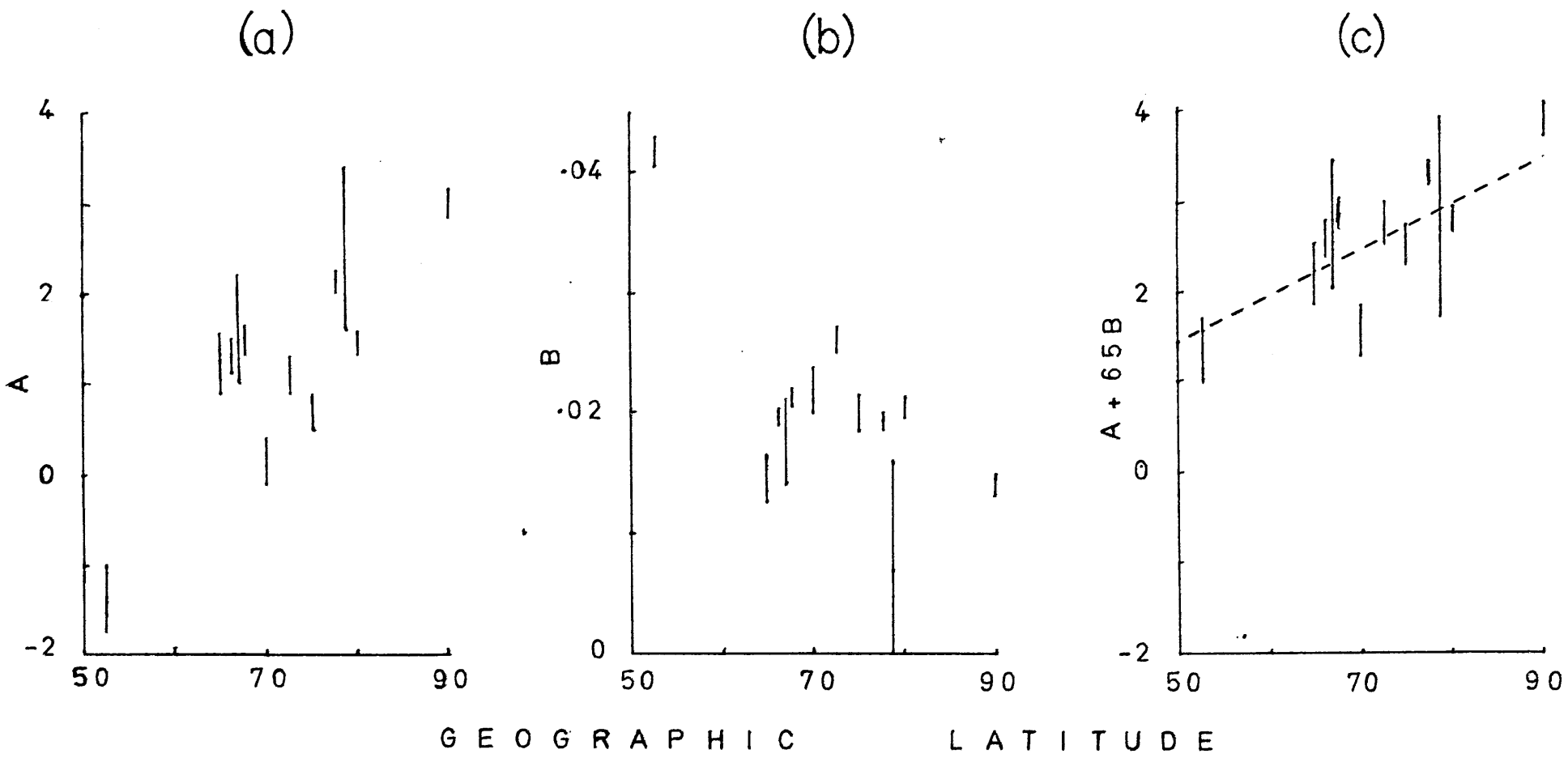
(a)
(b)
(c)
A
B
A + 65B
4
2
0
-2
.04
.02
0
50
70
90
GEOGRAPHIC LATITUDE

ionization produced by solar EUV alone will account for the behaviour of the F2 region over Antarctica.

The point which deviates furthest from the straight line in Fig. 8(c) is that for SANAE (at 70°S) and the deviation is seen to be negative. This may be significant since this station shows an unusually high percentage of ionospheric disturbances (Gledhill, Torr and Torr[53]) owing to its proximity to the South Atlantic Geomagnetic Anomaly, and these disturbances do generally involve a decrease in f_oF2.

The three quantities A, B and A+65B were also plotted against geomagnetic latitude, dip angle and L-value (Figs. 9, 10 and 11) but in each case the ordering of the points was noticeably less convincing.

The coefficients C and D (Table 7) on the other hand, do not appear to correlate with geographic latitude, geomagnetic latitude, dip angle or L-value. In fact the coefficient C which measures the effect of changes of the solar zenith angle on the average value of f_oF2, behaves in an extremely puzzling way. Although at Cape Hallett, Terre Adelie and Wilkes the values of C are comparable, at the neighbouring station Mirnyy its value is of the order of a quarter of these. Its value at SANAE, Byrd and Campbell Island exceeds 6 MHz, but at Halley Bay, which lies between SANAE and Byrd, it is only 4.5 MHz. At South Pole, Vostok and Terre Adelie, stations which are very close to the geographic, geomagnetic and dip poles respectively, C does not take on extreme values.

Similarly the coefficients E and F were plotted against geographic latitude, geomagnetic latitude, dip angle and L-value but failed to correlate with any of them. With the exception of two values of very

low/...

FIGURE 9

A, B and A + 65 B plotted against geomagnetic latitude

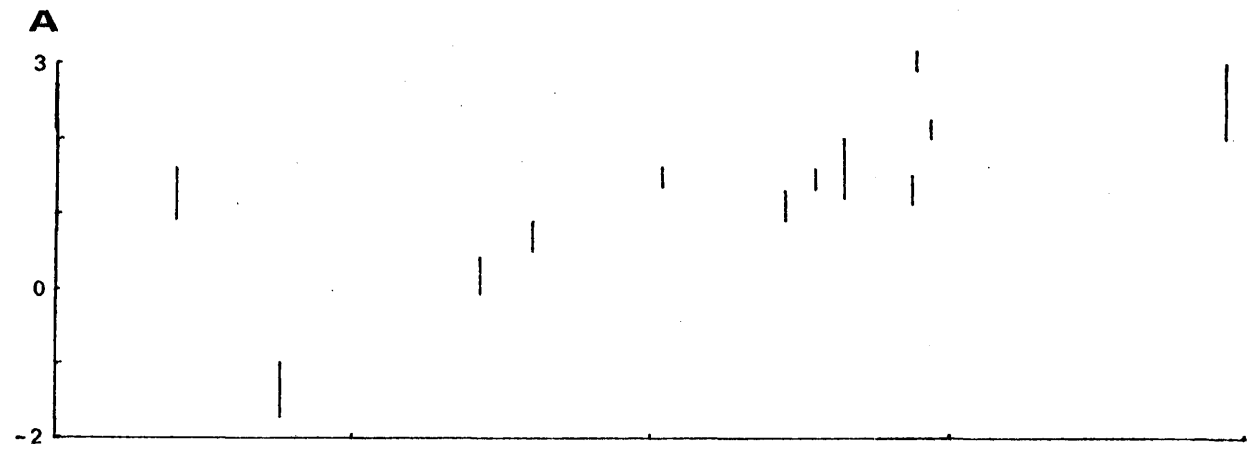
A
3
0
-2

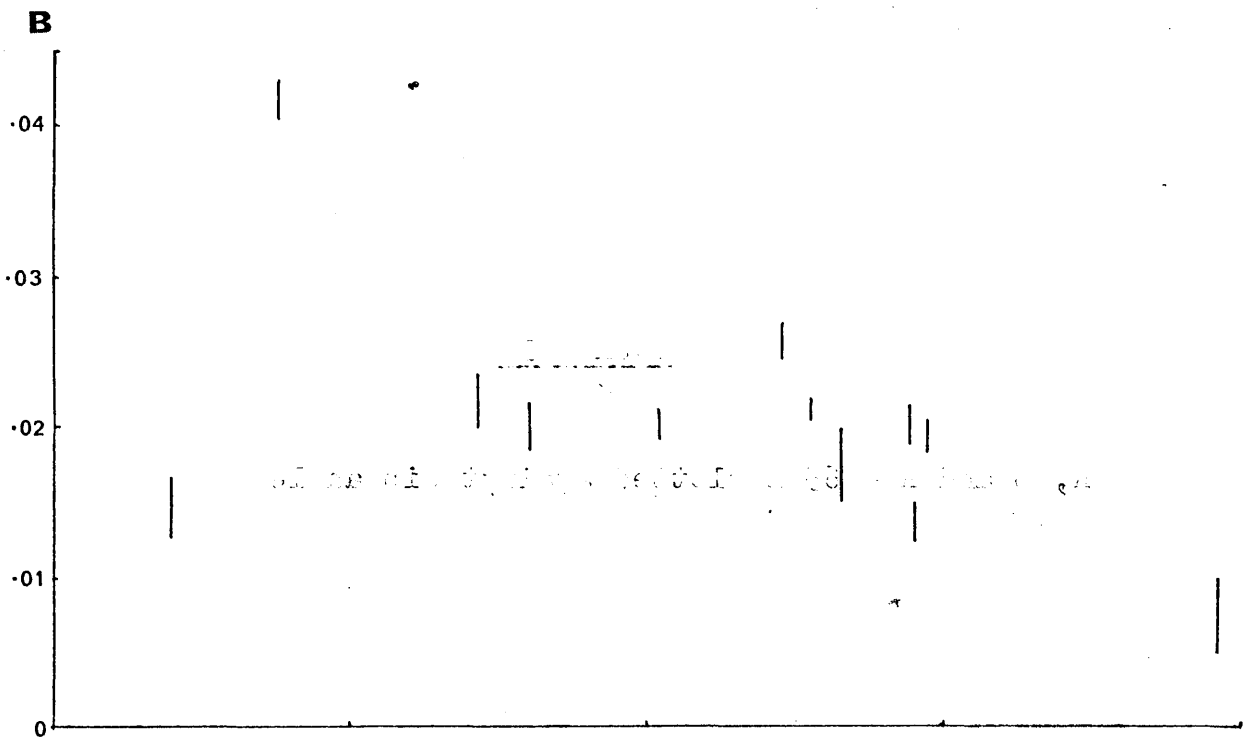
B
·04
·03
·02
·01
0

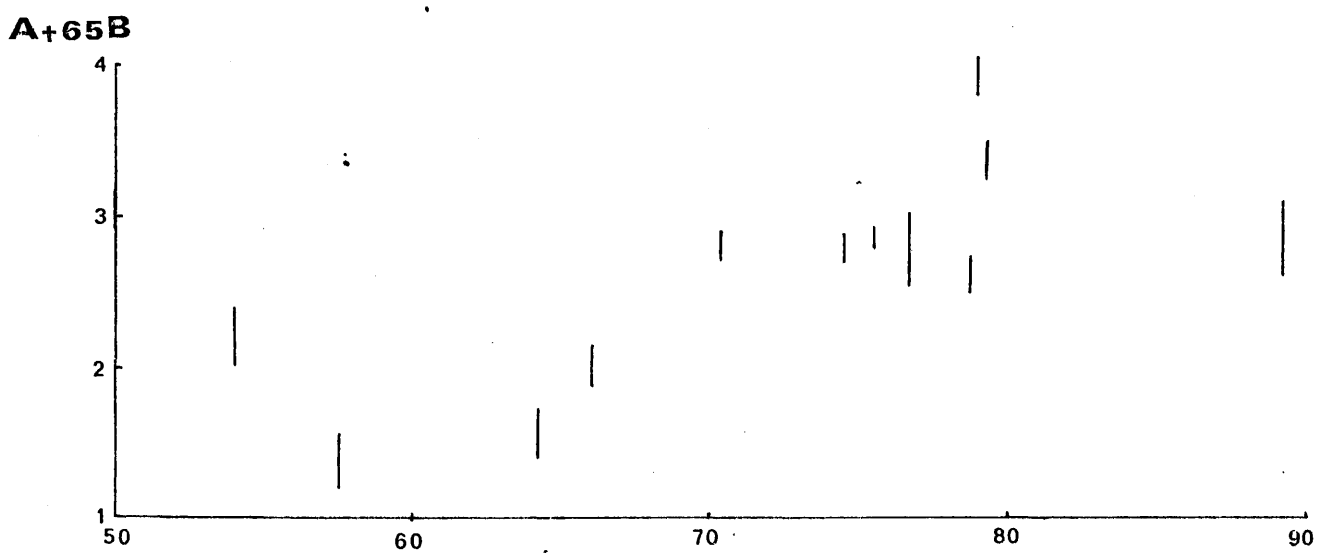
A+65B
4
3
2
1
50
60
70
80
90

FIGURE 10

A, B and A + 65 B plotted against dip angle

Pb1

FIGURE 11

A, B and A + 65 B plotted against L-value

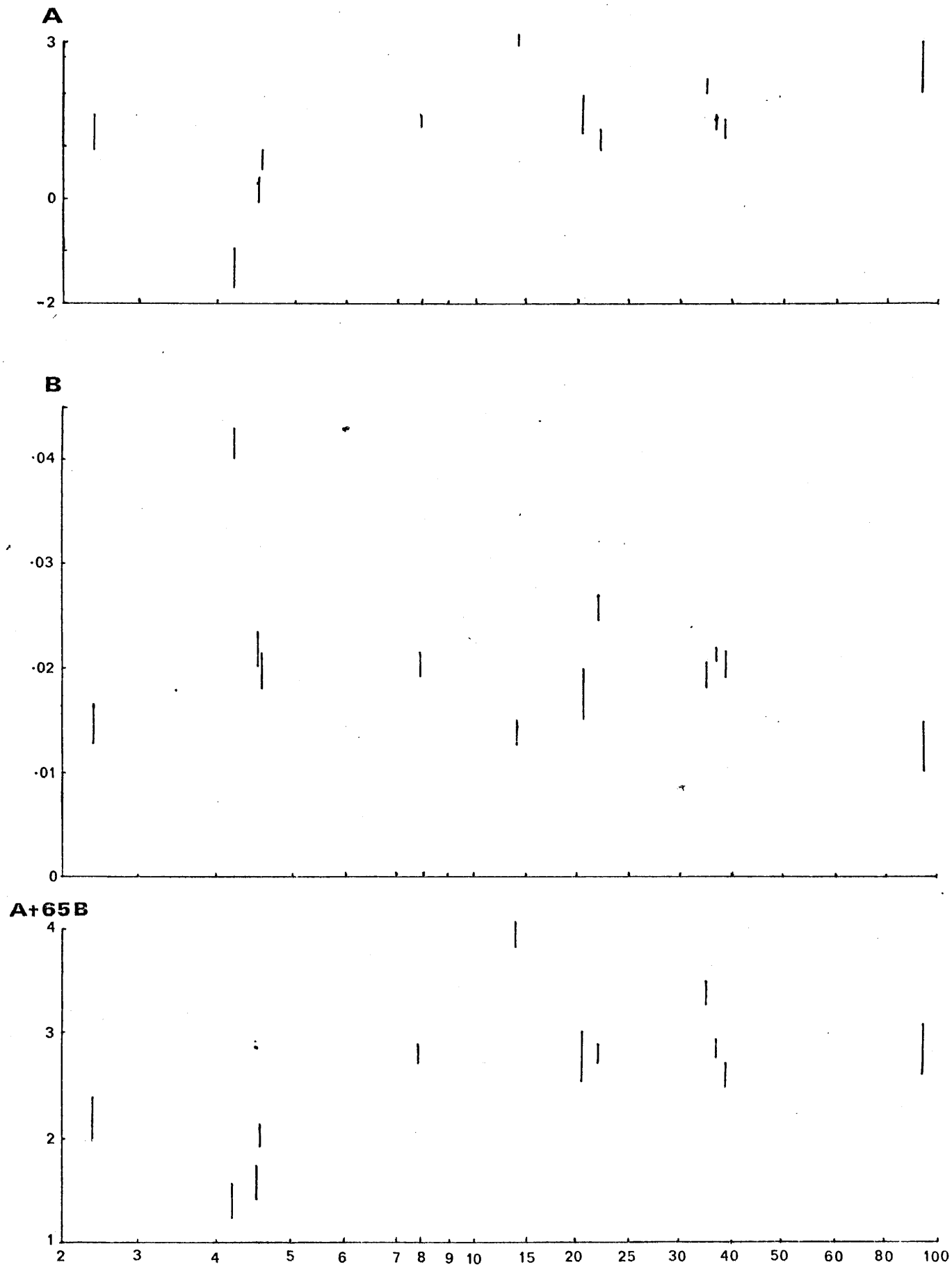
A
3
0
-2
B
·04
·03
·02
·01
0
A+65B
4
3
2
1
2
3
4
5
6
7
8
9
10
15
20
25
30
40
50
60
80
100

low weight from Vostok and Mirnyy (for which stations only data near sunspot minimum were available), F is always positive. This shows that solar activity definitely influences the semi-annual variation of A_0 and tends to increase it.

1.6 THE DATE OF CHANGEOVER

The transition between local time control and UT control of the ionosphere is sometimes very sharp, taking place within a few days (Piggott and Shapley[114], Rishbeth[125]). An example of this for SANAE is shown in Fig. 12. To investigate whether this phenomenon shows any dependence on solar activity, the dates of changeover for five stations for which the changeover was easy to detect, are shown in Tables 8 and 9. From these tables it appears that the changeover dates for each station are approximately the same from year to year. This is shown more clearly in Fig. 13 where the changeover periods between UT and LT controlled behaviour for SANAE are shown for the period 1962-1970 (where data were available). Tables 8 and 9 also support the idea put forward by Piggott and Shapley that the changeover occurs on different dates at different stations.

To investigate the difference in changeover date between different stations, the average changeover date for each of these stations is plotted against geographic latitude (Fig. 14). However, no simple pattern emerges from this figure. Attempts to correlate the changeover dates with geomagnetic latitude and L-value also failed (see Fig. 15).

The average changeover dates (averaged over

several/...

Figure 12

The time of day of maximum f_oF2 at SANAE is plotted against date to illustrate the rapid transition between local time and universal time control of the Ionosphere.

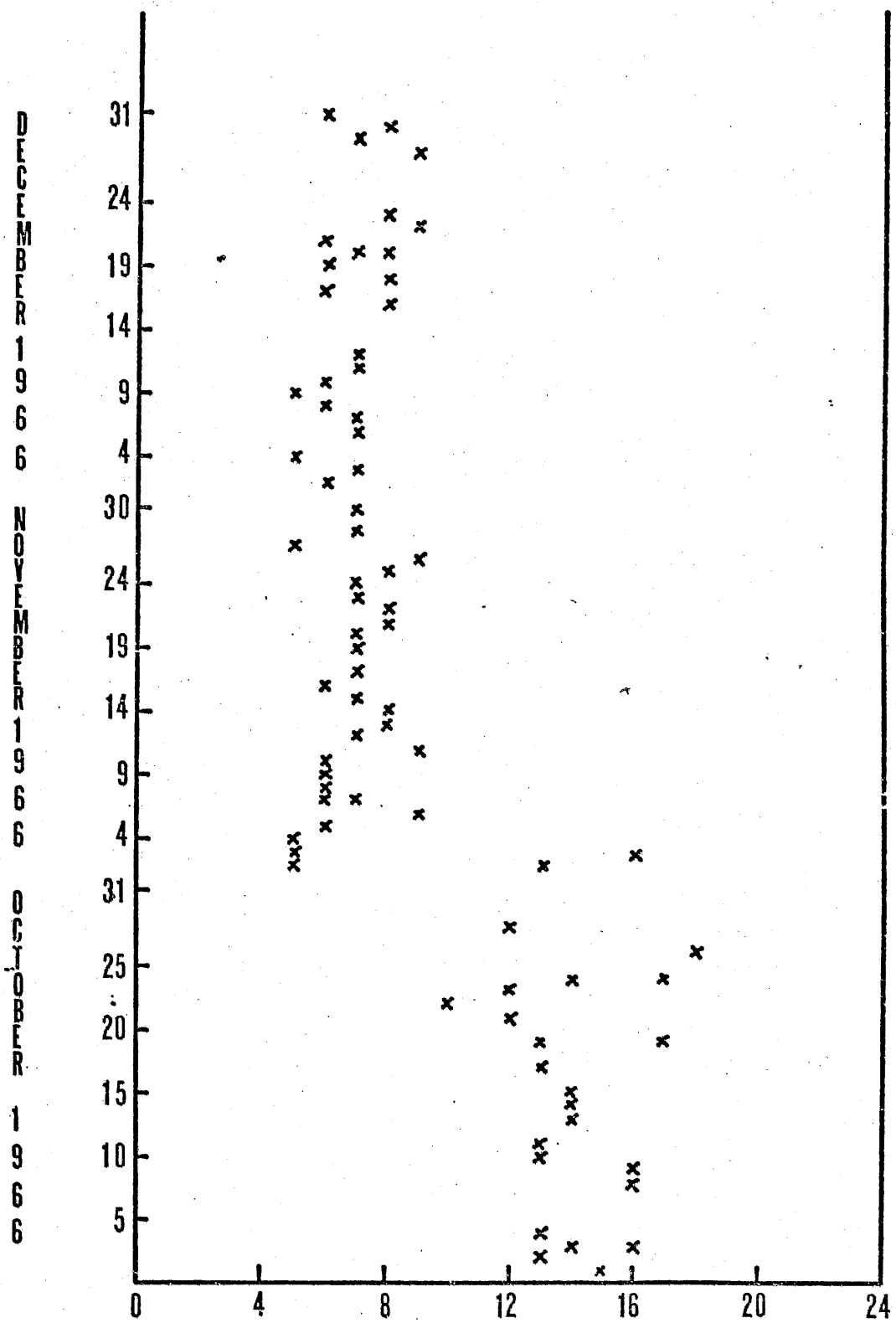
DECEMBER 1966 NOVEMBER 1966 OCTOBER 1966
31
24
19
14
9
4
30
24
19
14
9
4
31
25
20
15
10
5
0
4
8
12
16
20
24

TABLE 8

DATES OF CHANGEOVER FROM SUMMER TO WINTER BEHAVIOUR.

YEAR	CAMPBELL ISLAND	SANAE	HALLEY BAY	PORT LOCKROY	BYRD
1958					MAY 19(±0)
1959	MAR 11(±5)				MAY 4(2)
1960	MAR 8(3)				MAY 6(4)
1961	MAR 11(7)		MAR 14(±9)		MAY 6(3)
1962	MAR 27(5)		FEB 27(1)		
1963	FEB 17(8)	FEB 21(±1)	MAR 14(8)	MAR 3(±2)	
1964	FEB 29(2)	FEB 25(4)		MAR 23(1)	
1965	MAR 24(2)		MAR 17(7)	MAR 14(0)	
1966	MAR 10(0)	MAR 2(0)	MAR 8(7)	MAR 1(1)	
1967		FEB 22(2)	MAR 9(7)	FEB 25(3)	
1968		MAR 3(0)		MAR 10(1)	
1969		MAR 3(1)	MAR 16(10)	FEB 25(0)	
1970		MAR 9(2)			

NOTE: Since the changeover usually took place over a period of several days, the date recorded is the mid-point of the transition period and the figure in brackets an estimate of half the length of the transition period in days.

TABLE 9

DATES OF CHANGEOVER FROM WINTER

TO SUMMER BEHAVIOUR.

YEAR	CAMPBELL ISLAND	SANAE	HALLEY BAY	PORT LOCKROY	BYRD
1957	NOV 25(±5)				JUL 27(±1)
1958	NOV 21(3)				JUL 28(4)
1959	NOV 10(5)				AUG 3(2)
1960	NOV 1(3)				JUL 28(2)
1961	NOV 5(6)		SEP 13(±2)		AUG 11(2)
1962	OCT 15(6)	OCT 29(±2)	SEP 29(3)	OCT 2(±2)	
1963	NOV 1(0)		OCT 6(1)		
1964		OCT 31(0)	OCT 7(5)	OCT 3(2)	
1965	OCT 31(1)		OCT 15(3)	OCT 12(1)	
1966	OCT 5(2)	OCT 30(2)		OCT 22(1)	
1967		OCT 29(1)	OCT 13(4)	OCT 24(3)	
1968		OCT 21(1)	OCT 16(4)	OCT 26(2)	
1969		OCT 31(3)	OCT 24(7)	OCT 29(1)	

TABLE 10

THE AVERAGE CHANGEOVER DATES FOR THE TRANSITION BETWEEN UT AND LT-CONTROLLED BEHAVIOUR AT FIVE ANTARCTIC STATIONS.

STATION	LT TO UT TRANSITION		UT TO LT TRANSITION	
	DATE	NO. OF DAYS BEFORE DEC. 22	DATE	NO. OF DAYS AFTER DEC. 22
SANAE	OCT 28	55	MAR 1	69
HALLEY BAY	OCT 8	75	MAR 11	79
PORT LOCKROY	OCT 17	66	MAR 6	74
CAMPBELL ISLAND	NOV 6	46	MAR 10	78

STATION	LT TO UT TRANSITION		UT TO LT TRANSITION	
	DATE	NO. OF DAYS BEFORE JUNE 21	DATE	NO. OF DAYS AFTER JUNE 21
BYRD	MAY 9	43	AUG 1	41

Figure 13

The dates of changeover between LT and UT behaviour for SANAE plotted against year for the period 1962 - 1970.

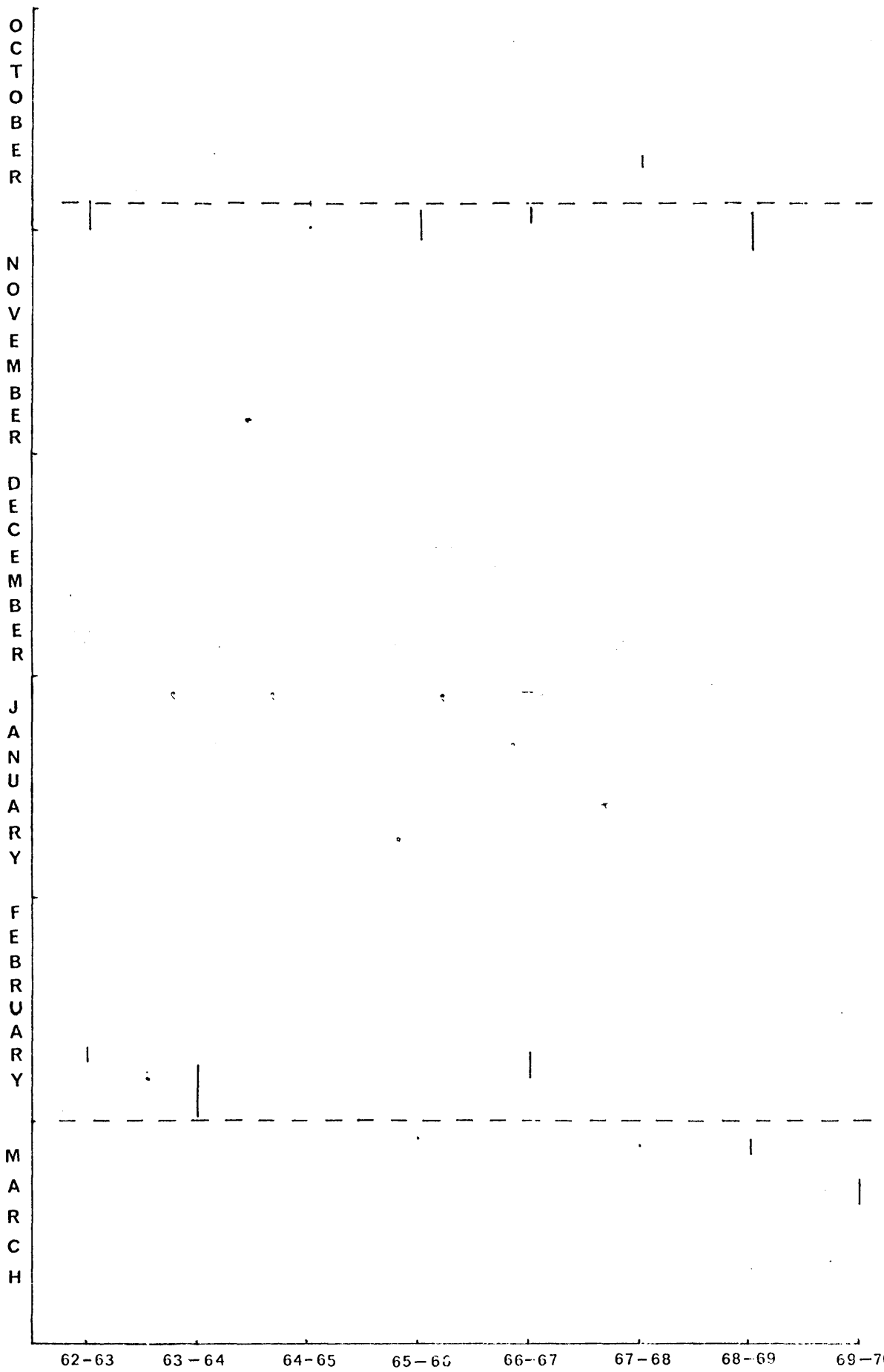
OCTOBER
NOVEMBER
DECEMBER
JANUARY
FEBRUARY
MARCH
62-63
63-64
64-65
65-66
66-67
67-68
68-69
69-70

Figure 14

The average changeover dates for the transition between LT and UT behaviour plotted against geographic latitude for five stations:- Byrd, Halley Bay, SANAE, Port Lockroy and Campbell Island. The average changeover date is represented by a point and the period of UT control is shown.

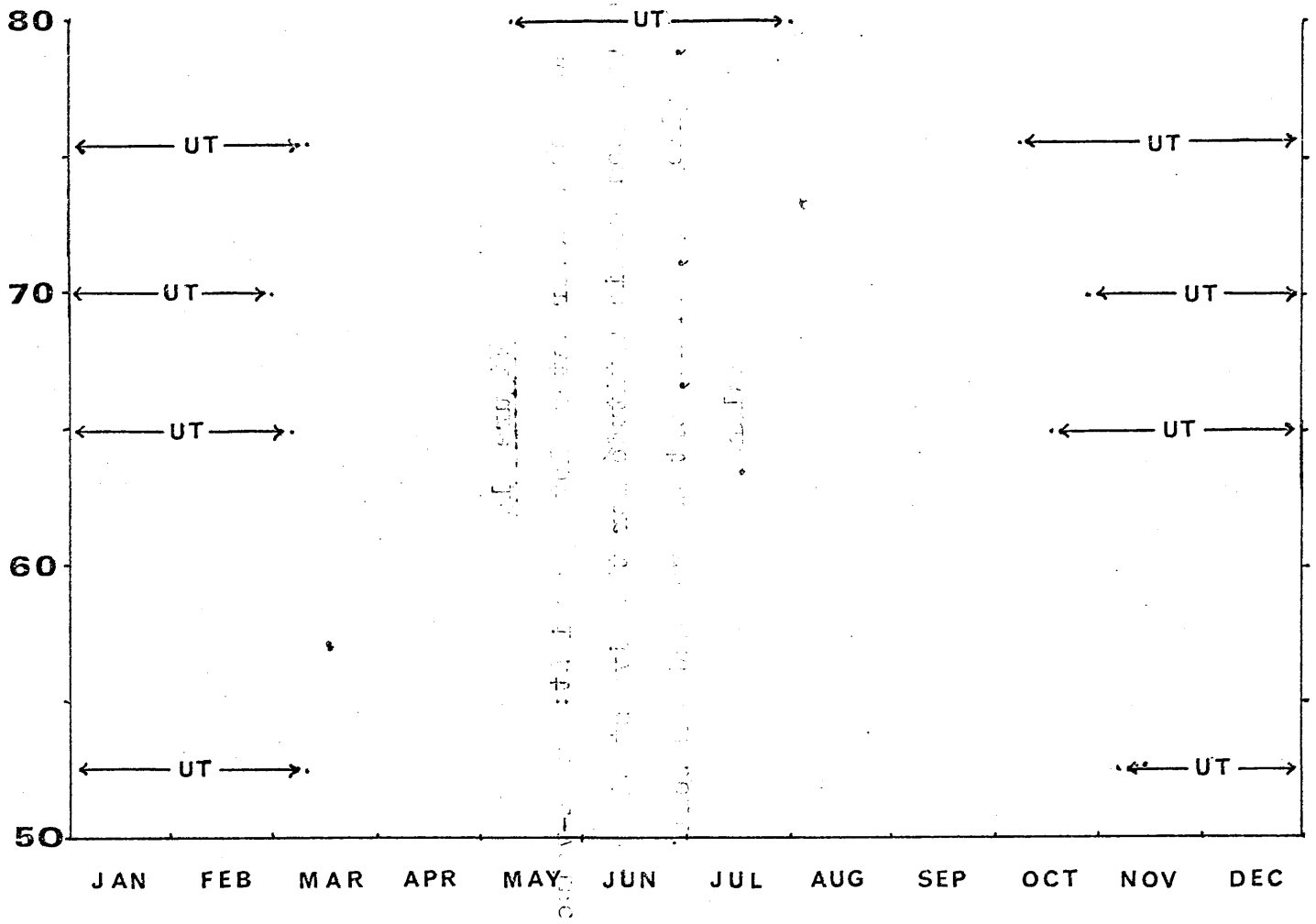
80
70
60
50
UT
UT
UT
UT
UT
UT
UT
UT
JAN
FEB
MAR
APR
MAY
JUN
JUL
AUG
SEP
OCT
NOV
DEC

Figure 15

The mean changeover dates plotted against: (a) L-value and (b) geomagnetic latitude for the five stations:- Byrd, Halley Bay, SANAE, Port Lockroy and Campbell Island.

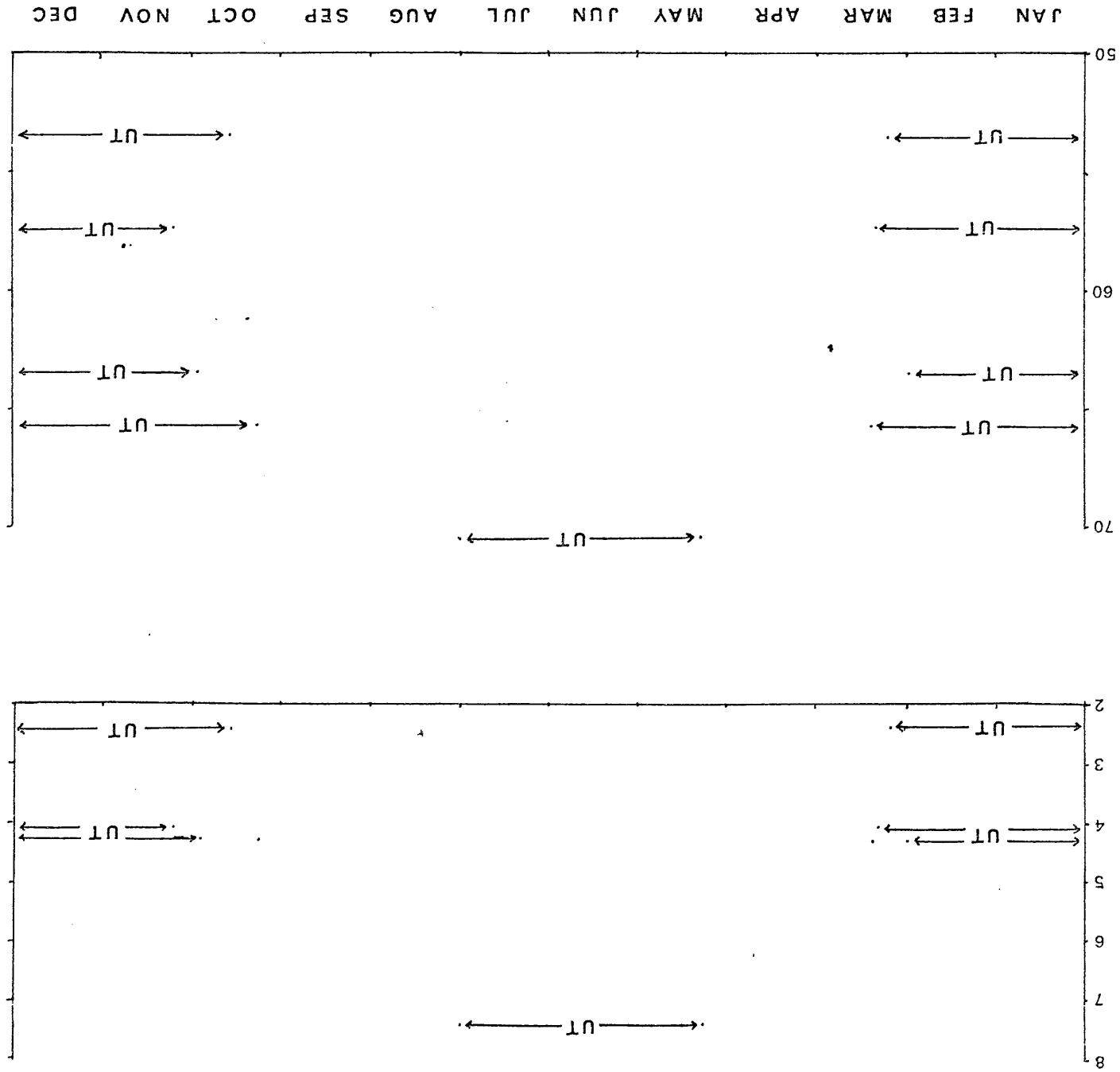
JAN
FEB
MAR
APR
MAY
JUN
JUL
AUG
SEP
OCT
NOV
DEC
50
60
70
GEOMAGNETIC LATITUDE
(b)
2
3
4
5
6
7
8
L - VALUE
(a)
UT

several years) for the five stations considered, are shown in Table 10. This table shows that for the three stations in the Weddell Sea area, the changeover from LT-controlled behaviour to UT control usually occurs first at Halley Bay, then Port Lockroy and finally SANAE while the changeover from UT control back to LT control occurs in the reverse order, viz. SANAE-Port Lockroy-Halley Bay. This order of changeover does not appear to be related to magnetic latitude, geographic latitude, dip angle or L-value. Another thing which is apparent from Table 10 is that the period of UT control for the three stations in the Weddell Sea area is centred on the December solstice (December 22nd) and the average changeover dates for each station are roughly symmetrical about this date (i.e. the changeover from LT to UT control occurs approximately the same number of days before Dec. 22 as the changeover from UT to LT control occurs after it). Similarly, the period of UT control at Byrd is centred on the June solstice, 21st June, and the average changeover dates are approximately symmetrical about this date. Campbell Island is the exception in this table, as the changeover dates in this case are not symmetrical about one of the solstices. However, in the light of a recent report by King, Eccles and Kohl[82] who investigate the case of Macquarie Island, it seems very likely that the "UT behaviour" observed at Campbell Island during summer is not the same as the UT controlled behaviour observed at Antarctic stations (i.e. an increase of f_0F2 at about 06 UT), but, like the behaviour at Macquarie Island, is merely a "midday bite-out" effect which by chance produces a maximum near 06 UT during summer.

It is unfortunate that the majority of the stations

used/...

used in the least squares analyses lie near the 120°E longitude and hence it is impossible to determine when the changeover occurs for these stations. Without values for these stations the analysis is incomplete and it is difficult to say anything further about the significance of the changeover date.

1.7 SUMMARY AND DISCUSSION

To summarize, the following results have emerged from these analyses:

(1) The constant term, A_0, which is the mean value of f_0F2 for the ten magnetically quiet days of each month, has the same general pattern of behaviour at all Antarctic stations for which data were obtained. During years of low solar activity, it varies almost sinusoidally with its maximum in summer, while when solar activity is high, it reaches a maximum twice a year in March/April and September/October. In addition there appears to be a long term dependence on solar activity, A_0 increasing with increasing solar flux; Table 2 which compares the June values of A_0 for different stations, shows this dependence very clearly.

(2) The behaviour of A_0 can be described by a function of the form

$$A + BS + Cf(\cos\chi) + DSf(\cos\chi) + Eg(\cos\delta) + FSg(\cos\delta)$$

where the term BS takes account of the dependence on solar activity, $Cf(\cos\chi) + DSf(\cos\chi)$ the dependence on the position of the sun in the sky and $Eg(\cos\delta) + FSg(\cos\delta)$ the semi-annual equinoctial maxima.

(3) The $\cos\chi$ functions which fit the A_0 data best, are $\overline{\cos\chi_m}$ and $\overline{\cos\chi}$, the two functions which include negative values of the cosine of the solar zenith angle.

(4) The/...

(4) The amplitude of the 24-hour component, A_1, at Port Lockroy, SANAE and Halley Bay (the three stations lying in the area of the Weddell Sea anomaly) has two well-defined maxima about the equinoxes each year and an additional one around December. Its behaviour at other stations is less distinct, although, with the exception of Campbell Island, it does still show peaks at the equinoxes.

(5) The transition between local time control and UT control of the ionosphere occurs at approximately the same date each year for a given station, irrespective of solar activity.

The average changeover date is different for different stations. In the Weddell Sea area the changeover from LT to UT control usually occurs first at Halley Bay then Port Lockroy and finally at SANAE; the transition from UT control to LT control follows the reverse order.

The periods of UT control for SANAE, Halley Bay and Port Lockroy are symmetrical about the summer solstice; for Byrd the period of UT control is symmetrical about the winter solstice; for Campbell Island the period of UT control occurs in summer but is not symmetrical about the summer solstice.

Points (4) and (5) suggest that the stations exhibiting so-called UT-controlled behaviour can be divided into three classes:

(a) stations in the Weddell Sea area. For these stations the period of UT control is centred on the summer solstice and changeover dates are symmetrical about 22nd December. The amplitude of the 24-hour component, A_1, has well-defined maxima about the equinoxes and in December.

(b) stations/...

(b) stations in the Ross Sea area. These stations have their period of UT control centred on the winter solstice and changeover dates are symmetrical about 21st June. A_1 has maxima about the equinoxes but these are less distinct.

(c) stations such as Campbell Island and Macquarie Island. In these cases the changeover dates are not symmetrical about a solstice and A_1 does not display distinct maxima about the equinoxes.

The mechanisms responsible for the UT behaviours of (a) and (b) may be the same or different. The one responsible for the UT behaviour of (c) is different and is probably due to a midday bite-out effect.

There are four possible mechanisms which may explain the behaviour of the constant term, A_0, as outlined in the first point of the summary above:

(a) the effect of winds in the F2-region of the ionosphere;

(b) the temperature-dependent balance between production by solar EUV and loss in the ionosphere;

(c) the effect of the annual variation in the neutral atmospheric density on production and loss in the ionosphere;

(d) the effects of particle precipitation from the magnetosphere.

The merits and demerits of each of these explanations will be considered in the next part.

PART II

POSSIBLE EXPLANATIONS OF THE BEHAVIOUR OF THE ANTARCTIC F2-REGION

"We will listen instead to the wind's text

.....

Wrong from the start, for nature's truth

Is primary and her changing seasons

Correct out of a vaster reason"

(R.S. Thomas)

Horizontal winds at ground level in Antarctica

CHAPTER 2

THE SIGNIFICANCE OF HORIZONTAL NEUTRAL WINDS

2.1 INTRODUCTION

Many authors have suggested that particular ionospheric phenomena may be ascribed to the action of horizontal neutral winds. Examples of such phenomena include the evening enhancement of f_0F2 observed at middle latitudes (Ratcliffe[120], Allen[2]), the "midday bite-out" (Ratcliffe[120], Kohl and King[92]) and the "diurnal anomaly" observed at low latitudes in which the highest critical frequencies occur several hours after noon (King[81]). In particular, several authors have proposed the effect of winds as the explanation of the peculiar UT behaviour of f_0F2 in the Antarctic (e.g. Knecht[90], Rastogi[116], Kohl and King[92]). Kohl, King and Eccles[93] attempted to prove that the early morning maximum of f_0F2 at Port Lockroy is due to an equatorward wind which blows in the F-region in the late evening and early morning and which gives rise to an upward drift of ionization at these times. Hill[64] showed on the basis of magnitude alone that winds might explain the anomalous Antarctic behaviour generally, without going into detail about the directions which such winds should have. King et al[84] tried to explain the UT behaviour of f_0F2 observed in the Ross Sea area in terms of winds "blowing ionization" up or down the magnetic lines of force. However, no-one has yet proved that winds are the cause of the phenomenon (Challinor[19], Duncan[38]). For this reason this chapter has been devoted to a study of F-region drift velocities and critical frequencies in order to clarify the

part/...

part played by horizontal neutral winds in determining the behaviour of the F2 peak.

First we shall look at the evidence in favour of the wind argument, viz. the correlation between theoretical wind velocities and observed f_oF2, then the evidence against the wind argument, i.e. where the wind argument fails. The next part of the chapter deals with a study of experimentally measured wind velocity data. The only station for which suitable data were available, was Halley Bay. Data for this station obtained during the IGY (1957-1958) were analyzed by Bellchambers et al[11] and several of their tables have been included in this chapter. In section 2.6 a study of the IQSY data is undertaken. Then an analysis of f_oF2 values for several pairs of stations at the same geographic latitude was undertaken, the purpose of which was to look for trends in the behaviour of f_oF2 stations at the same latitude which might be attributed to winds. Finally winds are considered as a possible explanation of the results of the harmonic analysis outlined in Chapter 1.

2.2 THE WIND EXPLANATION OF KING ET AL

Making certain assumptions about the pressure gradients, electron densities, scale heights, etc., Kohl and King[92] obtained solutions of the equation of motion of the neutral atmosphere for equinoctial conditions at sunspot maximum and sunspot minimum. Figure 16 shows the temperature distribution with latitude and longitude (Jacchia's model) which Kohl and King assumed while Figure 17 shows the results which they calculated for sunspot minimum.

Furthermore they suggested that the effect that an horizontal neutral wind will have on the ionosphere,

will/...

Figure 16

The exospheric temperature distribution used by Kohl and King[92]. Copy of Fig. 1 of their paper.

FIGURE 16

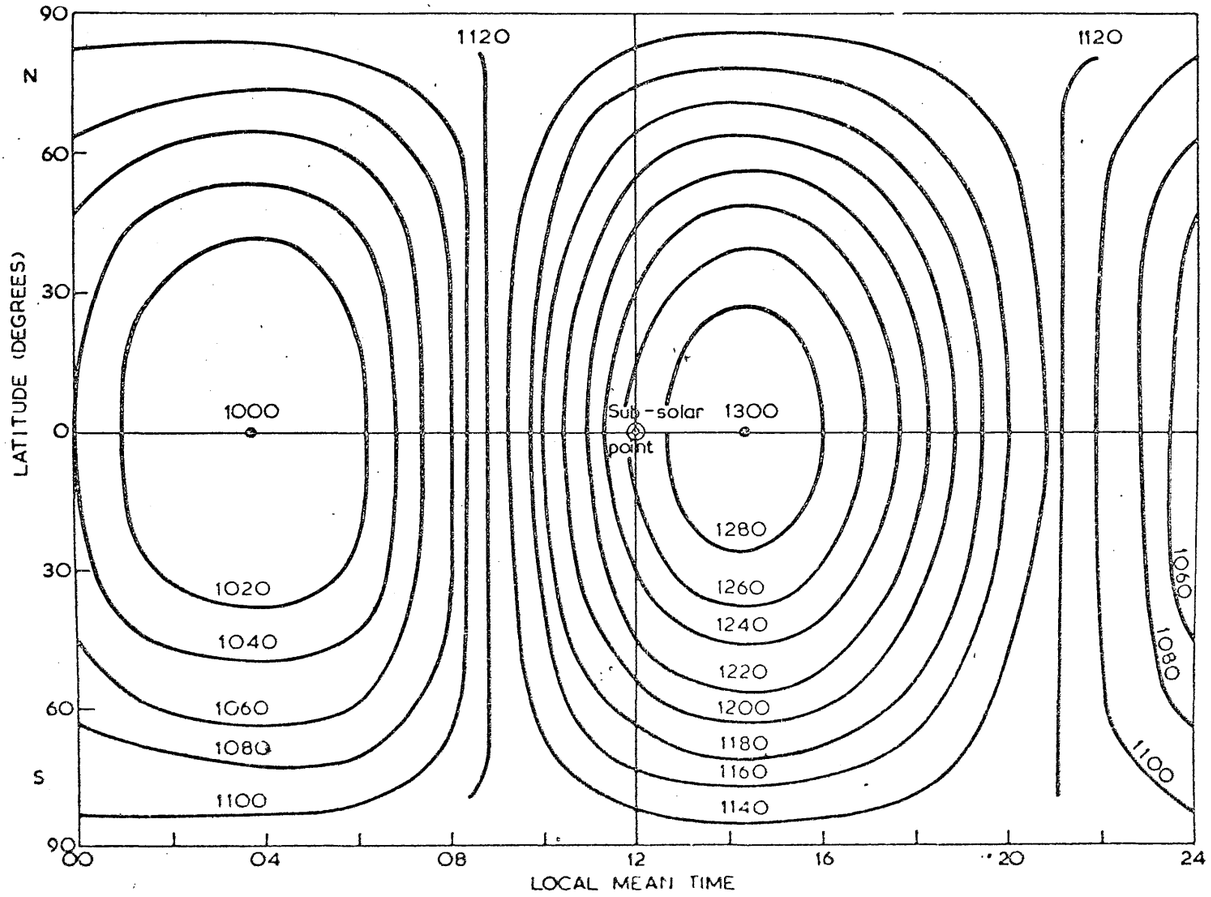

Fig. 1 : Equinox exospheric temperature distribution for medium solar cycle conditions (after Jacchia (1965)). The isothermal contours are approximately concentric circles around the atmospheric bulge which occurs on the equator at 1430 L.M.T.

Figure 16

Figure 17

The wind pattern calculated by Kohl and King[92] for equinoctial conditions near sunspot minimum. (Copy of Fig. 6 of their paper.)

FIGURE 17

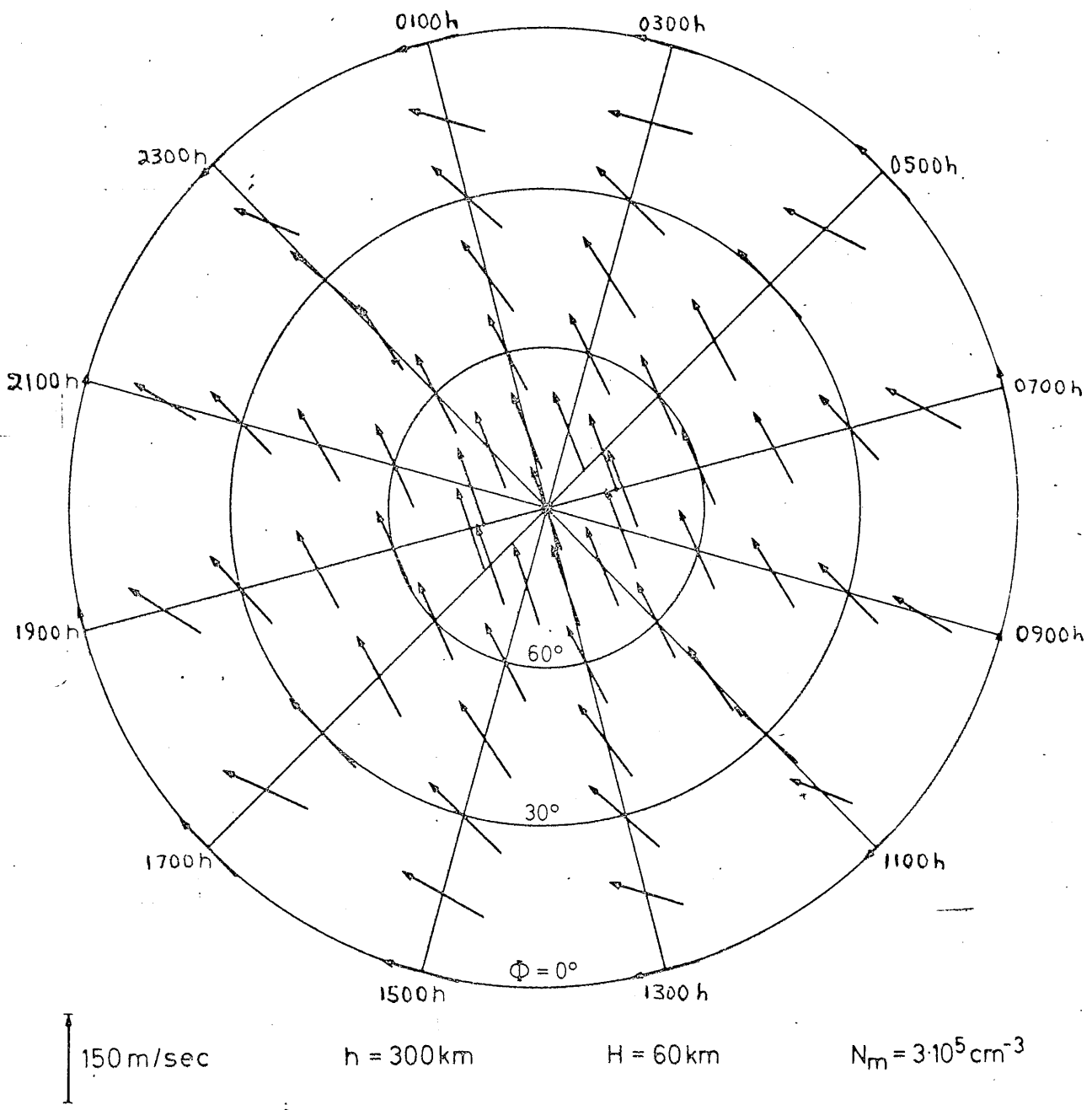
0100h
0300h
0500h
0700h
0900h
1100h
1300h
1500h
1700h
1900h
2300h
2100h
60°
30°
Φ = 0°
150 m/sec
h = 300 km
H = 60 km
$N_m = 3 \cdot 10^5 cm^{-3}$

will be as follows. If the wind drives ionization down the lines of force, the layer will move into "a region of greater loss rate" which would result in a decrease in the critical frequency and the height at which it occurs. If the wind results in an upward drift of ionization, the ionization will be driven into "a region of smaller loss rate" and thereby will cause the critical frequency and height of the F2 layer to be greater than what they would otherwise have been.

From this wind pattern and its postulated effect, King et al[84] suggested that the UT behaviour of f_0F2 in Antarctica might be explained as follows. Although the Antarctic stations which experience maximum f_0F2 values near 06 to 07 hours UT have widely varying geographic longitudes, they all lie on the same side of the magnetic pole (see Fig. 18) and should therefore have similar magnetic longitudes. This being so, winds blowing at about 06 to 07 hours UT will produce a maximum upward drift of ionization at all these stations at about this time and hence explain the UT phenomenon.

The wind theory has been taken a step further by Challinor and Eccles[20] who show that, because of the variation of magnetic dip and magnetic declination with longitude at geographic latitude 45° South, the magnitude of the vertical velocity at any given local time is dependent on the longitude. Further, for any given local time, the longitude at which the maximum upward or minimum downward drift occurs, is one for which the specified local time is equal to 06 UT. Eccles et al[40] obtained a similar result by solving the continuity equation for various longitudes at a latitude of $50^{\circ}S$ and suggest that this might explain the 07 UT effect observed at Antarctic stations.

These/...

Figure 18

Copy of King et al's[84] Figure 3 (showing Antarctic stations and directions of winds).

FIGURE 18

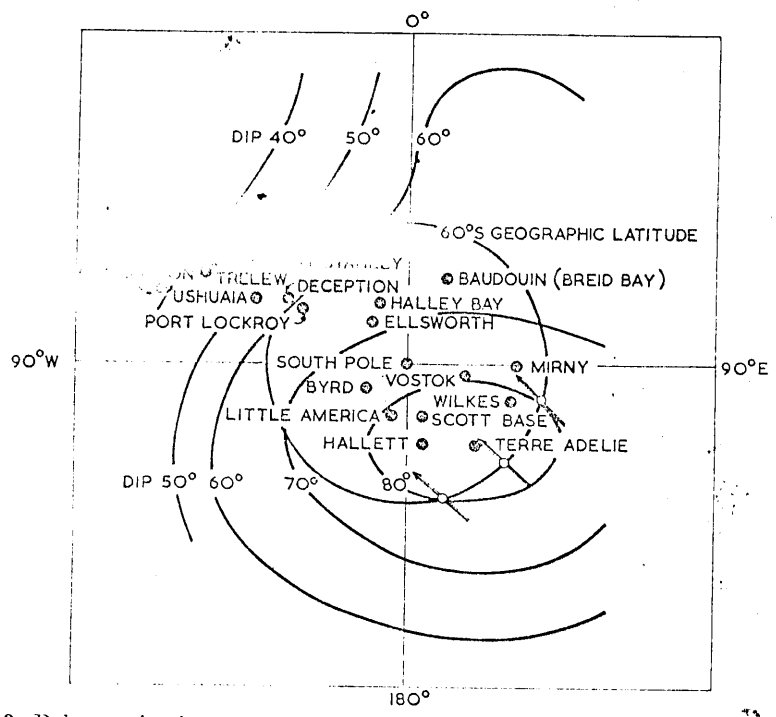

Fig. 3. Polar projection map showing the positions of the Antarctic and South American ionospheric observatories. (After PIGGOTT and SHAPLEY, 1962.) The vectors which have been included indicate the direction of the atmospheric winds calculated by KOHL and KING (1967) for three different localities on the 60° parallel at 06.00 U.T.

TABLE 11

The geographic co-ordinates, geomagnetic longitude and magnetic declination (Barish[5]) at the twelve Antarctic stations used in the analysis of section 2.2.

STATION	GEOGRAPHIC LATITUDE ^{o}S	GEOGRAPHIC LONGITUDE ^{o}E	GEOMAGNETIC LONGITUDE ^{o}E	MAGNETIC DECLINATION
Byrd	79.98	-120.02	336.0	68
Cape Hallett	72.32	170.22	278.2	104
Campbell Island	52.55	169.15	253.0	28
Halley Bay	75.52	-26.60	24.3	-1
Mawson	67.40	62.50	103.0	-61
Mirnyy	66.57	92.92	146.6	-80
Port Lockroy	65.25	-64.27	3.9	16
SANAE	70.30	-2.35	44.1	-20
Scott	77.85	166.75	294.4	+141
Terre Adelie	66.67	140.02	230.9	-74
Vostok	76.48	106.50	92.6	-115
Wilkes	66.20	110.35	179.0	-89

Figure 19

The monthly quiet-day average f_0F2 (in MHz) is plotted against time of day for the three stations Port Lockroy, Halley Bay and SANAE. Beneath the summer and winter f_0F2 curves for each station is plotted the vertical drift velocity for that station,(as calculated from Kohl and King's predicted horizontal neutral wind system for sunspot minimum conditons.)

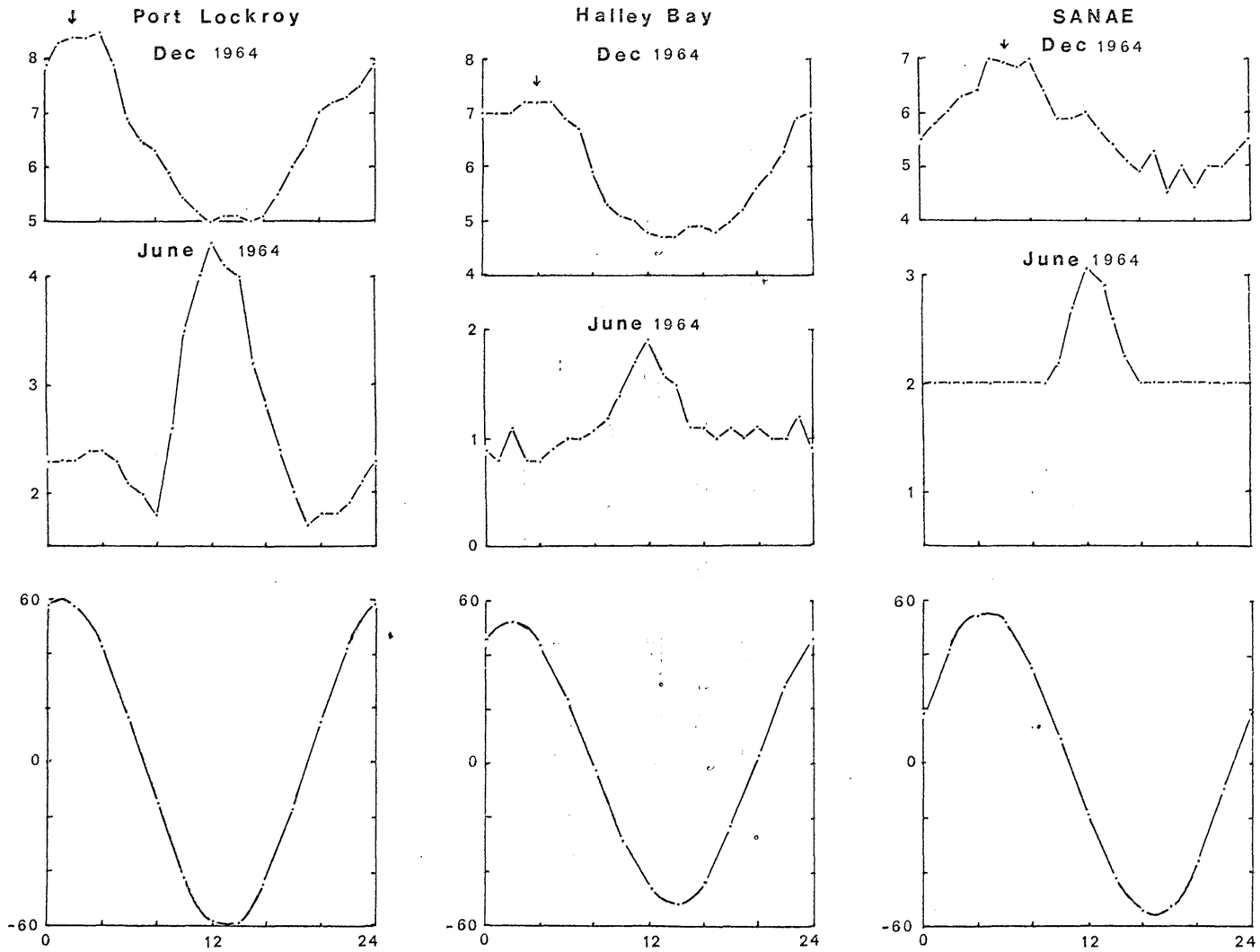
Port Lockroy
Dec 1964
June 1964
Halley Bay
Dec 1964
June 1964
SANAE
Dec 1964
June 1964
8
7
6
5
4
3
2
1
0
60
-60
0
12
24

Figure 20

The monthly quiet-day average f_0F2 (in MHz) is plotted against time of day for one summer and one winter month for Scott, Cape Hallett and Terre Adelie. Beneath the summer and winter f_0F2 curves for each station, the vertical drift velocity for that station is plotted.

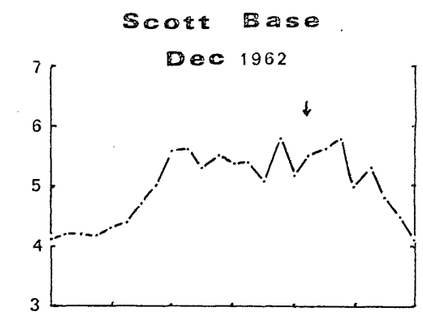
Scott Base
Dec 1962
7
6
5
4
3

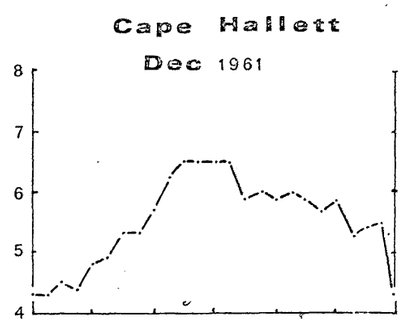
Cape Hallett
Dec 1961
8
7
6
5
4

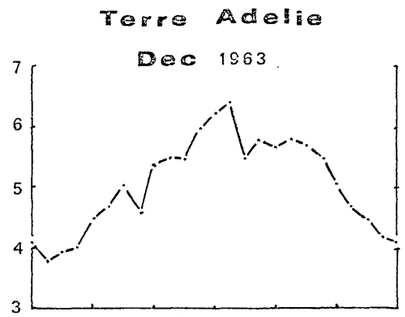
Terre Adelie
Dec 1963
7
6
5
4
3

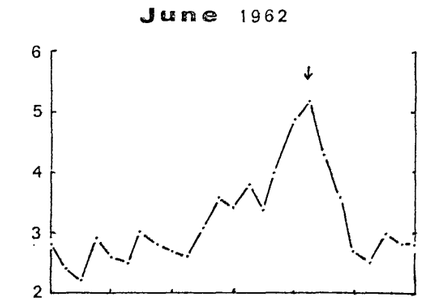
June 1962
6
5
4
3
2

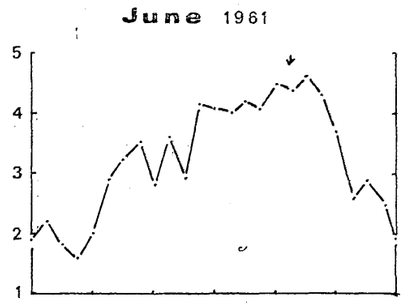
June 1961
5
4
3
2
1

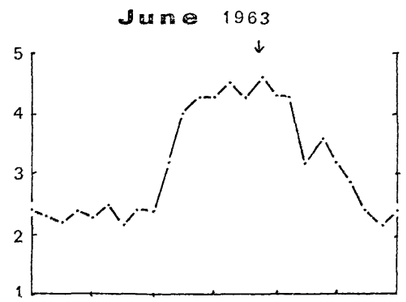
June 1963
5
4
3
2
1

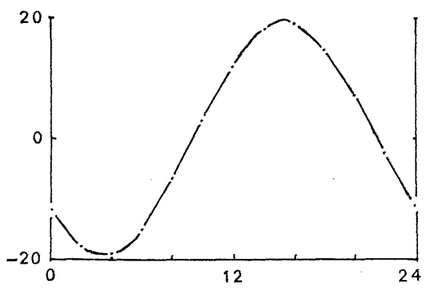
20
0
-20
0
12
24

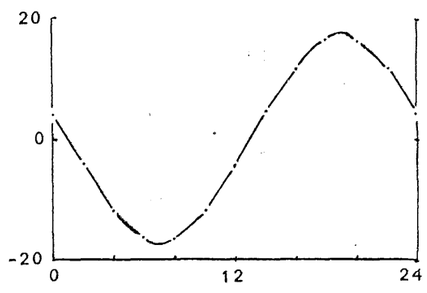
20
0
-20
0
12
24

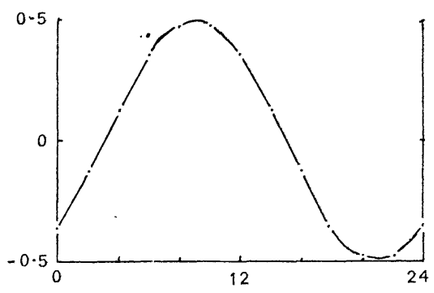
0·5
0
-0·5
0
12
24

Figure 21

The monthly quiet-day average f_oF2 (in MHz) is plotted against time of day for one summer and one winter month for Mirnyy, Vostok and Wilkes. Beneath the summer and winter curves for each station , the vertical drift velocity for that station is plotted.

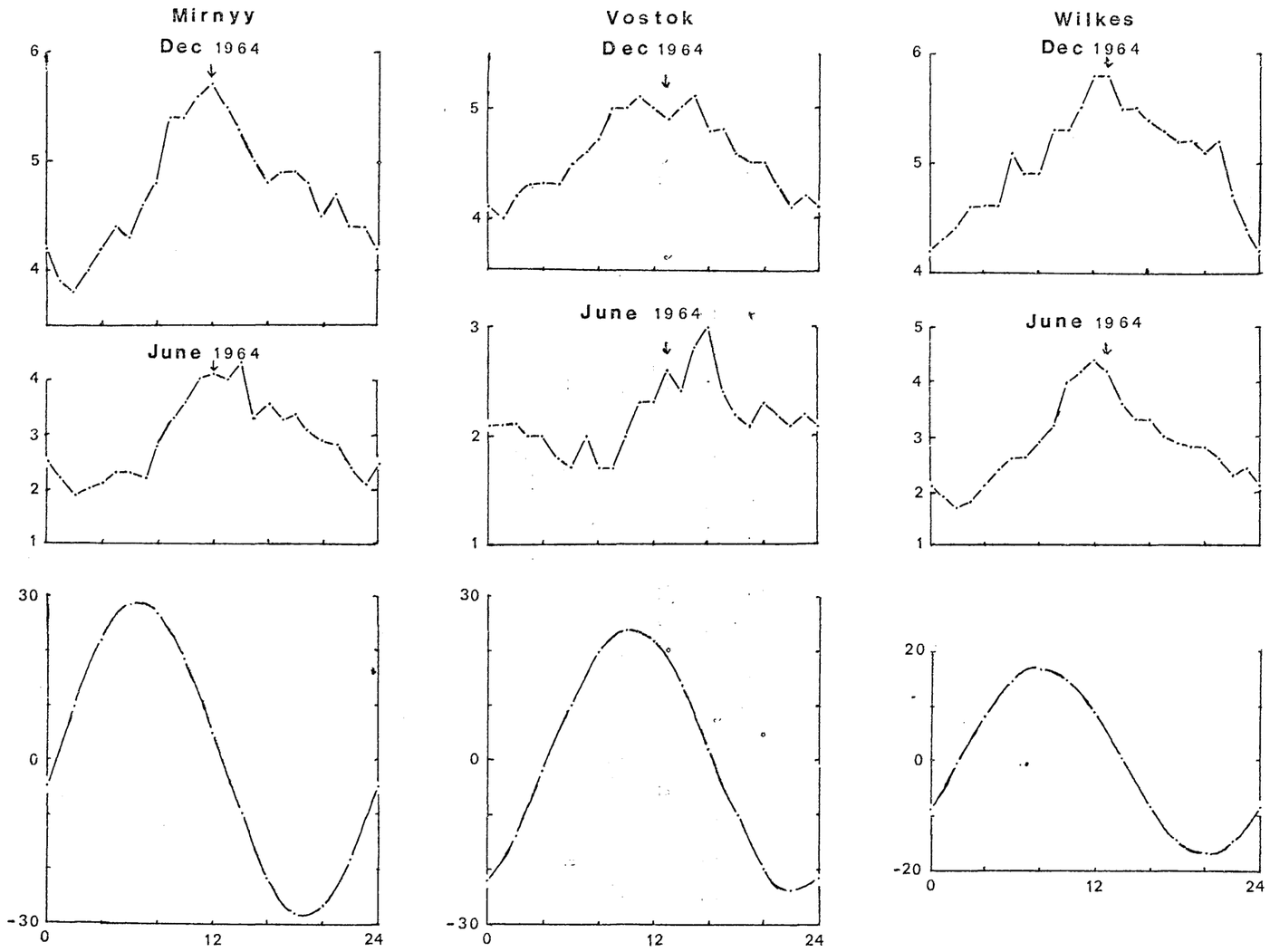
Mirnyy
Dec 1964
June 1964
Vostok
Dec 1964
June 1964
Wilkes
Dec 1964
June 1964
6
5
4
3
2
1
30
0
-30
20
-20
0
12
24

Figure 22

The monthly quiet-day average f_oF2 (in MHz) is plotted against time of day for one summer and one winter month for Byrd, Campbell Island and Mawson. Beneath the summer and winter curves for each station, the vertical drift velocity for that station is plotted.

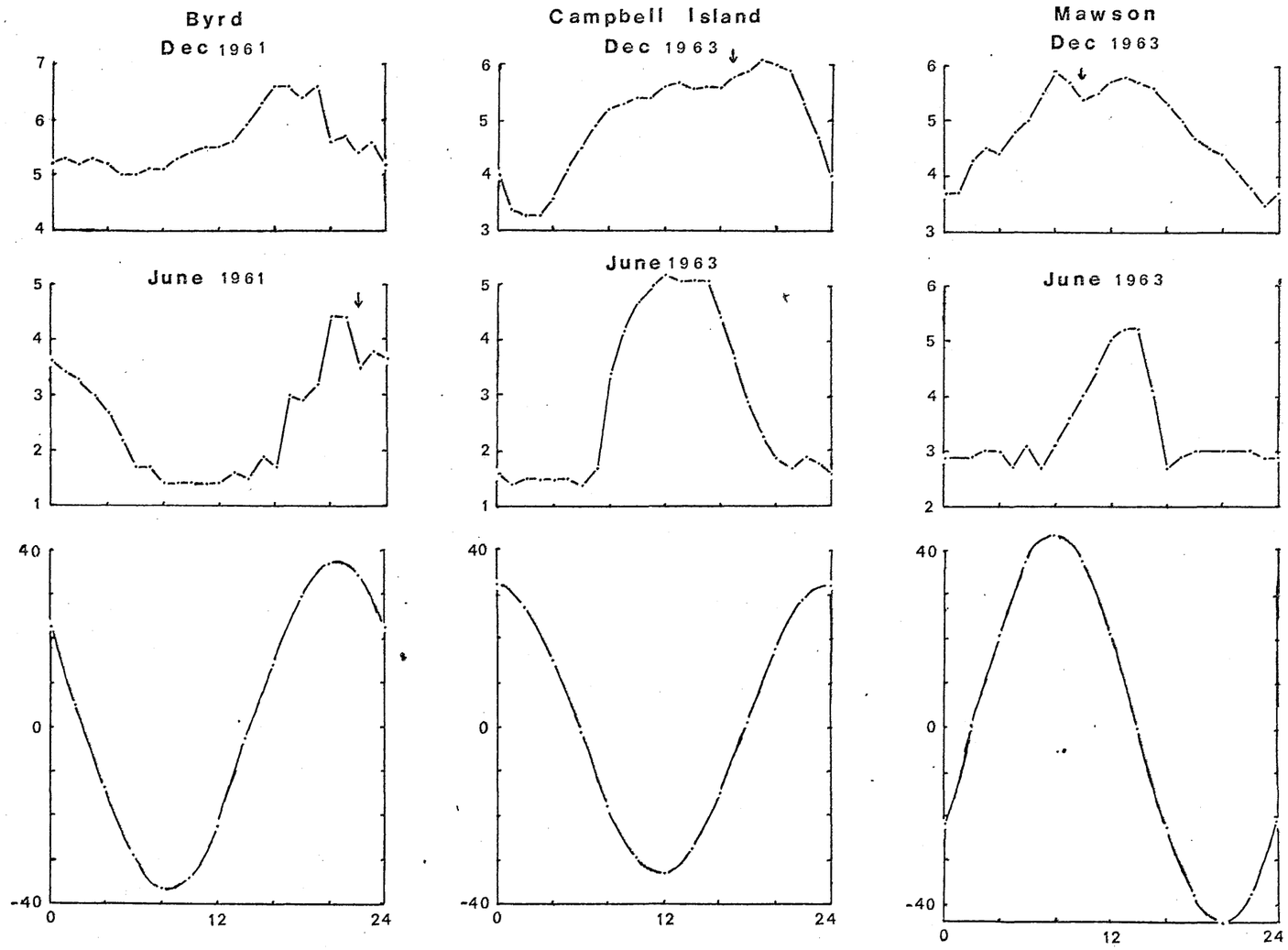
Byrd
Dec 1961
June 1961
Campbell Island
Dec 1963
June 1963
Mawson
Dec 1963
June 1963
40
0
-40
0
12
24

These analyses are all fairly general. However, they do not consider what happens at individual stations in Antarctica. A good test of the theory would, therefore, be to calculate the vertical drift of ionization caused by horizontal neutral winds at a number of Antarctic stations and compare this with the behaviour of f_oF2 at the same stations. This was done for twelve stations (see Table 11) using the horizontal neutral wind velocities calculated by Kohl and King[92] for equinoctial conditions around sunspot minimum. These vertical drift velocities have been plotted together with the mean monthly values of f_oF2 for December and June for each station in Figs. 19 to 22. Also shown is the local time corresponding to 06 hours UT for each station. These figures show a very good correlation between the time of maximum upward vertical drift and the maximum of f_oF2 observed at about 06 hours UT at most stations. At Port Lockroy, Halley Bay, SANAE and Mawson the early morning maximum which occurs at about 06-07 UT in summer, may be accounted for by winds and at Scott, Cape Hallett and Byrd the 06 UT maximum in winter occurs at the same time as the maximum upward vertical drift caused by winds. At Mirnyy, Vostok and Wilkes, 06 UT coincides approximately with local noon and it is difficult to isolate wind effects from those due to the variation in solar zenith angle. At Terre Adelie the magnitude of the vertical drift is too small to have much effect on f_oF2 while at Campbell Island the maximum at about 06-08 UT during summer may be due to a midday bite-out effect.

At this stage one might note that the vertical drift velocities shown are those calculated for equinoctial

conditions/...

Figure 23

Global view of the exospheric temperature distribution for

(a) southern hemisphere summer

(b) southern hemisphere winter

and (c) equinox conditions.

The dotted line indicates the daily path of a high-latitude station in the southern hemisphere. Solid lines represent isotherms.

(a)

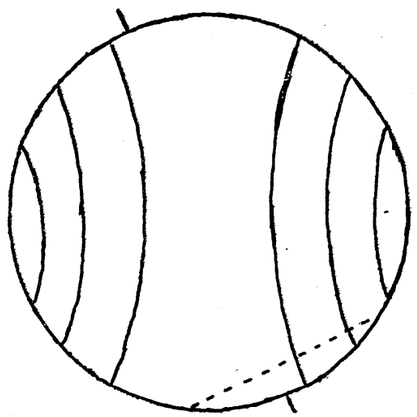

SOUTHERN HEMISPHERE
SUMMER

(b)

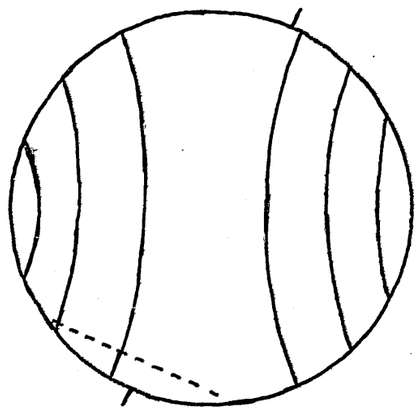

SOUTHERN HEMISPHERE
WINTER

(c)

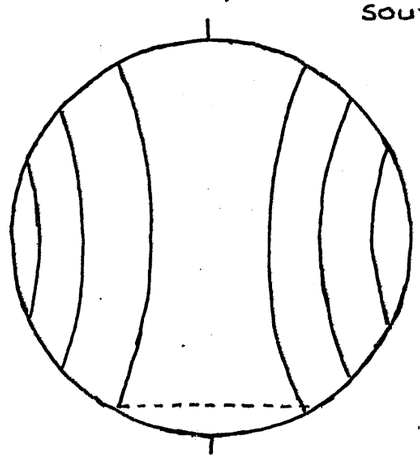

EQUINOX

conditions, while the values of f_0F2 are for summer and winter. However, extrapolating Kohl and King's[92] calculations, the wind velocities for summer and winter should be very similar to those for the equinoxes. This is due to the fact that the most important factor affecting wind velocity is the pressure gradient, and Kohl and King assume this to be directly proportional to the temperature gradient. Viewed globally (Fig. 23), the temperature gradients do not change very much from summer to winter - the individual stations merely cross different isotherms during different seasons. Thus since the magnitude of the velocity is much the same between latitudes 30^o and 90^o south (Fig. 17), there is very little change in magnitude with season at any station. The change in phase of the wind velocity with season at any station (i.e. the change in the time of day at which winds blow in the direction of the magnetic field) is determined by the change in geographic longitude of the sub-solar point at a particular geomagnetic longitude. At all stations except Terre Adelie the change in this geographic longitude between summer and winter is less than 15^o - so that the variation in time of day of maximum upward vertical drift at these stations during the year is less than one hour. At Terre Adelie the variation amounts to several hours but at this station the magnetic inclination is close to 90^o and the component of the horizontal neutral velocity along the field line is negligible.

The comparison between vertical drift velocities and F2 critical frequencies is also illustrated in Figs. 24 and 25. In Fig. 24 the time of day of maximum f_0F2 in winter is plotted against geographic latitude for several stations in the Ross Sea area. In the upper diagram time is measured in LST while in the lower one it is measured

in/...

Figure 24

The time of day of maximum f_oF2 in winter for several stations in the Ross Sea area is plotted against geographic latitude. To the right of this is plotted the time of day of maximum upward vertical drift for the same stations. (Upper diagrams show time in LST, lower diagrams give time in UT.)

ROSS SEA AREA WINTER

LT OF MAXIMUM f_0F2

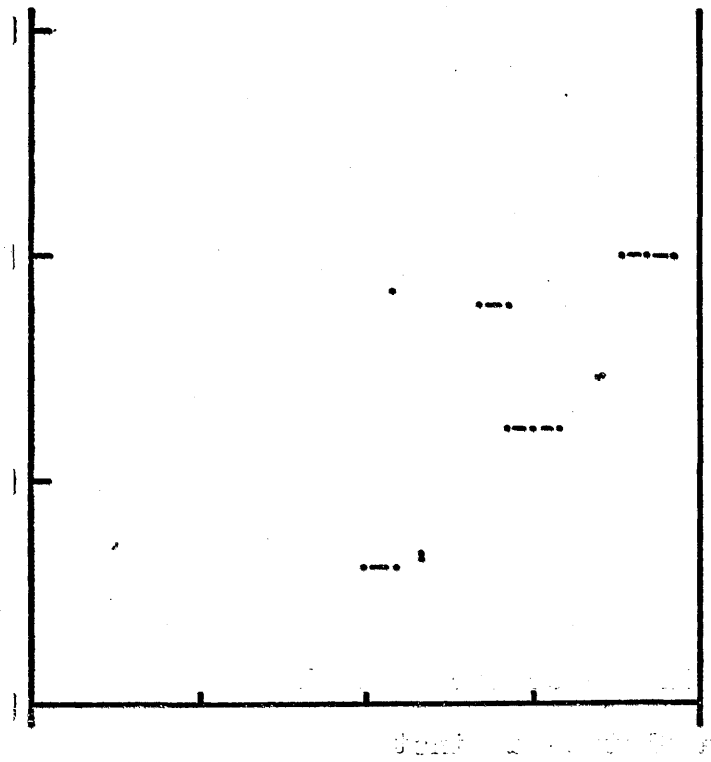

LT OF MAXIMUM VERTICAL DRIFT

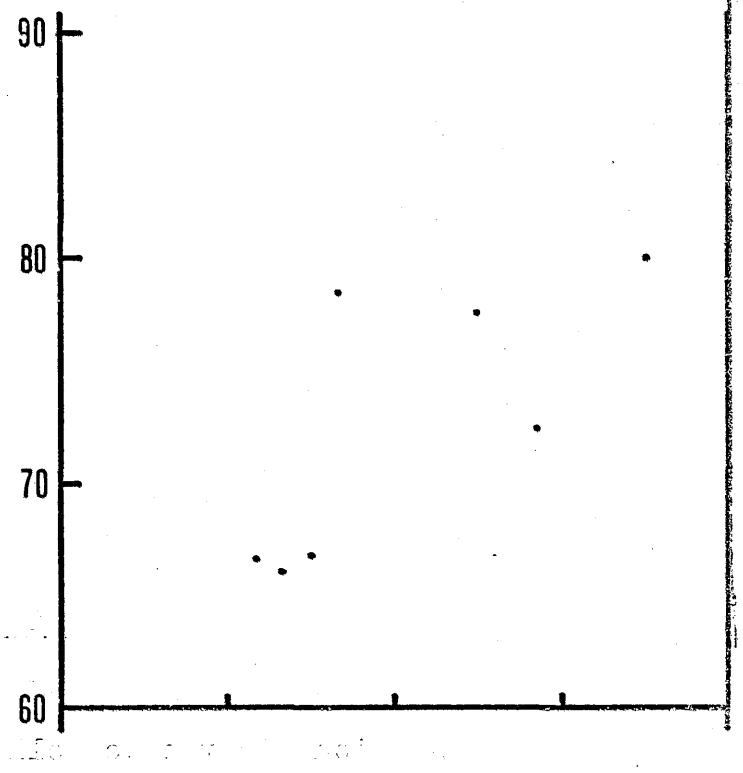

UT OF MAXIMUM f_0F2

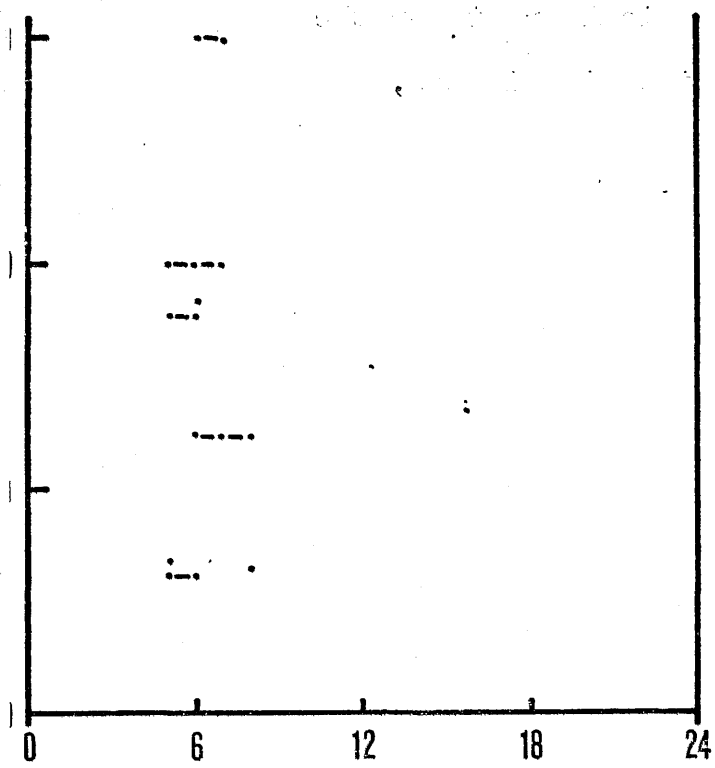

UT OF MAXIMUM VERTICAL DRIFT

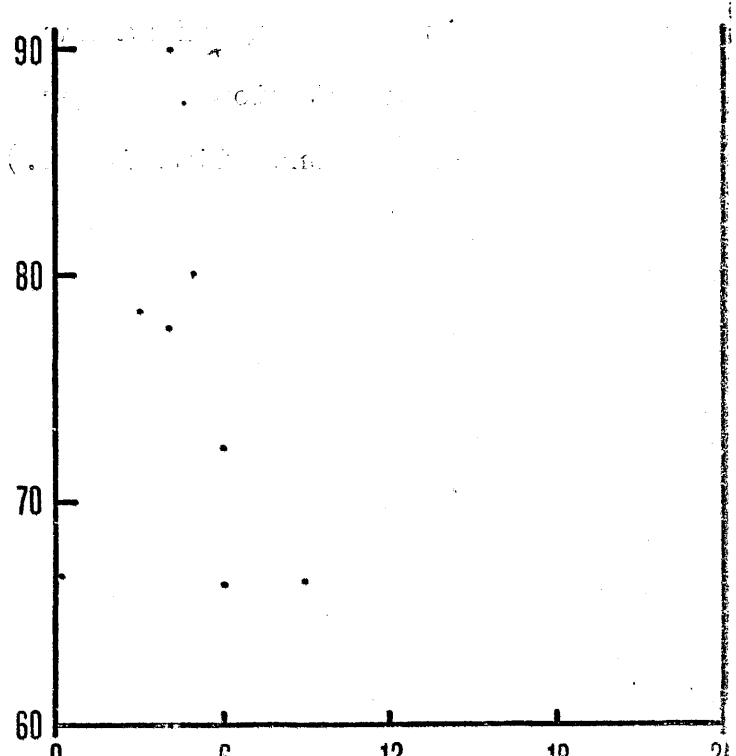

Figure 25

The time of day of maximum f_oF2 in summer for several stations in the Weddell Sea area plotted against geographic latitude. The right-hand diagram shows the time of day of maximum upward vertical drift for the same stations. (Upper diagrams give time in LST, lower ones time in UT.)

WEDDELL SEA SUMMER

LT OF MAXIMUM f_0F2

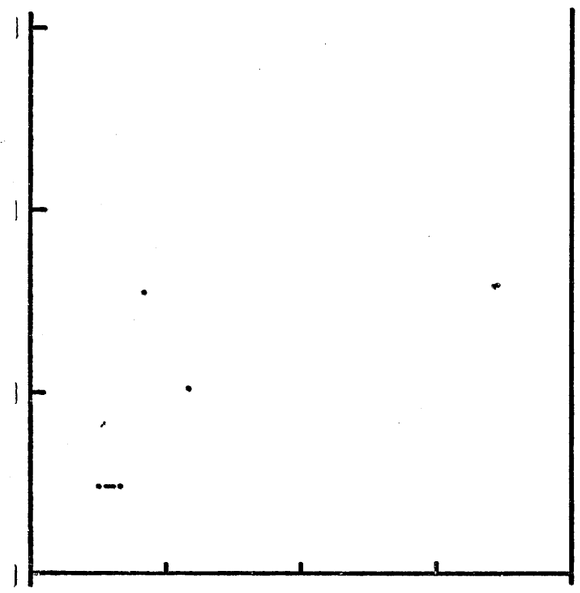

LT OF MAXIMUM VERTICAL DRIFT

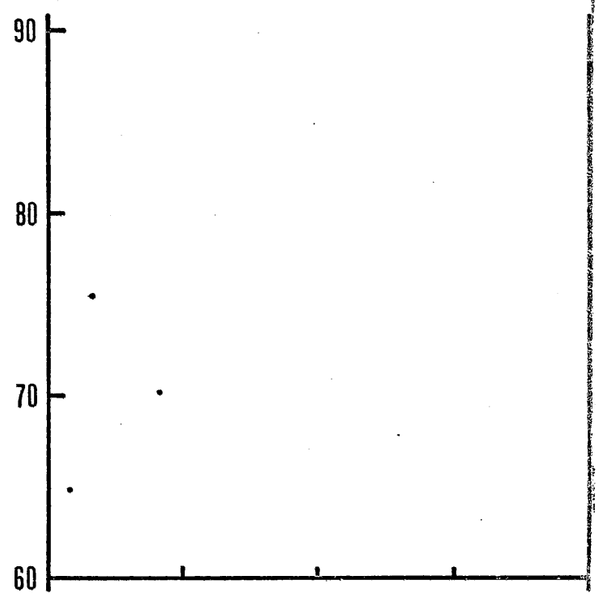

UT OF MAXIMUM f_0F2

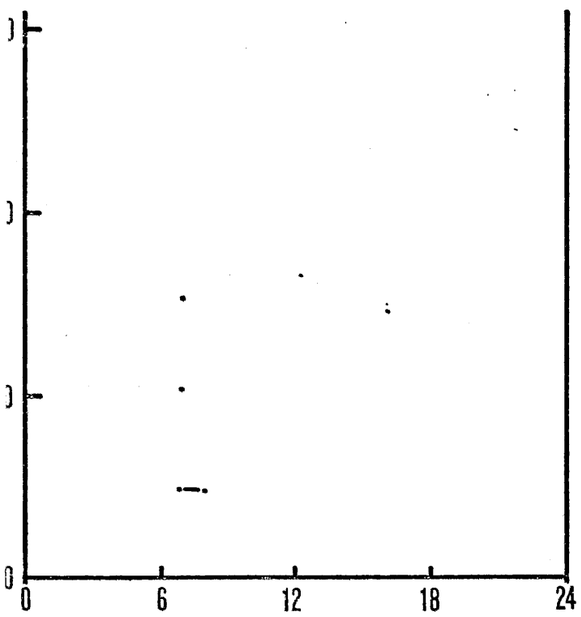

UT OF MAXIMUM VERTICAL DRIFT

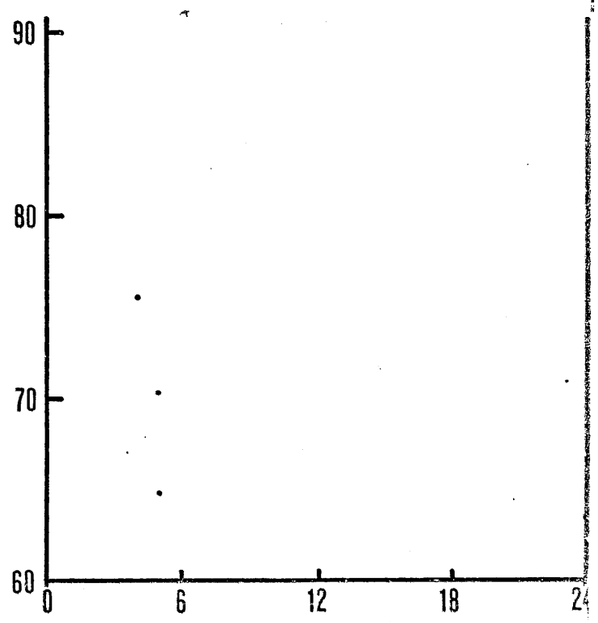

in UT. To the right of these are diagrams showing the times of day of maximum upward vertical drift (due to horizontal neutral winds) at these stations, plotted against geographic latitude. Once again the upper diagram gives time in LST, the lower one gives time in UT. Fig. 25 contains a similar analysis of data from stations in the Weddell Sea area during summer. Both figures show that the time of maximum upward vertical drift occurs at approximately 04-06 UT and this may perhaps account for the 06-07 UT maximum in f_0F2. The two points on the "UT of maximum vertical drift" graph for the Ross Sea area which show large deviations from the 04-06 UT region are those for Terre Adelie (maximum upward vertical drift at 00 UT) and for Mirnyy (maximum at 09 UT). However, in the case of Terre Adelie the effect of winds is negligible.

After the completion of this analysis a paper was published by King et al[82] in which the continuity equation and the equation of motion of the neutral atmosphere are solved simultaneously for several Antarctic stations. The results which they obtained are similar to those enunciated here.

2.3 DRAWBACKS OF KING'S MODEL

There are three aspects of the Antarctic f_0F2 behaviour which are not accounted for by this model. They are:

(i) in the Weddell Sea area stations experience a large well-defined maximum in f_0F2 at about 06-07 hours UT during summer, but during winter there is no obvious maximum at this time. Stations in the Ross Sea area, however, observe a well-defined maximum in f_0F2 at about 06-07 hours UT during winter, while during summer there

is/...

is no definite maximum at this time.

The presence of a UT maximum at stations in the Weddell Sea area during summer may be explained by the fact that there is sufficient ionization present (due to incoming solar EUV) at 06 UT for the vertical drift to drive upwards and hence cause a noticeable increase in f_0F2. During winter there is very little ionization present at 06 UT at stations in the Weddell Sea area and this is already concentrated at fairly large heights so that the effect of an upward vertical drift is not noticeable.

However, the presence of a UT maximum during winter and not during summer at stations in the Ross Sea area conflicts with the above reasoning and no explanation for this has yet been found.

(ii) the transition period from LT-controlled behaviour to UT-controlled behaviour and vice versa is often very sharp (Piggott and Shapley[114]) and occurs at different times for different stations. However, the transition period for any particular station occurs at approximately the same time each year (Tables 8 and 9).

Bullen[17] found that radical changes in atmospheric circulation over Antarctica take place abruptly during October. This suggests a possible way in which the wind theory could account for the rapid transition between LT and UT control of f_0F2 at Weddell Sea stations. However, no radical circulatory changes have been observed during February-March, when the reverse transition (UT control to LT control) takes place. Similarly there is a rapid transition from LT to UT control of f_0F2 at Byrd during May and the reverse transition occurs at about the beginning of August. Once again radical changes in

atmospheric/...

atmospheric circulation are not observed at these times either. Thus the radical changes in circulation observed in October do not account generally for the rapid transition between LT and UT-controlled behaviour of f_oF2.

(iii) winds and production due to solar EUV are not sufficient to account for the magnitudes of the observed critical frequencies in winter. King et al[82] have stated that in solving the continuity equation and the equation of motion of the neutral atmosphere for winter conditions, it is necessary to include an additional source of ionization , such as particle precipitation, in order to explain the observed magnitudes of f_oF2.

2.4 OTHER THEORETICAL WIND MODELS

Before leaving the subject of theoretically determined neutral winds, let us consider the wind patterns which have been predicted theoretically by several other workers. Fig. 26 shows the diurnal variation of the North-South component of horizontal neutral wind velocity as calculated by Stubbe[146], Geisler[183] and Bailey et al[4] for mid-latitude equinoctial conditions around sunspot minimum. In Fig. 27 the component of the horizontal neutral wind velocity along the magnetic field as calculated by Kohl and King[92] and Torr[162] for two stations with similar magnetic inclinations at sunspot minimum are shown. The discrepancy in the magnitude of velocity predicted by the different workers is striking.

Besides this discrepancy in magnitude, there is also a difference in opinion as to the effect which the vertical drift set up by this horizontal wind will have on the F2 peak. Kohl and King's suggestion that an upward vertical drift causes an increase in f_oF2 while a downward drift decreases it, has already been mentioned. From the

results/...

Figure 26

The North-South component of horizontal neutral wind velocity as predicted by several workers for mid-latitude equinoctial conditions around sunspot minimum plotted against time. (Positive values represent winds blowing towards the Equator.)

.-.-.-.-.-. Stubbe[146]

\- - - - - - Geisler[183]

..... Bailey et al[4]. Curve A.

_____ Bailey et al[4], Curve F.

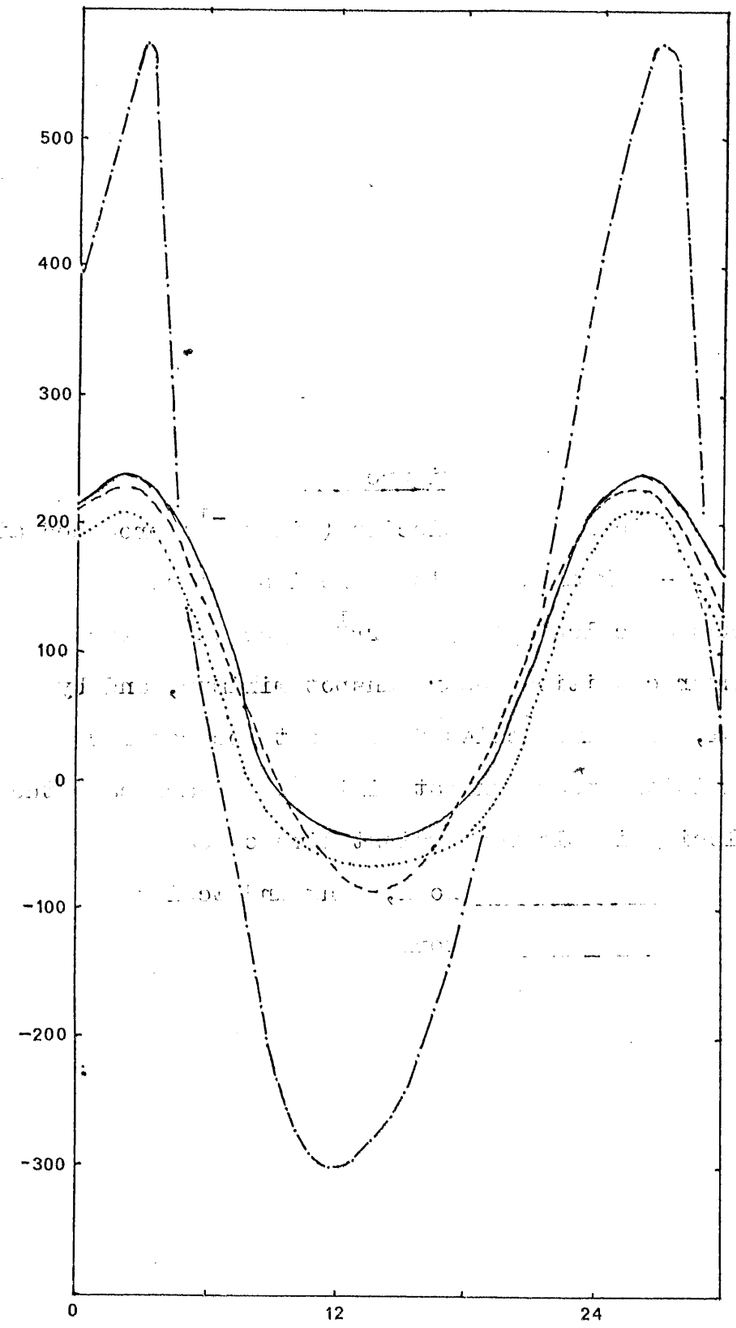
500
400
300
200
100
0
-100
-200
-300
0
12
24

Figure 27

The vertical drift velocity (in ms^{-1}) produced at the F2-peak as a result of horizontal neutral winds as calculated by Torr[162] for SANAE for summer conditions near sunspot minimum, and by Kohl, King and Eccles[93] for Port Lockroy for conditions near sunspot minimum. In each case the velocity is plotted against time of day.

_____ Kohl, King and Eccles

\- - - - - - Torr

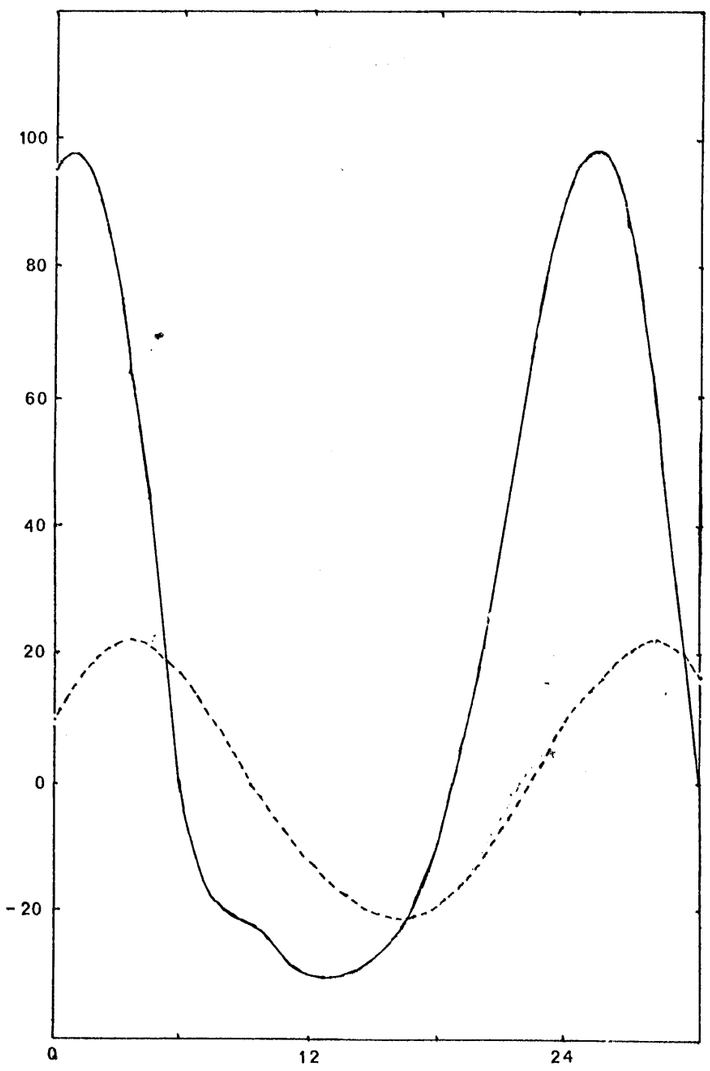
100
80
60
40
20
0
-20
0
12
24

results of Bailey et al[4] who obtain numerical solutions of the continuity equation of the ionosphere, the effect of a downward drift velocity about midday is to decrease the value of N_mF2 in agreement with the results of Kohl and King. However, their results also show (cases A and C in their paper) that the value of N_mF2 at night decreases when an upward drift velocity is included - which does not agree with the suggestions of Kohl and King.

One can deduce from Torr and Torr's[164] results (Figs. 38 and 40 in their report) for SANAE that the inclusion of a downward drift of ionization around midday gives rise to a very slight increase in N_mF2 and an increase in the height at which it occurs. A similar but more noticeable increase can be seen in the early hours of the morning when an upward drift of ionization is included.

Rüster[131], on the other hand, obtains results from a solution of the continuity equation which agree with Kohl and King's ideas.

The results of these four groups of workers are summarized in Table 12.

TABLE 12. The effect of the vertical drift of ionization due to horizontal winds on N_mF2 as predicted by several workers.

WORKER	EFFECT CALCULATED FOR	EFFECT ON N_mF2 CAUSED BY DOWNWARD DRIFT	UPWARD DRIFT
Kohl et al[92]	Port Lockroy, summer	Decr. in N_mF2	Incr. in N_mF2
Bailey et al[4]	Latitude 45°, equinox	Decr. in N_mF2	Decr. in N_mF2
Torr[162]	SANAE, summer	Incr. in N_mF2	Incr. in N_mF2
Rüster[131]	Lindau, equinox	Decr. in N_mF2	Incr. in N_mF2

This/...

This shows that there is no general agreement about the effect of an upward or downward vertical drift and that its effect may depend on factors such as latitude, season and time of day. From Figs. 4, 5 and 22 of Stubbe's[146] paper on solving the continuity equation for equinoctial conditions at Lindau (51.6°N), N_mF2 can be seen to drop steadily between 19 and 04 hours LMT while the upward vertical drift (caused by horizontal winds) increases considerably. On the other hand h_mF2 first increases (19 to 01 hours LMT) and then decreases (01 to 04 hours LMT). This is further indication that the effect of an upward drift velocity is not as simple as Kohl and King suggest; and since their model depends partly on the idea that an upward drift velocity raises the level of the layer and causes an increase in f_oF2, while a downward drift decreases the value of f_oF2, their argument may be weakened. This question is investigated further in the next section (Chapter 6) which is concerned with solving the continuity equation of the ionosphere under various conditions.

2.5 ANALYSIS OF WIND DATA AROUND SUNSPOT MAXIMUM

Bellchambers et al[11] conducted an analysis of the drift velocities measured at Halley Bay (deduced from the spaced receiver method - using three closely spaced antennas) during the IGY. They divided their analysis into E-W(v_x) and N-S(v_y) components of drift velocity in the E and F-regions. However, since the declination of the magnetic field at Halley Bay is so small (1.2° W of N), the East-West component of horizontal wind velocity has very little effect on the critical frequency and, for the purpose of this investigation, can be neglected.

We/...

We shall consider, therefore, the results which they obtained for the North-South component of drift velocity in the F-region. The average monthly values of v_y for the year 1958 are shown in Fig. 28. This is a copy of Fig. 67 in the paper by Bellchambers et al. This figure shows that the average value of this component is positive (i.e. northwards) during March, April and May while for the remainder of the year (except for July when it is approximately zero) the average value is negative (southwards). This would suggest that, if winds did have any considerable effect on the ionosphere, the behaviour during the aforementioned three months (when the average v_y is positive) might be extreme and noticeably distinct from the behaviour during the rest of the year. However, as is well known, it is the behaviour in November, December and January which is extreme and distinct from the rest of the year.

Bellchambers et al have also plotted the average hourly values of the N-S component for the four seasons of the year (see Fig. 29). From this figure the average value of the N-S component in summer is seen to be approximately zero between 19 hours UT (17 hours LMT) and 06 hours UT (04 hours LMT). During this period the average value of f_oF2 increases from about 6.8 MHz to about 8.0 MHz. Thus since production due to solar EUV is a minimum at this time, if the N-S component of the wind velocity is zero during this period, it cannot be responsible for the early morning maximum in f_oF2 at Halley Bay.

Table 13 (Table 67 of Bellchambers et al) contains a summary of the average N-S component of F-region drift velocities for all hours of the day for every month during the IGY. Extracts from this table are compared with average values of f_oF2 for the same period in Table 14.

Two/...

Figure 28

Copy of Figure 67 from Bellchambers et al[11]. This shows the variation of the monthly average drift velocities in the F-region during 1958.

FIGURE 28

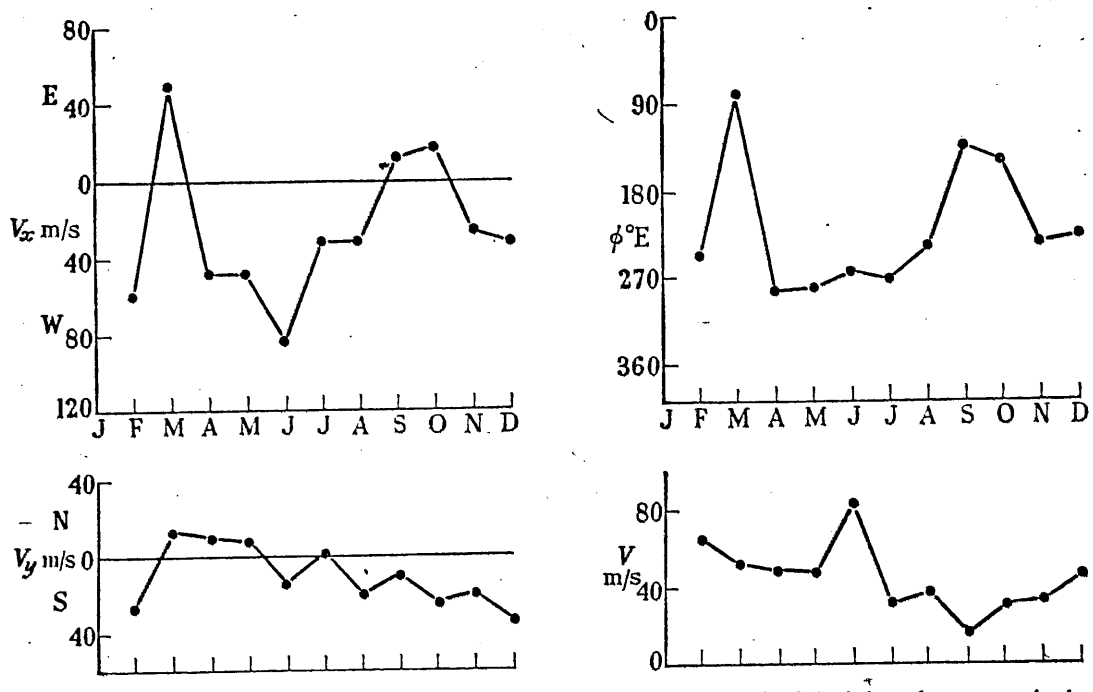

FIGURE 67. Variation of the *F* region drift velocities during 1958. The method of deriving the curves is described in the text.

Figure 29

Average hourly values of V_x, V_y, V and ϕ for the four seasons of the year, taken from Bellchambers et al[11].

FIGURE 29

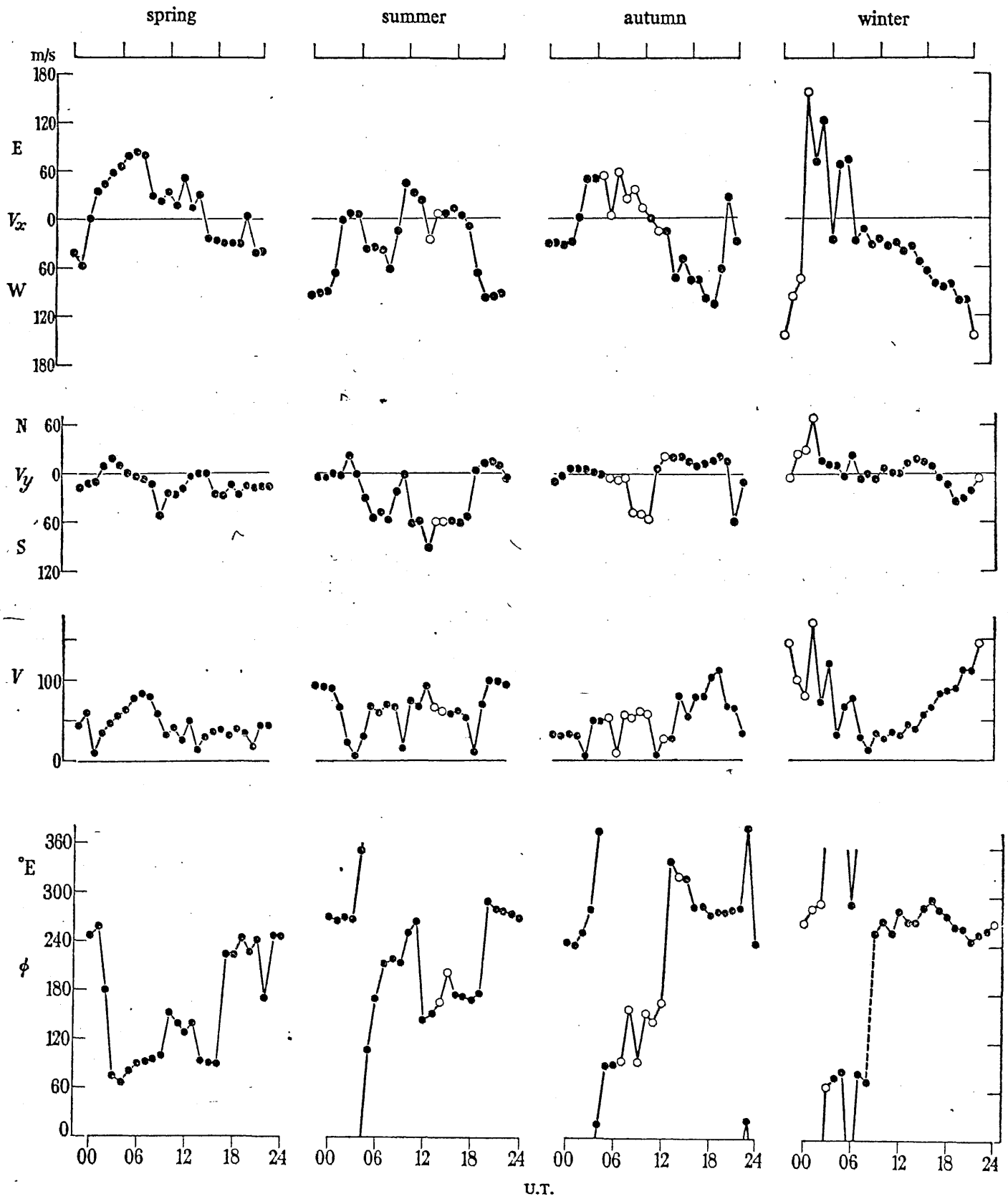

FIGURE 71. Diurnal variations of the *F* region drift velocities for each of the four seasons of 1958. The count for each hour is denoted: ○, 6 to 9; ●, ⩾ 10.

Table 13. Hourly values of the N-S component of drift velocity, v_y, at Halley Bay during the IGY, taken from Bellchambers et al[11].

TABLE 67. *F* REGION DRIFT VELOCITIES: HOURLY MEDIAN VALUES OF THE NORTH-SOUTH COMPONENT, V_y, IN UNITS OF 1 M/S

hour U.T.	00	01	02	03	04	05	06	07	08	09	10	11	12	13	14	15	16	17	18	19	20	21	22	23
month																								
1957																								
June	..	..	..	..	..	..	..	..	..	..	..	−74	−37	−180	−9	+2	−8	..	+33	..	..	..	..	..
July	..	..	..	..	..	..	..	..	..	..	..	−119	+69	−112	−58	−41	−25	+67	−5	−24	−84	..	..	..
Aug.	..	..	..	..	..	0	..	..	+41	..	+27	−10	..	..	+23	+40	−113	..	+50	−33	..	−18	+3	−125
Sept.	−32	+19	−26	+1	+46	+50	+9	0	−42	..	..	..	..	..	..	..	..	..	..	..	−19	..	..	−10
Oct.	..	..	..	..	..	+27	..	..	..	..	..	..	..	..	..	..	..	..	..	..	..	..	..	..
Nov.	..	..	..	..	..	..	..	..	..	..	..	..	..	..	..	..	..	..	..	..	..	..	..	..
Dec.	..	..	..	..	..	..	..	..	..	..	..	..	..	..	..	..	..	..	..	..	..	..	..	..
1958																								
Jan.	..	..	..	..	..	..	..	..	..	..	..	..	..	..	..	..	..	..	..	..	..	..	..	..
Feb.	−80	+116	−28	+6	+6	−30	−1	−34	..	..	..	..	−1	−89	..	−213	−56	..	−25	+66	−43	+31	+22	−48
March	−40	−10	+59	+6	+29	+150	..	+119	+122	−48	+35	..	..	..	−50	..	..	−205	−43	0	+20	+21	+27	+178
April	..	..	..	..	..	..	..	..	−8	−5	−18	−62	−70	+21	+58	+218	+44	+21	+5	+16	+34	−49	..	..
May	..	..	..	..	+141	−2	+16	..	−10	+62	−186	+53	+22	+64	−4	+30	+34	+51	−2	+8	−3	−10	−4	−36
June	−5	+35	−18	−38	+254	−105	..	..	−13	..	−28	+68	−43	−17	−46	−80	+43	+20	−10	0	−74	+38	−8	−77
July	+12	..	+47	+53	+48	−16	0	+64	−4	+13	+58	−8	−30	+78	−50	+34	−45	+18	+14	+1	−71	−78	−78	−30
Aug.	−111	−17	..	−73	+32	+60	−198	+50	+6	0	−59	−54	+10	−22	−2	+100	−20	−38	−16	−50	+22	−123	−24	−54
Sept.	−17	−9	+22	−7	+21	+18	−3	+14	−19	−56	−52	−61	−26	−20	−27	+46	−85	+77	−31	−2	+30	−40	−5	−11
Oct.	−30	−80	−23	−34	+43	+6	+10	−420	+22	..	+28	−96	−24	−40	−20	+66	−158	−12	−47	−48	−59	−39	−2	+12
Nov.	−53	+8	−5	+22	−52	−8	+6	..	−56	−10	−104	−348	+61	−62	−90	0	+128	−34	−45	−185	+11	..	−43	−12
Dec.	−7	+17	+12	−11	+59	+52	−62	−43	−89	−22	..	−34	+60	−116	−59	−101	−52	−91	−63	−61	+14	−106	+1	+40

TABLE 14. A comparison between the monthly average N-S component of drift velocity for particular hours of day measured at Halley Bay during the IGY and average values of f_oF2 for the same periods.

MONTH	PERIOD	HOURLY AVERAGES OF N-S COMPONENT OF WIND VELOCITY IN m/s					CORRESPONDING HOURLY AVERAGES OF f_oF2 IN MHz				
Feb. 58	00-04	-80	+116	-28	+6	+6	8.2	6.7	6.7	7.4	6.5
	18-21	-25	+66	-43	+31		7.3	7.1	7.3	8.1	
Mar. 58	07-10	+119	+122	-48	+35		5.9	6.2	6.2	6.4	
	19-23	0	+20	+21	+27	+178	7.9	6.6	5.7	4.6	4.6
Apr. 58	11-15	-62	-70	+21	+58	+218	8.4	9.3	10.6	11.0	11.2
May 58	04-06	+141	-2	+16			5.7	5.7	4.6		
	08-12	-10	+62	-186	+53	+22	4.6	5.2	6.2	7.4	8.8
June 58	01-05	+35	-18	-38	+254	-105	2.1	2.7	2.6	3.7	4.0
	10-13	-28	+68	-43	-17		4.1	4.8	5.9	5.8	
	14-18	-46	-80	+43	+20	-10	5.3	4.4	3.8	3.0	2.3
	19-23	0	-74	+38	-8	-77	1.9	1.7	1.9	2.0	2.1
July 58	10-14	+58	-8	-30	+78	-50	4.3	5.1	6.0	6.1	6.0
	14-18	-50	+34	-45	+18	+14	6.0	5.0	4.4	3.5	2.7
Aug. 58	03-07	-73	+32	+60	-198	+50	4.0	4.3	4.1	4.1	4.5
	13-17	-22	-2	+100	-20	-38	9.4	8.9	8.5	7.5	6.6
Sept. 58	14-18	-27	+46	-85	+77	-31	11.3	11.3	11.4	10.8	9.9
Oct. 58	04-08	+43	+6	+10	-420	+22	7.9	7.6	7.9	7.5	7.6
	13-17	-40	-20	+66	-158	-12	9.2	9.5	9.6	9.8	9.9
Nov. 58	09-13	-10	-104	-348	+61	-62	8.6	8.0	7.8	7.5	7.6
	14-18	-90	0	+128	-34	-45	7.3	7.2	7.5	7.6	7.9
Dec. 58	11-15	-34	+60	-116	-59	-101	6.6	6.6	6.6	6.6	6.6

The third column of this table (headed "HOURLY AVERAGES ...") contains the monthly average N-S component of wind velocity for each hour of the period specified (second column). The final column contains the monthly average f_oF2 for the same hours.

Two conclusions which may be drawn from these two tables are:

(a) that large hour-to-hour fluctuations in the average measured values of wind velocity (including fluctuations in which the N-S component of velocity changes direction) do not seem to affect the corresponding hourly values of f_0F2, and

(b) that month-to-month variations in the average N-S component of wind velocity at a particular hour of day are too large to reflect a consistent behaviour pattern. For example, compare the average velocities between 10 and 12 LMT for May with those for June and Jule - there is no apparent consistency at all between the values at times 10, 11 and 12 LMT for these three winter months.

The data from Table 14 are portrayed in a different form in Fig. 30(a). For this figure the mean of the hourly average N-S components of wind velocity for each 3-4 hour period shown in Table 14, was calculated. The difference between each individual hourly average and the mean for the period, Δv, was then plotted against Δf_0F2, the difference between each individual hourly average of f_0F2 and the mean value of f_0F2 for the corresponding 3 or 4 hour period. This figure shows that there is no obvious relation between observed f_0F2 variations and changes in observed wind velocities.

In general, therefore, this analysis would seem to indicate that, at least during solar maximum, the wind velocities at Halley Bay do not account for the early morning maximum of f_0F2 in summer.

2.6 STUDY/...

Figure 30(a)

Δv (the difference between the value of v for a particular hour and the mean for the period) plotted against Δf_0F2 (the difference between the value of f_0F2 for the same hour and the mean for the period) - see text.

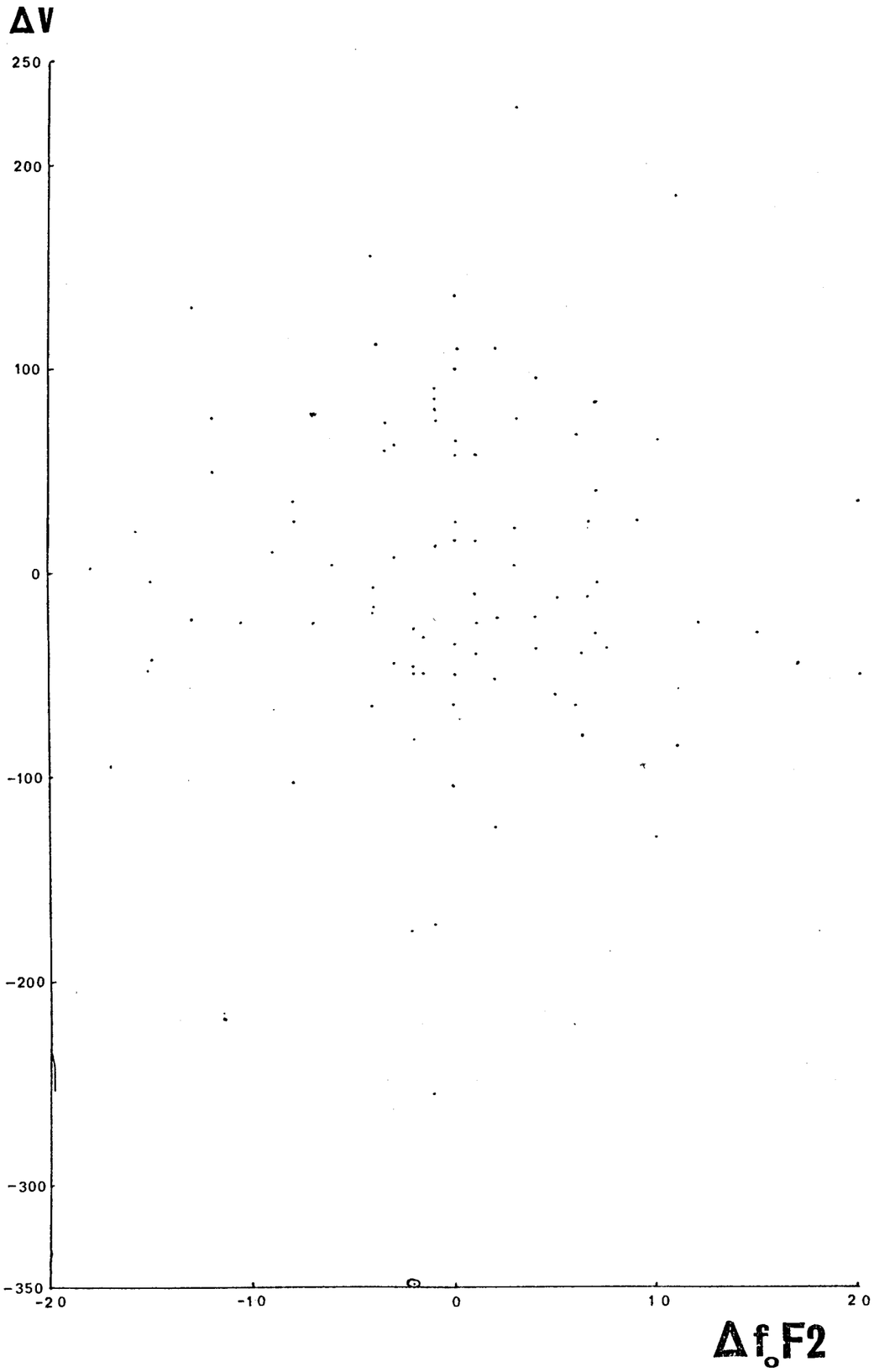
ΔV
250
200
100
0
-100
-200
-300
-350
-20
-10
0
10
20
ΔfoF2

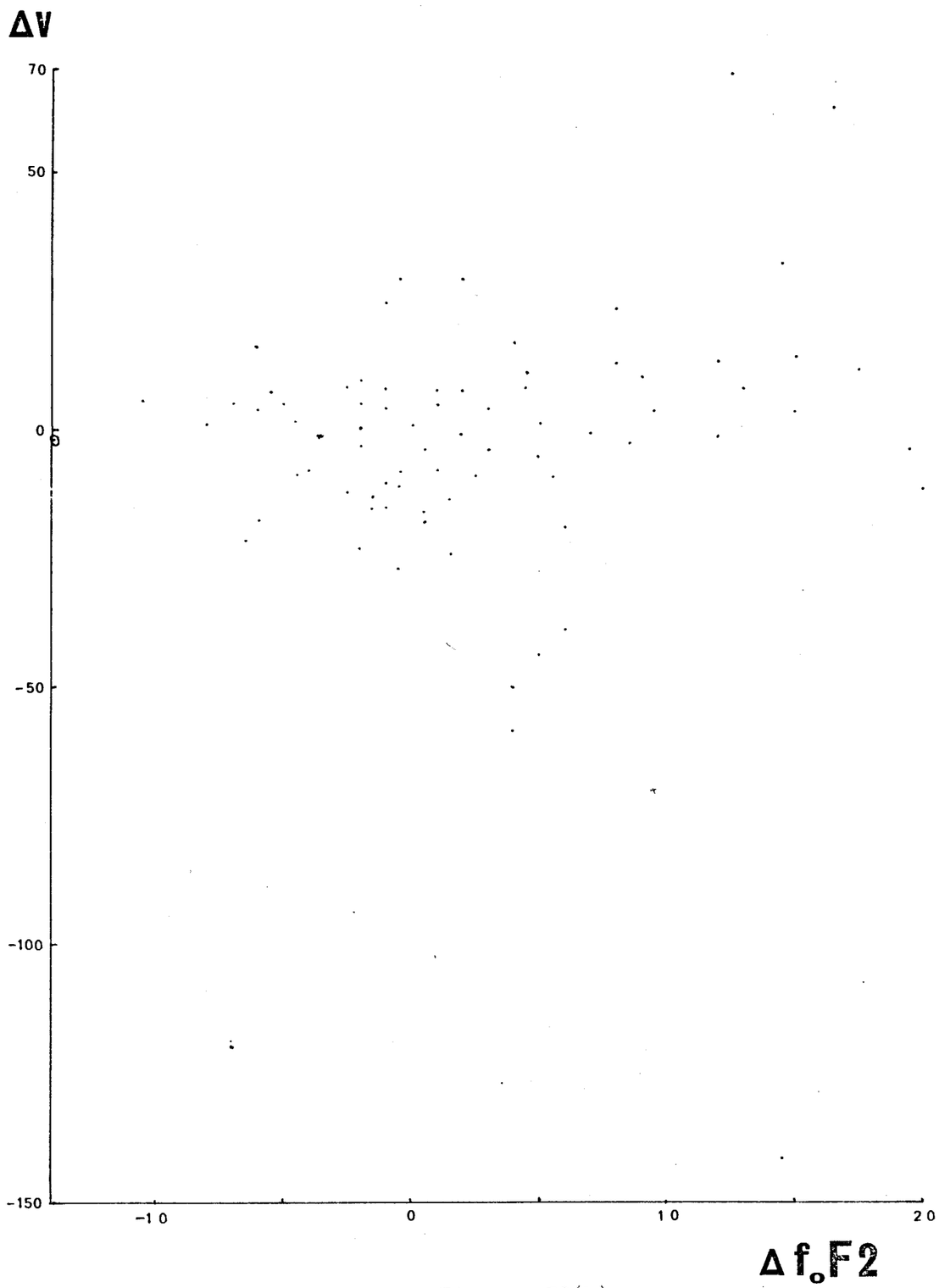

Figure 30(b)

Δv plotted against Δf_0F2 - see text.

2.6 STUDY OF WIND DATA AROUND SOLAR MINIMUM

Since drift velocity measurements obtained at Halley Bay during the IQSY (1964-65) were available, further study was carried out on some of these data. Tables A1 to A10 (Appendix 3) contain the hourly values of wind velocity data obtained for heights between 250 and 300 km above the surface of the earth during February, March, October, November and December 1965. These months were chosen because more measurements of F-region velocities were obtained during them than in the remaining 7 months of the year. Tables A1 to A5 contain the average N-S component of velocity determined with two or three antennas, tables A6 to A10 the N-S component as measured with a single antenna.

Values of the N-S component measured between 200 and 250 km in March and October 1965 are shown in Tables A11 and A12 (again these were the months with the largest number of observations). The measured values of velocity between 250 and 300 km are scarce but values between 200 and 250 km are even scarcer. For this reason the monthly averages have not been taken. However, one thing which is evident, despite the lack of readings, is the extreme variability present in the data.

The hourly values of the N-S component of velocity are compared with the corresponding hourly measurements of f_0F2 for some selected periods on particular days in Table 15. This comparison leads one to the same conclusion as the comparison in Table 14, viz. that the large hour-to-hour fluctuations in wind velocity are not accompanied by corresponding changes in f_0F2.

The difference between each hourly value of wind velocity given in Table 15 and the mean value over the

whole/...

TABLE 15. A comparison between hourly values of N-S component of drift velocity for particular hours of day measured at Halley Bay during the IQSY and corresponding hourly measurements of f_oF2 for the same periods.

MONTH	PERIOD (HRS LMT)	HOURLY AVERAGES OF N-S COMPONENT (m/s) DURING PERIOD SPECIFIED						CORRESPONDING HOURLY AVERAGES OF f_oF2 IN MHz					
Feb 10	01-04	10.9	-29.5	—	-61.7			4.9	4.5	4.55	5.0		
Feb 16-17	22-03	17.7	-23.7	2.7	-16.0	-6.9	1.8	5.4	5.7	5.9	5.6	4.9	5.5
Feb 25	02-04	-10.5	4.1	-14.2				3.3	3.5	3.9			
Feb 25	19-23	7.8	-111.2	—	—	-14.7		4.8	5.4	6.1	5.8	5.8	
Feb 27	21-24	32.8	0.1	—	29.7			5.1	5.7	4.5	-		
Mar 1	00-05	85.8	-37.5	-14.6	—	42.2	-189.8	5.0	4.9	4.3	4.0	4.25	4.5
Mar 4- 5	23-04	2.5	152.3	-10.7	8.4	14.6	-2.7	4.65	4.7	4.0	4.05	3.5	3.6
Mar 5	22-24	6.1	-1.6	31.3				4.6	3.9	3.45			
Mar 7	22-23	24.3	7.2					4.3	3.45				
Mar 13	21-23	-0.3	8.3	-9.0				4.0	3.9	3.65			
Mar 9	04-05	-31.1	20.8					3.6	4.3				
Mar 16	05-07	-19.1	-7.7	-0.4				3.0	3.3	3.45			
Mar 28	05-07	—	-36.9	-16.1				2.4	2.75	3.55			
Oct 1	00-02	-7.1	3.4	-17.2				3.7	3.6	3.5			
Oct 11	17-22	15.8	4.5	2.6	—	-1.6	-1.3	5.4	5.2	5.0	5.2	5.4	—
Oct 12	22-23	-15.4	-1.8					5.5	5.5				
Oct 13	22-23	5.7	22.7					4.0	-				
Oct 14	22-24	-7.0	—	-34.6				4.2	4.1	4.0			
Oct 16	00-04	-1.7	-6.5	-	-26.3	-10.0		5.1	4.8	4.6	4.3	4.25	
Oct 18	13-17	—	-14.8	0.0	—	12.8		5.2	4.9	4.8	5.15	5.4	
Oct 19	13-16	-4.5	2.3	7.2	-0.6			5.15	4.95	4.8	4.8		
Oct 22	09-14	-45.6	—	-15.8	-0.8	-3.2	16.1	5.0	4.8	4.7	4.8	5.0	5.6
Oct 26-27	22-03	-8.7	6.7	2.3	-3.1	6.7	-4.8	-	5.9	5.7	5.6	5.6	5.0
Oct 28	15-17	1.2	-12.6	-7.9				4.3	4.7	4.8			
Oct 29	02-03	-0.7	-17.1					3.7	4.0				
Oct 30	02-03	-0.6	26.8					4.2	4.25				
Oct 31	13-18	-16.9	-1.6	-1.5	-5.0	-6.0	-15.6	4.8	4.7	5.0	5.0	4.9	4.95

It is, of course, feasible that these "velocity" measurements obtained by the spaced receiver method at Halley Bay may be the phase or group propagation velocities associated with travelling disturbances or may result from irregularities generated by atmospheric gravity waves, instead of being measurements of the horizontal drift velocity due to neutral atmospheric winds (Hines and Raghava Rao). However, Wright and Fedor have shown that in the range 85 - 140 km the wind velocities deduced by the spaced-receiver method agree reasonably well with horizontal drift velocities determined by luminous trail releases from rockets. Föppl et al have measured wind velocities in the region 125 - 200 km in the Sahara and over Sardinia during 1964 and found velocities of between 40 and 130 ms^{-1} in this region. These velocities are larger than the velocities used in this analysis for sunspot minimum conditions but smaller than those obtained by Bellchambers et al for sunspot maximum conditions. For these reasons the measured values of drift velocity can be reasonably interpreted as being caused by horizontal neutral winds.

Föppl H., Haerendel G., Haser L., Loidl J., Lütjens P., Lüst R., Metzner F., Meyer B., Neuss H and Rieger E., Artificial Strontium and Barium Clouds in the Upper Atmosphere, 1967, Planet. Space Sci., vol 15, pp 357 - 372.

Hines C.O. and Raghava Rao R., Validity of Three-station Methods of Determining Ionospheric Motions, 1968, J. Atmosph. Terr. Phys., vol 30, pp 979 - 993.

Wright J.W. and Fedor L.S., Comparison of Ionospheric Drift Velocities by the Spaced Receiver Technique with Neutral Winds from Luminous Rocket Trails, 1967, Space Research VII, pp 67 - 72.

whole month for that particular hour, Δv, is plotted against Δf_0F2, the difference between the corresponding hourly measurement of f_0F2 and the mean value of f_0F2 for that particular hour. The result is shown in Fig. 30(b). Again this shows no relation between f_0F2 variations and wind velocity variations.

Another difference between the observed winds and those predicted theoretically by Kohl and King lies in their dependence on solar activity. The magnitudes of the wind velocities calculated by Kohl and King for sunspot minimum are about 150 ms^{-1} and for sunspot maximum about 40 ms^{-1}. However, the observed wind speeds are greater at sunspot maximum (Table 13) than at sunspot minimum (Appendix 3).

The results of this study are, therefore, the same as those obtained from the analysis of sunspot maximum data, namely:

(i) individual measurements of the N-S component of horizontal wind velocity (or monthly average of same) fluctuate so much from hour to hour that no underlying pattern of behaviour is obvious,

(ii) the variability of velocity is not accompanied by corresponding changes in f_0F2, and

(iii) the average hourly values of velocity observed in summer do not follow the theoretical pattern derived by King, Kohl and Pratt[83] for Halley Bay (see Fig. 31).

These results point to the conclusion that either velocity measurement techniques are not very accurate or horizontal neutral winds have very little effect on the ionosphere generally and fluctuate too much to be responsible for the regular early morning maximum observed at Halley Bay during summer.

2.7 A/...

Figure 31

The theoretical patterns of vertical drift velocity for Halley Bay and South Pole Station calculated from Kohl and King's model. A copy of Figures 3 and 4 in the paper by King et al[83].

FIGURE 31

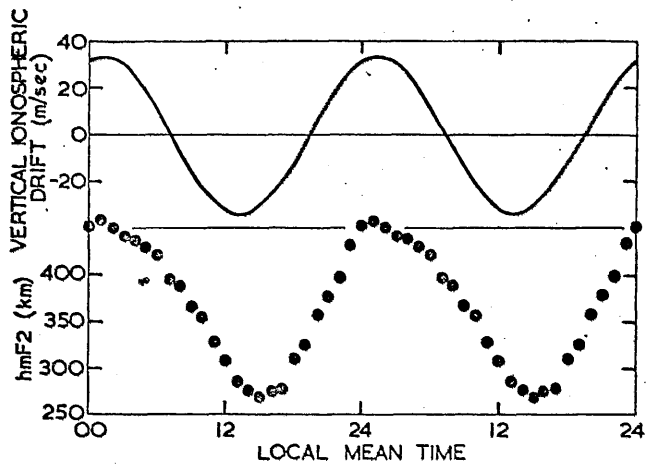

Fig. 3. Diurnal variation of the vertical ionospheric drift (positive upwards) and the monthly mean h_mF2 (June 1958) for Halley Bay.

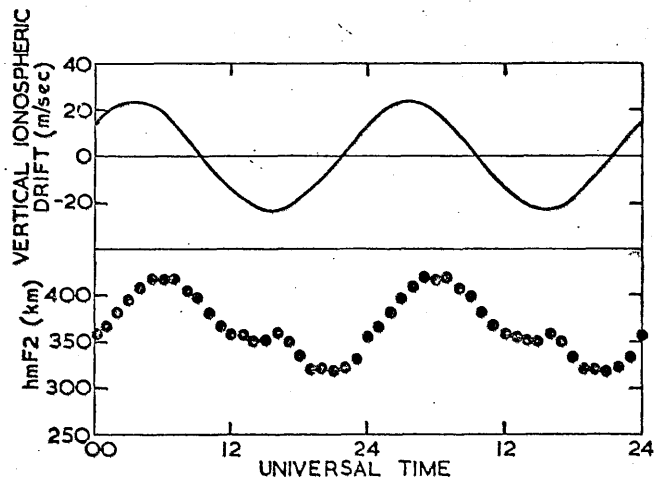

Fig. 4. Diurnal variation of the vertical ionospheric drift (positive upwards) and the monthly mean h_mF2 (June 1958) for the South Pole Station.

2.7 A COMPARISON OF f_0F2 BEHAVIOUR AT SEVERAL PAIRS OF ANTARCTIC STATIONS

Since there is so much uncertainty about the magnitude of winds derived theoretically and the effect which winds have on the F2 peak, it was decided to compare the observed values of f_0F2 at stations having the same geographic latitude in Antarctica but with different magnetic declinations in the hope that some trends in the behaviour of f_0F2 ascribable to winds may become apparent. It must be borne in mind that this is not meant to be an accurate hour-by-hour comparison, since stations at the same latitude but different longitudes in different parts of the world do very often show differences in the behaviour of f_0F2.

For the analysis three pairs of Antarctic stations were chosen (see Table 16) situated near geographic latitudes 65°, 70° and 75°S. The magnetic declinations at each pair of stations are sufficiently different to show up any effect which winds may have. In each case one of the stations falls inside the area of the Weddell Sea (Penndorf[113]) while the other is in the Ross Sea area.

The idea behind this analysis is to compare the observed variation of f_0F2 with local time at each pair of stations for specific months of the year. Since each pair of stations occurs at approximately the same geographic latitude, the contribution to the ionosphere from solar EUV will be much the same for both stations at any given time. If we assume that the contribution from precipitated particles is small compared with the effects produced by vertical drifts resulting from horizontal neutral winds, which many workers believe to be the case, it should be possible to compare the differences in observed f_0F2 at any

pair/...

T A B L E 16

List of Antarctic stations used

in this analysis

STATION	GEOGRAPHIC LAT.	GEOGRAPHIC LONG.	GEOMAGNETIC LAT.	GEOMAGNETIC LONG.	DIP ANGLE	MAGNETIC DECLINATION
Halley Bay	75.5°S	26.6°W	65.8°S	24.3°E	-65°	-1°
Scott	77.8°S	166.8°E	79.0°	294.4°	-83°	141°
SANAE	70.3°S	2.4°W	63.6°	44.1°	-64°	-20°
Cape Hallett	72.3°S	170.3°E	74.7°	278.2°	-85°	104°
Port Lockroy	64.8°S	63.5°W	53.4°	3.9°	-58°	16°
Terre Adelie	66.7°S	140.0°E	75.6°	230.9°	-88°	-74°

Figure 32

The vertical drift velocity (in ms^{-1}) at a height of 300 km plotted as a function of local time for 3 pairs of Antarctic stations at similar geographic latitudes. In each case the upper figure shows the drift velocity at each station; the lower figure displays the difference in drift velocity, Δv (ms^{-1}), between each pair of stations. The three pairs of stations are:

(a) Halley Bay (._._.) and Scott (.....)

(b) SANAE (.__.__.) and Cape Hallett (.....)

(c) Port Lockroy (._._.) and Terre Adelie (.....)

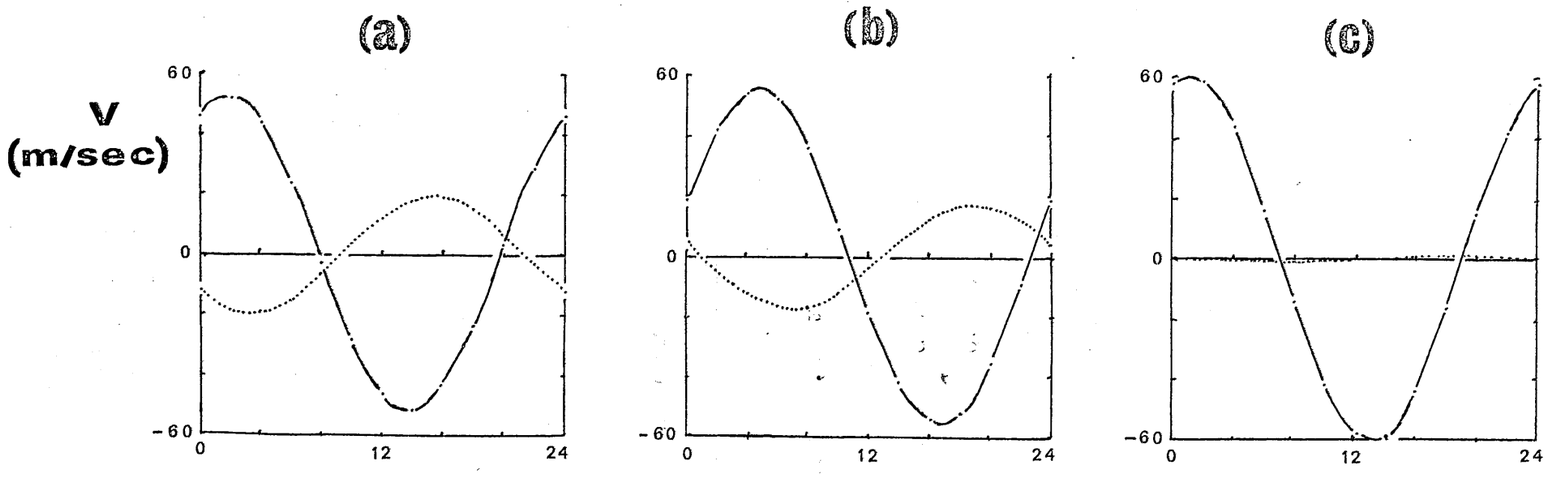
(a)
(b)
(c)
V
(m/sec)
60
0
-60
0
12
24
ΔV
(m/sec)
80
0
-80

Figure 33

Comparison of monthly quiet-day average f_0F2 values (in MHz) plotted against time of day for two stations situated at approximately 75°S geographic latitude, Halley Bay and Scott, during the equinoxes. Months shown are March and September 1962, September 1964 and March and September 1965. The two stations are represented as follows:

Halley Bay .-.-.-.

Scott .....

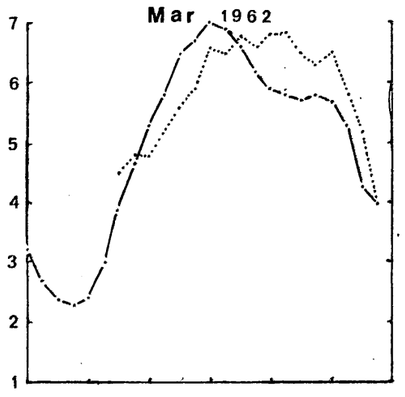
Mar 1962
7
6
5
4
3
2
1

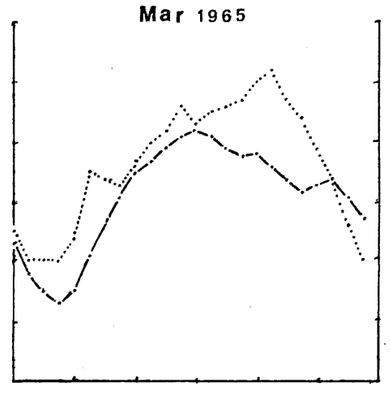
Mar 1965

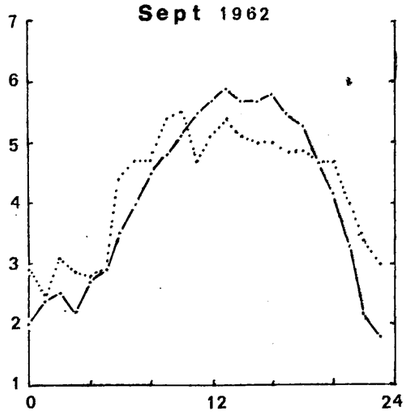
Sept 1962
7
6
5
4
3
2
1
0
12
24

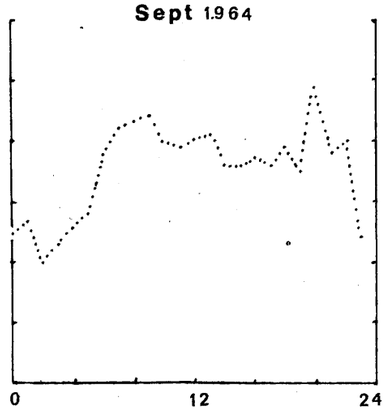
Sept 1964
0
12
24

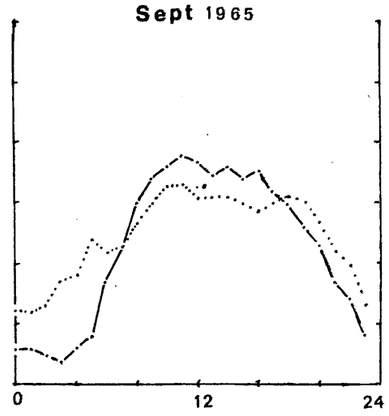
Sept 1965
0
12
24

Figure 34

Comparison of monthly quiet-day average f_0F2 values (in MHz) at Halley Bay and Scott during the equinoxes. Months shown are March and September 1960 and 1961 and September 1958 and 1968.

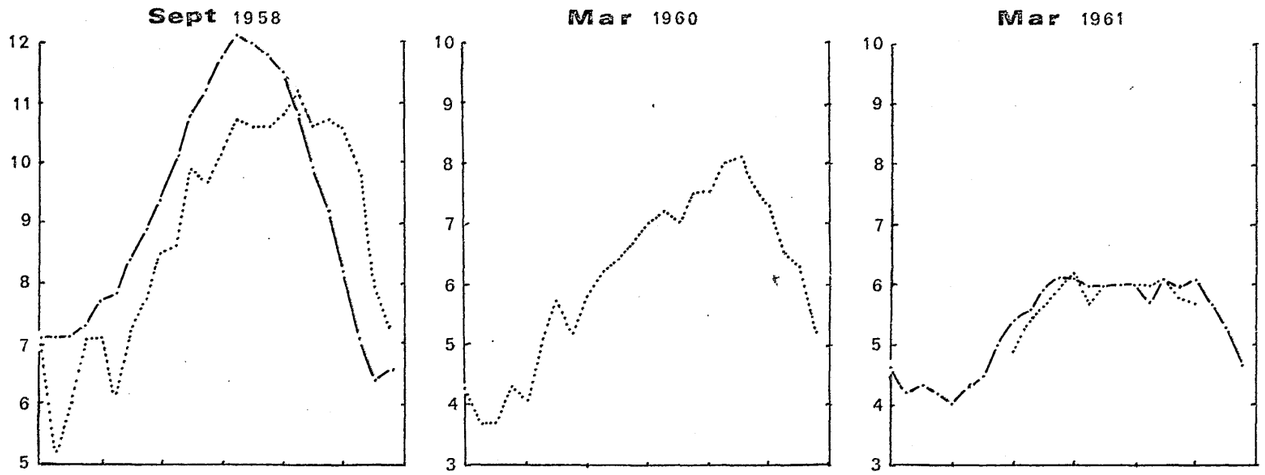
Sept 1958
Mar 1960
Mar 1961
12
11
10
9
8
7
6
5
4
3

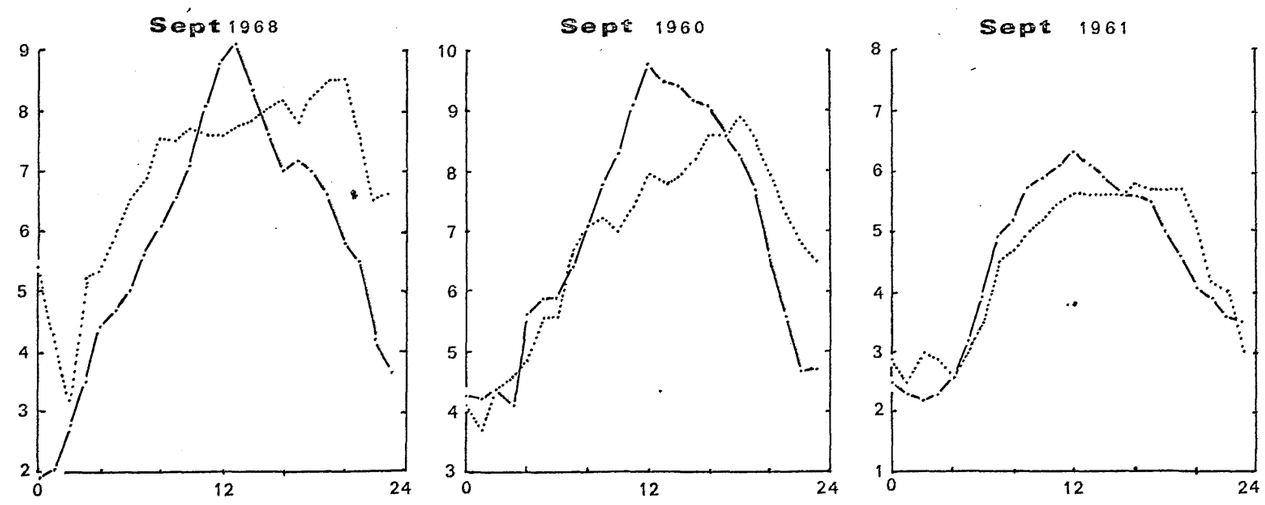
Sept 1968
Sept 1960
Sept 1961
9
8
7
6
5
4
3
2
10
1
0
12
24

pair of stations with the differences in vertical drift velocity between the two stations. If the theory put forward by King et al[84] (in section 2.1) is correct, the differences in observed f_0F2 should correlate well with the differences in vertical drift velocity predicted by Kohl and King[92].

Thus the vertical drift velocities which might be expected at each station during the equinoxes at sunspot minimum have been calculated using the theoretical wind distribution of Kohl and King[92]. These are compared in Fig. 32. The relative differences between the vertical drift velocities at each pair of stations at the same local times are also shown. These differences can be seen to be largest soon after midnight and shortly after midday. The vertical drift velocities for summer and winter as derived from Kohl and King's model are not very different from the equinoctial drift velocities (see section 2.2).

The mean of the hourly quiet-day values of f_0F2 for the months March, June, September and December have been plotted for each station and are compared below.

(a) HALLEY BAY AND SCOTT (75^oS)

Figs. 33 and 34 show the behaviour of f_0F2 at these two stations during the equinoxes. From Fig. 32, which shows the theoretically calculated winds, one would expect the largest differences in f_0F2 due to winds to occur at about 02 and 14 hours LMT. From Figs. 33 and 34 it is clear that the critical frequency at Halley Bay is larger than that at Scott at about midday (7 cases out of 9) while soon after midnight the values at Scott are larger than those at Halley Bay.

Another noticeable feature of Figs. 33 and 34 is that, with the exception of September 1958, 1960 and 1968

(months/...

Figure 35

Comparison of monthly quiet-day average f_0F2 values (in MHz) at Halley Bay and Scott during the solstices. The months shown are December and June 1962, 1964 and 1965. The two stations are represented as follows:

Halley Bay .-.-.-.

Scott .....

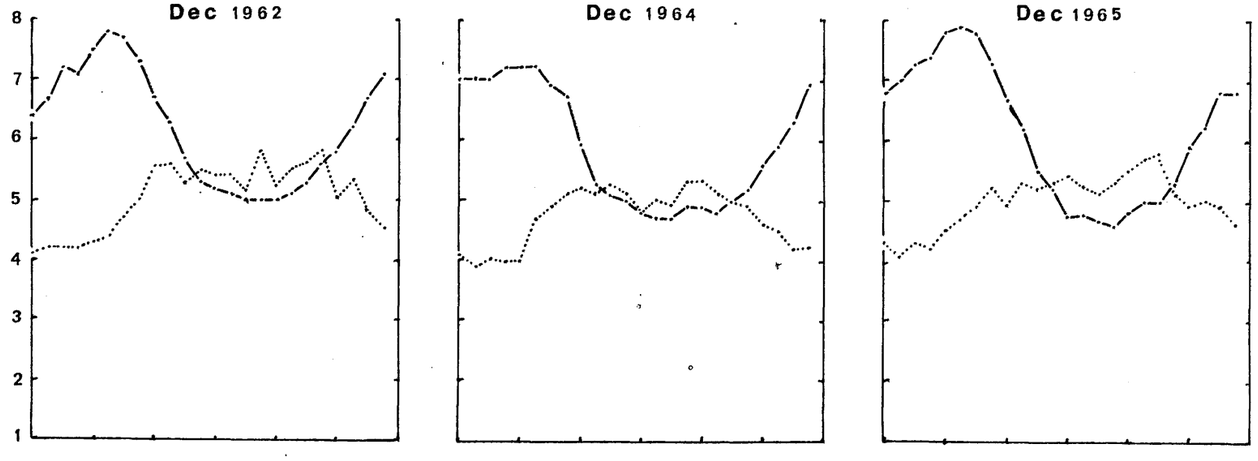
Dec 1962
Dec 1964
Dec 1965
8
7
6
5
4
3
2
1

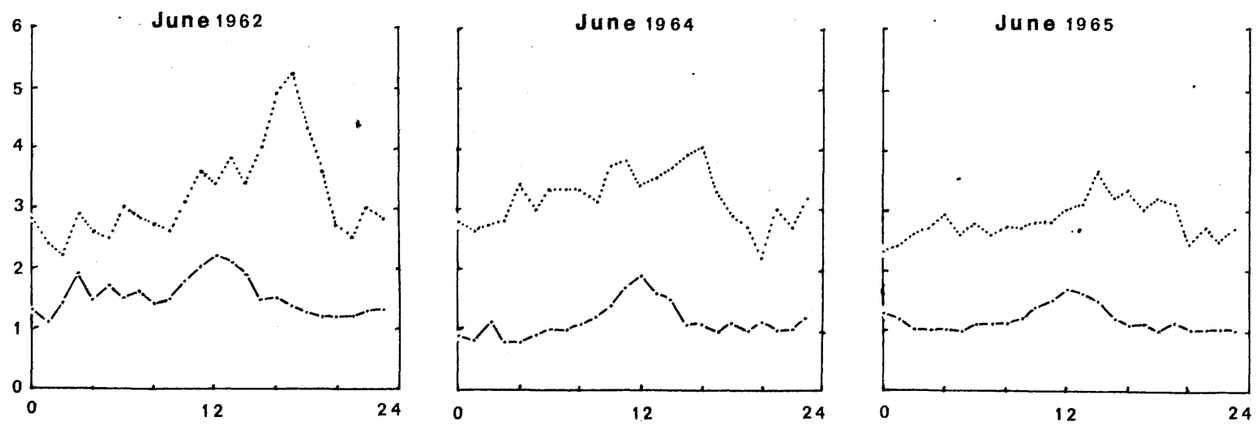
June 1962
June 1964
June 1965
6
5
4
3
2
1
0
0
12
24
0
12
24
0
12
24

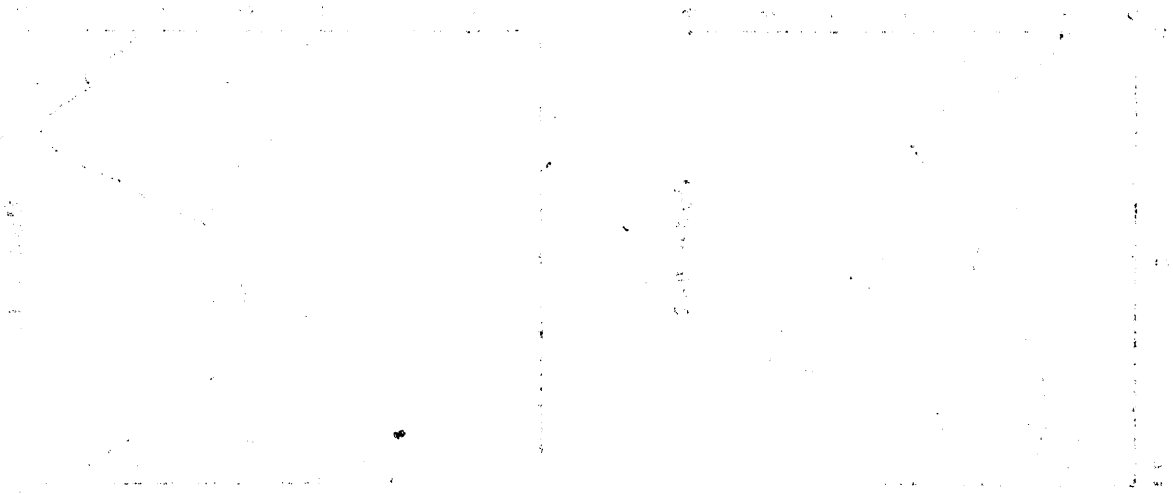

Figure 36

Comparison of monthly quiet-day average f_oF2 values (in MHz) at Halley Bay and Scott during the equinoxes. Months shown are June and December 1958, 1960 and 1961.

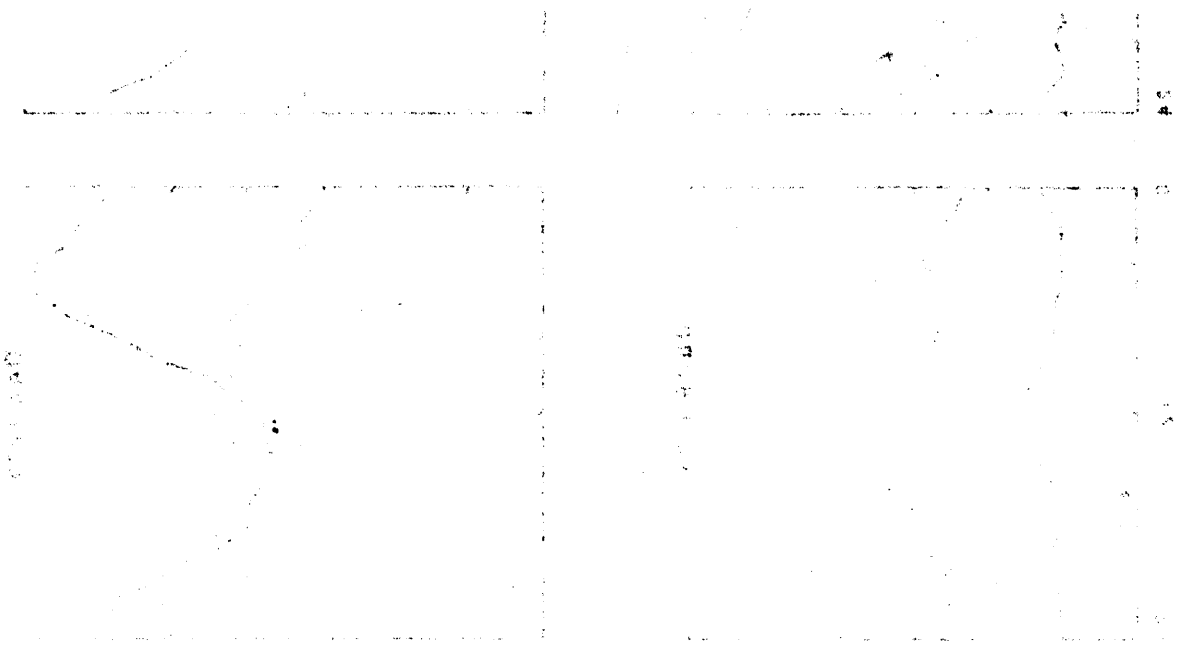

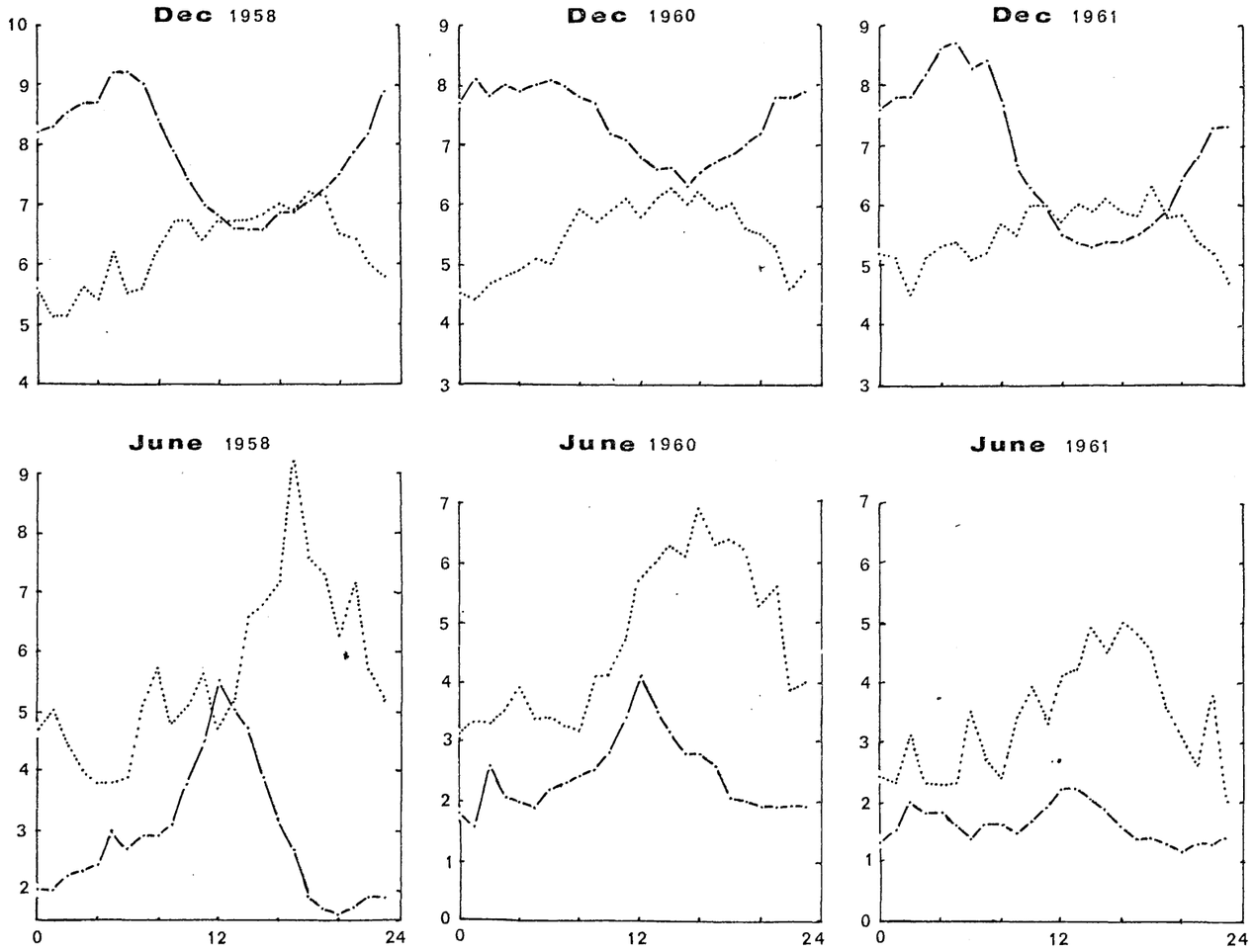
Dec 1958
Dec 1960
Dec 1961
June 1958
June 1960
June 1961
0
12
24

(months for which the level of solar activity was reasonably high - R_z = 201, 127 and 117 compared with $R_z < 64$ for the remaining months), the values of f_oF2 at the two stations are very similar. On relatively few occasions were there differences of more than 1 MHz between values of f_oF2 at the two stations, and on no occasion was the difference larger than 1.6 MHz.

In Figs. 35 and 36 the variation of f_oF2 at these stations during June and December is shown. Here a completely different picture emerges. During June the difference between f_oF2 values at the two stations is seldom less than 1 MHz and differences in excess of 4 MHz can be seen at solar minimum (at solar maximum even larger differences can be seen - on one occasion the difference exceeded 6 MHz). During December differences greater than 3 MHz are observed for each of the years under consideration. In June the largest difference occurs at 16-17 hours local time (=05 to 06 hours UT for Scott) and in December it appears to be at about 04-05 hours local time (=06 to 07 hours UT for Halley Bay). This is some 2 to 3 hours after the maximum difference of wind velocity.

(b) SANAE AND CAPE HALLETT (70°S)

Unfortunately, much fewer data were available for these two stations. In June and September values of f_oF2 at SANAE during the night fell below the usual value of f-min. In these cases a value of 2 MHz has been plotted although the actual value of f_oF2 is unknown and is less than this.

The equinoctial behaviour at these two stations is shown in Fig. 37. It has similar features to the behaviour observed at Halley Bay and Scott during the equinoxes (shown in Figs. 33 and 34), viz. the difference

in/...

Figure 37

Comparison of monthly quiet-day average f_0F2 values (in MHz) plotted against time for two stations situated at approximately 70°S geographic latitude, SANAE and Cape Hallett, during the equinoxes. Months shown are March and September 1962, 1963 and 1964. The two stations are represented as follows:

SANAE .-.-.

Cape Hallett .....

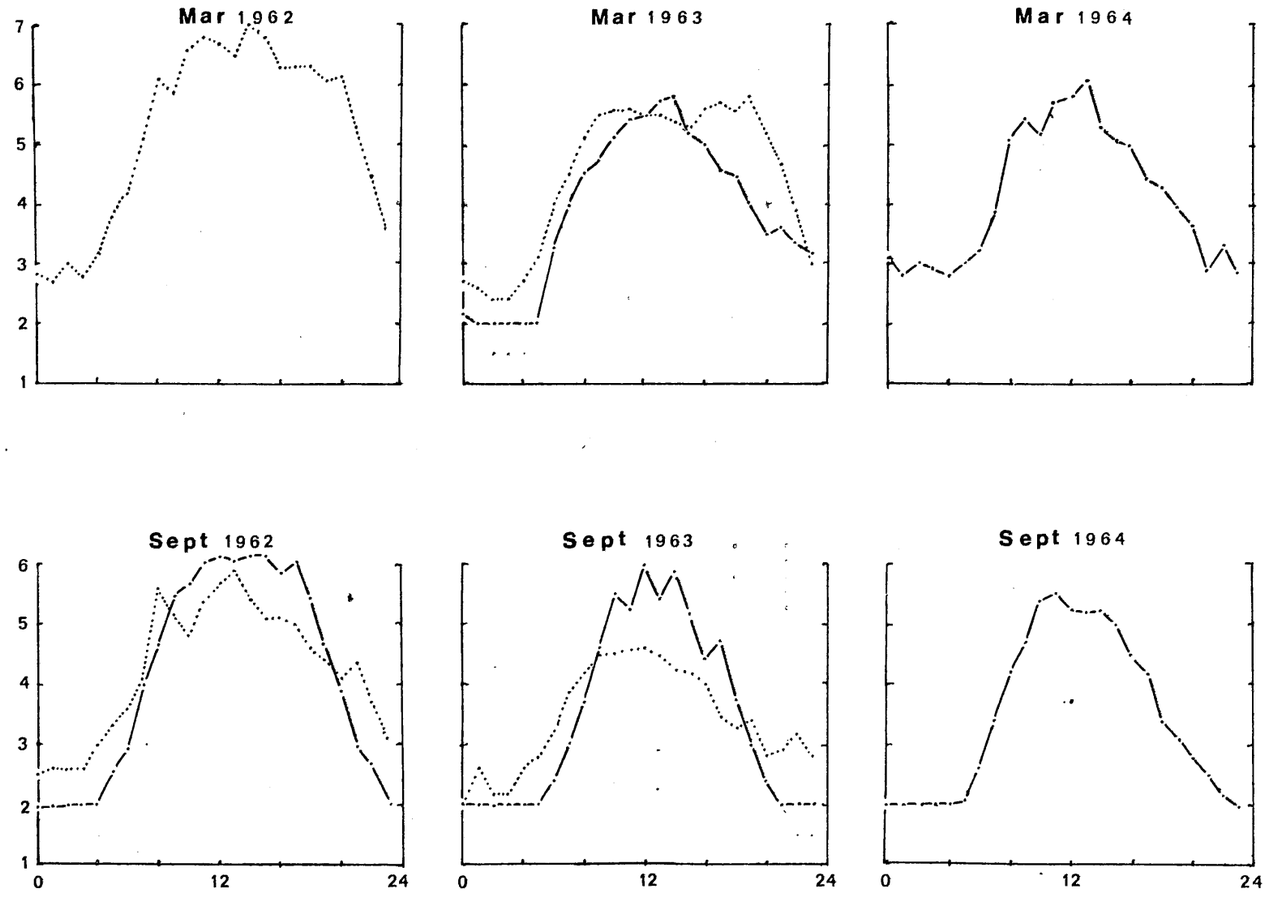
Mar 1962
Mar 1963
Mar 1964
Sept 1962
Sept 1963
Sept 1964
7
6
5
4
3
2
1
0
12
24

Figure 38

Comparison of monthly quiet-day average of f_oF2 values (in MHz) at SANAE and Cape Hallett during the solstices. Months shown are December and June 1962, 1963 and 1964. The two stations are represented as follows:

SANAE .—.—.

Cape Hallett .....

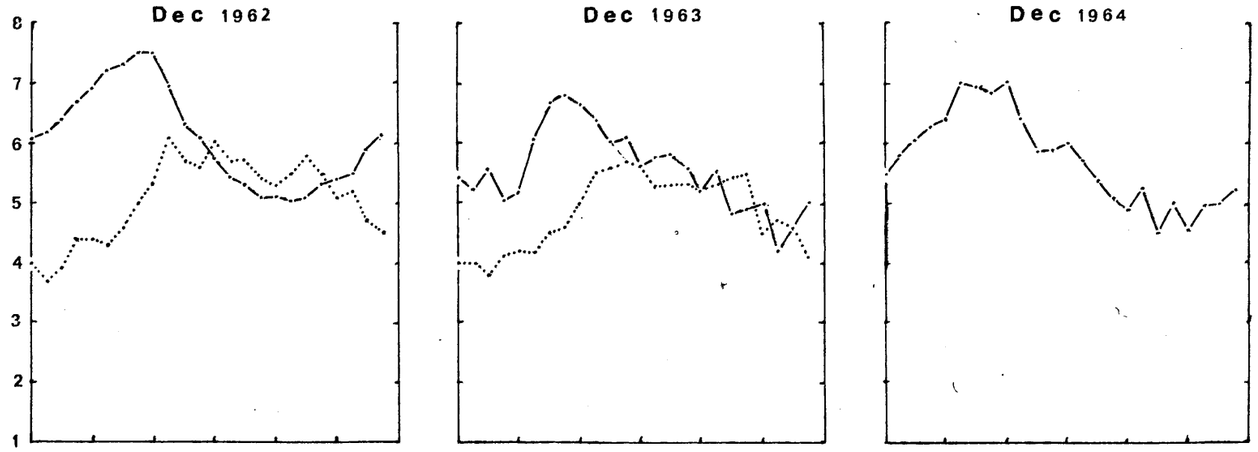
Dec 1962
Dec 1963
Dec 1964
8
7
6
5
4
3
2
1

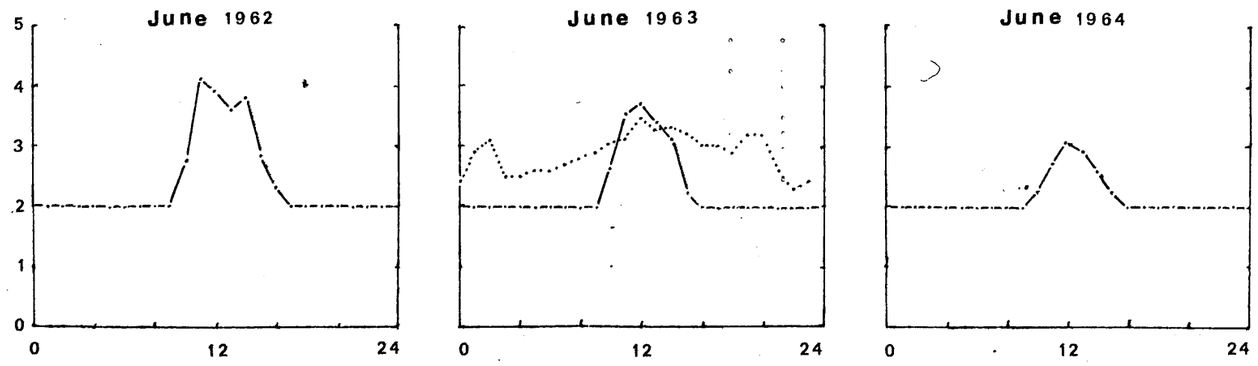
June 1962
June 1963
June 1964
5
4
3
2
1
0
0
12
24

4/e

Figure 39

Comparison of monthly quiet-day average f_oF2 values (in MHz) plotted against time for two stations situated at approximately 65°S geographic latitude, Port Lockroy and Terre Adelie, during the equinoxes. Months shown are March and September 1962, 1963 and 1964. The two stations are represented as follows:

Port Lockroy .—.—.—.

Terre Adelie .....

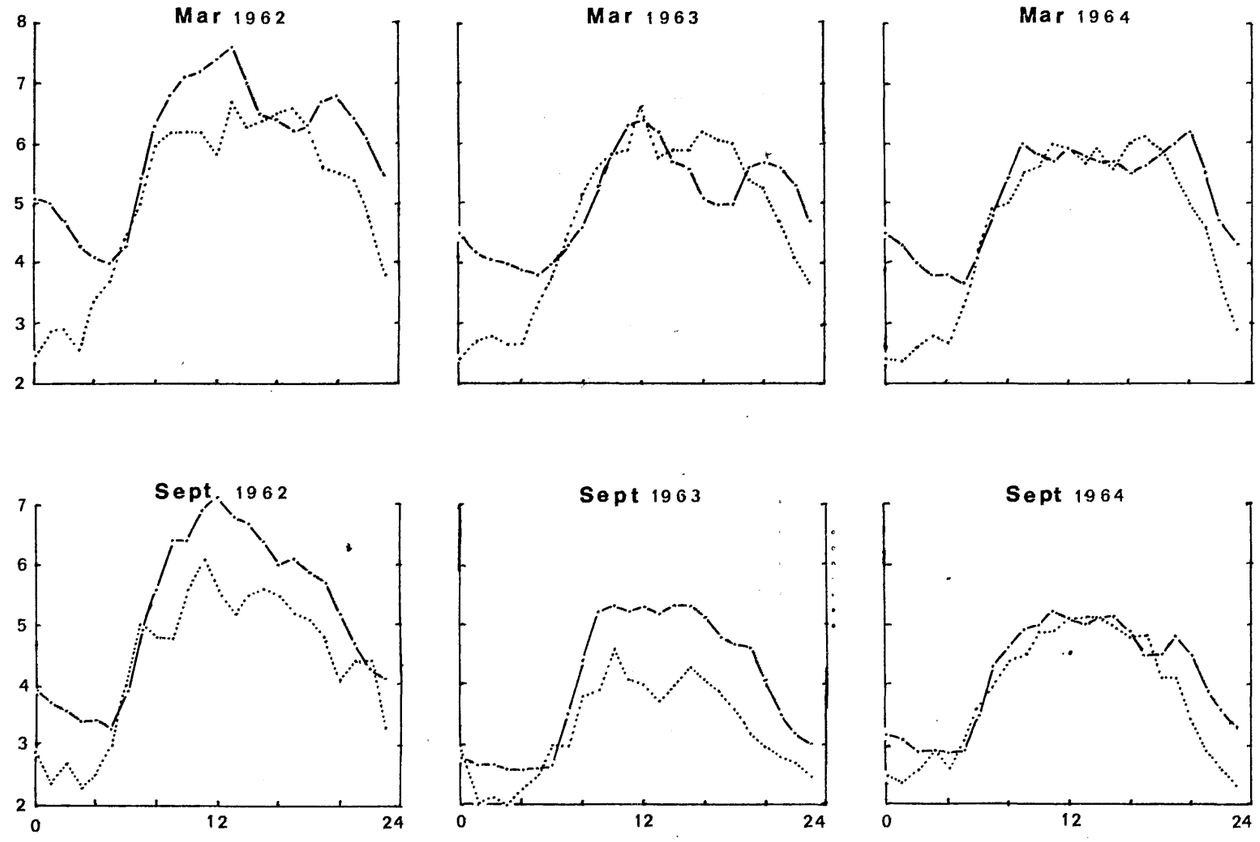
Mar 1962
Mar 1963
Mar 1964
Sept. 1962
Sept 1963
Sept 1964
8
7
6
5
4
3
2
0
12
24

Figure 40

Comparison of monthly quiet-day average f_0F2 values (in MHz) at Port Lockroy and Terre Adelie during the solstices. Months shown are December and June 1962, 1963 and 1964. The two stations are represented as follows:

Port Lockroy .-.-.-.

Terre Adelie .....

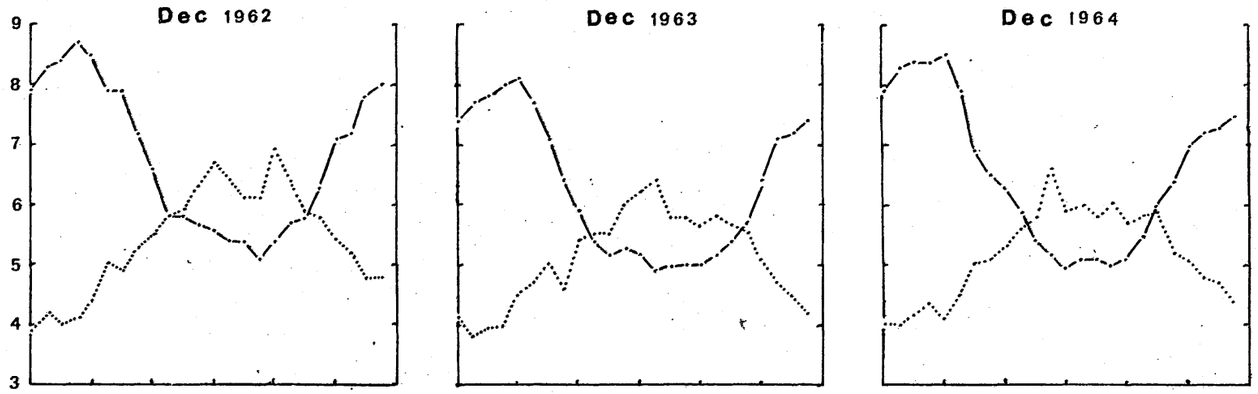
Dec 1962
Dec 1963
Dec 1964
9
8
7
6
5
4
3

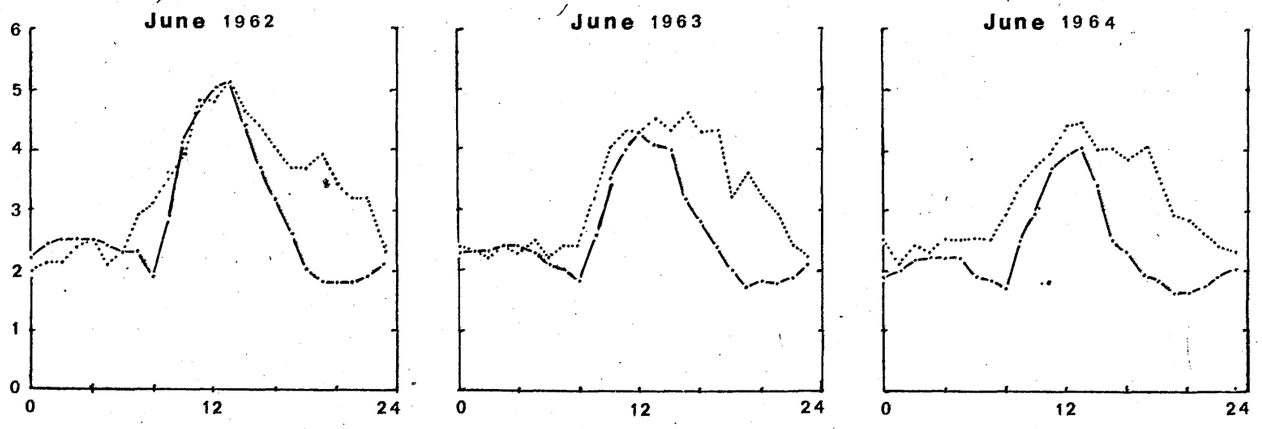
June 1962
June 1963
June 1964
6
5
4
3
2
1
0
0
12
24

in f_0F2 between the two stations at a particular time of day is seldom larger than 1 MHz and the differences are largest about noon and in the late evening (in agreement with the theoretical winds shown in Fig. 32). The values of f_0F2 at SANAE are larger than those at Cape Hallett about midday and those at Cape Hallett larger than SANAE values around midnight.

Again the values of f_0F2 for the two stations in June and December (Fig. 38) are markedly different, the maximum difference in December occurring at about 06-07 LMT (=06 - 07 UT for SANAE) while the maximum difference in June occurs at 18 - 19 LMT (=07 - 08 UT for Cape Hallett).

(c) PORT LOCKROY AND TERRE ADELIE (65^{o}S)

The equinoctial behaviour shown in Fig. 39 follows a similar pattern to that observed at the other stations. From Fig. 32, the times of maximum difference of vertical drift velocity between the two stations occur at 01 and 13 hours LMT. From Fig. 39 the critical frequency at Terre Adelie usually exceeds the value observed at Port Lockroy in the early afternoon while at about midnight f_0F2 at Port Lockroy is greater. In general values of f_0F2 at Port Lockroy are larger than those at Terre Adelie but this may be due to the fact that Terre Adelie is so close to the Magnetic Dip Pole (and hence vertical diffusion will have a greater influence on the F2 peak).

The solstitial behaviour (Fig. 40) is once again quite different from the equinoctial behaviour, the values of f_0F2 at the two stations sometimes differing by more than 4 MHz during summer. In December the difference is largest at about 03 to 04 hours local time (=07 to 08 hours UT at Port Lockroy) while in June the largest difference occurs at about 17 hours local time (=08 hours UT at Terre Adelie).

This/...

Figure 41

The constant term, A_0, from the harmonic analysis (see Chapter 1) plotted against time for six Antarctic stations. The stations are:

Upper Diagram : Halley Bay (._._.) and Scott (.....)

Middle Diagram : SANAE (._._.) and Cape Hallett (.....)

Lower Diagram : Port Lockroy (._._.) and

Terre Adelie (.....)

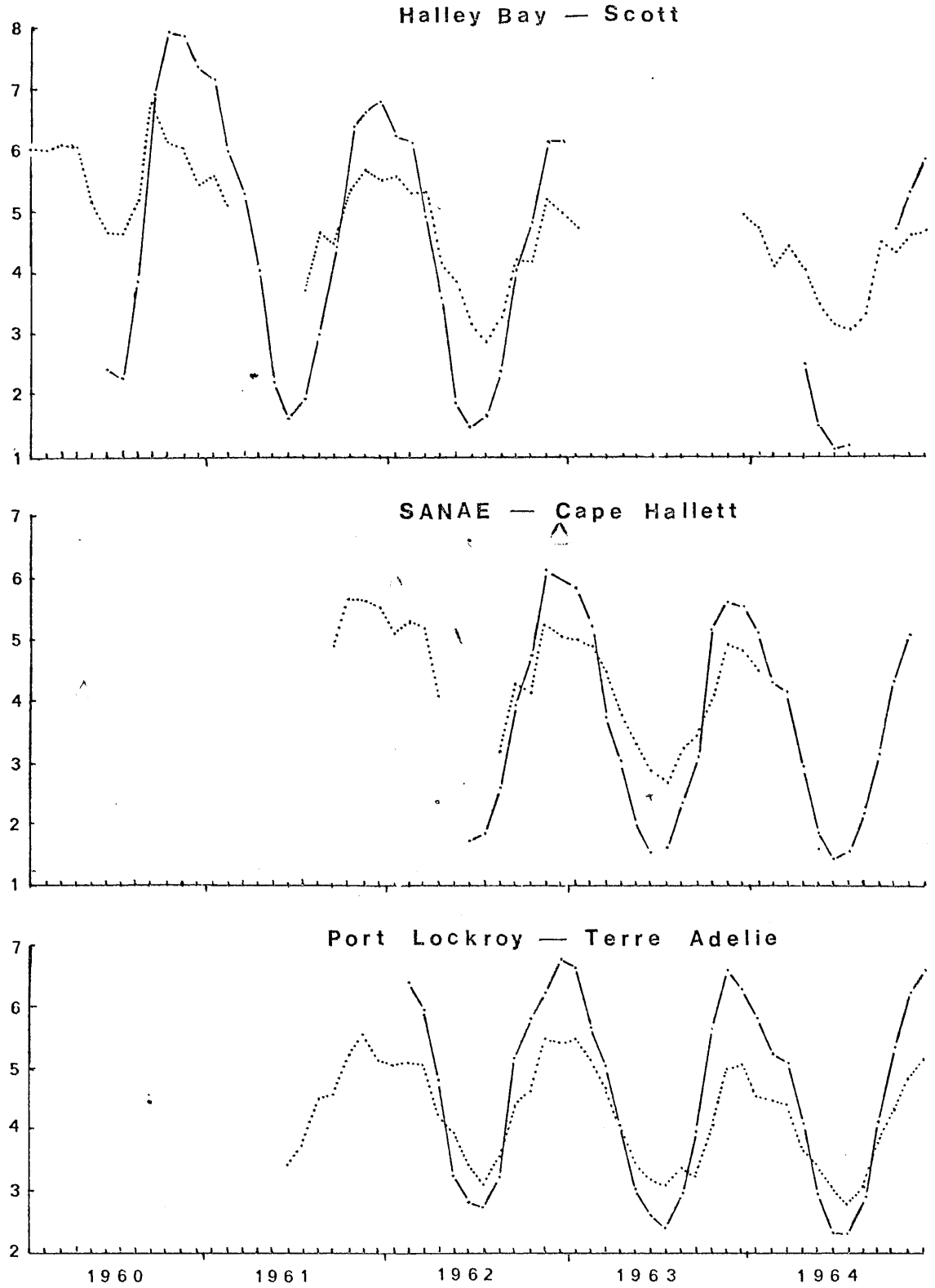
Halley Bay — Scott
8
7
6
5
4
3
2
1
SANAE — Cape Hallett
7
6
5
4
3
2
1
Port Lockroy — Terre Adelie
7
6
5
4
3
2
1960
1961
1962
1963
1964

Figure 42

The average difference in f_oF2 between Halley Bay and Scott, Δf_oF2, is plotted against time. The upper diagram contains $\overline{\Delta f_oF2}$ (in MHz) for December, the middle diagram $\overline{\Delta f_oF2}$ (in MHz) for the equinoxes (March and September) and the lower diagram Δv (the difference in vertical drift velocity between the two stations) in ms^{-1}.

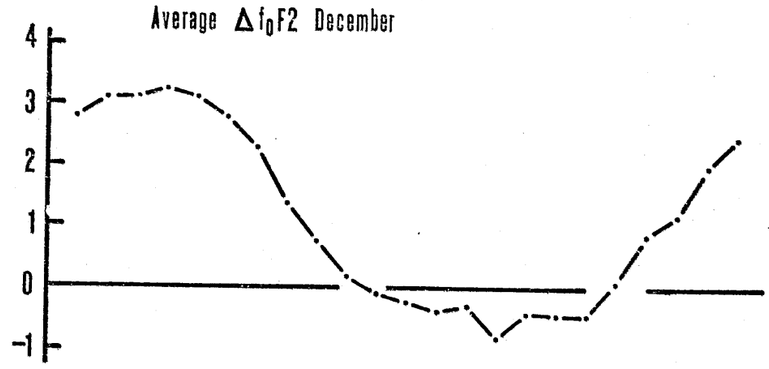
Average Δf_0F2 December
4
3
2
1
0
−1

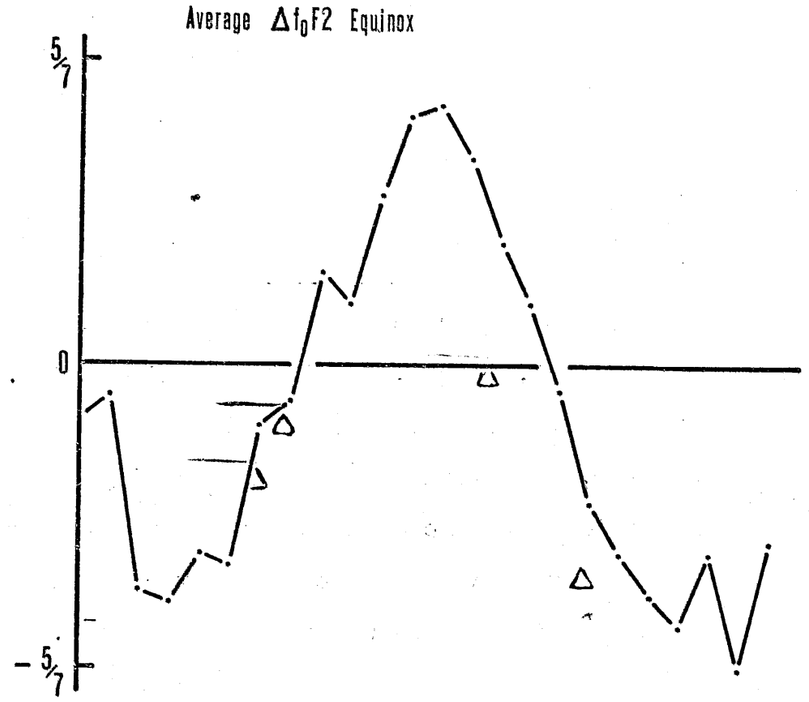
Average Δf_0F2 Equinox
5/7
0
−5/7

ΔV

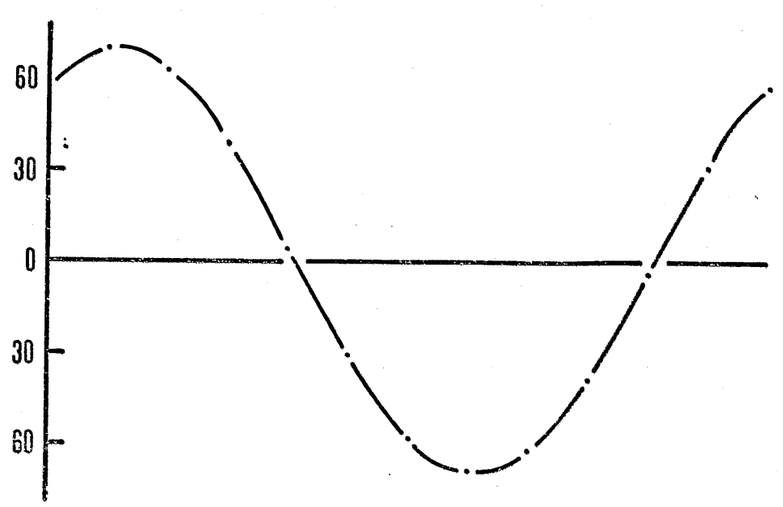
60
30
0
30
60

Figure 43

The average difference in f_oF2 between SANAE and Cape Hallett, $\overline{\Delta f_oF2}$, is plotted against time. The upper diagram contains $\overline{\Delta f_oF2}$ (in MHz) for December, the middle diagram $\overline{\Delta f_oF2}$ (in MHz) for the equinoxes (March and September) and the lower diagram Δv (the difference in vertical drift velocity between the two stations) in ms^{-1}.

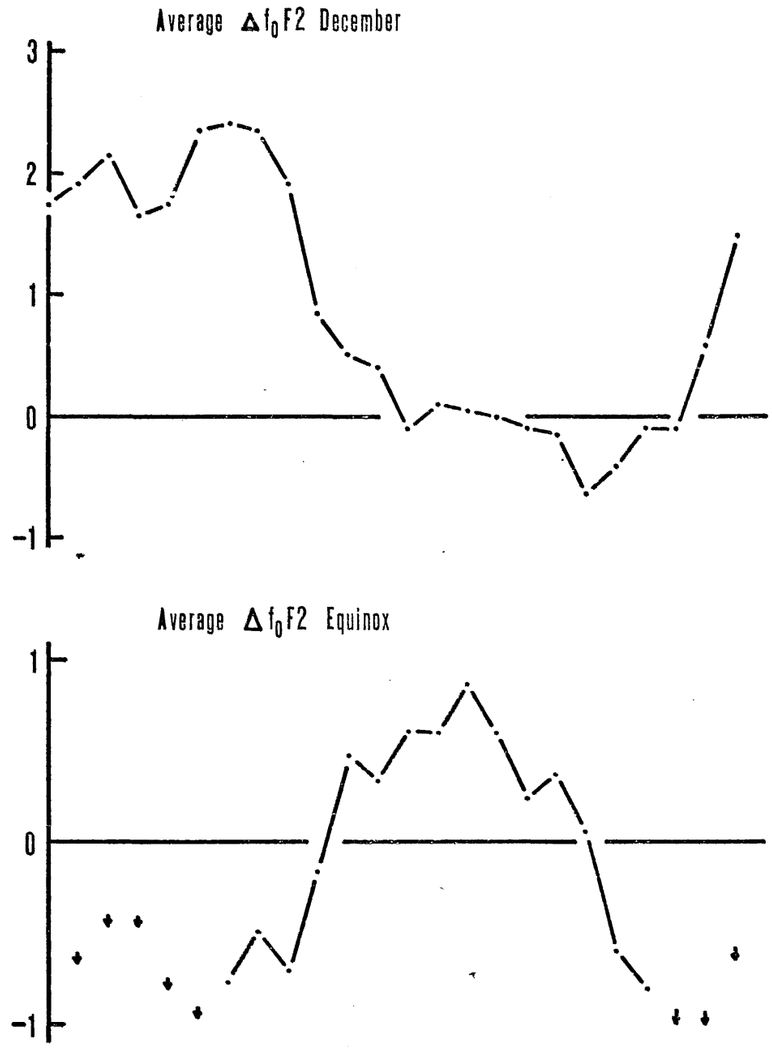
Average Δf_0F2 December
3
2
1
0
-1
Average Δf_0F2 Equinox
1
0
-1
ΔV
60
30
0
-30
-60

This is several hours after the time of maximum difference in vertical drift velocity at the two stations.

As further evidence of the seasonal variation, the means of all the hourly quiet-day values of f_0F2 for each month (i.e. the constant term, A_0, in the harmonic analysis) have been plotted for each pair of stations in Fig. 41. From this it is clear that during summer the average quiet-day value of f_0F2 is higher at stations in the area of the Weddell Sea than at stations at the same geographic latitude in the Ross Sea area, while in winter the reverse is true. During the equinoxes there is much less difference between the average f_0F2 at stations at the same latitude in the two areas. Since Kohl and King's wind model predicts approximately the same wind velocities in summer and winter, it is not clear how such a wind system can account for these differences.

The difference between the Ross Sea and Weddell Sea stations is also evident in Fig. 42 which shows how the average difference in f_0F2 between the two stations Halley Bay and Scott varies with local time. In the upper diagram the average differences, $\overline{\Delta f_0F2}$, between f_0F2 measured at Halley Bay and that measured at Scott at the same local time during December (for the years 1961, 1962, 1964 and 1965) are plotted against local time. The middle diagram shows the average differences during the equinoctial months for these two stations. The lower diagram illustrates the variation of Δv, the average difference in vertical drift velocity between the two stations at the same local time. Fig. 43 shows the same quantities for SANAE and Cape Hallett. These figures both show that the values of f_0F2 at either pair of stations are not very different during the equinoxes (in the case of Halley Bay and Scott the maximum average

difference/...

difference is about 0.7 MHz during the equinoxes compared with about 3.2 MHz during December).

The values of $\overline{\Delta f_0 F2}$ vary approximately sinusoidally with a mean value of about zero during the equinoxes while during December the differences are unevenly distributed about zero (for Halley Bay - Scott they vary from -0.8 MHz to +3.2 MHz). The difference in the time of maximum $\overline{\Delta f_0 F2}$ between equinox and summer is striking. It is not clear how a wind system which causes f_0F2 values at Halley Bay to be <u>smaller</u> than f_0F2 values at Scott at midday in both summer and winter (see Figs. 35 and 36), can also explain why f_0F2 values at Halley Bay are <u>larger</u> than those at Scott at midday during the equinoxes.

To sum up, the following conclusions have become apparent from this analysis:

(i) The differences in f_0F2 values between stations at the same geographic latitude in Antarctica are very much larger in June <u>and</u> December than the differences observed during the equinoxes.

(ii) The maximum difference in f_0F2 between two stations at the same latitude (one in the Weddell Sea area, the other in the Ross Sea area) in summer occurs at a local time corresponding to about 06-07 UT for the Weddell Sea station. The maximum difference in winter occurs at about 06-07 UT for the Ross Sea station. On the other hand during the equinoxes the maximum differences occur at about local midday and midnight and are not dependent on universal time.

(iii) In summer the differences in f_0F2 between any of the pairs of stations are very large in the early hours of the morning but fairly small around midday. During

the/...

the equinoxes the differences around midnight and midday are roughly equal.

(iv) In summer the monthly average quiet-day f_0F2 is larger in the area of the Weddell Sea than in the area of the Ross Sea. In winter the reverse is true, while during the equinoxes the monthly average quiet-day f_0F2 for the two areas is approximately equal.

(v) If the differences in f_0F2 observed in summer are to be accounted for by Kohl and King's[92] wind model then an upward vertical drift must result in an increase of f_0F2 while a downward drift will decrease f_0F2. However, the differences in f_0F2 observed during the equinoxes point to the conclusion that the value of f_0F2 is enhanced by a downward vertical drift and decreased by an upward drift.

These results all point to the conclusion that Kohl and King's simple wind model does not adequately explain the differences in behaviour observed at pairs of Antarctic stations situated at the same latitude.

2.8 EXPLANATION OF THE RESULTS OF THE HARMONIC ANALYSIS

The constant term A_0 of the harmonic analysis (Chapter 1) reaches a maximum twice a year in March/April and September/October during years of high solar activity. This is true for stations in either the Ross Sea or Weddell Sea areas. Since the sun is above the horizon for only half the day during the equinoxes while it remains above the horizon all day during summer, the average production due to solar EUV at F-region heights during the day should be greater in summer than during the equinoxes. If winds are responsible for redistributing ionization in the F-region in such a way that the average value of f_0F2 during the equinoxes is increased, then one

would/...

would expect the average value of f_0F2 during summer to increase too. In fact no wind system could be found which would explain the fact that the average value of f_0F2 during the equinoxes is higher than the average value of f_0F2 during December for all stations near solar maximum.

2.9 SUMMARY AND CONCLUSIONS

In this chapter the effects of vertical drifts produced by horizontal neutral winds have been studied as a possible explanation of the peculiar behaviour of f_0F2 over Antarctic stations. In this connection the following arguments have been discussed and conclusions reached:

(i) The phase of the diurnal variation of wind velocity (as proposed by Kohl and King) at most Antarctic stations is such that a maximum upward vertical drift occurs at about 05-07 UT for these stations. This could explain the diurnal variation of h_mF2 at these stations[83]. It could also account for the 06-07 UT maximum in f_0F2.

(ii) Stations in the Weddell Sea area experience a maximum at about 06-07 UT in summer while stations in the Ross Sea area experience the UT maximum in winter. This could not be accounted for by the wind theory alone.

(iii) The transition period between local-time and UT-controlled behaviour of the ionosphere is often very sharp and occurs at different times for different stations. It is not clear how the wind theory could explain this.

(iv) Winds together with production by solar EUV are not sufficient to account for the magnitudes of observed critical frequencies in winter (King et al[82]). An additional source of ionization, such as particle precipitation, must be included in a solution of the continuity equation if the observed magnitudes of f_0F2

are/...

are to be explained.

(v) There is not yet general agreement that a downward drift velocity decreases the value of F_0F2 while an upward drift increases it. This will be discussed further in the next section. There is also no general agreement about the magnitudes of wind velocities.

(vi) The experimentally measured values of wind velocity obtained at Halley Bay around sunspot maximum and sunspot minimum do not agree with Kohl and King's simple model. The velocities observed at sunspot maximum are so different from the theoretical wind velocities that they could not be responsible for an 06 UT maximum in f_0F2.

(vii) The observed wind velocities fluctuate excessively from hour to hour so that it does not seem likely that they could be responsible for the 06-07 UT maximum in f_0F2 which is a regular and stable feature of the Antarctic ionosphere.

(viii) There does not appear to be any correlation between fluctuations in observed wind velocity and corresponding changes in f_0F2 at Halley Bay.

(ix) Kohl and King show that the horizontal neutral wind velocity during sunspot maximum is about 40 ms^{-1} while during sunspot minimum it is about 150 ms^{-1} (more than three times as large). The observed wind velocities at Halley Bay on the other hand are larger at sunspot maximum than at sunspot minimum.

(x) A comparison of f_0F2 behaviour at several pairs of Antarctic stations with similar geographic latitudes reveals that the equinoctial values of f_0F2 at any local time for a pair of Antarctic stations at the same latitude are very similar. However, values of f_0F2 during June and December are very different. Kohl and King's wind model predicts wind velocities for June and December which are

very/...

very similar to those for the equinoxes.

(xi) If Kohl and King's wind model is to account for differences in f_0F2 observed between two stations at the same geographic latitude in summer, then an upward vertical drift must cause an increase in f_0F2 while a downward drift should decrease f_0F2. However, differences in f_0F2 observed during the equinoxes point to the opposite conclusion, viz. that the value of f_0F2 is enhanced by a downward vertical drift and decreased by an upward drift.

(xii) In summer the monthly average quiet-day f_0F2 is larger in the area of the Weddell Sea than in the area of the Ross Sea, while in winter the reverse is true. During the equinoxes the monthly average quiet-day f_0F2 for the two areas is approximately equal. It is not evident how winds might account for this.

(xiii) The constant term A_0 of the harmonic analysis (Chapter 1) has a semi-annual variation during years of sunspot maximum, with maxima at the equinoxes. No wind system could be found to explain this.

The chief conclusions which one may draw from this evidence are that:

(a) the wind velocities observed in practice are very different from those predicted by the simple wind model proposed by Kohl and King.

(b) neither the observed wind velocities nor velocities obtained from the simple theoretical wind model are capable of explaining many facets of the Antarctic f_0F2 behaviour.

Some suggestions for future research are:

(a) An analysis of experimentally measured wind velocities

over/...

over a number of Antarctic stations - when more stations take such measurements.

(b) A detailed investigation of the methods used to calculate winds theoretically is called for, if only to obtain agreement about the magnitude and effect of horizontal neutral winds.

(c) Measurements of f_0F2 are required at intermediate points between the stations used in this analysis. This will enable more detailed f_0F2 maps to be drawn up and will yield more precise information concerning the area which is under UT control and how this varies with time.

(d) The comparison of f_0F2 values at pairs of Antarctic stations could be extended to include pairs of Arctic stations at similar geographic latitudes. Since the UT behaviour in the Arctic is much less pronounced than in the Antarctic, the comparison may provide useful information about the effects of horizontal neutral winds.

(e) The analysis of Challinor and Eccles[20] on vertical drift velocities at a latitude 45° South could be carried out for stations at 70° South to see whether the same results are true.

CHAPTER 3

THE EFFECTS OF TEMPERATURE AND NEUTRAL ATMOSPHERIC DENSITY ON PRODUCTION AND LOSS IN THE IONOSPHERE

3.1 INTRODUCTION

The second possible mechanism for explaining the Antarctic f_0F2 behaviour is based on the suggestion by Torr and Torr[160] that the early-morning maximum in f_0F2 observed at SANAE during summer could be accounted for by the temperature-dependent balance of the production and loss terms in the continuity equation. In this chapter the method is reviewed and evidence against it is examined.

Also considered here is the semi-annual variation of neutral atmospheric density observed by King-Hele and Walker[89] and others. Although this has no connection with the UT behaviour of f_0F2, it may be related to the variation in the monthly quiet-day average value of f_0F2 (A_0 in the harmonic analysis of Chapter 1) which also has a semi-annual variation during months of high solar activity.

3.2 TORR AND TORR'S EXPLANATION

3.2.1 DIURNAL BEHAVIOUR OF f_0F2

The suggestion which Torr and Torr have put forward to explain the summertime early morning maximum of f_0F2 at SANAE may be understood by means of the following simplified argument. If the transport term is neglected, the continuity equation for electrons in the

F-region/...

FIGURE 44

Copy of Torr and Torr's[160] Fig. 2.

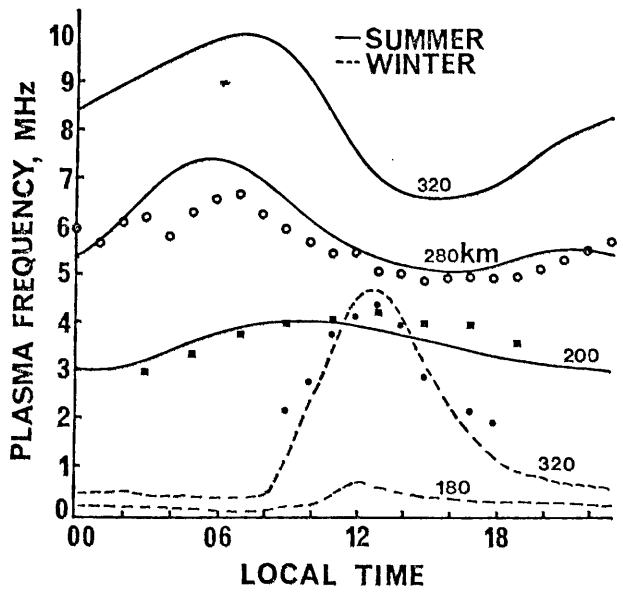

FIG. 2

Theoretical diurnal variation of plasma frequency at fixed heights at SANAE for January 1963 and June 1962. Also shown are median values of f_0F_2 (0) and f_0F_1 (■) for January 1963 and f_0F_2 for June 1962 (⊛).

F-region of the ionosphere may be written in the approximate form

$$\frac{\partial N}{\partial t} = q - \gamma n(N_2)N \qquad (3.1)$$

Since the sun is permanently above the horizon during the summer, $\frac{\partial N}{\partial t}$ is always negligible and we may write equation (3.1) in the form

$$N = \frac{q}{\gamma n(N_2)}$$

where q is the electron production rate due to photoionization, γ is a rate constant roughly independent of temperature and $n(N_2)$ and N the number densities of nitrogen molecules and electrons respectively. At midnight N has some value depending on the ratio $\frac{q}{\gamma n(N_2)}$; $\gamma n(N_2)$ is determined by the exospheric temperature, which is relatively low at this time. During the early morning the temperature increases. Initially q increases faster than $\gamma n(N_2)$ so that N increases correspondingly. By about 08 LMT the rate of increase of $\gamma n(N_2)$ overtakes that of q, so that N decreases after this time until late in the afternoon, when the rate of decrease of $\gamma n(N_2)$ falls below that of q and N begins to increase again after about 16 LMT.

The result for a station at latitude 70^{o} South has been calculated by Torr and Torr and is shown in Fig. 44.

3.2.2 SEASONAL BEHAVIOUR OF AVERAGE f_0F2

The argument just outlined may be extended to explain the equinoctial maxima in A_0 (from the harmonic analysis of Chapter 1) as follows. During winter, temperatures are low and production and loss rates are small. As summer approaches the average production due

to/...

to solar EUV increases as does the temperature. If the average value of q were to increase at a faster rate than $\gamma n(N_2)$ at the end of winter and then, as the temperature increased further, $\gamma n(N_2)$ were to increase more rapidly than q as summer approached, it might be found that during the equinoxes the average electron density was a maximum.

3.3 DRAWBACKS OF TORR AND TORR'S THEORY

The ideas expounded in section 3.2 are dependent on several basic assumptions. To begin with the figures given by Torr and Torr were based on the CIRA[24] model atmosphere 3. In this model the ratio of day-time maximum to night-time minimum exospheric temperatures is 1.5, whereas Jacchia[72] and Jacchia and Slowey[73] have shown that the ratio is unlikely to exceed 1.3. In addition, the CIRA model is only intended to apply to middle latitudes; Jacchia's model on the other hand, includes a factor which takes account of variation with latitude. The maximum value of the exospheric temperature at SANAE during the summer day considered by Torr and Torr is 830 K according to Jacchia's model (which agrees with satellite measurements[140, 121]) but 1184 K for the CIRA model 3 atmosphere. With the lower temperature predicted by Jacchia, the loss rate will not increase as rapidly and will not produce the same summer behaviour as that predicted by Torr and Torr. This problem is considered further in the next section where solutions of the continuity equation are discussed.

Furthermore, since no longitude-dependent term appears in the continuity equation solved by Torr and Torr, the solution which they obtained ought to be

independent/...

Figure 45

A comparison of the quiet-day average diurnal behaviour of f_oF2 (in MHz) during December 1963 at four stations situated at approximately 70°S geographic latitude: SANAE (70.3°S), Wilkes (66.3°S), Mawson (67.6°S) and Cape Hallett (72.3°S).

SANAE

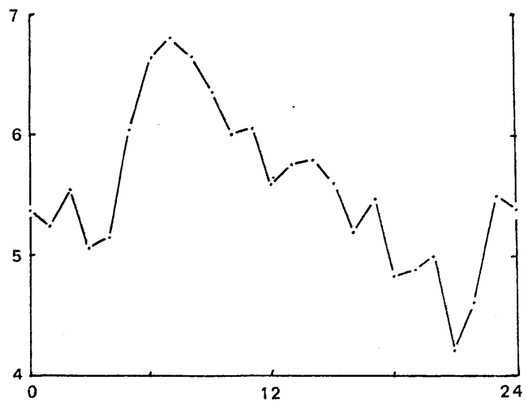

Wilkes

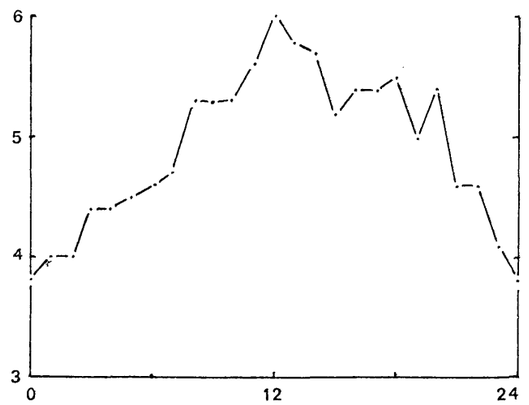

Mawson

Cape Hallett

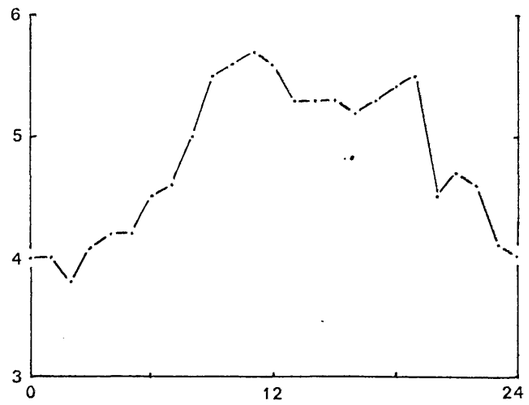

independent of longitude and the 08 LMT maximum which they predict for SANAE should be observed at all stations at about 70°S during the summer. This is certainly not the case at Cape Hallett, Mawson or Wilkes (as can be seen from Fig. 45).

Not only is the solution obtained by Torr and Torr independent of longitude, but it is also not restricted to the southern hemisphere. The behaviour of f_0F2 which they predict for any station at a latitude 70°S in December, applies also to any station at a latitude 70°N in June. However, stations situated near 70°N do not show this 08 LMT maximum either.

Thus since the 07-08 LMT maximum is not present at stations other than SANAE, but an 06-07 UT maximum is present at other stations in Antarctica, it seems reasonable to associate the behaviour at SANAE with the generally observed UT phenomenon rather than to try and explain the behaviour on a local time basis as an isolated instance.

Another aspect of the Antarctic f_0F2 behaviour is the sharp transition between local time control and UT control (see section 1.6). This transition often takes place within a few days and occurs at approximately the same date each year for a given station. However, the production due to solar EUV and the temperature at any height vary very slowly during the year and there does not seem to be any reason why either or both of these two quantities should suddenly undergo a large change within a period of a few days at a set time each year. Moreover, the order in which the changeover from LT to UT-controlled behaviour occurs for stations in the Weddell Sea area (viz. Halley Bay-Port Lockroy-SANAE) does

not/...

not appear to be related to geographic latitude.

The monthly average quiet-day f_0F2 (A_0) is larger at stations in the Weddell Sea area during summer than at stations at the same latitude in the area of the Ross Sea. In winter the reverse is true. During the equinoxes A_0 for the two areas is approximately equal. However, the temperature theory as presented by Torr and Torr is not dependent on longitude and, therefore, predicts the same monthly average f_0F2 for stations at the same latitude in Antarctica during summer.

3.4 THE SEMI-ANNUAL VARIATION OF NEUTRAL ATMOSPHERIC DENSITY

The semi-annual variation of air density, originally established by Paetzold[111] from the orbit of Sputnik 3 during the period 1958-60, has since been confirmed by many workers[87, 88, 85, 167, 168]. King-Hele and Hingston[86] observed a semi-annual variation of air density at 191 km during 1966-67 from an analysis of the orbit of the satellite Secor 6 (1966-51B). Maximum densities were observed in October 1966 and April 1967, minimum densities in July 1966 and January 1967. King-Hele and Walker[89] observed a similar variation at heights between 160 and 190 km for the period July 1968 to September 1969 from the orbit of the satellite A.T.S.2. Maximum densities occurred at the end of October 1968 and in March 1969, minima in July 1968, January 1969 and July 1969.

The semi-annual variation is also noticeable at intermediate and great heights. Cook[26] analysed the orbits of 5 satellites and found a semi-annual variation in air density at heights between 300 and 500 km during

1967-68/...

1967-68 while Cook and Scott[27] and Cook[25] found a distinct semi-annual variation at heights near 1100 km between 1964 and January 1967 and from 1967 to 1968 respectively using the orbit of Echo 2.

The dependence of the semi-annual variation of density on the level of solar activity has been investigated by several workers. Cook and Scott[27] showed that the magnitude of the semi-annual variation, measured by the ratio $\left(\frac{\text{maximum density}}{\text{minimum density}}\right)$, appears to increase with increasing solar activity, while Cook[25] suggests that there is no definite dependence of the semi-annual variation on the level of solar activity.

Thus, viewed in the light of explaining the semi-annual variation of the monthly average quiet-day f_oF2, A_0, the semi-annual variation of air density will have an effect on the production rate, the loss rate and the diffusion rate at any given height. The nett effect on the elctron density at F-region heights may be visualized if an increase in air density is assumed to be caused by an increase in exospheric temperature (since this should produce roughly the same effect). With this assumption the semi-annual variation of density may be regarded as a semi-annual variation of temperature with maxima in March-April and October and minima in January and July.

Since there is no semi-annual variation of 10.7cm solar flux, this variation of temperature must be regarded as being independent of the 10.7cm solar flux. In this case an increase in temperature would not be accompanied by an increase in I_{max} (see section 5.3) and from the results of section 6.3, the temperature maxima in March-April and October should be associated with <u>minimum</u> values of A_0, unless the increase in

temperature/...

temperature during these months is associated with an increase in electron and ion production (for example, by precipitation of trapped particles). This case will be considered in the next Chapter.

3.5 CONCLUSIONS

It is generally accepted that the early morning maximum in f_oF2 in the Weddell Sea area occurs at about 06-07 UT during summer and the cause of the phenomenon is probably the same for all stations in this area. Torr and Torr have suggested a mechanism which might explain the f_oF2 behaviour at SANAE, but which cannot explain behaviour at Halley Bay or Port Lockroy. This mechanism which might explain behaviour at SANAE predicts an 08 LMT maximum in f_oF2 for all stations at a latitude of 70^oS or N. In fact this is not observed. It does not account for differences between average f_oF2 behaviour at Weddell and Ross Sea stations, nor does it explain the rapid transition between local time and universal time control of the ionosphere. In general it is unlikely that this mechanism can account for Antarctic f_oF2 behaviour.

The semi-annual variation of neutral atmospheric density is considered as a possible explanation of the semi-annual variation of A_0 during years of high solar activity. However, unless the increased atmospheric density at the equinoxes is accompanied by an increase in particle precipitation, the variation of A_0 cannot be accounted for.

The effect of particles

An aurora observed at SANAE during 1968

CHAPTER 4

PARTICLE PRECIPITATION IN THE ANTARCTIC IONOSPHERE

4.1 INTRODUCTION

A low-energy electron influx has been suggested by several workers as a possible explanation of such ionospheric problems as the high observed values of electron density as compared with those calculated from laboratory measured reaction rates (Torr and Torr[163]), the maintenance of the night-time ionosphere (Ivanov-Kholodny[70]) and the winter anomaly (Maehlum[97]). Similar suggestions have been put forward to explain the anomalous behaviour of f_0F2 over Antarctica. For example, Duncan[37] suggested that dumping of particles (due to oscillations set up by the transport of the eccentric geomagnetic field through the interplanetary plasma) could explain the UT variation of f_0F2 in Antarctica.

To determine whether particles are in fact being precipitated in sufficient quantities at about 06-07 UT to explain the observed variation in f_0F2, one would require satellite measurements of low-energy particle fluxes over Antarctic stations. Unfortunately very little data of this type are available. For this reason no analysis of particle data could be conducted and this chapter merely reviews the idea of particle precipitation as a possible cause of Antarctic f_0F2 behaviour.

4.2 THE DIURNAL BEHAVIOUR OF f_0F2

4.2.1 THE/...

4.2.1 THE NECESSITY OF PARTICLES

As mentioned in Chapter 2, King et al[82] solved the continuity equation and the equation of motion of the neutral atmosphere simultaneously for several Antarctic stations. They found that in order to explain the observed magnitudes of f_0F2 in winter, it is necessary to include an additional source of ionization, such as particle precipitation.

A similar conclusion was reached by Keating and Prior[79] who, from an analysis of neutral atmospheric densities derived from the orbits of the Explorer XIX and Explorer XXIV satellites, found that the atmospheric densities observed around the northern polar region in winter were higher than the densities predicted by Jacchia's empirical model[71]. They suggest that heating due to particle precipitation in winter may be responsible for this.

Rothwell[129] analysed electron concentrations at heights between 400 and 1200 km and found a pronounced maximum in observed electron densities at about 07 UT in the southern hemisphere during local winter and a smaller maximum at about 20 UT in the northern hemisphere during local summer (unfortunately her analysis did not include observations for the southern hemisphere during summer, nor the northern hemisphere during winter). She proposed that the effect is due to precipitation of particles, particularly at heights just above the F2 layer.

Stuart and Titheridge[142] used satellite observations to analyse the small-scale variations of electron content in the Antarctic ionosphere. They noticed that the irregularities increased throughout most of the Antarctic at about 04 UT in winter at sunspot minimum. At sunspot maximum the degree of irregularity

shows/...

shows a peak near 06 UT in winter. This increase in the irregularity of the ionosphere they ascribe to a highly ionized region above the normal F-layer, which in turn they attribute to the soft zone of precipitating electrons.

4.2.2 OBSERVATIONS OF PARTICLES

Several analyses have been performed on low-energy electron fluxes in the northern polar region. Maehlum[98] discovered that a UT variation is present in the low-energy electron fluxes in the northern polar exosphere during summer and that these fluxes reach a maximum at about 18-20 UT. This result supports Rothwell's suggestion (see section 4.2.1). Thomas and Andrews[153] (and Andrews and Thomas[3]) analysed satellite data for the northern hemisphere and found that maximum electron density enhancements due to particle precipitation occur between 19 and 21 UT during winter as well.

Both Schield and Frank[133] and Sharp et al[137] have measured large fluxes of ~~the~~ low-energy electrons in the polar regions and from their results Torr and Torr[166] have suggested that there is an almost permanent corpuscular enhancement at SANAE.

Burch[18] found that a region of low-energy electron fluxes (50eV to 10keV) exists in the polar regions in both northern and southern hemispheres near magnetic local noon and midnight (see Fig. 46). Pike[115] compared F-layer electron densities for the southern polar region with low energy electron flux measurements obtained by Burch[18] and found that the variations in f_0F2 between different stations in Antarctica might be

explained/...

Figure 46

Copy of Figure 9 in the paper by Thomas and Andrews[153], showing the positions of magnetic noon and magnetic midnight.

FIGURE 46

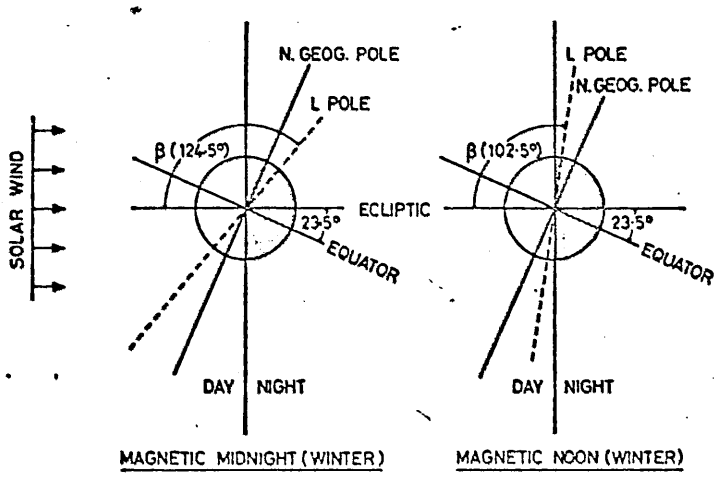

FIG. 9. SCHEMATIC DIAGRAM SHOWING MAGNETIC NOON AND MIDNIGHT AND THE CORRESPONDING VALUE OF THE ANGLE β BETWEEN THE GEOMAGNETIC AXIS AND THE EARTH–SUN LINE.

explained qualitatively by the effects of the observed low-energy electron fluxes. He suggested that the UT control of the F-layer in winter is due to precipitation of low-energy electron fluxes and that such precipitation reaches a maximum between 2 to 4 hours after local noon at the corrected geomagnetic pole (i.e. 2 to 4 hours after 04 UT). Present satellite measurements do not, however, account for the UT control in the Weddell Sea area in summer, although this may be caused by particle precipitation too[115].

4.2.3 THE PARTICLE EXPLANATION

If enhanced particle precipitation does occur at about 06 UT in the Ross Sea area in winter, this could certainly explain the maximum in f_0F2 observed at about this time at stations in this area. It could also account for the fact that the monthly average quiet-day f_0F2 (A_0) is larger at stations in the Ross Sea area than at stations at the same geographic latitude in the Weddell Sea area in winter. Furthermore, since the enhanced precipitation at this time appears to result from the geometrical configuration of the Earth's magnetic field in relation to the solar wind[153], it is possible that there may be a rapid transition (over a period of a few days, say) between normal "background" precipitation (where no noticeable enhancement is present) and a state in which particle precipitation is enhanced at about 06 UT. In this case one would expect the transition from normal "background" precipitation to "enhanced" precipitation and the reverse transition to be symmetrical about the June solstice.

If enhanced particle precipitation occurs in the

Weddell/...

Weddell Sea area at about 06 UT in summer, this could account for

(a) the maximum in f_0F2 observed at stations in this area at about this time;

(b) the sharp transition between local time and UT-controlled behaviour of f_0F2;

(c) the fact that the date for the transition between LT and UT control and the date for the reverse transition are symmetrical about the December solstice;

(d) the fact that the monthly average quiet-day values of f_0F2 at stations in the Weddell Sea area are larger than at stations at the same latitude in the Ross Sea area; and

(e) the results of the analysis comparing the behaviour of f_0F2 at pairs of Antarctic stations at the same geographic latitude (section 2.7).

Assuming that during the equinoxes the tilt of the earth's magnetic field with respect to the solar wind is such that there is no enhancement of low-energy electron fluxes at 06 UT in either region, then if the effects of horizontal neutral winds are small (as suggested in section 2.6), one might expect that average quiet-day f_0F2 values for stations at the same geographic latitude in the two regions would be similar. This agrees with results obtained in section 2.7.

4.3 THE SEASONAL BEHAVIOUR OF f_0F2

The semi-annual variation of the monthly average quiet-day f_0F2 during years of high solar activity (obtained from the harmonic analysis described in Chapter 1) could also be accounted for by precipitation of low-energy

particles/...

particles (the "background" precipitation mentioned in section 4.2.3) Bartels[6, 7] has shown that a semi-annual variation in geomagnetic activity is present with maxima about the equinoxes and Knecht[90] and Duncan[37] have pointed out that corpuscular radiation reaches a maximum at the same time. Kühn[94] has discovered that more riometer absorption events occur at SANAE in the equinoctial months than at any other time of the year, which might well signify more precipitation of particles in these months.

Boller and Stolov[14] associate the semi-annual variation of geomagnetic activity with the semi-annual variation in the Kelvin-Helmholtz instability along the flanks of the magnetosphere. The latter has maximum instability during the equinoxes which, it is suggested, may be the cause of the increased geomagnetic activity at this time. This could also account for a semi-annual variation in the low-energy electron fluxes which are precipitated (normal "background" precipitation) in the polar regions. During the solstices the Kelvin-Helmholtz instability has a UT variation in which maximum instability is reached at about 0430 UT in June (i.e. there is a maximum likelihood of particles entering the magnetosphere at this time), while during December the probability of instability is smaller and has a maximum at about 1630 UT. This may explain the enhancements in low-energy particle fluxes observed by Maehlum[98], Thomas and Andrews[153] and Burch[18].

Another thing which may be relevant is the fact that the semi-annual variation of A_o only becomes noticeable when the sunspot number exceeds 100 (i.e.

between/...

between July 1957 and December 1960). In this way it is similar to the winter spur phenomenon (also only observed when the sunspot number is greater than 100). This latter phenomenon is thought to be caused by precipitated electrons (Thomas[152]).

4.4 CONCLUSIONS

It is generally accepted that low-energy electron fluxes are precipitated in the northern and southern polar regions of the ionosphere. Several workers have found a UT variation in these fluxes which could account for the UT behaviour of f_0F2.

A simple model which assumes that enhanced precipitation of fluxes occurs at about 06 UT in the Ross Sea area during winter and a separate enhanced precipitation of fluxes occurs at about 06 UT in the Weddell Sea area in summer, may account for all aspects of the UT phenomenon (cf. results for wind theory - section 2.9). The semi-annual variation of the monthly average quiet-day f_0F2 during years of high solar activity could also be accounted for by a semi-annual variation of "background" particle precipitation.

However, justification for this simple model can only be obtained by conducting a detailed analysis on observed low-energy particle fluxes in the two regions.

PART III

SIMULATING THE ANTARCTIC IONOSPHERE

CHAPTER 5

SOLVING THE CONTINUITY EQUATION

5.1 INTRODUCTION

The idea of simulation, i.e. the construction of a mathematical model of a situation or process and the subsequent solution of the mathematical equations as functions of time to see how the model behaves, has for many years been applied to the ionosphere in the form of the continuity equation. This equation has been written in many different forms and solved by many different methods. Although a complete solution to this equation which will account for the observed data in detail, has not yet been found, much has been learnt regarding the part played by the different terms of the equation and their influence on the behaviour of the electron density.

In its most general form, the equation is

$$\frac{\partial N_i}{\partial t} = q_i - L_i - \mathrm{div}(N\bar{v})_i \qquad (5.1)$$

where q_i = production of i^{th} ion species (due to photoionization by solar EUV, to charge-exchange processes or to ionization from precipitated particles),

L_i = loss of i^{th} ion species by chemical processes (charge-exchange, dissociative recombination, etc.),

$\bar{v}$ = effective velocity of i^{th} ion species, and

$\mathrm{div}(N\bar{v})_i$ = effect of transport of i^{th} ion species (including mechanisms such as ambipolar diffusion, vertical drifts caused by horizontal neutral winds, electric fields, etc.).

The/...

The simplest approach to solving this equation, which was used by most workers until quite recently, is based on the assumption that, since O^+ is virtually the only ion species present at F-region heights, the other ion species can be ignored. In this case the continuity equation reduces to a single equation

$$\frac{\partial [O^+]}{\partial t} = q_{O^+} - L_{O^+} - \text{div}(N\bar{v})_{O^+} \qquad (5.2)$$

The earlier solutions to this equation neglected the effects of winds, electric fields and precipitated particles so that q_{O^+} represents production due to photoionization by solar EUV and $\text{div}(N\bar{v})_{O^+}$ represents transport due to ambipolar diffusion. The loss functions, L_{O^+}, which were used, were fairly simple. For example, Gliddon and Kendall[55] used a function of the form

$$L = KN$$

where K is a constant and N the electron (or ion) density; Rishbeth[122] used

$$L = KN \exp(-k \int_{h_o}^{h} \frac{dh}{H})$$

while Bailey et al[4] have as their loss function

$$L = KN \exp(-1.75(\frac{h - 180}{H}))$$

The effect of horizontal neutral winds on the behaviour of the F2 peak was first investigated by Rishbeth[123, 124] who used values of wind velocity calculated by Geisler[182, 183]. Kohl and King[92] calculated numerical values of the wind velocity and included these pre-calculated values in their solution of the continuity equation. However, both treatments of the problem suffer from the drawback that the wind equations are solved independently of the continuity equation whereas in fact the value of the horizontal

neutral/...

neutral wind velocity depends considerably on the ion density (Kohl and King[92]).

Stubbe[144] overcame the problem by solving the continuity equation and the equations of motion of the neutral atmosphere "simultaneously". Since then Kohl, King and Eccles[93] and Torr and Torr[161, 164] have used this same approach. Stubbe also included the effects of a horizontal electric field of the order of 5 to 10 V/km in order to explain the night-time behaviour of the ionosphere over Lindau/Harz.

A more comprehensive solution to the ionospheric continuity equation should, however, take account of the behaviour of all the important ion species in the height range under consideration. Thus instead of solving only the continuity equation for O^+ ions, several equations of the form demonstrated in equation (5.1) must be solved simultaneously. This has been done by Torr and Torr[161] and Stubbe[146].

Torr and Torr[161] also include a term to take account of production of ionization by corpuscular radiation. Their analysis is devoted solely to explaining the behaviour of the F2 layer over SANAE in January 1963. Although they manage to account for the behaviour of N_mF2, they fail to achieve a suitable behaviour for h_mF2.

The non-equilibrium between ion and electron temperatures, T_i and T_e, has recently been considered to play an important role in determining F-region electron densities. Thomas and Venables[150] solved the continuity equation for $T_e \neq T_i$ and since then several workers have included the non-equilibrium terms in the continuity equation. Herman and Chandra[63] and Chandra

and/...

and Herman[22] solved the coupled differential equations for heat conduction for electrons, ions and neutral gas together with the continuity equation for electrons and obtained solutions (T_e, T_i, T and N) which are in rough agreement with observation. Stubbe[146] incorporated this idea into a general solution which takes account of four ion species. He solved simultaneously the four ion continuity equations, four heat conduction equations (electrons, neutral gas and O^+ and H^+ ions) and the equations of motion of the neutral atmosphere, this time neglecting the effect of electric fields. He shows results for Lindau/Harz (52^oN) during equinox.

In the present analysis an attempt was made (in 1966) to solve the set of four continuity equations for O^+, O_2^+, N_2^+ and NO^+ ions without taking into account the effects of horizontal neutral winds. The computer used was an ICL 1301 with 800 words of core store. However, since this small memory was used to store data, program instructions and subroutines (all floating point arithmetic was done by software), the remaining data, program instructions and subroutines not in use being stored on a drum store, this made the execution of the program extremely slow. Although much was done to reduce the execution time (including writing large sections of the program in machine code), a complete solution for a 24-hour period was never obtained. This was partly due to the fact that the step-length used was small - less than one minute - but the main problem was the enormous amount of time which had to be wasted on transferring program instructions and data to and from the drum store.

At the end of 1969 Rhodes University acquired a 1901A computer with 16K words of core store and hardware

facilities/...

facilities for performing floating point arithmetic. This made the solution of the set of continuity equations possible even with the small step-length of less than one minute. The method was then modified and a step-length of 5 minutes was found to give sufficient accuracy. The computer time required for integrating the equations over a 24-hour period by this method is about 5 hours. The effect of winds has also been included.

5.2 ASSUMPTIONS CONCERNING THE ATMOSPHERIC MODEL

Before one can set about solving the continuity equation, certain basic assumptions must be made concerning the composition and temperature of the neutral atmosphere and the ion constituents. Until several years ago fairly drastic assumptions were made, such as an isothermal atmosphere consisting only of O and N_2 and having a single ion species O^+. Recently, however, solutions have become more general. The following assumptions have been made in the present analysis:

5.2.1 CONSTITUENTS OF NEUTRAL ATMOSPHERE

The neutral atmosphere was assumed to consist of four constituents O, O_2, N_2 and NO. Of these O, O_2 and N_2 were assumed to be in diffusive equilibrium above a height of 120 km, i.e. they each independently obey the barometric law

$$n_i = n_{io} \frac{T_o}{T} \exp\left(-\int_{h_o}^{h} \frac{dh}{H_i}\right) \qquad (5.3)$$

where n_i = number density of particles (species i) at height h,

T = neutral/...

T = neutral gas temperature at height h ,

n_{io} = number density at a reference height h_o (h_o = 120 km),

T_o = temperature at reference height,

H_i = scale height of species $i = \frac{kT}{m_i g}$

and m_i = mass of single atom or molecule of species i.

The number densities at 120 km, n_{io} , are those given by Jacchia[71] , viz.

$$n_o(O) = 7.6 \times 10^{10} \text{ cm}^{-3} ,$$

$$n_o(O_2) = 7.5 \times 10^{10} \text{ cm}^{-3} ,$$

$$n_o(N_2) = 4.0 \times 10^{11} \text{ cm}^{-3} .$$

The number density of NO at any height was determined using the approximation suggested by Mitra[104] , viz.

$$n(NO) = 0.4 \exp\left\{\frac{-3700}{T}\right\} n(O_2) + 5 \times 10^{-7} n(O)$$

5.2.2 TEMPERATURE OF THE NEUTRAL ATMOSPHERE

Jacchia[71] has shown that the time dependent temperature models of Harris and Priester[181] can be very closely approximated by an exponential distribution. Similarly Torr[159] demonstrated the very good fit obtained when an exponential distribution is fitted to CIRA (1965)[24] data. Thus, following Jacchia[71], the distribution of temperature with height in the neutral atmosphere has here been assumed to be exponential and of the form

$$T = T_\infty - (T_\infty - T_o) \exp\left[-s(h - h_o)\right] \qquad (5.4)$$

where T_∞ is the exospheric temperature ,

T_o is the temperature at the reference level h_o ,

$s = 0.0291 \exp(-0.5x^2)$

and $$x = \frac{T_\infty - 800}{750 + 1.722 \times 10^{-4}(T_\infty - 800)^2}$$

The/...

The temperature at the reference level (h_o = 120 km) was assumed to be T_o = 355 K (Harris and Priester[181]; Jacchia[71]). The exospheric temperature, T_∞, depends on a number of factors such as latitude, time of day, average 10.7 cm solar flux, etc. Once again Jacchia's model has been used since it predicts values which (at least where observations are available) are in better agreement with observed data than the values predicted by CIRA[24] (Jacchia[72]). Hence for average quiet geomagnetic conditions (Jacchia[71]; Jacchia and Slowey[74])

$$T_\infty = T'(1 + R\sin^m\theta)(1 + R\frac{\cos^m\eta - \sin^m\theta}{1 + R\sin^m\theta}\cos^n\frac{\tau}{2}) \quad (5.5)$$

where $\tau = H + \beta + p\sin(H + \gamma)$,

H = hour angle of the sun (= 0 at local noon),

$\theta = \frac{1}{2}|\phi + \delta|$,

$\eta = \frac{1}{2}|\phi - \delta|$,

ϕ = geographic latitude,

δ = declination of the sun,

$$T' = 418 + 3.60\overline{F}_{10.7} + 1.8(F_{10.7} - \overline{F}_{10.7}) + (0.37 + 0.14\sin 2\pi\frac{d-151}{365})\overline{F}_{10.7}\sin 4\pi\frac{d-59}{365},$$

d = number of days from January 1,

$F_{10.7}$ = 10.7 cm solar flux,

$\overline{F}_{10.7}$ = 10.7 cm solar flux smoothed over 5 months,

R, m, n, β, γ and p are constants.

The values used for the constants were

$R = 0.28$

$n = 2.5$

$\beta = -45^o$

$p = 12^o$

$\gamma = 45^o$

and $m = 1.25$ (Jacchia and Slowey[74]).

The/...

The assumption of an exponential temperature distribution of the form

$$T = T_\infty - Be^{-C(h-120)}$$

makes it possible to obtain an explicit solution to the barometric law, equation (5.3), governing the neutral number density distribution. From equation (5.3),

$$n_i = n_{io} \frac{T_o}{T} \exp\left(- \int_{120}^{h} \frac{dh}{H_i}\right)$$

and

$$\int_{120}^{h} \frac{dh}{H_i} = \frac{m_i g}{k} \int_{120}^{h} \frac{dh}{T}$$

$$= \frac{m_i g}{k} \int_{120}^{h} \frac{dh}{T_\infty - Be^{-C(h-120)}}$$

By changing variable ($h' = h - 120$), this reduces to a standard integral, the solution to which is

$$\frac{m_i g}{k} \left[\frac{1}{T_\infty} \left(h - 120 + \frac{1}{B} \ln \frac{T}{T_o}\right)\right]$$

Thus equation (5.3) becomes

$$n_i = n_{io} \frac{T_o}{T} \exp\left(- \frac{\left(h - 120 + \frac{1}{B} \ln \frac{T}{T_o}\right)}{H_{i\infty}}\right) \qquad (5.6)$$

where

$$H_{i\infty} = \frac{kT_\infty}{m_i g}$$

5.2.3 ION CONSTITUENTS

Four ion species have been considered in this analysis : O^+, O_2^+, N_2^+ and NO^+. Since each ion species can be regarded as being controlled by its own separate continuity equation, equation (5.1) becomes a set of four interrelated equations

/...

$$\begin{aligned}
\frac{\partial n(O^+)}{\partial t} &= q_{O^+} - L_{O^+} - \mathrm{div}(N\bar{v})_{O^+} \\
\frac{\partial n(O_2^+)}{\partial t} &= q_{O_2^+} - L_{O_2^+} - \mathrm{div}(N\bar{v})_{O_2^+} \\
\frac{\partial n(N_2^+)}{\partial t} &= q_{N_2^+} - L_{N_2^+} - \mathrm{div}(N\bar{v})_{N_2^+} \\
\frac{\partial n(NO^+)}{\partial t} &= q_{NO^+} - L_{NO^+} - \mathrm{div}(N\bar{v})_{NO^+}
\end{aligned} \qquad (5.7)$$

The percentage distribution of these ions with height was assumed to be similar in form to those measured by Johnson et al[76], Taylor and Brinton[149] and Istomin[69]. From this assumption a further simplification can be made. Since the diffusion term is only significant at F-region heights and since at these heights there is very little O_2^+, N_2^+ or NO^+, the diffusion term can be left out of the continuity equations for these ions. Thus equations (5.7) become

$$\begin{aligned}
\frac{\partial n(O^+)}{\partial t} &= q_{O^+} - L_{O^+} - \mathrm{div}(N\bar{v})_{O^+} \\
\frac{\partial n(O_2^+)}{\partial t} &= q_{O_2^+} - L_{O_2^+} \\
\frac{\partial n(N_2^+)}{\partial t} &= q_{N_2^+} - L_{N_2^+} \\
\frac{\partial n(NO^+)}{\partial t} &= q_{NO^+} - L_{NO^+}
\end{aligned} \qquad (5.8)$$

Finally, electrical neutrality was assumed, i.e. at any height

$$N_e = n(O^+) + n(O_2^+) + n(N_2^+) + n(NO^+)$$

5.2.4 ION AND ELECTRON TEMPERATURES

The ion temperature, T_i, at any height was assumed to be the same for all ion species and to be

equal/...

equal to the neutral gas temperature, T, at that height. Since solutions of the continuity equation were only obtained for summer conditions in Antarctica, the problem of sunrise effects is eliminated and hence the above assumption is probably a good one.

The electron temperature, T_e, was assumed to be equal to the ion temperature, T_i, (i.e. the ratio $\tau = \frac{T_e}{T_i} = 1$) at heights of 120 and 800 km (Geisler and Bowhill[51]). At intermediate heights values of τ obtained by Evans[180] at Millstone Hill (43°N) were used, since he has obtained measurements of τ throughout the day for several days at different times of year.

5.3 THE PRODUCTION TERM

The only source of ionization which will be considered here is photoionization due to solar ultra-violet radiation. The rate of production of the i^{th} ion species by this mechanism (Rishbeth and Garriott[127]) is given by

$$q_i = \sum_{\lambda} \sigma'_{i\lambda}\, n_i I_{\infty\lambda} \exp\left\{ -\sum_{j} \sigma_{j\lambda} n_j H_j Ch(\chi, j) \right\} \qquad (5.9)$$

where $\sigma'_{i\lambda}$ = ionization cross-section of i^{th} atmospheric constituent,

$\sigma_{j\lambda}$ = absorption cross-section of j^{th} atmospheric constituent,

χ = solar zenith angle,

$Ch(\chi, j)$ = Chapman function for j^{th} atmospheric constituent,

H_j = scale height of j^{th} constituent

and $I_{\infty\lambda}$ = intensity of ionizing radiation of frequency λ beyond the atmosphere.

The values of the absorption and photoionization

cross-sections/...

cross-sections and of $I_{\infty\lambda}$ used here were taken from Watanabe and Hinteregger[172], Hinteregger and Watanabe[67], Hall et al[60] and Hinteregger et al[66]. The solar flux data ($I_{\infty\lambda}$) refer to low solar activity but since the purpose of the simulation is to explain the behaviour of the Antarctic ionosphere at solar minimum, this is in order.

5.4 THE LOSS TERM

The simplest forms of the loss term are those suggested by Gliddon and Kendall[55]

$$L = KN ,$$

by Ratcliffe[118]

$$L = \frac{\alpha\beta N^2}{\beta + \alpha N}$$

and by Kohl and King[92]

$$L = 8 \times 10^{-13} n(N_2) N$$

However, a more realistic loss rate is obtained when the individual ion species present in the ionosphere are considered separately. The following are regarded as being the most important reactions governing the ion concentrations in the F-region.

(1) $O^+ + N_2 \xrightarrow{k_1} NO^+ + N$

(2) $O^+ + O_2 \xrightarrow{k_2} O_2^+ + O$

(3) $N_2^+ + O \xrightarrow{k_3} NO^+ + N$

(4) $O_2^+ + NO \xrightarrow{k_4} NO^+ + O_2$

(5) $N_2^+ + O_2 \xrightarrow{k_5} O_2^+ + N_2$

(6) $O_2^+ + e^- \xrightarrow{\alpha_1} O' + O''$

(7) $N_2^+ + e^- \xrightarrow{\alpha_2} N' + N''$

(8) $NO^+ + e^- \xrightarrow{\alpha_3} N + O$

Thus/...

Thus the loss terms in equations (5.8) become

$$-L_{O^+} = -\left[k_1 n(N_2) + k_2 n(O_2)\right] n(O^+)$$

$$-L_{O_2^+} = -\left[k_4 n(NO) + \alpha_1 N\right] n(O_2^+) + k_2 n(O_2) n(O^+) + k_5 n(O_2) n(N_2^+)$$

$$-L_{N_2^+} = -\left[k_3 n(O) + k_5 n(O_2) + \alpha_2 N\right] n(N_2^+)$$

$$-L_{NO^+} = -\alpha_3 N n(NO^+) + k_1 n(N_2) n(O^+) + k_3 n(O) n(N_2^+) + k_4 n(NO) n(O_2^+) \quad (5.10)$$

5.4.1 THE REACTION RATES

For many years there was much uncertainty about the values of the rate constants, and as recently as 1965, Nicolet[107] gave the rate constants of reactions (1) and (2) as $10^{-12\pm1}$ $cm^3 s^{-1}$. In the past few years, however, more consistent results have been obtained and the values of the constants at 300 K are now known to within a factor of about two (Ferguson[46]). One problem which is still outstanding is the dependence of these reaction rates on temperature. This is due partly to the lack of data at temperatures other than 300 K.

Different methods which have been employed to measure the reaction rates include the steady-state afterglow flow technique used by Fehsenfeld et al[43, 42], Ferguson et al[47] and Goldan et al[56], the transient afterglow method developed by Dickinson and Sayers[33] and modified by Copsey et al[28] and the photoionization mass spectrometer used by Warneck[169]. In the tables which follow, reaction rates obtained from laboratory measurements are denoted by an L while those deduced from ionospheric composition data are signified by an I. Values derived theoretically or from the work of

others/...

TABLE 17

Some Values of the Rate Constant k_1

VALUE OF RATE CONSTANT	TEMP.	OBTAINED BY	LAB. OR IONOSPHERE
$4.7(\pm 0.5)\times10^{-12}$ $cm^3\ s^{-1}$	300 K	Langstroth and Hasted [95]	L
$\leq 6.75\times10^{-12}$	300 K	Talrose et al [148]	L
2×10^{-12}		Whitten and Popoff [173]	I
$3\ (\pm 1) \times 10^{-12}$	~ 300 K	Fehsenfeld et al [44]	L
4×10^{-12}		Donahue [34]	I
$2.4(\pm 0.4)\times10^{-12}$	300 K	Copsey et al [28]	L
3.72×10^{-12}	300 K	Nakshbandi and Hasted [106]	L
7×10^{-12}	~ 550 K	Bohme et al [13]	L
$4.6(\pm 1.1)\times10^{-12}$	700 -1400 K	Warneck [169,171]	L
1.8×10^{-12}	300 K	Schmeltekopf et al [134]	L
$1.3(\pm 0.2)\times10^{-12}$	300 K	Schmeltekopf et al [135]	L
1.2×10^{-12}	300 K	Dunkin et al [39]	L

others are denoted by a blank in the rightmost column of each table.

k_1: Values of k_1 obtained by different workers are shown in Table 17. Schmeltekopf et al[134, 135] have shown that early measurements of this reaction rate obtained from stationary afterglows gave values which were too large. This is because N_2 is vibrationally excited when it is discharged and this greatly increases the value of k_1. Thus the values obtained by Fehsenfeld et al[44] (3×10^{-12} cm^3s^{-1}), Copsey et al[28] (2.4×10^{-12} cm^3s^{-1}) and Warneck[169, 171] (4.6×10^{-12} cm^3s^{-1}) are probably too high and the actual value at 300 K should be less than 2×10^{-12} cm^3s^{-1} as suggested by Schmeltekopf et al[134, 135] and Dunkin et al[39].

The temperature dependence of this rate coefficient is very uncertain. Apparently the only three groups of workers who have measured its value at different temperatures are Nakshbandi and Hasted[106], Warneck[169, 171] and Dunkin et al[39]. The results obtained by these three groups are somewhat confusing. Nakshbandi and Hasted found that k_1 increases slightly with increasing temperature, Warneck maintained that it remains constant (at least for temperatures between 700 K and 1400 K) and Dunkin et al showed clearly that the rate coefficient decreases with increasing temperature. Stubbe[145] attempted to explain the results theoretically but these discrepancies made it almost impossible to draw any general conclusions about this reaction rate. If Dunkin's measurements are reliable (6×10^{-13} cm^3s^{-1} at 600 K), Stubbe has shown that k_1 has a value between 5×10^{-13} and 7×10^{-13} cm^3s^{-1} for F-region temperatures and does not vary very much with temperature in the

range/...

TABLE 18.

Measured Values of the Rate constant k_2

VALUE OF RATE CONSTANT	TEMP.	OBTAINED BY	LAB. OR IONOSPHERE
$2.5(\pm 0.4)\times 10^{-11}$ $cm^3\ s^{-1}$	~300 K	Dickinson and Sayers [33]	L
2×10^{-11}		Whitten and Popoff [173]	I
$4(\pm 1)\times 10^{-11}$	~300 K	Fehsenfeld et al [43]	L
$1.64(\pm 0.05)\times 10^{-11}$	292 K	Batey et al [8]	L
$2.0(^{+0.4}_{-0.3}) \times 10^{-11}$	300 K	Copsey et al [28]	L
4×10^{-11}		Donahue [34]	I
1.69×10^{-11}	300 K	Nakshbandi and Hasted [106]	L
2×10^{-11}	~550 K	Bohme et al [13]	L
$2.0(\pm 0.5) \times 10^{-11}$	300 K	Warneck [169, 171]	L
2.6×10^{-11}	300 K	Schmeltekopf et al, unpublished results (Ferguson [46])	L
$2.1(\pm 0.1) \times 10^{-11}$	300 K	Smith and Fouracre [138]	L
2×10^{-11}	300 K	Dunkin et al [39]	L
2.0×10^{-11}	300 K	Schmeltekopf et al [135]	L
1.9×10^{-11}	300 K	Stubbe [145]	

range 600-2000 K. Thus Stubbe[146] used the value 5×10^{-13} cm^3s^{-1} independent of temperature for this rate constant in his solution of the continuity equation.

Ghosh[52] has suggested the form

$$k_1 = 4.2 \times 10^{-12} \exp(-\frac{470}{RT})$$

This corresponds to a value of 2×10^{-12} cm^3s^{-1} at 300 K and also does not vary very much with temperature in the range 700 - 2000 K. Torr and Torr[164] have used this form in their solution of the continuity equation. However, for a temperature of 1200 K this rate constant is almost six times larger than that suggested by Stubbe. Rishbeth et al[128] use the value 6×10^{-13} cm^3s^{-1} independent of temperature while Rüster[130] has used the same form as that employed by Stubbe.

The constant value 5×10^{-13} cm^3s^{-1} has been used in this present analysis, although the form suggested by Ghosh has also been tried and its effect is commented on in section 6.2.

k_2: The values determined for this rate constant at about 300 K are in much closer agreement than the values for k_1, and they are shown in Table 18. In this case there is little doubt that the value of k_2 at 300 K is about 2×10^{-11} cm^3s^{-1}. Batey et al[8] and Smith and Fouracre[138] have obtained a $T^{-0.5}$ dependence on temperature for temperatures in the range 185 to 576 K while values obtained by Dunkin et al[39] in the range 300 to 600 K are in very good agreement with these observations. Nakshbandi and Hasted[106] also investigated the effect of temperature (in the range 77 - 375 K) and their results are in fair agreement with the results of the others. However, there are still different opinions as to the behaviour of k_2 at higher temperatures.

Smith/...

Smith and Fouracre have suggested that the rate constant is represented by a function of the form

$$k_2 = 3.4(\pm 0.5) \times 10^{-10}\ T^{-(0.48\pm0.05)}$$

which decreases with increasing temperature and Torr and Torr[164] have used this form, i.e.

$$k_2 = 3.4 \times 10^{-10}/\sqrt{T} \qquad (5.11)$$

Stubbe[145], however, has studied the dependence of this rate coefficient on temperature from a theoretical point of view using the collision theory approach. He finds that for temperatures above 750 K the variation with temperature is almost linear and can be approximately described by

$$k_2 = 1.1 \times 10^{-11}\ (1 + \frac{T}{1660}) \qquad (5.12)$$

which <u>increases</u> with increasing temperature. At a temperature of 1000 K, the difference between the values predicted by these two formulae is not very large (k_2 = 1.0 x 10^{-11} cm^3s^{-1} and 1.76 x 10^{-11} cm^3s^{-1} respectively). Rishbeth et al[128] use a constant value of 1.3 x 10^{-11} cm^3s^{-1} independent of temperature for this reaction rate.

All three forms of the coefficient were tried.

k_3: Values are given in Table 19.

Unfortunately there have been very few determinations of the value of this reaction rate. Three laboratory measurements of its value at 300 K are shown in the table; and nothing is known about its dependence on temperature. Ghosh[52] has suggested the form

$$k_3 = 1.0 \times 10^{-7} \exp\ (-\frac{3560}{RT})$$

which was adopted by Torr and Torr[164]. This corresponds to a value of 2.5 x 10^{-10} cm^3s^{-1} at 300 K. Stubbe[146]

and/...

TABLE 19

Values of the Rate Constant k_3

VALUE OF RATE CONSTANT	TEMP.	OBTAINED BY	LAB. OR IONOSPHERE
$2.5(\pm 1) \times 10^{-10}$ $cm^3\ s^{-1}$	~300 K	Fehsenfeld et al [45]	L
$2.5(\pm 1) \times 10^{-10}$	300 K	Ferguson et al [47]	L
5×10^{-10}		Donahue [34]	I
2.5×10^{-10}	300 K	Ghosh [52]	
1.4×10^{-10}	300 K	Fehsenfeld et al [42]	L

TABLE 20

Values of the Coefficient k_4

VALUE OF RATE CONSTANT	TEMP.	OBTAINED BY	LAB. OR IONOSPHERE
8×10^{-10} $cm^3\ s^{-1}$	300 K	Ferguson et al [48]	I
$8(+2, -5) \times 10^{-10}$	300 K	Goldan et al [56]	L
$7.7(\pm 1.5) \times 10^{-10}$	300 K	Warneck [169]	L
8×10^{-10}	300 K	Wolf and Turner [176]	L
8×10^{-10}	300 K	Ghosh [52]	
$6.3 \times 10^{-10}(\pm 30\%)$	300 K	Fehsenfeld et al [42]	L
8×10^{-10}	300 K	Monro [105]	

T A B L E 21

Values of the Coefficient k_5

VALUE OF RATE CONSTANT	TEMP.	OBTAINED BY	LAB. OR IONOSPHERE
2×10^{-10} cm^3 s^{-1}	300 K	Fite et al [50]	L
2×10^{-10}		Whitten and Popoff [173]	I
2.0×10^{-10}		Ferguson et al [48]	I
$1.0(\pm 0.5) \times 10^{-10}$	~300 K	Fehsenfeld et al [45]	L
2×10^{-10}		Donahue [34]	I
$1.0(+0.2,-0.6) \times 10^{-10}$	300 'K	Goldan et al [56]	L
4.9×10^{-10}	~300 K	Shahin [136]	L
$1.07(\pm 0.2) \times 10^{-10}$	300 'K	Warneck [169,170]	L
7.8×10^{-11}	300 K	Golden et al [57]	L
4.7×10^{-11}	300 K	Dunkin et al [39]	L

and Rüster[130] use the value 2.5×10^{-10} cm^3s^{-1} independent of temperature. In this analysis the value 2.0×10^{-10} cm^3s^{-1} independent of temperature has been used (since the most recent measurement suggests a lower value than 2.5×10^{-10} cm^3s^{-1}).

k_4 and k_5: These reactions are of less importance and have not been considered by Torr and Torr. However, for the sake of completeness they have been included in this present study. Tables 20 and 21 contain values of these constants at 300 K.

Wolf and Turner[176] have suggested that k_4 is approximately independent of temperature (increasing from 8.0×10^{-10} cm^3s^{-1} at 300 K to 8.5×10^{-10} cm^3s^{-1} at 1200 K) and Stebbings et al[141] have shown that k_5 also varies very little with temperature (1.0×10^{-10} cm^3s^{-1} at 300 K to 1.1×10^{-10} cm^3s^{-1} at 1500 K). Besides these there has been no further investigation into the temperature dependence of either coefficient.

The value of k_4 at 300 K is usually taken to be 8×10^{-10} cm^3s^{-1}. This value was used in this analysis (independent of temperature). In the case of the constant k_5, once again, with the exception of Shahin's[136] determination, the values obtained recently are lower than the earlier determinations. A value of 1×10^{-10} cm^3s^{-1} independent of temperature was used in this analysis.

α_1: From Table 22, the value of this coefficient at 300 K is about 2.0×10^{-7} cm^3s^{-1}. Swider[147], Donahue[34] and Norton et al[109] have suggested that from ion composition data, this coefficient should vary as T_e^{-1}. Kasner and Biondi[78] arrived at the same conclusion from

laboratory/...

TABLE 22

Values of Recombination Coefficient α_1

VALUE OF RATE CONSTANT	TEMP.	OBTAINED BY	LAB. OR IONOSPHERE
2×10^{-7} $cm^3 s^{-1}$		Norton et al[109]	I
1×10^{-7}		Swider[147]	I
2×10^{-7}		Nicolet[107]	I
1.2×10^{-7}		Donahue[34]	I
$1.7(\pm 1) \times 10^{-7}$	300 K	Biondi[12]	L
$2.2(\pm 0.4) \times 10^{-7}$	300 K	Chan[21]	L
$2.2(\pm 0.2) \times 10^{-7}$	295 K	Kasner and Biondi[78]	L
$2.1(\pm 0.3) \times 10^{-7}$	295 K	Smith and Goodall[139]	L
2×10^{-7}	300 K	Mitra[104]	
$1.95(\pm 0.2) \times 10^{-7}$	300 K	Mehr and Biondi[101]	L

TABLE 23

Values of Recombination Coefficient α_2

VALUE OF RATE CONSTANT	TEMP.	OBTAINED BY	LAB. OR IONOSPHERE
$4.0(\pm 0.3) \times 10^{-7}$ $cm^3 s^{-1}$	400 K	Faire and Champion[41]	L
1.2×10^{-7}	300 K	Mentzoni[102]	L
2.0×10^{-6}	295 K	Hackam[59]	L
$2.7(\pm 0.3) \times 10^{-7}$	300 K	Kasner[77]	L
$2.9(\pm 0.3) \times 10^{-7}$	300 K	Biondi[12]	L
3×10^{-7}	300 K	Ghosh[52]	
3×10^{-7}	300 K	Mitra[104]	
$1.8(^{+0.4}_{-0.2}) \times 10^{-7}$	300 K	Mehr and Biondi[101]	L

laboratory measurements. However, Smith and Goodall[139] favour a $T_e^{-0.5}$ dependence for temperatures in the range 300 to 630 K. They show that this gives good agreement not only with their observations but also with those of Mentzoni, and Kasner and Biondi[78]. Mehr and Biondi[101], on the other hand, find that this reaction rate varies with $T_e^{-0.70}$ over the range 300 K $\leqslant T_e \leqslant$ 1200 K. Since the $T_e^{-0.7}$ dependence is suitably intermediate and cannot be very far wrong, this was selected for this analysis, with the rate coefficient starting at a value 2.0×10^{-7} cm^3s^{-1} at 300 K. Thus

$$\alpha_1 = 2.0 \times 10^{-7}\left(\frac{300}{T_e}\right)^{0.7} = 1.08 \times 10^{-5} T_e^{-0.7}$$

is the form of the recombination coefficient for O^+ ions which was used. At 1000 K this yields a value 0.86×10^{-7} cm^3s^{-1} as compared with the values 1.09×10^{-7} cm^3s^{-1} and 0.6×10^{-7} cm^3s^{-1} which the $T^{-0.5}$ and T^{-1} models predict.

α_2: Values are shown in Table 23. Ignoring Hackam's[59] very high value, the laboratory measurements of this reaction rate at 300 K lie in the range 1.2×10^{-7} to 2.9×10^{-7} cm^3s^{-1}. Ghosh[52] and Mitra[104] have suggested the value 3×10^{-7} cm^3s^{-1} independent of temperature which seems a little high in view of the laboratory results. However, if one takes into account the slight temperature dependence of α_2, this approximation may be quite good.

Donahue[34] suggested that α_2 varies with $T_e^{-0.2}$. Kasner[77] found no significant temperature dependence over the temperature range 205 to 480 K while Mehr and Biondi[101] have shown that this recombination coefficient varies as $T_e^{-0.39}$ over the range 300 K $\leqslant T_e \leqslant$ 5000 K.

From/...

TABLE 24

Values of the Recombination Coefficient for NO^+, α_3

VALUE OF REACTION RATE	TEMP.	OBTAINED BY	LAB. OR IONOSPHERE
3×10^{-7} $cm^3 s^{-1}$		Norton et al[109]	I
5×10^{-7}		Nicolet[107]	I
$4.6(^{+0.5}_{-1.3}) \times 10^{-7}$	298 K	Gunton and Shaw[58]	L
5×10^{-7}		Donahue[34]	I
$5(\pm 2) \times 10^{-7}$	300 K	Young and St.John[179]	L
$5(\pm 1) \times 10^{-7}$	300 K	Biondi[12]	L
$4.5(^{+3.5}_{-1.9}) \times 10^{-7}$	300 K	Mentzoni and Donohoe[103]	L
3.5×10^{-7}	300 K	Ghosh[52]	
1 to 4 x 10^{-7}		Mitra[104]	

From their results α_2 should have a value of about 2.6×10^{-7} cm^3s^{-1} at 750 K and about 3.2×10^{-7} cm^3s^{-1} at 1500 K.

In view of this the value 3×10^{-7} cm^3s^{-1} independent of temperature was used in this solution of the continuity equation.

α_3: In this case both laboratory measurements of this coefficient at 300 K and estimates from ionospheric data (shown in Table 24) point to the value 5×10^{-7} cm^3s^{-1}. However, Torr and Torr[160] deduced the value 3.5×10^{-7} cm^3s^{-1} for this coefficient at 300 K from data given by Whitten and Popoff[173], and Stubbe[146] and Rüster[130] used a formula which yields the value 2.9×10^{-7} cm^3s^{-1} at 300 K.

Norton et al[109] have suggested that this coefficient has a $\frac{1}{T_e}$ dependence on temperature while Donahue[34] proposed a $T_e^{-1.4\pm0.1}$ dependence. From laboratory measurements, Gunton and Shaw[58] obtained the dependence on temperature as $T_e^{-1.2}$. This latter dependence was also suggested by Mitra[104].

The form used by Stubbe[146] and Rüster[130] for this recombination coefficient was that due to Whitten and Popoff[174], viz.

$$\alpha_3 = 4.7 \times 10^{-8}\left(\frac{1000}{T_e}\right)^{1.5} \qquad (5.13)$$

while Torr and Torr[160] used the function

$$\alpha_3 = \frac{1.16 \times 10^{-4}}{T_e} - 3.7 \times 10^{-8} \qquad (5.14)$$

Both of these functions were tried in this analysis. Besides these a function of the form

$$\alpha_3 = 5 \times 10^{-7}\left(\frac{300}{T_e}\right)^{1.2} \qquad (5.15)$$

was also tried. This function yields the value 5×10^{-7} cm^3s^{-1} at 300 K and is thus in agreement with

measured/...

measured values of this coefficient.

5.5 THE TRANSPORT TERM

The two chief mechanisms responsible for the motion of ions and electrons up or down magnetic field lines are ambipolar diffusion and drifts caused by horizontal neutral winds. The transport term of the continuity equation is thus

$$-\mathrm{div}(N\bar{v}) = -\frac{\partial}{\partial h}(Nv_D) - \frac{\partial}{\partial h}(Nv_W) \qquad (5.16)$$

where v_D = vertical drift velocity due to ambipolar diffusion ,

v_W = vertical drift velocity due to horizontal neutral winds

(see Appendix 10).

5.5.1 AMBIPOLAR DIFFUSION

The simplest form of the ambipolar diffusion term is that for an isothermal atmosphere consisting of atomic oxygen with $T_e = T_i$. In this case (see Appendix 10)

$$v_D = -D'\sin^2 I\left[\frac{1}{N}\frac{\partial N}{\partial h} + \frac{1}{H(O)}\right]$$

and

$$-\frac{\partial}{\partial h}(Nv_D) = D'\sin^2 I\left\{\frac{\partial^2 N}{\partial h^2} + \frac{3}{2H(O)}\frac{\partial N}{\partial h} + \frac{N}{2H(O)^2}\right\} \qquad (5.17)$$

where D = ambipolar diffusion coefficient

and H(O)= scale height of atomic oxygen.

This form was used in most of the early solutions and even in some more recent ones (e.g. Kohl and King[92]). If the atmosphere is not assumed to be isothermal, the vertical drift due to ambipolar diffusion is given by

/...

$$v_D = -D'\sin^2 I \left[\frac{1}{N}\frac{\partial N}{\partial h} + \frac{1}{T}\frac{\partial T}{\partial h} + \frac{1}{H(O)} \right]$$

and the diffusion term is

$$-\frac{\partial}{\partial h}(Nv_D) = D'\sin^2 I \left\{ \frac{\partial^2 N}{\partial h^2} + \left[\frac{5}{2T}\frac{\partial T}{\partial h} + \frac{3}{2H} \right] \frac{\partial N}{\partial h} + N \left[\frac{1}{2T^2}\left(\frac{\partial T}{\partial h}\right)^2 + \frac{7}{4HT}\frac{\partial T}{\partial h} + \frac{1}{T}\frac{\partial^2 T}{\partial h^2} + \frac{1}{2H^2} - \frac{1}{2H^2}\frac{\partial H}{\partial h} \right] \right\} \tag{5.18}$$

as was used by Torr[159] (Case 1). However, this is still based on the assumption that $T_e = T_i$. The most general form of the diffusion term (for diffusion in an atmosphere consisting only of atomic oxygen and for which $T_e \neq T_i$) is

$$v_D = -D\sin^2 I(1+\tau) \left[\frac{1}{N}\frac{\partial N}{\partial h} + \frac{1}{T}\frac{\partial T}{\partial h} + \frac{1}{(1+\tau)}\frac{\partial \tau}{\partial h} + \frac{1}{(1+\tau)H} \right]$$

and

$$-\frac{\partial}{\partial h}(Nv_D) = D\sin^2 I \left\{ (1+\tau)\frac{\partial^2 N}{\partial h^2} + \left[(1+\tau)\left(\frac{5}{2T}\frac{\partial T}{\partial h} + \frac{1}{H}\right) + \left(2\frac{\partial \tau}{\partial h} + \frac{1}{H}\right) \right] \frac{\partial N}{\partial h} + \left[\frac{(1+\tau)}{T} \left\{ \frac{1}{2T}\left(\frac{\partial T}{\partial h}\right)^2 + \frac{1}{H}\frac{\partial T}{\partial h} + \frac{\partial^2 T}{\partial h^2} \right\} + \frac{\partial T}{\partial h}\frac{1}{2T}\left(\frac{3}{H} + 5\frac{\partial \tau}{\partial h}\right) + \frac{1}{H}\left(\frac{\partial \tau}{\partial h} + \frac{1}{H}\right) - \frac{1}{H^2}\frac{\partial H}{\partial h} \right] N \right\} \tag{5.19}$$

which was the form used by Torr and Torr[161].

If one considers an atmosphere consisting of more than one neutral constituent - say atomic oxygen and molecular nitrogen - the simplest form for the diffusion velocity for a non-isothermal atmosphere is

$$v_D = -D'\sin^2 I \left[\frac{1}{N}\frac{\partial N}{\partial h} + \frac{1}{T}\frac{\partial T}{\partial h} + \frac{\mu}{H_i} \right]$$

and the diffusion term becomes

/...

$$-\frac{\partial}{\partial h}(Nv_D) = D\sin^2 I\left\{\frac{\partial^2 N}{\partial h^2} + \frac{\partial N}{\partial h}\left[\frac{5}{2T}\frac{\partial T}{\partial h} + \frac{1}{n}\left(\frac{n(O)}{H(O)} + \frac{n(N_2)}{H(N_2)}\right) + \frac{\mu}{H_i'}\right]\right.$$
$$+ N\left[\frac{1}{2T^2}\left(\frac{\partial T}{\partial h}\right)^2 + \frac{1}{T}\frac{\partial^2 T}{\partial h^2} + \frac{1}{nT}\left(\frac{n(O)}{H(O)} + \frac{n(N_2)}{H(N_2)}\right)\frac{\partial T}{\partial h}\right.$$
$$+ \frac{\mu}{2nH_i'}\left(\frac{n(O)}{H(O)} + \frac{n(N_2)}{H(N_2)}\right) + \frac{1}{4H_i'T}\frac{\partial T}{\partial h} - \frac{\mu}{H_i'(h+R_E)}$$
$$\left.\left. + \frac{1}{2H_i}\frac{\partial \mu}{\partial h}\right]\right\} \qquad (5.20)$$

where $\mu = \dfrac{m(O^+)}{2\left(\dfrac{m(O)n(O) + m(N_2)n(N_2)}{n(O) + n(N_2)}\right)}$.

This is similar to Torr's[159] case 2, except that Torr considered more than two components. Stubbe[144] used the formula

$$-\frac{\partial}{\partial h}(Nv_D) = D\sin^2 I\left\{(1+\tau)\frac{\partial^2 N}{\partial h^2} + \frac{\partial N}{\partial h}\left[\frac{1}{H_i} + (1+\tau)\left(\frac{p}{H_i} + \frac{3}{T}\frac{\partial T}{\partial h}\right)\right]\right.$$
$$\left. + N\left[\frac{p}{H_i^2} + \frac{1}{H_i T}\frac{\partial T}{\partial h} - \frac{2}{(R_E+h)H_i} + (1+\tau)\frac{p}{H_i T}\frac{\partial T}{\partial h}\right]\right\} \qquad (5.21)$$

where $p = \dfrac{n(O) + 2.496\, n(N_2)}{n(O) + 1.426\, n(N_2)}$

for diffusion in a non-isothermal atmosphere consisting of atomic oxygen and molecular nitrogen with $T_e \neq T_i$.

Torr[159] found that there was no significant difference between the solutions obtained using the diffusion term for an atmosphere consisting entirely of atomic oxygen and the results for a 4-component neutral atmosphere. Besides this there does not appear to have been any other investigation into the effects of the different forms of the diffusion term. An attempt has therefore been made (see Chapter 6) to investigate the effect of using different diffusion terms.

5.5.2 HORIZONTAL/...

5.5.2 HORIZONTAL NEUTRAL WINDS

Since Kohl and King[92] proposed that the inclusion of the effects of horizontal neutral winds into the continuity equation could explain the anomalous behaviour of f_oF2 observed at Port Lockroy and other Antarctic stations, several workers[1, 4, 128, 164, 146] have solved the continuity equation with the transport term due to winds. Stubbe[144] suggested that, instead of simply inserting the neutral gas velocity numerically into the continuity equation, the continuity equation and the equation of motion of the neutral atmosphere ought to be solved simultaneously since the neutral gas velocity depends on the electron concentration.

The equation of motion (in the N-S direction) of the neutral atmosphere (see Appendix 10) is:

$$\frac{\partial U}{\partial t} = -\frac{1}{\rho}\frac{\partial p}{\partial x} + \zeta\frac{\partial^2 U}{\partial x^2} + \frac{Nm_i\nu_i}{N_n m_n}\times$$

$$\left\{\cos I\sin I\left[W - D(1+\tau)\left(\frac{1}{N}\frac{\partial N}{\partial h} + \frac{1}{T}\frac{\partial T}{\partial h} + \frac{1}{H_i(1+\tau)}\right)\right] - U\sin^2 I\right\} \qquad (5.22)$$

where ζ = kinematic viscosity = $\frac{\eta}{\rho}$,

η = coefficient of viscosity = $3.34 \times 10^{-6} T^{0.71}$ (Dalgarno and Smith[32]),

ρ = neutral atmospheric density,

$\frac{\nu_i}{N_n}$ = $4.6 \times 10^{-11} T^{0.4}$ (Dalgarno[31]),

U = horizontal component of velocity of neutral air,

W = vertical component of velocity of neutral air

and $\frac{\partial p}{\partial x}$ = pressure gradient of the neutral atmosphere in the N-S direction, calculated from Jacchia's[71] temperature model assuming that p is directly proportional to T.

Vertical/...

Vertical drifts due to electric fields have been neglected (see Appendices 10 and 11).

The wind term in the continuity equation is

$$-\frac{\partial}{\partial h}(Nv_W) = -\frac{\partial N}{\partial h}(W\sin^2 I + U\sin I\cos I)$$
$$- N\left(\frac{\partial W}{\partial h}\sin^2 I + \frac{\partial U}{\partial h}\sin I\cos I\right) \qquad (5.23)$$

Thus it can be seen that the two equations are interdependent. Stubbe's[144] method of solving the pair of equations "simultaneously" was used in this analysis.

5.5.3 THE DIFFUSION COEFFICIENT

Measured values for the diffusion coefficient,

$$D_a = \frac{kT}{m\nu} ,$$

have been obtained by Knof et al[91] and these are in fairly good agreement with the theoretically predicted values of Ferraro[49], Cowling (see Dalgarno[30]) and Dalgarno[31]. The means of these values at different temperatures are shown in Table 25.

TEMPERATURE	MEAN DIFF. COEFF. x n
300 K	$3.1\ (\pm 0.5) \times 10^{18} cm^{-1}s^{-1}$
400 K	$3.86(\pm 0.5) \times 10^{18} cm^{-1}s^{-1}$
500 K	$4.4\ (\pm 0.4) \times 10^{18} cm^{-1}s^{-1}$
700 K	$5.8\ (\pm 0.3) \times 10^{18} cm^{-1}s^{-1}$
1000 K	$7.8\ (\pm 0.9) \times 10^{18} cm^{-1}s^{-1}$

TABLE 25. n x (mean diffusion coefficient obtained by several workers).

/...

Fitting a function of the form

$$D = \frac{bT^{\frac{1}{2}}}{n} \qquad (5.24)$$

to these values, the best value of b is found to be 2.1×10^{17} $cm^{-1}s^{-1}$ $K^{-\frac{1}{2}}$. This is very close to the form of the diffusion coefficient used by King, Kohl and Eccles, viz.

$$D = \frac{2.2 \times 10^{17} T^{0.6}}{[n(0) + 1.4\ n(N_2)]}$$

as well as that used by Thomas and Venables[150], viz.

$$D = \frac{2.26 \times 10^{17} \sqrt{T}}{n(0)}$$

Torr[159], on the other hand, uses the form of the diffusion coefficient given in equation (5.24) but calculates the value of b from

$$b = \frac{3}{8\sigma^2} \left(\frac{k}{\pi m(0)}\right)^{\frac{1}{2}}$$

where $k = 1.38 \times 10^{-16}$ ergs/K,

$m(0) = 2.65 \times 10^{-23}$ grams

and $\sigma = 2.0 \times 10^{-8}$ cm

The value of b in this case is 1.21×10^{18} $cm^{-1}s^{-1}$ $K^{-\frac{1}{2}}$ which is about six times larger than measured values. Torr and Torr[161] have tried both $\sigma = 2.0 \times 10^{-8}$ cm and $\sigma = 6.0 \times 10^{-8}$ cm in their solution. The latter value gives a value of $b = 1.34 \times 10^{17}$ $cm^{-1}s^{-1}$ $K^{-\frac{1}{2}}$ which is much closer to the measured values.

If a function of the form

$$D = \frac{bT}{n} \qquad (5.25)$$

is fitted to the means of the measured values in Table 25, the value of b which results, is $b = 0.90 \times 10^{16}$ $cm^{-1}s^{-1}$ K^{-1}. Stubbe[144] uses this form of the diffusion coefficient with a value of 1.2×10^{16} $cm^{-1}s^{-1}$ K^{-1} for b.

In/...

In this analysis the values which have been used for D are

$$D = \frac{bT}{n}$$

where $b = 0.90 \times 10^{16}$ $cm^{-1}s^{-1}K^{-1}$, and

$$D = \frac{bT^{\frac{1}{2}}}{n}$$

where $b = 2.1 \times 10^{17}$ $cm^{-1}s^{-1}K^{-\frac{1}{2}}$. The effect of setting $b = 1.21 \times 10^{18}$ $cm^{-1}s^{-1}K^{-\frac{1}{2}}$ has also been tried (see section 6.1) but owing to the discrepancy between values of the diffusion coefficient obtained in this way and the measured values of the diffusion coefficient, this value was not used generally.

5.6 THE METHOD OF SOLUTION

The equations to be solved are given in Appendix 11. They consist basically of a set of coupled partial differential equations which express the unknown variables N (electron density or ion densities) and U as functions of each other and of the independent variables h and t.

As mentioned in section 5.5.2, these equations must be solved simultaneously and for this reason, the method suggested by Stubbe[144] was used. In this method one starts with initial profiles for N and U (as functions of height) at time t_o. Both profiles are used to solve the continuity equation(s) to obtain the N(h) profile at time $t_o + \Delta t$. This new N(h) profile is used together with the old U(h) profile for time t_o to solve the equation of motion of the neutral atmosphere. This gives the U(h) profile for time $t_o + \Delta t$, and so on. This can be represented schematically as follows:

/....

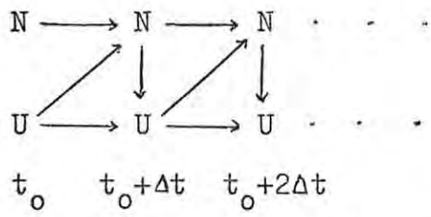

where N represents an N(h) profile, U a U(h) profile. This method has also been adopted by Kohl, King and Eccles[93] and by Torr and Torr[161].

Problems arise when trying to solve the continuity equations and the equation of motion of the neutral atmosphere, since these include partial derivatives with respect to both time and height. Several methods have been used to separate the variables. For example, Stubbe[144] used Lagrange's interpolation formula to replace time derivatives by difference coefficients, viz.

$$\frac{\partial N}{\partial t} = \frac{1}{\Delta t}(1.5N(t) - 2N(t-\Delta t) + 0.5N(t-2\Delta t))$$

The Runge-Kutta method was then used to solve the height-dependent equations. Kohl, King and Eccles[93] employed a simple finite difference technique in which the two basic differential equations were replaced by a system of difference equations. Torr and Torr[161] used the Du Fort-Frankel method, in which, in order to calculate electron density N(1,2), the values N(2,1), N(1,0) and N(0,1) are required, i.e.

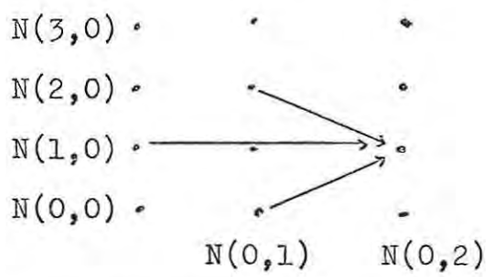

It is interesting to note the time step-length required in each of the solutions. Stubbe found that a step-length, Δt, of 5 minutes gave sufficiently accurate results. Kohl, King and Eccles used a

step/...

step-length of 20 minutes while Torr and Torr required Δt to be 1 to 2 minutes in order to obtain accurate solutions. Bailey et al[4] and Rishbeth et al[128] used a step-length of 5 minutes for their solution (using simple difference quotients) while Abur-Robb and Windle[1], using the Crank-Nicolson technique, found that a step-length of 6 minutes gave sufficient accuracy.

Initially a difference technique was used in this analysis. Newton's backward and central difference formulae were used (to the 12^{th} differences) to obtain expansions for $\frac{\partial N}{\partial h}$ and $\frac{\partial^2 N}{\partial h^2}$. However, it was found that the step-length required for stable solutions using this method was less than 1 minute and the calculation time (on the 1301) was prohibitive.

For this reason different methods were tried. Although these also took too long, the advent of the 1901A Computer at Rhodes University enabled a solution to be obtained. The method used is as follows. Consider the continuity equation for O^+ ions. An initial profile for n_{O+} was calculated for noon (t_o) assuming that $\frac{\partial n_{O+}}{\partial t} = 0$ at this time. Then the values of $\frac{\partial n_{O+}}{\partial t}$ (= 0 initially) and the values of n_{O+} at time t_o, $n_{O+}(t_o)$, are used to solve the height-dependent continuity equation for time $t_o+\Delta t$. The values $n_{O+}(t_o+\Delta t)$ obtained from the solution, provide one with a better estimate for $\frac{\partial n_{O+}}{\partial t}$. Using these new values of $\frac{\partial n_{O+}}{\partial t}$ and the original values of $n_{O+}(t_o)$ one recalculates the values of $n_{O+}(t_o+\Delta t)$. This process is repeated until the desired accuracy is obtained. The final values of $\frac{\partial n_{O+}}{\partial t}$ used to calculate $n_{O+}(t_o+\Delta t)$ are then used as the initial values of $\frac{\partial n_{O+}}{\partial t}$ in the calculation of $n_{O+}(t_o+2\Delta t)$, and so on.

The/...

The Runge-Kutta method was used to solve the height-dependent equation. The step-lengths used in this solution were $\Delta h = 2$ km and $\Delta t = 5$ minutes. Boundary conditions are the same as those used by Stubbe, Kohl et al, etc. At the lower boundary the effect of diffusion is neglected and the neutral gas velocity is assumed to be zero (i.e. $U = 0$). The continuity equation for O^+ thus becomes

$$\frac{\partial n_{O^+}}{\partial t} = q_{O^+} - L_{O^+}$$

At the upper boundary, the rate of change of neutral gas velocity with height is assumed to be zero (i.e. $\frac{\partial U}{\partial h} = 0$) and the O^+ ion density is assumed to be in diffusive equilibrium, i.e. to have a distribution of the form

$$n_{O^+} = n_o e^{-f(h)}$$

(Torr and Torr[161]). The integration was always started at midday and was usually continued to midnight of the following day (i.e. 36 hours in all), thus allowing for the solution to settle down. Time taken for such a solution is about 7 hours. The program was originally written in MAC for the 1301 computer and was converted to EMA and developed further for the 1901A computer. To reduce the volume of output, densities were printed every 4 km instead of every 2 km.

CHAPTER 6

RESULTS OBTAINED FROM CONTINUITY EQUATION SOLUTIONS

The continuity equation has been solved using the parameters (latitude, angle of dip, etc.) for summer conditions at SANAE. Although the analysis is incomplete (for reasons given in section 6.6), these are some of the results which have been obtained thus far.

6.1 THE EFFECT OF THE AMBIPOLAR DIFFUSION TERM

As has been pointed out in section 5.5.1, there is no general agreement as to the form of the ambipolar diffusion term which should be used for solving the continuity equation. Depending on the assumptions one makes, there are various forms which one can use. Torr[159] has compared results obtained using two different terms, and found that there was no significant difference between the two solutions. In this analysis the effects of four different diffusion terms , equations 5.17, 5.18, 5.19 and 5.21 (pages 82, 83 and 84), are compared. The fifth form of the diffusion term (equation 5.20) discussed in section 5.5.1 is not included in this analysis, since Torr has found that the results obtained using this form are not significantly different from those obtained using equation 5.18.

The continuity equation has been solved using each of the aforementioned diffusion terms in turn with the following values for the rate coefficients:

.../..

$$O^+ + N_2 \longrightarrow NO^+ + N \quad : \quad k_1 = 5.0 \times 10^{-13} \qquad cm^3 s^{-1}$$

$$O^+ + O_2 \longrightarrow O_2^+ + O \quad : \quad k_2 = 3.4 \times 10^{-10}/\sqrt{T} \qquad cm^3 s^{-1}$$

$$N_2^+ + O \longrightarrow NO^+ + N \quad : \quad k_3 = 2.0 \times 10^{-10} \qquad cm^3 s^{-1}$$

$$O_2^+ + NO \longrightarrow NO^+ + O_2 \quad : \quad k_4 = 8.0 \times 10^{-10} \qquad cm^3 s^{-1}$$

$$N_2^+ + O_2 \longrightarrow O_2^+ + N_2 \quad : \quad k_5 = 1.0 \times 10^{-10} \qquad cm^3 s^{-1}$$

$$O_2^+ + e^- \longrightarrow O' + O'' \quad : \quad \alpha_1 = 1.08 \times 10^{-5} T_e^{-0.7} \qquad cm^3 s^{-1}$$

$$N_2 + e^- \longrightarrow N' + N'' \quad : \quad \alpha_2 = 3.0 \times 10^{-7} \qquad cm^3 s^{-1}$$

$$NO^+ + e^- \longrightarrow N + O \quad : \quad \alpha_3 = 4.7 \times 10^{-8} \left(\frac{1000}{T_e} \right)^{1.5} \qquad cm^3 s^{-1}$$

Since the diffusion term will affect chiefly the O^+ ion density at about the F2 peak (and, of course, above it), the differences between the effects produced by the four diffusion terms can be seen by comparing the values of f_oF2 obtained in each solution. Thus Tables 26 and 27 contain values of f_oF2 at hourly intervals throughout the day obtained from the respective solutions. From these tables it would appear that if the form of the diffusion term given in equation 5.20 is used, resulting values of f_oF2 are slightly lower (< 0.1 MHz) than those obtained using equations 5.17 or 5.18, while equation 5.19 produces f_oF2 values which are a little higher ($\lesssim 0.1$ MHz).

The height of the F2 peak, h_mF2, varies very little throughout the day (for Antarctic summer conditions) as expected [82] and has an average value of about 270 km for $F_{10.7} \sim 70 - 80 \times 10^{-22} Wm^{-2} Hz^{-1}$ (sunspot minimum) when using diffusion terms 5.17, 5.18 and 5.21, and is about 4km higher when using 5.19. Thus in general it would not seem to make much difference whichever form of the diffusion term is used.

In/...

TABLE 26

Comparison of f_0F2 at each hour of the day calculated by solving the continuity equation for SANAE (summer conditions at sunspot minimum) using four different diffusion terms. $F_{10.7}$ was chosen to be $73 \times 10^{-22} Wm^{-2}Hz^{-1}$ and T_∞ varies from 812 to 855 K.

TIME IN HOURS	f_0F2 OBTAINED USING EQ^N. 5.18	EQ^N. 5.17	EQ^N. 5.19	EQ^N. 5.21
00	4.98	4.99	5.09	4.93
01	5.05	5.07	5.15	4.99
02	5.33	5.34	5.42	5.26
03	5.67	5.69	5.76	5.59
04	5.97	5.99	6.03	5.88
05	6.19	6.20	6.24	6.09
06	6.37	6.38	6.59	6.41
07	6.46	6.47	6.67	6.49
08	6.49	6.51	6.69	6.52
09	6.48	6.50	6.67	6.50
10	6.46	6.48	6.64	6.48
11	6.43	6.45	6.62	6.45
12	6.39	6.41	6.57	6.42
13	6.36	6.37	6.54	6.38
14	6.32	6.34	6.49	6.34
15	6.29	6.30	6.44	6.28
16	6.26	6.27	6.40	6.24
17	6.22	6.23	6.35	6.20
18	6.16	6.17	6.29	6.14
19	6.07	6.09	6.20	6.04
20	5.93	5.95	6.07	5.90
21	5.27	5.74	5.85	5.69
22	5.44	5.46	5.57	5.40
23	5.15	5.16	5.27	5.10

TABLE 27

Comparison of f_oF2 at each hour of the day calculated by solving the continuity equation for SANAE (summer conditions at sunspot minimum) using four different diffusion terms. $F_{10.7}$ was the same as that for Table 26 (viz. 73 x $10^{-22}Wm^{-2}Hz^{-1}$) and T_∞ was increased slightly (varied from 831 to 875 K).

TIME IN HOURS	f_oF2 OBTAINED USING EQ^N. 5.18	EQ^N. 5.17	EQ^N. 5.19	EQ^N. 5.21
00	4.74	4.76	4.84	4.70
01	4.82	4.84	4.91	4.77
02	5.11	5.13	5.20	5.05
03	5.47	5.49	5.55	5.40
04	5.78	5.80	5.84	5.69
05	6.01	6.02	6.05	5.91
06	6.20	6.21	6.41	6.24
07	6.29	6.30	6.49	6.33
08	6.33	6.35	6.52	6.36
09	6.33	6.34	6.50	6.34
10	6.30	6.32	6.47	6.32
11	6.28	6.30	6.45	6.30
12	6.24	6.28	6.41	6.27
13	6.21	6.24	6.38	6.24
14	6.18	6.19	6.34	6.19
15	6.14	6.15	6.28	6.14
16	6.10	6.12	6.24	6.09
17	6.06	6.07	6.19	6.04
18	5.99	6.01	6.12	5.97
19	5,90	5.91	6.02	5.87
20	5.74	5.76	5.87	5.72
21	5.52	5.54	5.64	5.49
22	5.22	5.24	5.34	5.19
23	4.91	4.93	5.03	4.87

TABLE 28

Comparison of f_oF2 values obtained on solving the continuity equation for SANAE (summer conditions at sunspot minimum) using three different forms of the diffusion coefficient :

(a) equation 5.24 with b = $2.1 \times 10^{17} cm^{-1}s^{-1}K^{-\frac{1}{2}}$

(b) equation 5.24 with b = $1.21 \times 10^{18} cm^{-1}s^{-1}K^{-\frac{1}{2}}$

(c) equation 5.25 with b = $0.90 \times 10^{16} cm^{-1}s^{-1}K^{-1}$

TIME IN HOURS	(a)	(b)	(c)
00	4.98	5.13	5.00
01	5.05	5.19	5.07
02	5.33	5.45	5.35
03	5.67	5.79	5.69
04	5.97	6.08	5.99
05	6.19	6.29	6.21
06	6.37	6.46	6.39
07	6.46	6.54	6.47
08	6.49	6.58	6.51
09	6.48	6.57	6.50
10	6.46	6.55	6.47
11	6.43	6.51	6.44
12	6.39	6.46	6.41
13	6.36	6.44	6.37
14	6.32	6.41	6.34
15	6.29	6.38	6.30
16	6.26	6.35	6.27
17	6.22	6.32	6.24
18	6.16	6.27	6.18
19	6.07	6.19	6.09
20	5.93	6.06	5.96
21	5.72	5.86	5.75
22	5.44	5.59	5.47
23	5.15	5.30	5.17

In section 5.5.3 several forms of the ambipolar diffusion coefficient, D, are discussed. To see what effect these different forms may have on a solution of the continuity equation, the latter was solved using the diffusion term given in equation 5.18, the rate coefficients as outlined earlier in this section, and the following values for the diffusion coefficient

(a) equation 5.24 with $b = 2.1 \times 10^{17} cm^{-1}s^{-1}K^{-\frac{1}{2}}$

(b) equation 5.24 with $b = 1.21 \times 10^{18} cm^{-1}s^{-1}K^{-\frac{1}{2}}$

and (c) equation 5.25 with $b = 0.90 \times 10^{16} cm^{-1}s^{-1}K^{-1}$.

The results (hourly values of f_oF2 obtained from the solutions) are shown in Table 28. This shows that cases (a) and (c) above produce almost exactly the same values of f_oF2 , while case (b) (i.e. the diffusion coefficient used by Torr[159] which is very much larger than measured values) gives values of f_oF2 which are slightly larger (approx. .05 to .15 MHz). Thus at least at sunspot minimum the difference is not very significant.

6.2 THE EFFECT OF DIFFERENT LOSS RATES

The value used for k_1 in most of the solutions was $5 \times 10^{-13} cm^3 s^{-1}$, independent of temperature. However, the form suggested by Ghosh[52] for k_1, viz.

$$k_1 = 4.2 \times 10^{-12} \exp\left(\frac{-470}{RT}\right) cm^3 s^{-1} \qquad (6.1)$$

was also tried. This gives rise to a much larger loss rate for O^+ ions, and the values of f_oF2 which are obtained from such solutions are much smaller (about 2 MHz less than f_oF2 values obtained using $k_1 = 5 \times 10^{-13} cm^3 s^{-1}$). Since there is a strong argument in favour of using the value $5 \times 10^{-13} cm^3 s^{-1}$ for k_1, (see Section 5.4.1) and

since/...

Figure 47

Values of f_oF2 obtained on solving the continuity equation for various values of k_2:

(a) $k_2 = 3.4 \times 10^{-10}/\sqrt{T}$ cm^3s^{-1},

(b) $k_2 = 1.1 \times 10^{-11}(1 + \frac{T}{1660})$ cm^3s^{-1}

and (c) $k_2 = 1.3 \times 10^{-11}$ cm^3s^{-1}.

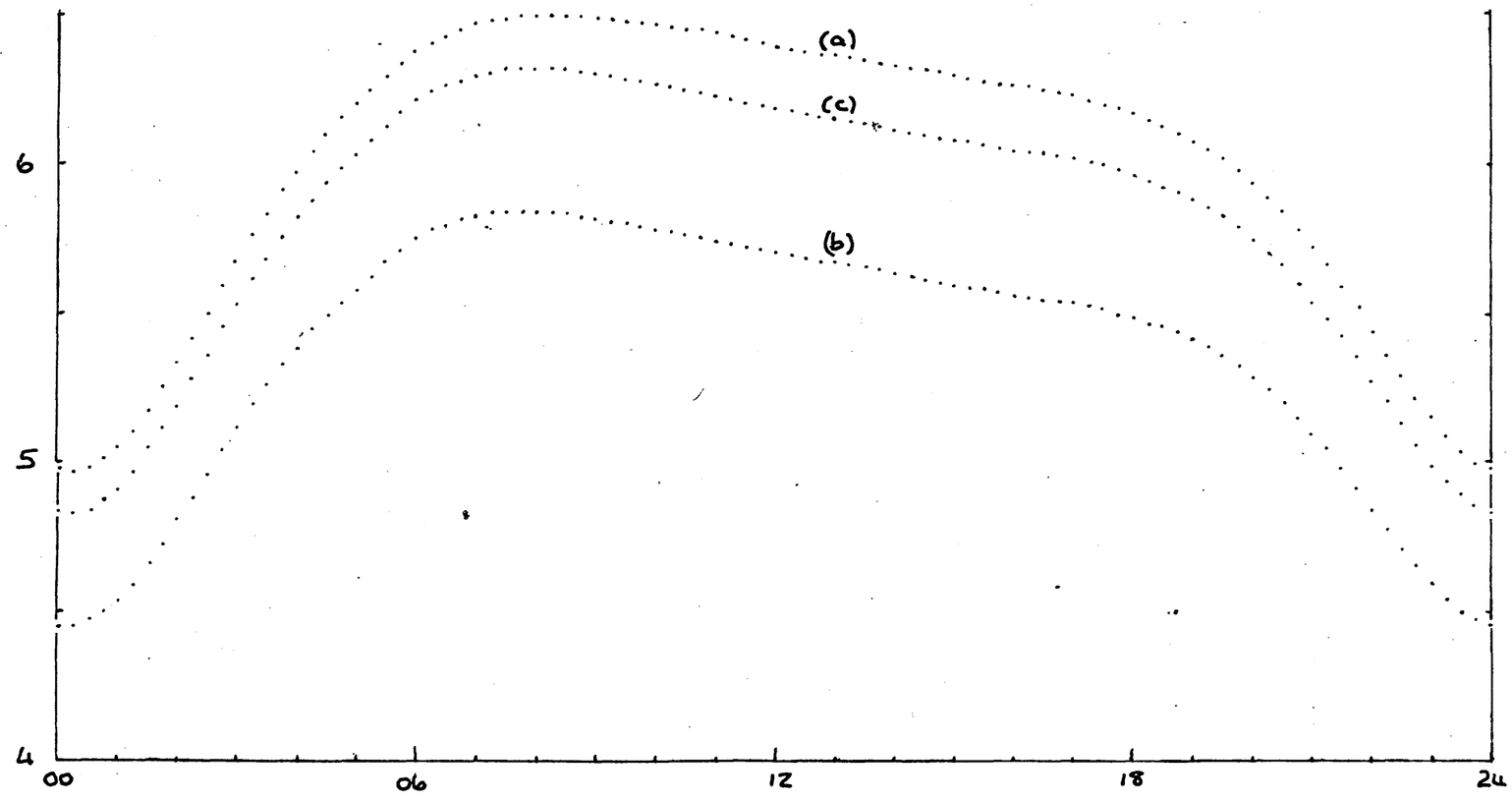
(a)
(c)
(b)
6
5
4
00
06
12
18
24

since the critical frequencies of f_oF2 obtained using this value are more realistic than those obtained using equation 6.1, $5 \times 10^{-13} cm^3 s^{-1}$ was used in all subsequent solutions.

The form of the loss rate coefficient, k_2, is less certain. The three forms outlined in Section 5.4.1 are :

$$(a)\ k_2 = 3.4 \times 10^{-10}/\sqrt{T}\ \ cm^3 s^{-1} \qquad (6.2)$$

$$(b)\ k_2 = 1.1 \times 10^{-11}\ (1 + \frac{T}{1660})\ cm^3 s^{-1} \qquad (6.3)$$

and $$(c)\ k_2 = 1.3 \times 10^{-11}\ \text{(independent of temp.)} \qquad (6.4)$$

Each of these forms has been used to solve the continuity equation, with values for the other rate coefficients as given in section 6.1 and with equation 5.18 for the diffusion term. The values of f_oF2 obtained from these solutions have been plotted in fig.47. From this it can be seen that the values of f_oF2 obtained using equation 6.3 (curve (b) in fig. 47) are about 0.4 to 0.5 MHz less than values obtained using equation 6.4 (curve (c)) which in turn are slightly less, (about 0.1 to 0. 2 MHz) than values obtained using equation 6.2 (curve (a)). There is little difference in the value of h_mF2 between the three solutions.

The value of k_3 has been taken as:

$k_3 = 2.0 \times 10^{-10} cm^3 s^{-1}$ (independent of temperature) throughout this analysis. However, since this is a little lower than the value used by Stubbe[146] and Rüster[130] (see Section 5.4.1) namely

$k_3 = 2.5 \times 10^{-10} cm^3 s^{-1}$,

the effect of this latter value has also been investigated.

The/...

Figure 48

NO^+ density obtained from continuity equation solutions, plotted against height. Various forms of the recombination coefficient α_3 were tried:

(i) $4.7 \times 10^{-8}(\frac{1000}{T_e})^{1.5}$ cm^3s^{-1},

(ii) $\frac{1.16 \times 10^{-4}}{T_e} - 3.7 \times 10^{-8}$ cm^3s^{-1}

and (iii) $5.0 \times 10^{-7}(\frac{300}{T_e})^{1.2}$ cm^3s^{-1}.

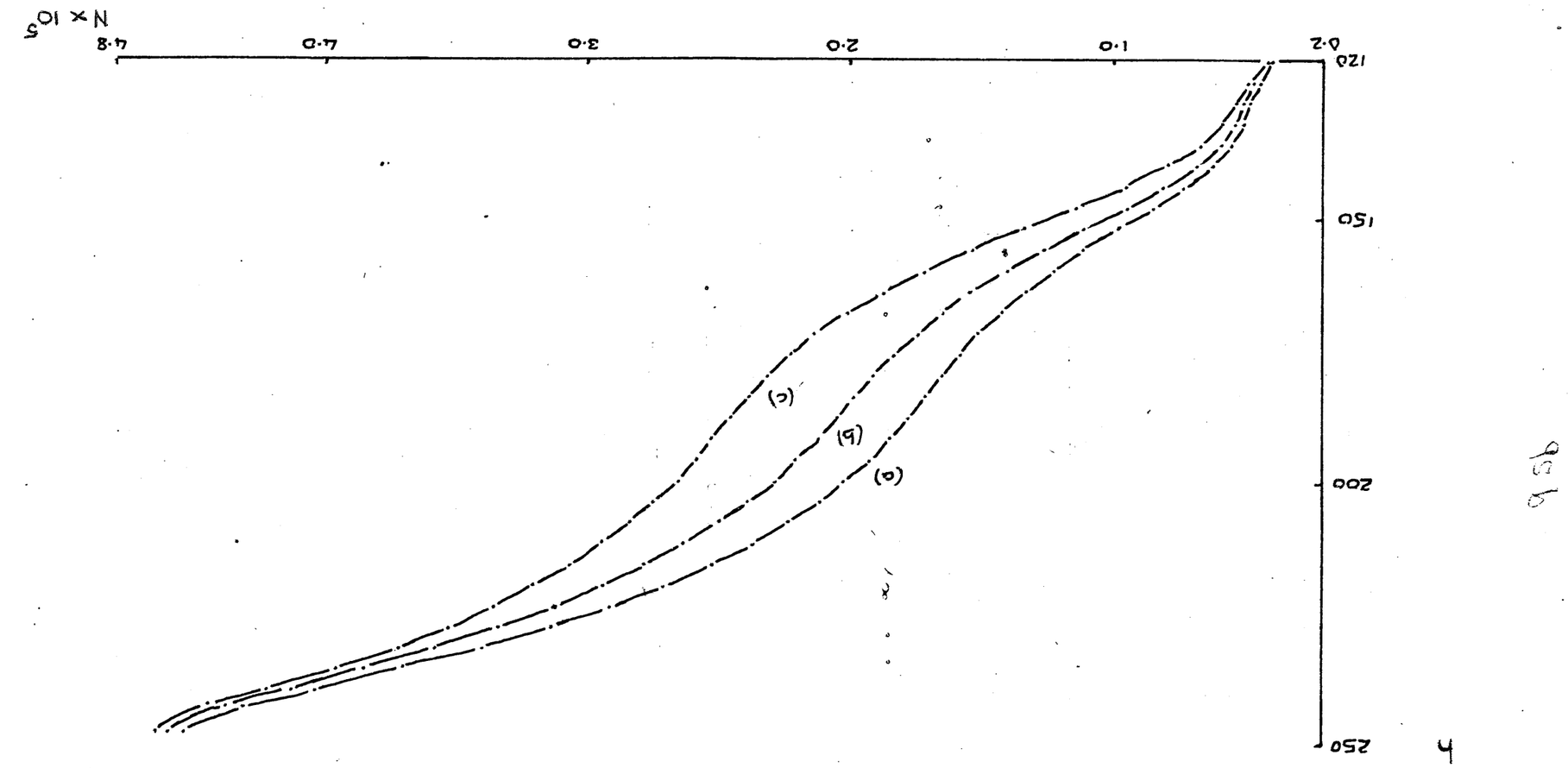

4

τ

Figure 49

Values of f_0F2 obtained from solutions of the continuity equation using different exospheric temperatures but the same solar flux, $\bar{S}_{10.7}$ (i.e. $I_{\infty\lambda}$ is kept constant). Diurnal temperature ranges used are:

(a) 745 to 784 K

(b) 812 to 855 K

and (c) 869 to 915 K.

$N \times 10^5$

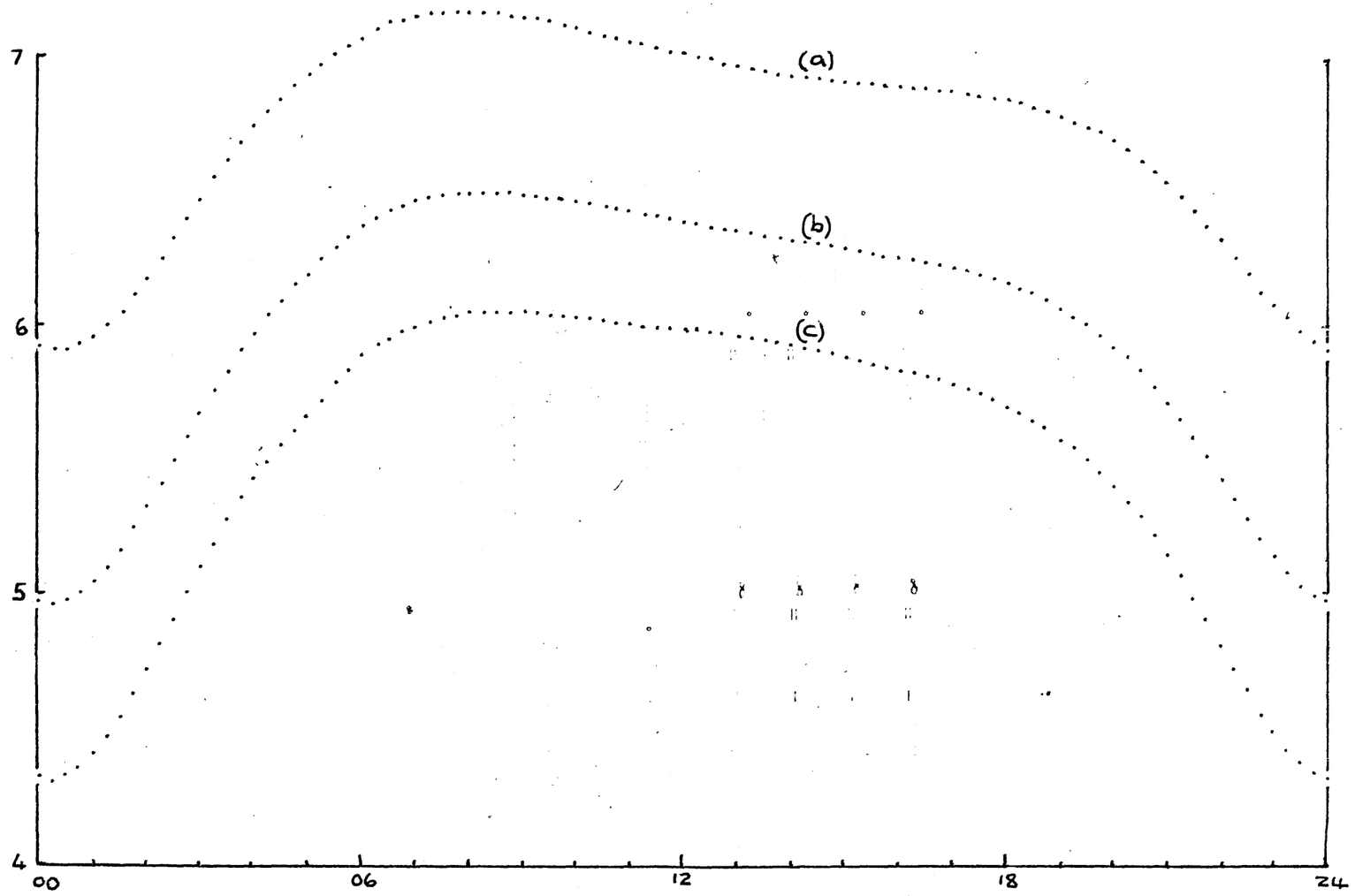
7
6
5
4
(a)
(b)
(c)
00
06
12
18
24

Figure 50

Values of f_0F2 obtained from solutions of the continuity equation using different solar fluxes and hence exospheric temperatures. Solar fluxes used were

(a) $\overline{S}_{10.7} = 61$ producing $T_\infty = 745 - 784$ K

(b) $\overline{S}_{10.7} = 73$ producing $T_\infty = 812 - 855$ K

(c) $\overline{S}_{10.7} = 92$ producing $T_\infty = 869 - 915$ K

(d) $\overline{S}_{10.7} = 115$ producing $T_\infty = 964 - 1014$ K

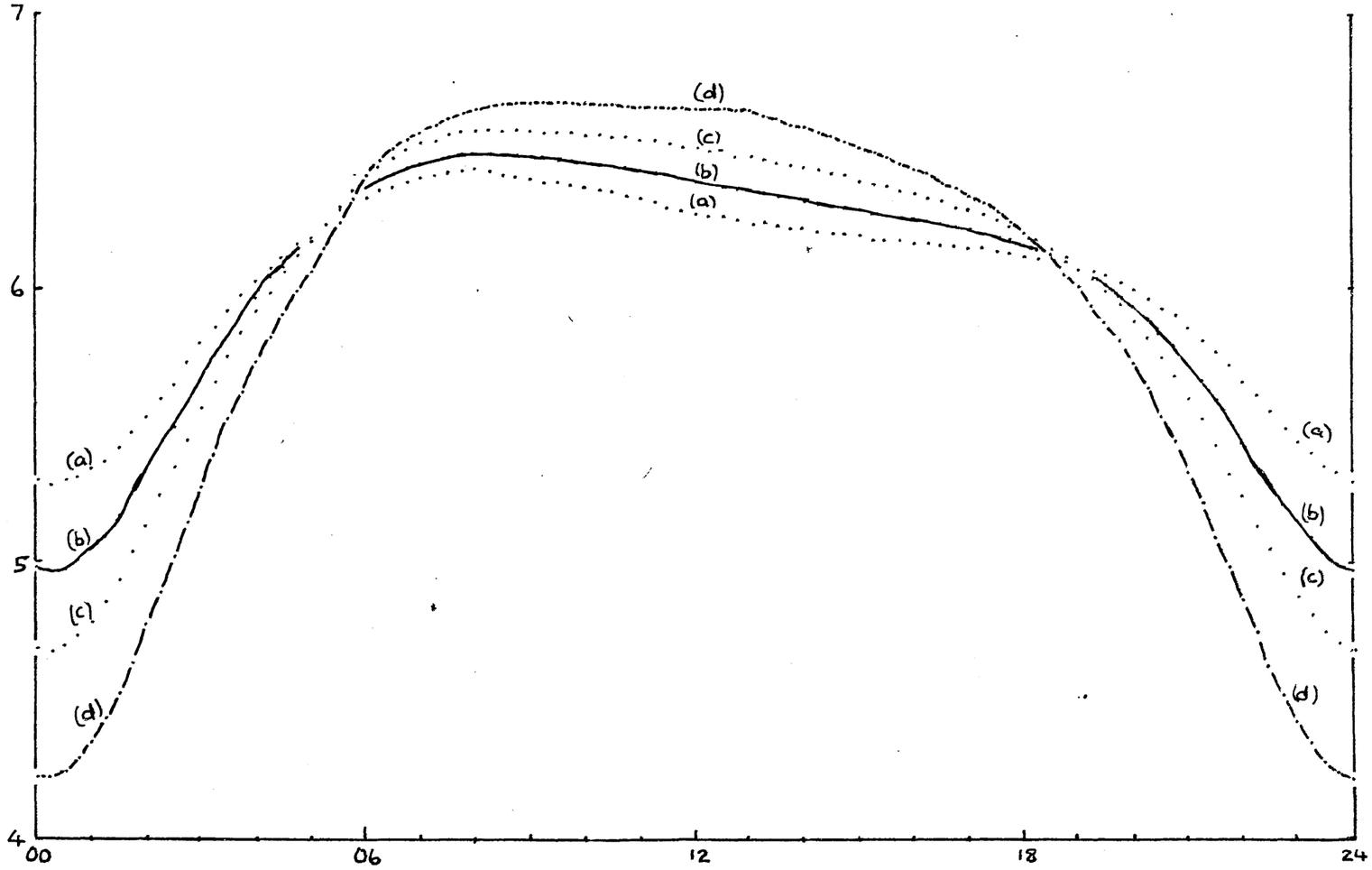
7
6
5
4
(d)
(c)
(b)
(a)
(a)
(b)
(c)
(d)
(a)
(b)
(c)
(d)
00
06
12
18
24

The reaction involved,

$$N_2^+ + O \longrightarrow NO^+ + N$$

affects the removal of N_2^+ ions from the ionosphere. However, since this rate coefficient is relatively large, the concentration of N_2^+ is always very small, and whether one uses the value $2.0 \times 10^{-10} cm^3 s^{-1}$ or the value $2.5 \times 10^{-10} cm^3 s^{-1}$, there should be little difference in the solution. This was found to be the case.

Various forms for the recombination coefficient for NO^+ ions have also been tried. The three forms

$$\text{(i)}\quad 4.7 \times 10^{-8} \left(\frac{1000}{T_e}\right)^{1.5} \qquad cm^3 s^{-1}$$

$$\text{(ii)}\quad \frac{1.16 \times 10^{-4}}{T_e} - 3.7 \times 10^{-8} \qquad cm^3 s^{-1}$$

and $$\text{(iii)}\quad 5.0 \times 10^{-7} \left(\frac{300}{T_e}\right)^{1.2} \qquad cm^3 s^{-1}$$

(see Section 5.4.1)

were used to obtain solutions of the continuity equation. However, as they affect the concentration of NO^+, the effect on the F2 peak is negligible (values of f_oF2 are never different by more than 0.05 MHz). In fact, the effect is only significant at heights between about 150 and 230 km, as can be seen from Fig. 48. Between about 170 and 200 km, values of NO^+ are about 25% lower if form (iii) above is used than if form (ii) is used. If form (i) is used, values of NO^+ are about 25% higher than values obtained using form (ii).

6.3/...

Figure 51

Comparison of f_oF2 values obtained when the continuity equation is solved

(a) with the wind term (equation 5.23)

(b) without the wind term

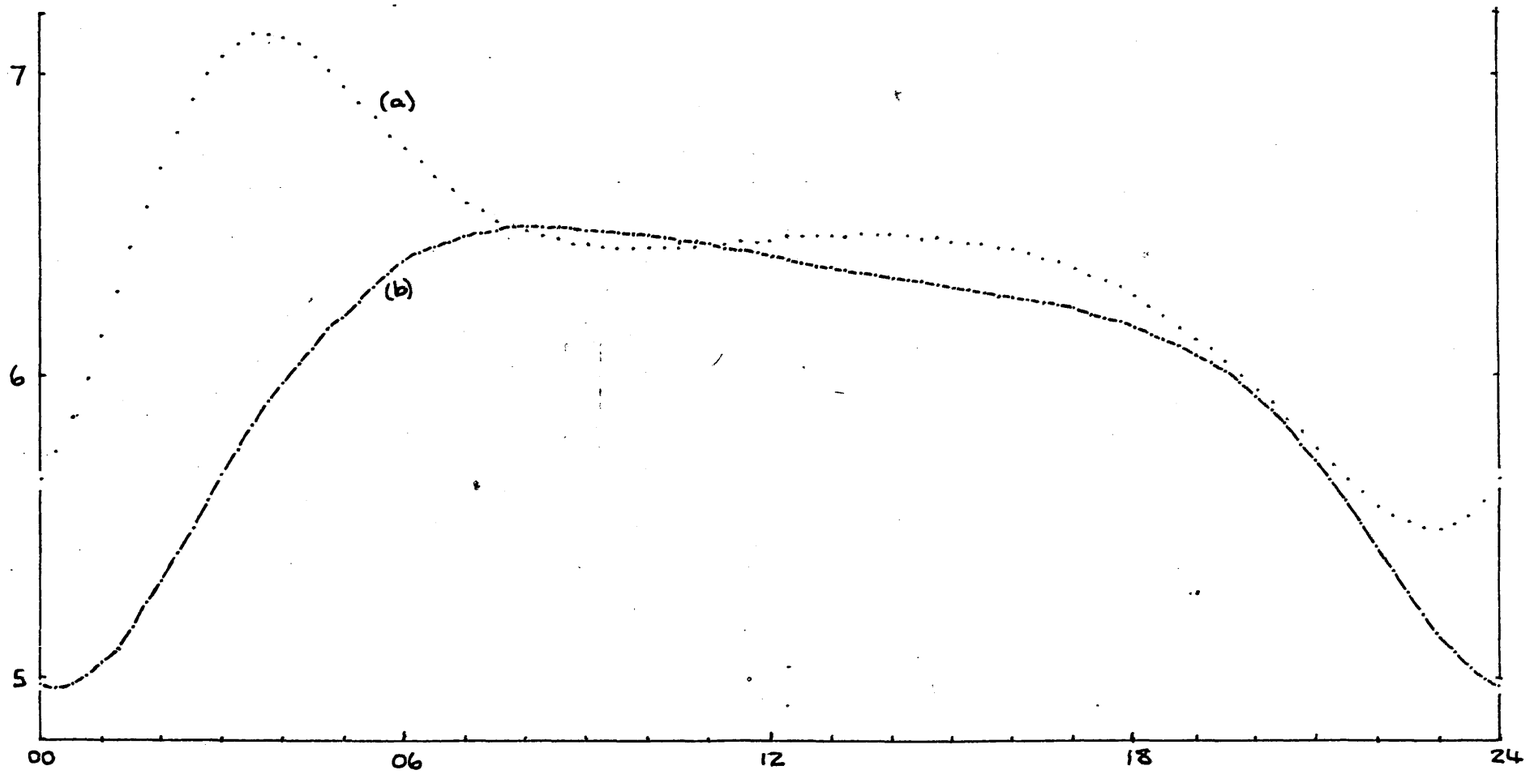
7
6
5
(a)
(b)
00
06
12
18
24

Figure 52

Comparison of h_mF2 values obtained when the continuity equation is solved

(a) with the wind term (equation 5.23)

(b) without the wind term

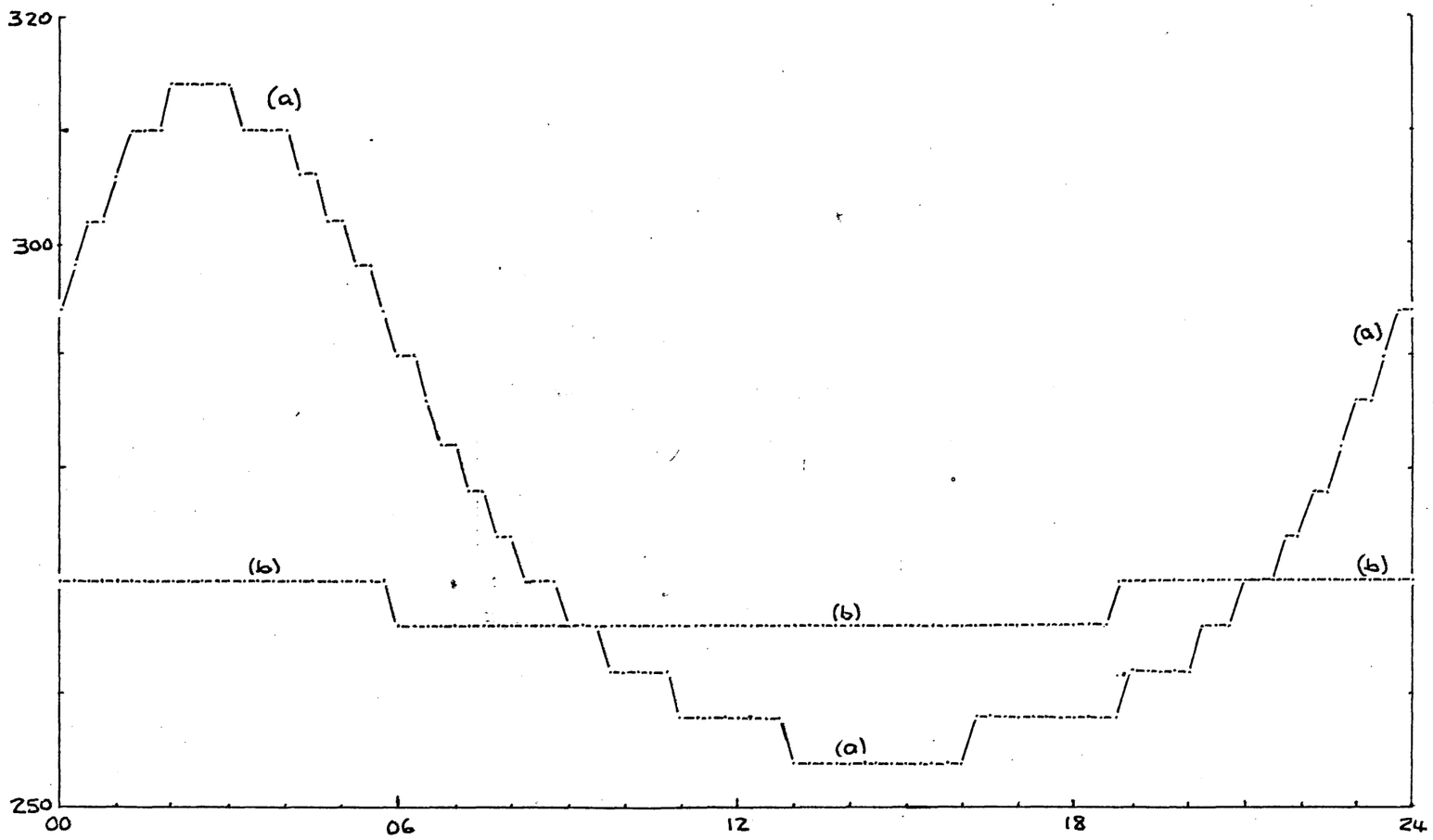
320
300
250
(a)
(b)
(b)
(a)
00
06
12
18
24

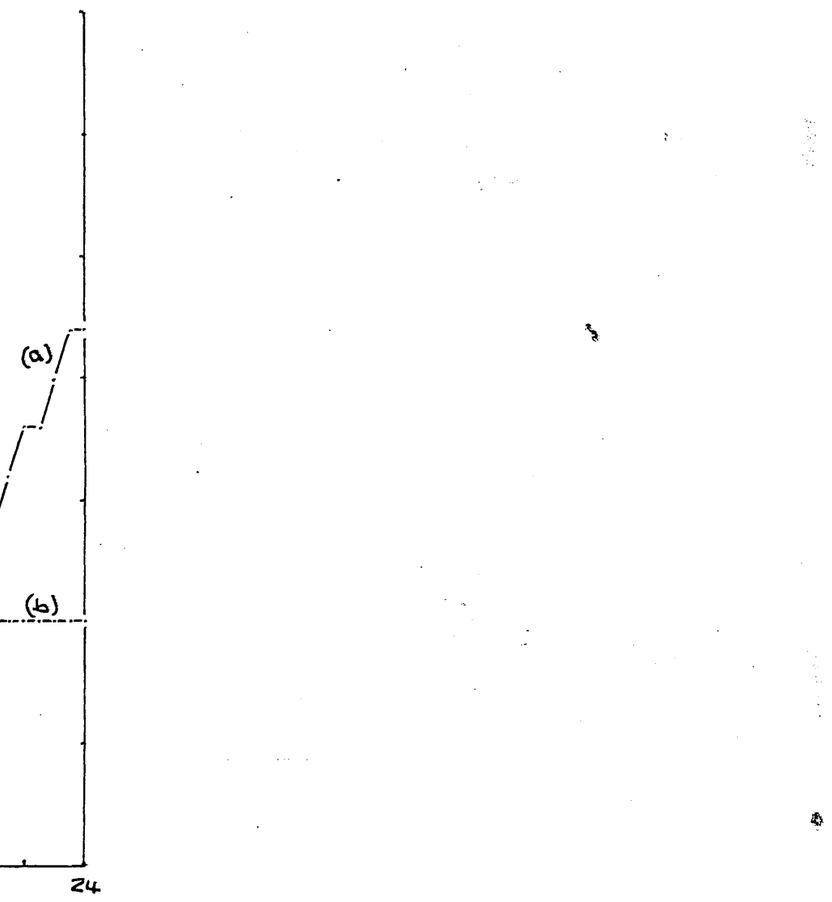
(a)
(b)

Figure 53

Comparison of calculated f_0F2 (in MHz) with observed variation at SANAE;

(a) shows the calculated f_0F2 for SANAE when the normal wind term is included,

(b) shows the calculated f_0F2 for SANAE when a slightly different wind term is included (with magnitude about two-thirds of that used in (a) and phase angle about 30° different) and

(c) contains the average quiet-day f_0F2 at SANAE during December 1963.

(a)

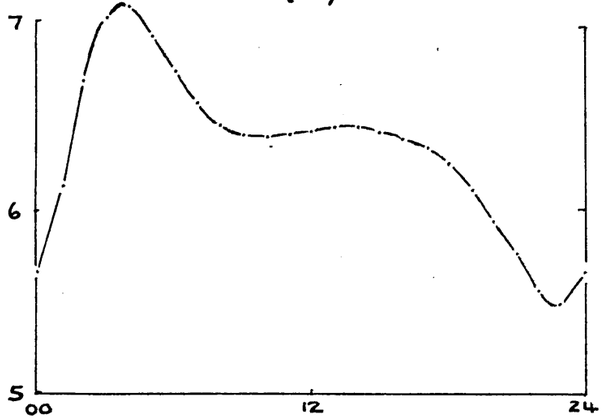

(b)

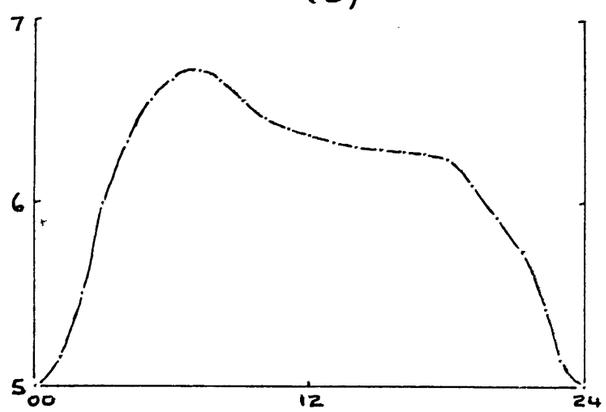

(c)

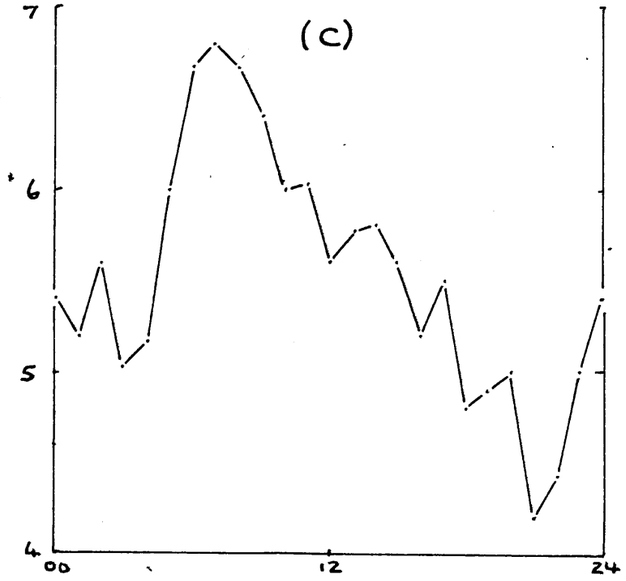

6.3 THE EFFECT OF TEMPERATURE

To investigate the effect of neutral atmospheric temperature on solutions of the continuity equation, the equation was solved using the diffusion term given in equation 5.18 and the values of the loss rate coefficients given in Section 6.1 for different values of T_∞. Initially the intensity of solar EUV outside the earth's atmosphere, $I_{\infty\lambda}$, was kept constant. Values of f_0F2 obtained from solutions for different exospheric temperatures are shown in Fig. 49, which points to the conclusion that the higher the exospheric temperature, the lower the value of f_0F2, at least in the range of T_∞ investigated.

Since an increase in exospheric temperature, which is caused by an increase in the 10.7 cm solar flux, will be accompanied by an increase in the intensity of solar EUV[175], the calculations were repeated assuming that the intensity of solar EUV outside the earth's atmosphere, $I_{\infty\lambda}$, is directly proportional to the intensity of the 10.7 cm solar flux. The variation of f_0F2 in this case has been plotted in Fig. 50. Here an increase in solar flux (resulting in an increase in both exospheric temperatures and $I_{\infty\lambda}$) will cause an increase in f_0F2 about midday when the production term has a large effect, but a decrease in f_0F2 at midnight, when the effect of solar EUV is small. This result is used in Section 3.4 where the effect of the semi-annual variation of neutral atmospheric density is discussed.

The effect of temperature on the height of the F2 peak was found to be small, an increase in temperature causing an increase in h_mF2.

6.4/...

TABLE 29

Comparison of f_0F2 values calculated from the continuity equation for SANAE (summer conditions at sunspot minimum) using three different $\tau(h,t)$ distributions :

(i) the τ distribution for Millstone Hill for Sept. 1963,

(ii) the τ distribution for Millstone Hill for Dec, 1963,

(iii) $\tau = 1$ at all heights and times of day.

TIME IN HOURS	f_0F2 CALCULATED FOR case(i)	case(ii)	case(iii)
00	4.98	4.95	4.95
01	5.05	5.03	5.03
02	5.33	5.32	5.31
03	5.67	5.67	5.66
04	5.97	5.98	5.96
05	6.19	6.21	6.18
06	6.37	6.36	6.33
07	6.46	6.44	6.41
08	6.49	6.47	6.44
09	6.48	6.47	6.43
10	6.46	6.44	6.40
11	6.43	6.41	6.36
12	6.39	6.38	6.32
13	6.36	6.34	6.29
14	6.32	6.31	6.26
15	6.29	6.28	6.23
16	6.26	6.24	6.21
17	6.22	6.21	6.17
18	6.16	6.15	6.12
19	6.07	6.06	6.04
20	5.93	5.92	5.90
21	5.72	5.70	5.69
22	5.44	5.42	5.41
23	5.15	5.12	5.12

6.4 THE EFFECT OF τ ($= \frac{T_e}{T_i}$)

Unfortunately, lack of time prevented much investigation into the effect which this quantity has on continuity equation solutions. However, three different $\tau(h,t)$ distributions were used to solve the continuity equation (diffusion term and loss rate coefficients as for section 6.3) ; they are

(i) the τ distribution for Millstone Hill for Sept.1963 (Evans[180])

(ii) the τ distribution for Millstone Hill for Dec. 1963 (Evans[180])

and(iii) $\tau = 1$ at all heights and times of day (i.e. $T_i = T_e$). The values of f_oF2 obtained are compared in Table 29. This shows that the values of f_oF2 are not affected very much by small variations in τ . The effect of large variations of τ (which Torr[162] suggests might be present because of particle precipitation) has not been investigated.

6.5 THE EFFECT OF WINDS

Thus far the results obtained have not included the effect of a horizontal neutral atmospheric wind. To see the effect of this on the solution, the continuity equation was solved (again using the diffusion term and loss rate coefficients as for section 6.3) with the wind term included (equation 5.23 on page 86),and the resulting values of f_oF2 and h_mF2 are compared with values of f_oF2 and h_mF2 obtained without the wind term in Figures 51 and 52. From Fig. 51, the value of f_oF2 is enhanced when either an upward vertical drift (maximum at 03 - 04 hours LMT) or a downward drift (maximum at about 15 - 16 hours LMT) is present. This agrees with the results of Torr[162] (see section 2.4).

The/...

The variation of h_mF2 (shown in Fig. 51) is unrealistically constant throughout the day when winds are neglected. This agrees with the results of King et al[82]. The variation of h_mF2 produced when winds are included is much larger with a maximum at about 02 - 03 LMT and a minimum at about 13 - 16 LMT. From the observed variations of N at fixed heights over SANAE during summer (see section 8.2) , the height of the F2 peak is seen to be at a maximum at about 05 - 07 LMT and at a minimum between 15 and 19 LMT. Thus there appears to be a difference of about two hours between the time of maximum (or minimum) values of f_oF2 calculated from the continuity equation including the wind term and that of the observed variation. Otherwise the observed behaviour of h_mF2 might be explained by the effect of horizontal neutral winds (cf. results of King et al[83]).

The values of f_oF2 produced from the above solution are also plotted in Fig. 53(a). Shown in Fig. 53(b) are the values of f_oF2 obtained if the wind velocities are decreased by a factor of two-thirds, and the declination is assumed to be about -45^o.(This changes the phase of the wind by about 30^o and produces a maximum of about 6.7 MHz at about 06 LMT to agree with Fig. 53 (c)). Fig. 53(c) shows the average quiet day f_oF2 measured at SANAE during December 1963. This shows that although the morning maximum at 06 LMT at SANAE can be explained by the effect of a horizontal neutral wind (with a reduced amplitude and with phase angle about 30^o different from that calculated using the parameters mentioned in Chapter 5), the subsequent rapid decrease in ionization is not obviously explained by this model.

6.6/...

6.6 CONCLUSIONS

Work on solving the continuity equation , with a view to explaining the behaviour of f_0F2 at SANAE, was begun during 1966 and continued in 1967. At the time Rhodes University had an ICL 1301 computer, which was very slow in operation owing to the size of its core memory (800 words) and consequently complete solutions of the continuity equation could not be obtained.

At the end of 1967 I went down to Antarctica, where I spent the whole of 1968 and the first part of 1969. During this time I began working on the harmonic analysis described in Part I. This analysis was completed using the 1301 computer after my return in 1969. In November of that year Rhodes University installed a 1901A computer, and since then it has become possible to solve the continuity equation. However, it has been decided to present this thesis now, and at this stage lack of time prevents a thorough study of continuity equation solutions, although it is hoped that the work will be continued by others along similar lines.

A further consideration is the fact that the computer time required to integrate the equation over a whole day is about seven hours. Strict limitations on the amount of computer time used have been imposed on computer users at Rhodes University this year (1971), and very little time could be allocated to long runs such as this. Nevertheless the following results have been obtained.

Solutions of the continuity equation show that the four forms of the diffusion term given in equations 5.17, 5.18, 5.19 and 5.21 (pages 82, 83 and 84) produce values of f_0F2 which are not significantly different. Three forms of the ambipolar diffusion coefficient were tried and found to

produce/...

produce approximately the same results, while different $\tau(h,t)$ distributions also had little effect on the solution.

The effect of an increase in exospheric temperature if $I_{\infty\lambda}$ is kept constant, causes a decrease in f_0F2. If $I_{\infty\lambda}$ is taken to be proportional to the 10.7 cm solar flux, an increase in the 10.7 cm solar flux (and hence temperature) at midday will cause an increase in f_0F2, while at midnight it will cause f_0F2 to decrease.

When the effect of horizontal neutral winds is included into a solution of the continuity equation, it has been found that both an upward and a downward vertical drift of ionization cause f_0F2 to increase. The increase in f_0F2 during the early morning in summer at SANAE could be explained by the effect of a horizontal neutral wind (provided that the time of maximum vertical drift is about two hours later than that calculated). However, the decrease in f_0F2 between 08 and 20 hours LMT observed at SANAE is much greater than can be accounted for by this simple wind model.

An attempt was made to solve the continuity equation for equinoctial conditions using a variable step-length (Δt) for the integration. However, a stable solution could not be obtained and, because of lack of time, this idea was abandoned. Torr and Torr[164] and King et al[82] were also unable to obtain stable solutions for equinoctial or winter conditions.

Suggestions for further research are, therefore,

(a) to investigate further the problem of solution of the continuity equation for equinoctial and winter conditions, and

(b)/...

(b) to obtain similar solutions using the dip angle and wind velocities for Cape Hallett and to compare these with the results obtained for SANAE. This may be extended further to include solutions for other Antarctic stations as well.

PART IV

REDUCTION OF IONOGRAMS BY COMPUTER

The ionosonde's aerial system at sunset

The ionosonde at SANAE

CHAPTER 7

COMPUTER PROGRAMS FOR CONVERTING IONOGRAMS TO N(h) PROFILES

7.1 INTRODUCTION

Although this section may seem to be slightly disjointed from the rest of the thesis, the original intention was that this should form an integral part of an investigation into the Antarctic ionosphere. The intention was to write a computer program which could be used to convert ionograms to N(h) profiles and use this to determine the variation of electron density at fixed heights during the day for several days during summer and winter at SANAE. One might then compare these measured values of electron density with densities predicted by the continuity equation solutions and adjust the parameters of the continuity equation until one could explain the observed densities, thus accounting for the observed behaviour and predicting values for parameters such as the diffusion coefficient, loss rate, etc.

In this chapter several methods of converting h'(f) curves to N(h) profiles will be considered. Computer programs have been developed for these methods and these are discussed (Sections 7.2 and 7.3). The two chief problems associated with ionogram reduction are the correction for the presence of low-lying ionization and the detection of and correction for valleys between ionospheric layers. Jackson[75], one of the first people to develop a systematic method for reducing ionograms, suggested that the inter-layer ionization density does not drop by more than a few percent of the density at

the/...

the layer maximum immediately below the valley. Thus as a first approximation one can determine heights above a suspected valley by calculating the linear segment between a point in the E- or F1-region which is nine-tenths of the critical density and the first point above the valley.

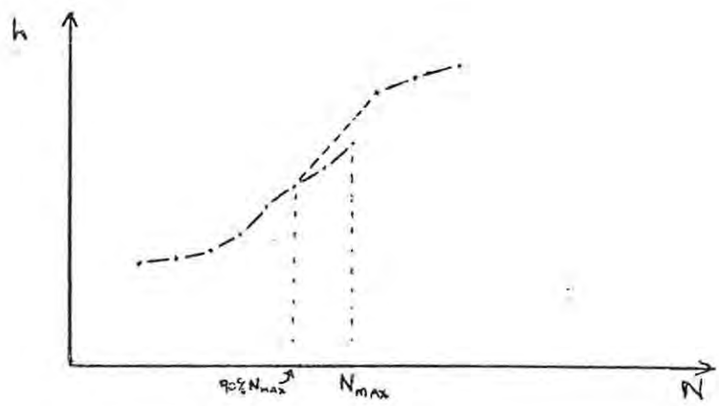

Titheridge[155] recognized the importance of using both ordinary and extraordinary ray traces in computing electron density profiles. He suggested that the ordinary ray h'(f) curve be used to calculate the normal monotonic N(h) curve. Then the extraordinary ray virtual heights corresponding to this N(h) curve can be calculated. Subtracting these calculated virtual heights from the observed values gives:

$$\Delta h'_x = h'_{x_{obs}} - h'_{x_{calc}}$$

These differences were then used in an approximate method to determine the dimensions of a wedge-shaped valley.

Another method of correcting for the effect of a valley used by the ITSA group (Howe and McKinnis[68], Wright[177]) is the "restart" technique. In this case, if a valley is suspected, the calculation is restarted above the layer peak, treating the ionization below the

peak/...

peak as low-lying ionization. Howe and McKinnis, who explain the method, give no account of how the presence of a valley is detected.

Unfortunately, not one of these methods produces an accurate correction for ionization in a valley under all conditions (Wright and Smith[178]). In fact, in most cases the method of correcting for a valley is outlined but no proper test of the method is ever described in the literature. In section 7.4 and Appendix 8 a method of correcting for the presence of a valley is outlined and a test of the method is described.

7.2 A LEAST SQUARES METHOD OF IONOGRAM REDUCTION

Initially a computer program was written which was based on the method proposed by Doupnik and Schmerling[36]. Their method entails the calculation of true heights from the virtual heights by fitting the true height profile with a set of parabolic laminations (cf. Paul and Wright[112]). This can be done in two ways:

(a) as a single mode analysis using points scaled entirely from the ordinary or entirely from the extraordinary ray trace;

(b) as a joint mode analysis in which both ordinary and extraordinary ray traces are scaled and a least squares fit is used to obtain maximum accuracy and provide a correction for underlying ionization.

In both cases the N(h) profile is represented by a series of parabolic segments of the form:

$$h = h_j + a_j(f_N - f_{N_j}) + b_j(f_N - f_{N_j})^2 \qquad (7.1)$$

where a_j, b_j are the coefficients of the j^{th} parabola,

/....

f_N is the plasma frequency in the interval $f_{N_j} \leq f_N \leq f_{N_{j+1}}$ (f_{N_j} and $f_{N_{j+1}}$ being the plasma frequencies corresponding to two successive frequencies scaled from an ionogram),

h_j is the true height corresponding to the plasma frequency f_{N_j}

and h the true height corresponding to frequency f_N.

The plasma frequency, f_N, is related to the wave frequency, f, as follows:

$$f_N \begin{cases} = f & \text{for the ordinary ray} \\ = \sqrt{f^2 - ff_h} & \text{for the extraordinary ray} \end{cases} \qquad (7.2)$$

where f_h is the gyrofrequency.

For continuity of slope between successive segments,

$$a_j = a_{j-1} + 2b_{j-1}(f_{N_j} - f_{N_{j-1}}) \qquad (7.3)$$

The well-known equation which relates true height, h, to virtual height, h', is

$$h'(f_k) = h_o + \int_o^{f_{N_k}} \mu' \frac{dh}{df_N} df_N \qquad (7.4)$$

where μ' is the group refractive index of either ordinary or extraordinary mode and h_o is the effective base of the ionosphere where $f_N = 0$.

7.2.1 THE SINGLE MODE ANALYSIS

From equations (7.1) and (7.4) one obtains

$$h'(f_k) = h_o + \sum_{j=0}^{k-1} \left[a_j \int_{f_{N_j}}^{f_{N_{j+1}}} \mu' df_N + 2b_j \int_{f_{N_j}}^{f_{N_{j+1}}} (f_N - f_{N_j}) \mu' df_N \right] \qquad (7.5)$$

At/...

At this stage one must make some assumption about h_o, the base of the ionosphere. One possibility is to use the first three virtual heights to calculate the coefficients of the first parabola (h_o, a_o, b_o), a second possibility is to assume that h_o = 95 km (since several workers have found from special low frequency ionograms that virtual heights near 75 kHz are relatively constant at 95 $\pm$ 15 km [36]) and use the first two virtual heights to solve for a_o and b_o, while a third possibility is to use the flat base assumption, viz. that the value of h_{min} (the virtual height corresponding to f_{min}) is taken as h_o. The latter two assumptions were used in the computer program. The reduction then follows in a step-by-step manner, at each stage calculating the coefficients a_j and b_j.

7.2.2 THE JOINT MODE ANALYSIS

In this case both ordinary and extraordinary ray virtual heights are used. Assume that M ordinary mode virtual heights have been scaled at frequencies f_1 to f_M and N' extraordinary mode virtual heights at frequencies f_{x_1} to $f_{x_{N'}}$. Equation (7.5) can be regarded as a set of equations:

/...

$$h'_o(f_1) = a_o D_{1,1} + b_o D_{1,2} + 0 + \ldots + 0 + h_o D_{1,M+2}$$

$$h'_o(f_2) = a_o D_{2,1} + b_o D_{2,2} + b_1 D_{2,3} + 0 + \ldots + 0 + h_o D_{2,M+2}$$

$$h'_o(f_M) = a_o D_{M,1} + b_o D_{M,2} + b_1 D_{M,3} + \ldots + b_{M-1} D_{M,M+1} + h_o D_{M,M+2}$$

$$h'_x(f_{x_1}) = a_o D_{M+1,1} + b_o D_{M+1,2} + \ldots + b_{j-1} D_{M+1,j+1} + 0 + \ldots + 0 + h_o D_{M+1,M+2} \qquad (7.6)$$

$$h'_x(f_{x_{N'}}) = a_o D_{M+N',1} + b_o D_{M+N',2} + \ldots + b_{k-1} D_{M+N',k+1} + 0 + \ldots + 0 + h_o D_{M+N',M+2}$$

where $h'_o(f)$ signifies the ordinary mode virtual height corresponding to a particular wave frequency f and $h'_x(f)$ the extraordinary mode virtual height corresponding to f. The coefficients $D_{j,k}$ are given in Appendix 5. These equations can be expressed in matrix notation as follows

$$DX_b = H' \qquad (7.7)$$

where D is the matrix of coefficients,

$$X_b = \begin{pmatrix} a_o \\ b_o \\ b_1 \\ \vdots \\ b_{M-1} \\ h_o \end{pmatrix} \quad \text{and} \quad H' = \begin{pmatrix} h'_o(f_1) \\ h'_o(f_2) \\ \vdots \\ h'_x(f_{x_{N'}}) \end{pmatrix}$$

From Appendix 5 the least squares solution to equation (7.7) is

$$D^t D X_b = D^t H' \qquad (7.8)$$

where D^t is the transpose of D. Equation (7.8) is solved to obtain X_b, from which the true heights are calculated.

7.2.3 THE/...

7.2.3 THE COMPUTER PROGRAM

Doupnik and Schmerling[36] assume parabolic laminations of the form given in equation (7.1) and the problem of finding true heights is thus reduced to that of solving an equation of the form

$$h'(f_k) = h_o + \int_0^{f_{N_k}} \mu' \frac{dh}{df_N}\, df_N$$

$$= h_o + \sum_{j=0}^{k-1} \left[a_j \int_{f_{N_j}}^{f_{N_{j+1}}} \mu'\, df_N + 2b_j \int_{f_{N_j}}^{f_{N_{j+1}}} (f_N - f_{N_j})\, \mu' df_N \right]$$

However, the accuracy of this method depends on the accuracy with which the above integrals can be calculated. Since the group refractive index μ' tends to infinity as the plasma frequency approaches the wave frequency, the integrals for the last frequency interval before reflection, $\int_{f_{N_{k-1}}}^{f_{N_k}} \mu'\, df_N$ and $\int_{f_{N_{k-1}}}^{f_{N_k}} (f_N - f_{N_{k-1}})\, \mu' df_N$, will be the most dominant and sensitive to error. Thus a better method which reduces the possibility of error arising from the fact that the value of μ' is infinite at the one end of this interval, is to introduce a new variable t defined by

$$t^2 = f_r^2 - f_N^2$$

$$\text{or } t = \sqrt{f_r^2 - f_N^2} \qquad (7.9)$$

where f_r = frequency of reflection. Hence

$$2tdt = - d(f_N^2)$$

and equation (7.4) becomes

/...

$$h'(f_k) = h_o + \int_0^{f_{N_k}^2} \mu' \frac{dh}{d(f_N^2)}\, d(f_N^2)$$

$$= h_o - \int_{\sqrt{f_{N_k}^2 - 0}}^{\sqrt{f_{N_k}^2 - f_{N_k}^2}} 2\mu' t \frac{dh}{d(f_N^2)}\, dt \qquad (7.10)$$

Since the independent variable is now f_N^2, it is more convenient to define parabolic laminations (equation 7.1) as

$$h = h_j + a_j(f_N^2 - f_{N_j}^2) + b_j(f_N^2 - f_{N_j}^2)^2 \qquad (7.11)$$

Equation (7.5) then becomes

$$h'(f_k) = h_o + \sum_{j=0}^{k-1} \left[a_j \int_{\sqrt{f_{N_k}^2 - f_{N_{j+1}}^2}}^{\sqrt{f_{N_k}^2 - f_{N_j}^2}} 2\mu' t\, dt \right.$$

$$\left. + b_j \int_{\sqrt{f_{N_k}^2 - f_{N_{j+1}}^2}}^{\sqrt{f_{N_k}^2 - f_{N_j}^2}} 2\mu' t(f_r^2 - t^2 - f_{N_j}^2)\, dt \right] \qquad (7.12)$$

and equation (7.3) changes to:

$$a_j = a_{j-1} + 2b_{j-1}(f_{N_j}^2 - f_{N_{j-1}}^2)$$

With these alterations to Doupnik and Schmerling's method, a computer program was written using the method in this form. The integrals were evaluated using Gaussian quadrature since this method gives the greatest accuracy for a given number of sample points. Initially 16-point and 8-point Gauss formulae were used[15]. However, it was found that a 4-point formula could be used for all but the last frequency interval before reflection without a

noticeable/...

noticeable loss of accuracy.

Various forms of the refractive index formulae for μ'_o and μ'_x were tried. Although in theory these different forms should give exactly the same values for the refractive index, in practice truncation errors (due to the fact that the computer can only store a number to a fixed degree of accuracy) caused the different formulae to yield slightly different results. The difference only becomes appreciable as X approaches 1 in the case of the ordinary ray and 1-Y for the extraordinary ray. The formulae which were tried, were

(a) those suggested by Doupnik and Schmerling[36],

(b) the formulae used by Becker[9, 10],

and(c) formulae derived directly from Ratcliffe[119].

The results for each set of formulae were compared with Walker's[184] and Becker's[9] results. In general the formulae of Doupnik and Schmerling involved more calculation and produced less accurate results than the other two. The formula for μ'_x used by Becker was not as accurate as that derived from Ratcliffe (for X within 1% of 1-Y). Hence the formula chosen for μ'_x was that derived from Ratcliffe, the formula for μ'_o was the one proposed by Becker (see Appendix 6).

One of the input parameters to the program determines whether a joint mode analysis using the least squares technique or a single mode analysis is to be conducted on the data. If the single mode analysis is selected, the program produces real height profiles (a) assuming that h_o = 95 km and (b) using the flat base assumption. In each case the first two virtual heights are used to calculate the first parabola (a_o, b_o). Each subsequent parabola has only one unknown, b_j, since the coefficient a_j is

determined/...

determined from the continuity of slope.

When the program was first written, it was written in MAC (for the ICL 1301 computer). However, the program did not always give reliable results for the joint mode analysis. It was later found that one of the standard ICL subroutines (the matrix inversion subroutine M/05/05/08) was in error. When Rhodes University replaced the 1301 computer by an ICL 1901A computer, the computer program was rewritten in EMA. Since the matrix inversion routine in EMA is correct, the program produced results which were consistent.

To test the method, one requires ionograms corresponding to known N(h) profiles. Since there were no standard ionograms at that time, a program was developed to convert N(h) profiles to ionograms. Initially the program was designed to read in a number of (frequency, real height) pairs and join these points with parabolas, matching the slopes at each intersection. From these real height parabolas, the virtual heights were calculated. However, this method proved unsuitable since the parabolas which were fitted, often caused the real heights to oscillate (see Fig. 54). The program was then altered so that the (frequency, real height) co-ordinates were connected by linear segments. However, unless one uses a large number of linear segments, the method produces unrealistic ionograms. Thus a third approach was tried in which selected functions were used to represent N(h) profiles. The functions used were parabolas, cubics and quartics. These produced realistic ionograms.

Typical ionograms obtained for a simple parabolic layer and for a cubic-parabolic combination are shown in Figs. 55 and 56. Several synthetic ionograms obtained in this way were then used as data for the ionogram

reduction/...

Figure 54

An illustration of the type of profile obtained when points on an N(h) profile were assumed to be connected by parabolic segments. The dotted line shows the expected profile, the solid line gives the actual profile obtained.

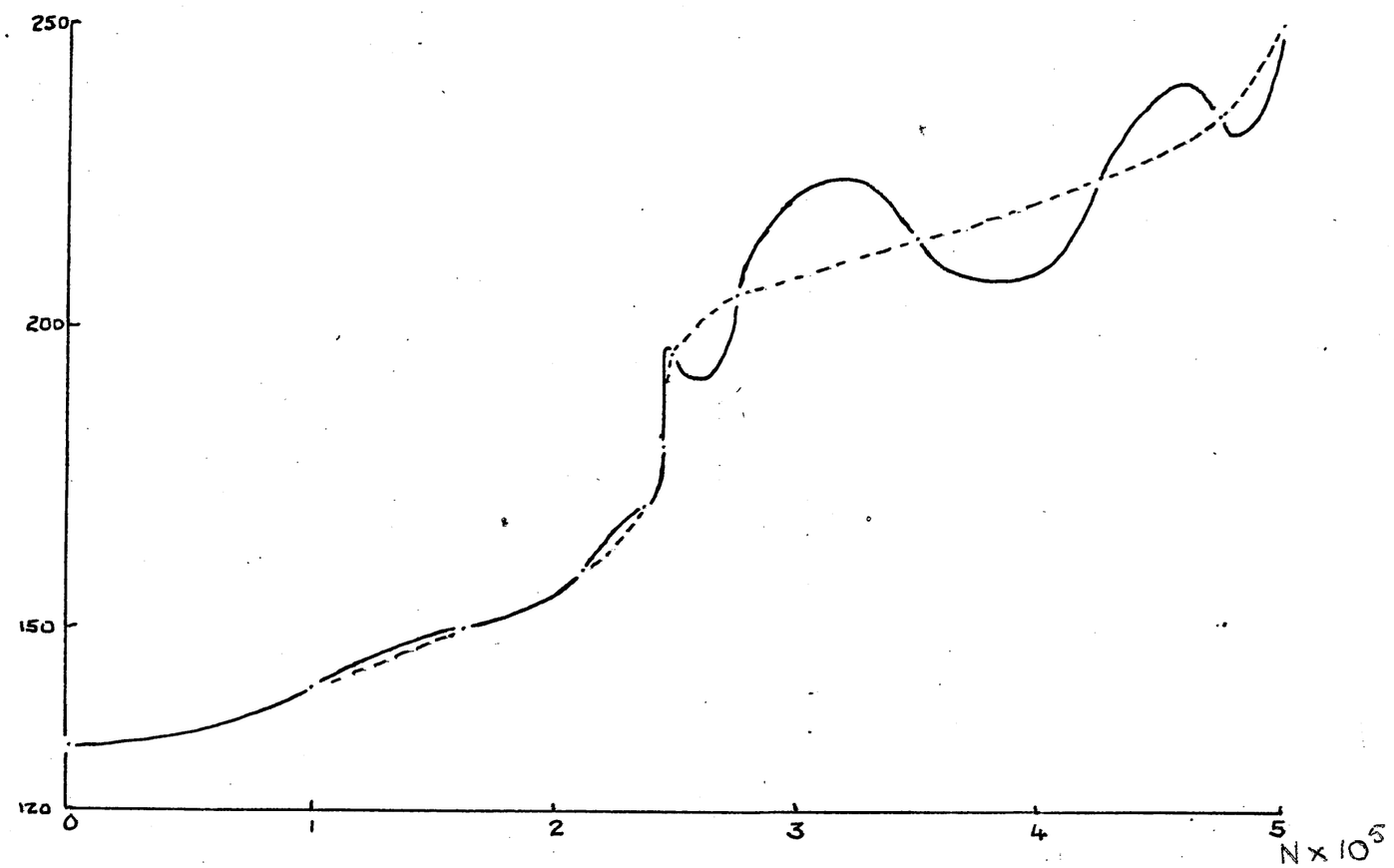
250
200
150
120
0
1
2
3
4
5
N x 10^5

Figure 55

Ionogram calculated for a simple parabolic layer. Upper diagram shows the ionogram; lower diagram gives the original N(h) profile.

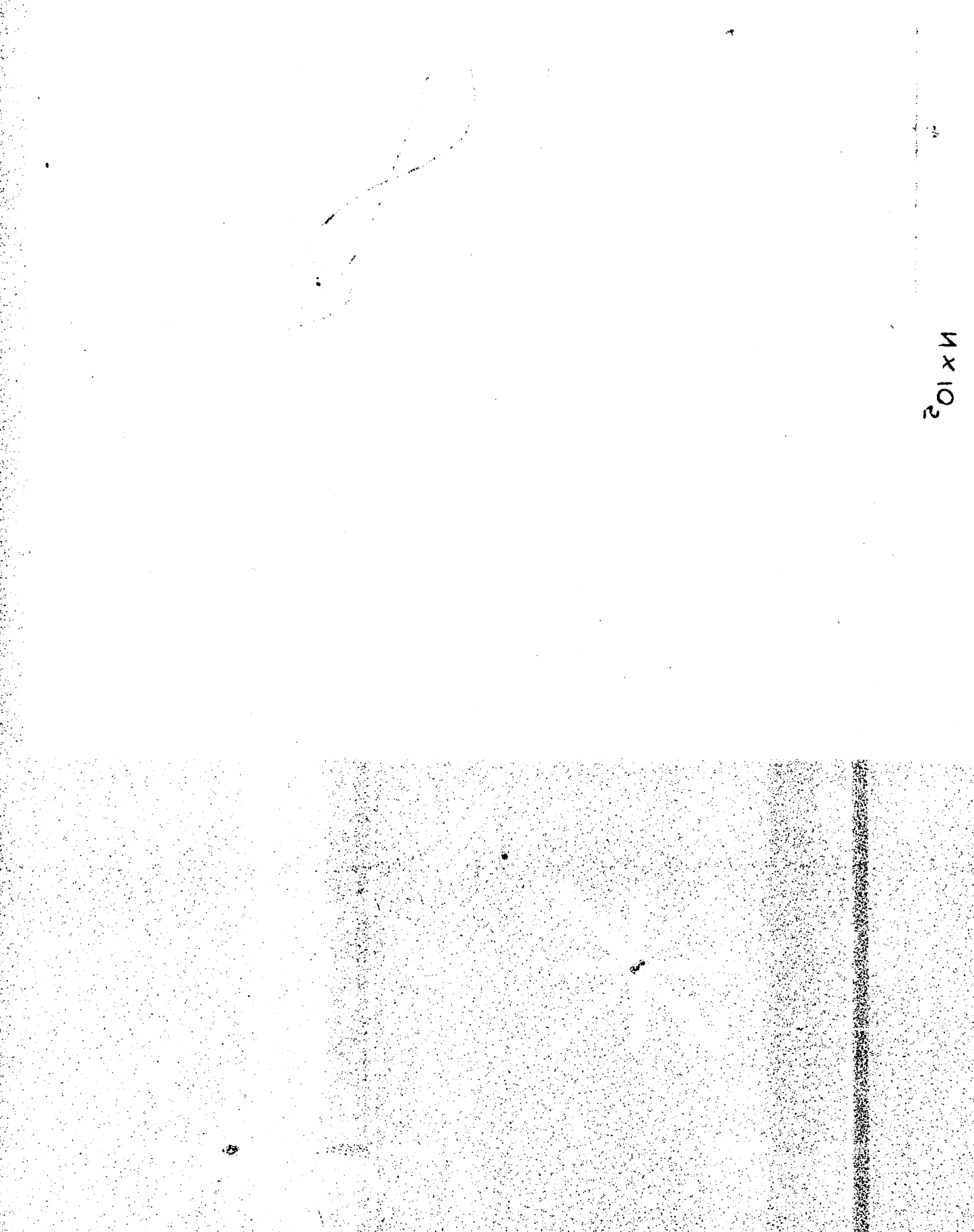

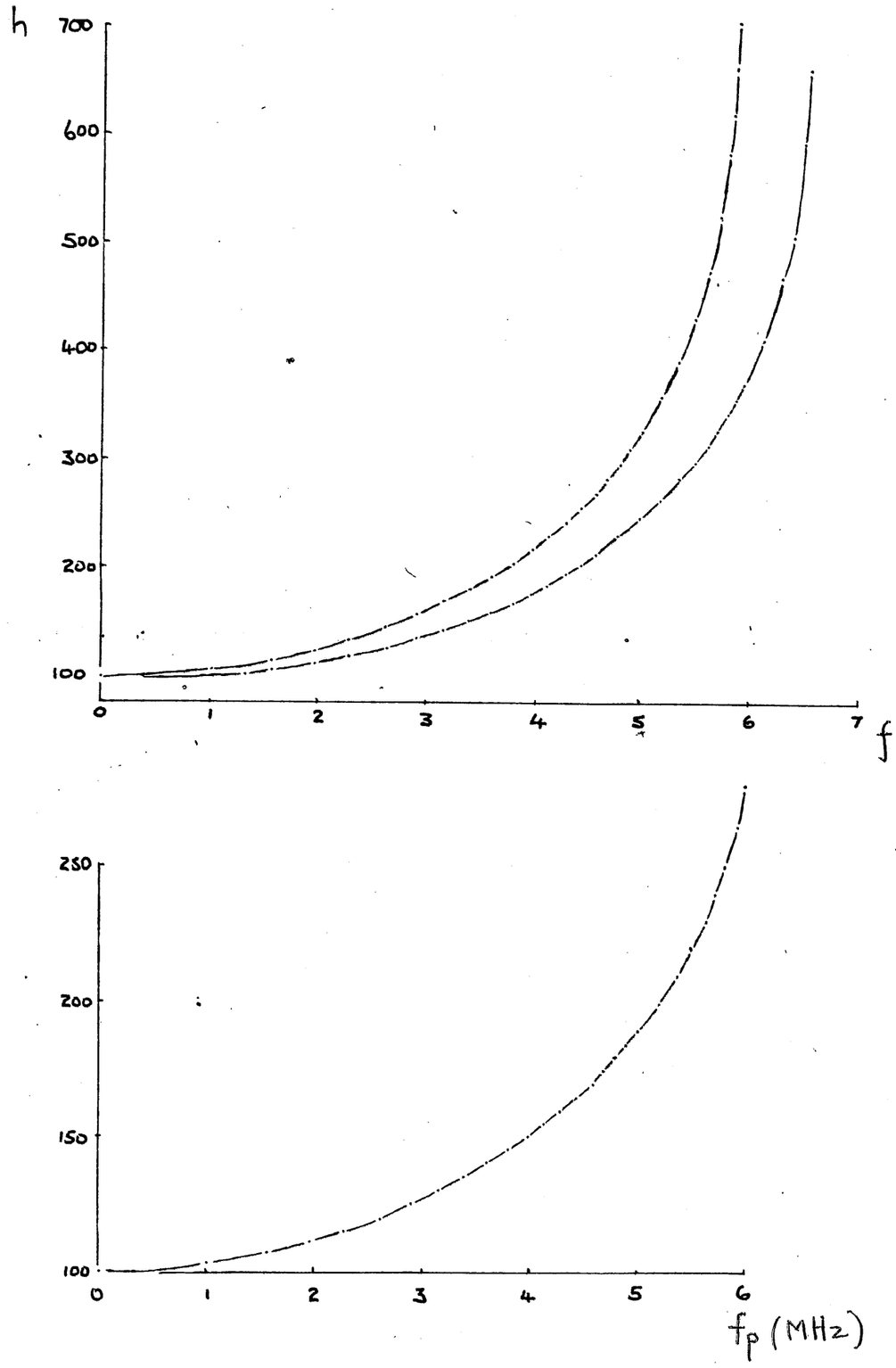
h
700
600
500
400
300
200
100
0
1
2
3
4
5
6
7
f
h
250
200
150
100
0
1
2
3
4
5
6
fp (MHz)

Figure 56

Ionogram calculated for a "cubic-parabolic" N(h) profile. Upper diagram shows the ionogram; lower diagram gives the original N(h) profile.

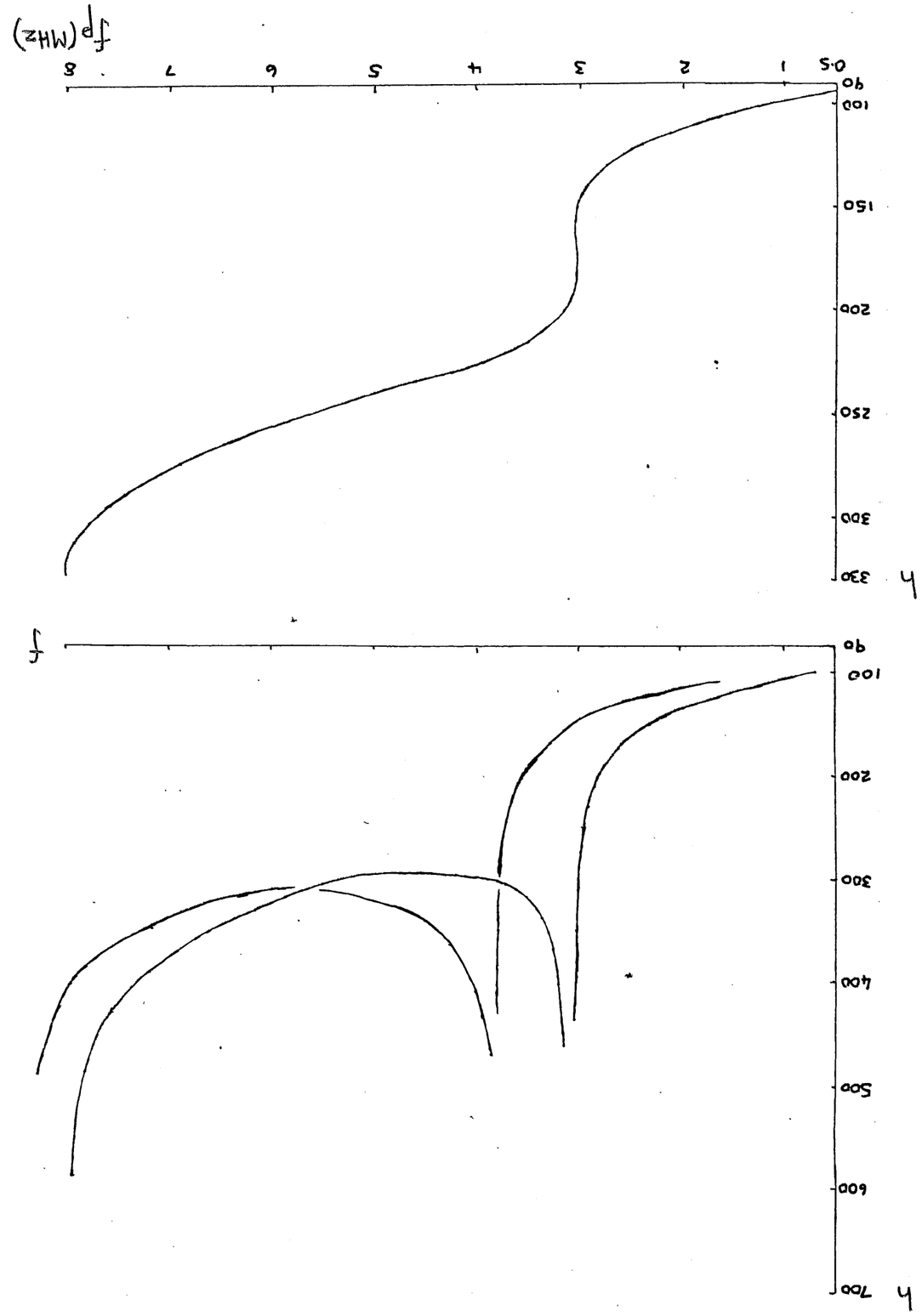
f_p (MHz)
0.5
1
2
3
4
5
6
7
8
90
100
150
200
250
300
330
h
f
90
100
200
300
400
500
600
700
h

TABLE 30

N(h) PROFILE WITHOUT VALLEY

ACTUAL HEIGHT	REAL HT CALCULATED BY LS	FLAT BASE	h_o=95km	Δh LS	FLAT BASE	h_o=95km
102.0	101.8	104.0	99.4	-0.2	2.0	-2.6
104.0	103.9	104.1	103.8	-0.1	0.1	-0.2
107.0	106.9	106.8	107.2	-0.1	-0.2	0.2
111.0	110.9	110.6	111.5	-0.1	-0.4	0.5
115.0	114.9	114.5	115.6	-0.1	-0.5	0.6
120.0	119.9	119.4	120.7	-0.1	-0.6	0.7
125.0	124.9	124.3	125.7	-0.1	-0.7	0.7
130.0	129.9	129.3	130.8	-0.1	-0.7	0.8
135.0	134.9	134.2	135.8	-0.1	-0.8	0.8
140.0	139.8	139.1	140.8	-0.2	-0.9	0.8
145.0	144.8	144.1	145.8	-0.2	-0.9	0.8
150.0	149.8	149.1	150.8	-0.2	-0.9	0.8
155.0	154.8	154.0	155.7	-0.2	-1.0	0.7
160.0	159.8	159.0	160.7	-0.2	-1.0	0.7
165.0	164.8	163.9	165.7	-0.2	-1.1	0.7
170.0	169.8	168.9	170.7	-0.2	-1.1	0.7
175.0	174.8	173.9	175.7	-0.2	-1.1	0.7
180.0	179.7	178.8	175.6	-0.3	-1.2	0.6
185.0	184.7	183.8	185.6	-0.3	-1.2	0.6
190.0	189.7	188.7	190.6	-0.3	-1.3	0.6
195.0	194.7	193.7	195.6	-0.3	-1.3	0.6
200.0	199.7	198.7	200.5	-0.3	-1.3	0.5
205.0	204.6	203.6	205.5	-0.4	-1.4	0.5
210.0	209.6	208.6	210.5	-0.4	-1.4	0.5
215.0	214.6	213.5	215.5	-0.4	-1.5	0.5
220.0	219.6	218.5	220.5	-0.4	-1.5	0.5
225.0	224.6	223.5	225.4	-0.4	-1.5	0.4
230.0	229.5	228.4	230.4	-0.5	-1.6	0.4
235.0	234.5	233.4	235.4	-0.5	-1.6	0.4
240.0	239.5	238.4	240.4	-0.5	-1.6	0.4
245.0	244.5	243.4	245.4	-0.5	-1.6	0.4
249.9	249.5	248.2	250.2	-0.5	-1.8	0.2
255.0	254.5	253.2	255.2	-0.5	-1.8	0.2

TABLE 31

N(h) PROFILE WITH VALLEY

ACTUAL HEIGHT	REAL HT CALCULATED BY LS	FLAT BASE	h_o=95 km	Δh LS	FLAT BASE	h_o=95km
95.00	-756.87	94.15	94.70	-851.87	-0.85	-0.30
99.70	162.83	95.54	95.35	63.13	-4.16	-4.35
104.40	22.25	101.44	101.23	-82.15	-2.96	-3.17
109.10	63.13	106.29	106.04	-45.97	-2.81	-3.06
113.80	70.15	111.12	110.85	-43.65	-2.68	-2.95
116.15	74.79	113.50	113.23	-41.36	-2.65	-2.92
118.50	78.21	115.87	115.60	-40.29	-2.63	-2.90
120.85	82.20	118.25	117.97	-38.65	-2.60	-2.88
123.20	86.38	120.60	120.32	-36.82	-2.60	-2.88
125.55	90.08	122.98	122.69	-35.47	-2.57	-2.86
127.90	93.57	125.32	125.03	-34.33	-2.58	-2.87
130.25	96.89	127.68	127.39	-33.36	-2.57	-2.86
132.60	99.99	130.00	129.71	-32.61	-2.60	-2.89
134.95	103.02	132.34	132.05	-31.93	-2.61	-2.90
137.30	105.93	134.73	134.44	-31.37	-2.57	-2.86
139.65	108.58	137.05	136.75	-31.07	-2.60	-2.90
142.00	111.29	139.37	139.07	-30.71	-2.63	-2.93
144.35	114.02	141.73	141.44	-30.33	-2.62	-2.91
146.70	116.55	144.02	143.73	-30.15	-2.68	-2.97
149.05	119.08	146.39	146.09	-29.97	-2.66	-2.96
151.40	121.67	148.78	148.49	-29.73	-2.62	-2.91
153.75	124.20	151.15	150.85	-29.55	-2.60	-2.90
156.10	126.38	153.30	153.00	-29.72	-2.80	-3.10
158.45	128.93	155.86	155.57	-29.52	-2.59	-2.88
191.35	139.42	166.26	165.97	-51.93	-25.09	-25.38
193.70	151.74	178.45	178.16	-41.96	-15.24	-15.54
196.05	154.01	180.13	179.84	-42.04	-15.92	-16.21
198.40	159.30	184.52	184.23	-39.10	-13.88	-14.17
200.75	161.93	187.23	186.93	-38.82	-13.52	-13.82
203.10	165.42	190.45	190.15	-37.68	-12.65	-12.95
205.45	168.66	193.35	193.05	-36.79	-12.10	-12.40
207.80	171.98	196.28	195.98	-35.82	-11.52	-11.82
210.15	175.34	199.18	198.88	-34.81	-10.97	-11.27
212.50	178.64	202.07	201.77	-33.86	-10.43	-10.73
214.85	181.97	204.95	204.65	-32.88	-9.90	-10.20
217.20	185.47	207.81	207.51	-31.73	-9.39	-9.69
219.55	188.92	210.64	210.33	-31.63	-8.91	-9.22
221.90	192.42	213.47	213.16	-29.48	-8.43	-8.74
224.25	195.76	216.26	215.95	-28.49	-7.99	-8.30
226.60	199.09	219.01	218.69	-27.51	-7.59	-7.91

TABLE 32

COSINE LAYER

36 Points

ACTUAL HEIGHT	REAL HT CALCULATED BY FLAT BASE	REAL HT CALCULATED BY h_o = 95 km	Δh FLAT BASE	Δh h_o = 95 km
115.00	125.04	109.38	10.04	- 5.62
120.01	124.47	121.04	4.46	1.03
125.01	127.95	126.86	2.94	1.85
129.99	131.91	132.40	1.92	2.41
135.01	136.23	137.80	1.22	2.79
140.00	140.72	143.06	0.72	3.06
145.01	145.35	148.28	0.34	3.27
150.00	150.05	153.42	0.05	3.42
155.00	154.82	158.55	- 0.18	3.55
160.00	159.62	163.65	- 0.38	3.65
165.01	164.47	168.74	- 0.54	3.73
170.00	169.33	173.80	- 0.67	3.80
174.99	174.21	178.85	- 0.78	3.86
180.01	179.13	183.92	- 0.88	3.91
185.01	184.05	188.96	- 0.96	3.95
190.01	188.97	194.00	- 1.04	3.99
195.01	193.90	199.03	- 1.11	4.02
200.01	198.85	204.06	- 1.16	4.05
205.00	203.79	209.08	- 1.21	4.08
209.99	208.73	214.09	- 1.26	4.10
215.00	213.71	219.12	- 1.29	4.12
220.00	218.67	224.14	- 1.33	4.14
225.01	223.65	229.16	- 1.36	4.15
230.01	228.62	234.18	- 1.39	4.17
235.00	233.59	239.18	- 1.41	4.18
240.00	238.57	244.19	- 1.43	4.19
245.01	243.56	249.21	- 1.45	4.20
249.98	248.52	254.20	- 1.46	4.22
254.99	253.52	259.22	- 1.47	4.23
259.98	258.49	264.21	- 1.49	4.23
265.02	263.53	269.27	- 1.49	4.25
269.98	268.48	274.24	- 1.50	4.26
275.03	273.53	279.30	- 1.50	4.27
279.98	278.49	284.27	- 1.49	4.29
284.93	283.45	289.24	- 1.48	4.31
289.86	288.43	294.22	- 1.43	4.36

TABLE 33

COSINE LAYER

28 Points

ACTUAL HEIGHT	REAL HT CALCULATED BY LS	FLAT BASE	h_o = 95 km	Δ h LS	FLAT BASE	h_o=95 km
115.00	115.82	125.38	108.90	0.82	10.38	- 6.10
125.01	125.67	126.50	130.57	0.66	1.49	5.56
135.01	135.51	135.40	140.86	0.50	0.39	5.85
145.01	145.41	144.53	151.31	0.40	- 0.48	6.30
155.00	155.34	154.05	161.51	0.34	- 0.95	6.51
165.01	165.30	163.73	171.66	0.29	- 1.28	6.65
174.99	175.25	173.48	181.73	0.26	- 1.51	6.74
185.01	185.25	183.33	191.83	0.24	- 1.68	6.82
195.01	195.22	193.19	201.87	0.21	- 1.82	6.86
200.01	200.21	198.14	206.90	0.20	- 1.87	6.89
205.00	205.20	203.08	211.90	0.20	- 1.92	6.90
209.99	210.17	208.02	216.90	0.18	- 1.97	6.91
215.00	215.18	213.00	221.93	0.18	- 2.00	6.93
220.00	220.17	217.96	226.94	0.17	- 2.04	6.94
225.01	225.18	222.94	231.96	0.17	- 2.07	6.95
230.01	230.17	227.91	236.97	0.16	- 2.10	6.96
235.00	235.16	232.88	241.98	0.16	- 2.12	6.98
240.00	240.16	237.86	246.98	0.16	- 2.14	6.98
245.01	245.16	242.85	252.00	0.15	- 2.16	6.99
249.98	250.14	247.81	256.99	0.16	- 2.17	7.01
254.99	255.15	252.80	262.00	0.16	- 2.19	7.01
259.98	260.13	257.78	266.99	0.15	- 2.20	7.01
265.02	265.18	262.82	272.05	0.16	- 2.20	7.03
269.98	270.14	267.77	277.01	0.16	- 2.21	7.03
275.03	275.20	272.82	282.08	0.17	- 2.21	7.05
279.98	280.16	277.78	287.04	0.18	- 2.20	7.06
284.93	285.13	282.74	292.01	0.20	- 2.19	7.08
289.86	290.11	287.72	297.00	0.25	- 2.14	7.14

TABLE 34.

COSINE LAYER

21 Points

ACTUAL HEIGHT	REAL HT CALCULATED BY LS	FLAT BASE	h_o=95 km	Δ h LS	FLAT BASE	h_o=95 km
115.00	115.88	125.38	108.90	0.88	10.38	-6.10
125.01	125.75	126.50	130.57	0.76	1.49	5.56
135.01	135.57	135.40	140.86	0.56	0.39	5.85
145.01	145.46	144.53	151.31	0.45	- 0.48	6.30
155.00	155.38	154.05	161.51	0.38	- 0.95	6.51
165.01	165.34	163.73	171.66	0.33	- 1.28	6.65
174.99	175.28	173.48	181.73	0.29	- 1.51	6.74
185.01	185.27	183.33	191.83	0.26	- 1.68	6.82
195.01	195.25	193.19	201.87	0.24	- 1.82	6.86
205.00	205.23	203.09	211.91	0.23	- 1.91	6.91
215.00	215.21	213.01	221.95	0.21	- 1.99	6.95
225.01	225.20	222.96	231.98	0.19	- 2.05	6.97
235.00	235.19	232.91	242.01	0.19	- 2.09	7.01
245.01	245.19	242.89	252.04	0.18	- 2.12	7.03
254.99	255.18	252.87	262.06	0.19	- 2.12	7.07
265.02	265.25	262.92	272.15	0.23	- 2.10	7.13
269.98	270.19	267.86	277.10	0.21	- 2.12	7.12
275.03	275.25	272.91	282.16	0.22	- 2.12	7.13
279.98	280.21	277.86	287.12	0.23	- 2.12	7.14
284.93	285.18	282.82	292.09	0.25	- 2.11	7.16
289.86	290.16	287.80	297.07	0.30	- 2.06	7.21

TABLE 35

PARABOLIC LAYER

43 Points

ACTUAL HEIGHT	REAL HT CALCULATED BY FLAT BASE	h_o = 95 km	Δh FLAT BASE	h_o = 95 km
101.00	101.78	98.37	0.78	-2.63
102.00	102.08	101.72	0.08	-0.28
103.00	102.99	103.03	-0.01	0.03
104.00	103.93	104.24	-0.07	0.24
105.00	104.89	105.36	-0.11	0.36
107.00	106.84	107.53	-0.16	0.53
109.00	108.81	109.64	-0.19	0.64
111.00	110.78	111.71	-0.22	0.71
113.00	112.77	113.77	-0.23	0.77
115.00	114.76	115.81	-0.24	0.81
119.99	119.73	120.88	-0.26	0.89
125.00	124.73	125.93	-0.27	0.93
130.01	129.72	130.97	-0.29	0.96
135.00	134.71	136.00	-0.29	1.00
140.00	139.70	141.01	-0.30	1.01
145.01	144.70	146.04	-0.31	1.03
150.01	149.70	151.06	-0.31	1.05
154.98	154.67	156.04	-0.31	1.06
160.00	159.69	161.07	-0.31	1.07
165.00	164.69	166.08	-0.31	1.08
170.02	169.70	171.10	-0.32	1.08
175.01	174.69	176.10	-0.32	1.09
180.00	179.68	181.10	-0.32	1.10
185.00	184.68	186.11	-0.32	1.11
190.00	189.68	191.11	-0.32	1.11
195.02	194.70	196.13	-0.32	1.11
199.99	199.67	201.11	-0.32	1.12
205.01	204.68	206.13	-0.33	1.12
209.99	209.66	211.11	-0.33	1.12
214.99	214.66	216.12	-0.33	1.13
219.99	219.67	221.13	-0.32	1.14
224.99	224.66	226.12	-0.33	1.13
229.96	229.63	231.09	-0.33	1.13
234.97	234.65	236.11	-0.32	1.14
240.04	239.71	241.18	-0.33	1.14
245.04	244.72	246.19	-0.32	1.15
249.94	249.62	251.09	-0.32	1.15
254.98	254.66	256.13	-0.32	1.15
260.04	259.72	261.19	-0.32	1.15
264.92	264.61	266.09	-0.31	1.17
269.97	269.67	271.14	-0.30	1.17
275.02	274.71	276.19	-0.31	1.17
280.02	279.73	281.21	-0.29	1.19

TABLE 36
PARABOLIC LAYER

28 Points

ACTUAL HEIGHT	REAL HT CALCULATED BY LS	FLAT BASE	h_o=95 km	Δh LS	FLAT BASE	h_o=95 km
101.00	101.036	101.812	98.26	0.04	0.81	-2.74
103.00	103.041	102.741	103.85	0.04	-0.26	0.85
105.00	105.032	104.702	105.98	0.03	-0.30	0.98
109.00	109.029	108.634	110.23	0.03	-0.37	1.23
113.00	113.022	112.611	114.32	0.02	-0.39	1.32
119.99	120.011	119.573	121.41	0.02	-0.42	1.42
130.01	130.021	129.568	131.49	0.01	-0.44	1.49
140.00	140.01	139.555	141.52	0.01	-0.44	1.52
150.01	150.03	149.561	151.56	0.02	-0.45	1.55
160.00	160.021	159.552	161.58	0.02	-0.45	1.58
170.02	170.032	169.562	171.60	0.01	-0.46	1.58
180.00	180.015	179.547	181.60	0.02	-0.45	1.60
190.00	190.015	189.549	191.62	0.02	-0.45	1.62
199.99	200.008	199.543	201.62	0.02	-0.45	1.63
209.99	210.008	209.546	211.63	0.02	-0.44	1.64
219.99	220.020	219.556	221.64	0.03	-0.43	1.65
224.99	225.011	224.546	226.64	0.02	-0.44	1.65
229.96	229.980	229.514	231.61	0.02	-0.45	1.65
234.97	234.998	234.530	236.62	0.03	-0.44	1.65
240.04	240.065	239.596	241.69	0.03	-0.44	1.65
245.04	245.066	244.597	246.69	0.03	-0.44	1.65
249.94	249.967	249.497	251.60	0.03	-0.44	1.66
254.98	255.009	254.538	256.64	0.03	-0.44	1.66
260.04	260.070	259.599	261.70	0.03	-0.44	1.66
264.92	264.960	264.488	266.59	0.04	-0.43	1.67
269.97	270.017	269.544	271.65	0.05	-0.43	1.68
275.02	275.065	274.593	276.70	0.05	-0.43	1.68
280.02	280.087	279.613	281.72	0.07	-0.41	1.70

TABLE 37

COMPLICATED MONOTONIC PROFILE

39 Points

ACTUAL HEIGHT	REAL HT CALCULATED BY FLAT BASE	h_o=95 km	Δ h FLAT BASE	h_o =95 km
81.49	82.79	89.09	1.30	7.60
82.98	82.98	83.36	0.00	0.38
84.47	84.32	83.99	-0.15	-0.48
85.95	85.72	84.95	-0.23	-1.00
87.44	87.15	86.10	-0.29	-1.34
88.93	88.59	87.35	-0.34	-1.58
90.41	90.05	88.66	-0.36	-1.75
91.89	91.50	90.00	-0.39	-1.89
93.37	92.97	91.38	-0.40	-1.99
94.85	94.43	92.76	-0.42	-2.09
96.32	95.89	94.17	-0.43	-2.15
97.79	97.35	95.58	-0.44	-2.21
99.25	98.80	96.99	-0.45	-2.26
100.70	100.25	98.41	-0.45	-2.29
102.13	101.67	99.81	-0.46	-2.32
103.52	103.06	101.18	-0.46	-2.34
104.89	104.43	102.53	-0.46	-2.36
106.12	105.67	103.76	-0.45	-2.36
111.90	110.93	108.99	0.03	-2.91
115.65	114.91	112.95	-0.74	-2.70
118.46	117.68	115.71	-0.78	-2.75
121.89	121.16	119.16	-0.73	-2.73
125.98	125.26	123.24	-0.72	-2.74
130.50	129.79	127.74	-0.71	-2.76
135.33	134.63	132.54	-0.70	-2.79
140.42	139.73	137.61	-0.69	-2.81
145.47	144.79	142.63	-0.68	-2.84
152.78	152.12	149.91	-0.66	-2.87
159.49	158.82	156.57	-0.67	-2.92
166.17	165.51	163.22	-0.66	-2.95
172.88	172.22	169.91	-0.66	-2.97
179.57	178.91	176.57	-0.66	-3.00
186.28	185.63	183.27	-0.65	-3.01
192.97	192.32	189.94	-0.65	-3.03
199.65	199.01	196.62	-0.64	-3.03
206.37	205.75	203.34	-0.62	-3.03
212.98	212.36	209.95	-0.62	-3.03
219.64	219.05	216.63	-0.59	-3.01
226.38	225.84	223.41	-0.54	-2.97

TABLE 38

COMPLICATED MONOTONIC PROFILE

31 Points

ACTUAL HEIGHT	REAL HT CALCULATED BY LS	FLAT BASE h_o=95 km		$\triangle h$ LS	FLAT BASE	h_o=95 km
81.49	82.15	82.84	89.41	0.66	1.35	7.92
84.47	85.09	83.82	81.50	0.62	-0.65	-2.97
87.44	87.93	86.74	84.16	0.49	-0.70	-3.28
90.41	90.84	89.66	86.79	0.43	-0.75	-3.62
93.37	93.77	92.60	89.57	0.40	-0.77	-3.80
96.32	96.68	95.53	92.40	0.36	-0.79	-3.92
99.25	99.59	98.46	95.26	0.34	-0.79	-3.99
102.13	102.47	101.35	98.10	0.34	-0.78	-4.03
104.89	105.25	104.14	100.87	0.36	-0.75	-4.02
106.12	106.48	105.36	102.08	0.36	-0.76	-4.04
111.90	111.74	110.62	107.32	0.16	-1.28	-4.58
115.65	115.72	114.60	111.28	0.07	-1,05	-4.37
118.46	118.49	117.37	114.04	0.03	-1.09	-4.42
121.89	121.97	120.85	117.49	0.08	-1.04	-4.40
125.98	126.06	124.94	121.57	0.08	-1.04	-4.41
130.50	130.60	129.48	126.08	0.10	-1.02	-4.42
135.33	135.43	134.31	130.88	0.10	-1.02	-4.45
140.42	140.53	139.41	135.95	0.11	-1,01	-4.47
145.47	145.59	144.46	140.98	0.12	-1.01	-4.49
152.78	152.91	151.79	148.26	0.13	-0.99	-4.52
159.49	159.61	158.49	154.93	0.12	-1.00	-4.56
166.17	166.30	165.18	161.59	0.13	-0.99	-4.58
172.88	173.02	171.90	168.28	0.14	-0.98	-4.60
179.57	179.71	178.58	174.94	0.14	-0.99	-4.63
186.28	186.42	185.30	181.64	0.14	-0.98	-4.64
192.97	193.11	191.99	188.32	0.14	-0.98	-4.65
199.65	199.80	198.68	194.99	0.15	-0.97	-4.64
206.37	206.54	205.42	201.72	0.17	-0.95	-4.65
212.98	213.15	212.03	208.33	0.17	-0.95	-4.65
219.64	219.84	218.72	215.01	0,20	-0.92	-4.63
226.38	226.64	225.52	221.80	0.26	-0.86	-4.58

reduction program. A typical result for an N(h) profile without a "valley" is shown in Table 30. Generally it was found that both the single mode and joint mode methods produce accurate results (average standard error for single mode analysis is usually about several km, for joint mode analysis usually less than 1 km) if the N(h) profile is monotonic, but if a valley is present, both methods yield incorrect results (see Table 31) as expected (Titheridge[155]).

More recently, Herbert[62] produced a paper in which he proposed a number of "standard" ionograms which might be used to compare the accuracy of different methods of ionogram reduction. The real heights calculated from his standard ionogram for a Cosine Layer Model are compared with the actual real heights in Tables 32, 33 and 34. In each case the error, Δh, i.e. the difference between the real height as calculated from the ionogram and the actual real height, is shown. It is clear from these tables that the real heights calculated by the single mode analysis assuming that h_o = 95 km are least accurate (standard errors are 3.9, 6.8 and 6.8 km respectively) while those calculated by the joint mode analysis are most accurate (standard errors are 0.29 and 0.37 km compared with 2.2, 2.7 and 2.9 km respectively for the single mode analysis using the flat base assumption).

Results for the Parabolic Layer are given in Tables 35 and 36 and results for the Complicated Monotonic Layer Model in Tables 37 and 38. In each case the results confirm the above conclusion.

However, as observed earlier, the method only produces accurate results for monotonic profiles.

The/...

TABLE 39

SIMPLE DEEP VALLEY

39 Points

ACTUAL HEIGHT	REAL HT CALCULATED BY FLAT BASE	h_o=95 km	Δh FLAt base	h_o=95 km
91.00	91.71	93.53	0.71	2.53
92.00	91.99	92.10	-0.01	0.10
93.00	92.91	92.82	-0.09	-0.18
94.00	93.86	93.64	-0.14	-0.36
95.00	94.83	94.53	-0.17	-0.47
96.00	95.81	95.45	-0.19	-0.55
97.00	96.79	96.39	-0.21	-0.61
98.00	97.78	97.34	-0.22	-0.66
99.00	98.77	98.31	-0.23	-0.69
100.00	99.76	99.28	-0.24	-0.72
101.00	100.75	100.26	-0.25	-0.74
102.00	101.75	101.24	-0.25	-0.76
103.00	102.75	102.22	-0.25	-0.78
104.00	103.75	103.22	-0.25	-0.78
105.00	104.74	104.21	-0.26	-0.79
106.00	105.74	105.20	-0.26	-0.80
107.01	106.76	106.21	-0.25	-0.80
108.00	107.76	107.21	-0.24	-0.79
162.46	114.37	113.81	-48.09	-48.65
163.65	119.12	118.55	-44.53	-45.10
164.65	121.55	120.98	-43.10	-43.67
166.02	124.95	124.37	-41.07	-41.65
167.84	128.88	128.29	-38.96	-39.55
170.13	133.42	132.83	-36.71	-37.30
172.90	138.42	137.82	-34.48	-35.08
176.22	143.95	143.34	-32.27	-32.88
179.98	149.72	149.10	-30.26	-30.88
186.33	158.72	158.08	-27.61	-28.25
192.70	167.07	166.41	-25.63	-26.29
199.04	174.92	174.26	-24.12	-24.78
205.41	182.50	181.83	-22.91	-23.58
211.75	189.81	189.13	-21.94	-22.62
218.12	196.96	196.27	-21.16	-21.85
224.46	203.94	203.25	-20.52	-21.21
230.80	210.79	210.10	-20.01	-20.70
237.18	217.60	216.90	-19.58	-20.28
243.45	224.20	223.50	-19.25	-19.95
249.77	230.79	230.09	-18.98	-19.68
256.17	237.42	236.71	-18.75	-19.46

The results of the single mode analysis of an N(h) profile with a valley can be seen in Table 39 which gives the results for Herbert's Simple Deep Valley case. In the joint mode analysis of this case the matrix D^tD was found to be singular and could not be inverted.

7.3 TITHERIDGE'S METHOD OF IONOGRAM REDUCTION

7.3.1 BASIS OF TITHERIDGE'S METHOD

The method outlinedabove does not yield correct results if a valley is present in the N(h) profile . Since the above method cannot easily be adapted to cater for N(h) profiles with valleys, a computer program was written which uses the method developed by Titheridge[154, 156, 157, 158] to convert h'(f) curves to N(h) profiles. This was then adapted to test and correct for the presence of a valley.

Titheridge assumes that an N(h) profile can be represented by a series of linear laminations. Taking the basic equation,

$$h' = \int_0^h \mu' \, dh \qquad (7.14)$$

Titheridge defines $\bar{\mu}'(r,n)$ (or $\bar{\mu}'(f_r,f_n)$) as the mean value of μ' over the lamination h_{r-1} to h_r (f_{r-1} to f_r) for a wave frequency f_n, i.e.

$$\bar{\mu}'(r,n) = \frac{1}{h_r - h_{r-1}} \int_{h_{r-1}}^{h_r} \mu' \, dh \qquad (7.15)$$

Then, using the flat base assumption, equation (7.14) can be written as

/....

$$h_0' = h_0$$
$$h_1' = h_1 + (\bar{\mu}'(1,1) - 1)(h_1 - h_0) \qquad (7.16)$$
$$h_2' = h_2 + (\bar{\mu}'(2,2) - 1)(h_2 - h_1) + (\bar{\mu}'(1,2) - 1)(h_1 - h_0)$$

Let $h_1 - h_0 = \Delta h_1$, $h_1' - h_0' = \Delta h_1'$, etc. Then subtracting successive equations gives:

$$\left.\begin{aligned}
\Delta h_1' &= \Delta h_1 + (\bar{\mu}'(1,1) - 1)\Delta h_1 = \bar{\mu}'(1,1)\Delta h_1 \\
\Delta h_2' &= \Delta h_2 + (\bar{\mu}'(2,2) - 1)\Delta h_2 + (\bar{\mu}'(1,2) - 1)\Delta h_1 \\
&\qquad - (\bar{\mu}'(1,1) - 1)\Delta h_1 \\
&= \bar{\mu}'(2,2)\Delta h_2 - (\bar{\mu}'(1,1) - \bar{\mu}'(1,2))\Delta h_1
\end{aligned}\right\} \qquad (7.17)$$

From this follow the equations

$$h_0 = h_0'$$
$$\Delta h_1 = \frac{1}{\beta_{11}}\Delta h_1'$$
$$\Delta h_2 = \frac{1}{\beta_{22}}(\Delta h_2' + \beta_{12}\Delta h_1) \qquad (7.18)$$
$$\Delta h_3 = \frac{1}{\beta_{33}}(\Delta h_3' + \beta_{13}\Delta h_1 + \beta_{23}\Delta h_2)$$

---

where $\beta_{nn} = \bar{\mu}'(n,n)$

$$\beta_{in} = \bar{\mu}'(i, n-1) - \bar{\mu}'(i,n) \qquad (7.19)$$

which is the basis of Titheridge's method.

/...

7.3.2 THE COMPUTER PROGRAM FOR TITHERIDGE'S METHOD

To simplify the calculation of coefficients, h is assumed to vary linearly with X rather than electron density N (as assumed by Jackson[75]) or plasma frequency f_N. Hence $\bar{\mu}'(i,n)$ becomes

$$\bar{\mu}'(i,n) = \frac{1}{\Delta h_i}\int_{h_{i-1}}^{h_i} \mu' \, dX \, \frac{dh}{dX}$$

$$= \frac{1}{\Delta h_i}\,\frac{\Delta h_i}{\Delta X_i}\int_{X_{i-1}}^{X_i} \mu' \, dX$$

$$= \frac{1}{X_{i,n} - X_{i-1,n}}\int_{X_{i-1}}^{X_i} \mu' \, dX$$

where $X_{i,n} = \dfrac{f_i^2}{f_n^2}$. Again the substitution

$$t^2 = f_r^2 - f_N^2$$

can be made, giving

$$\bar{\mu}'(i,n) = \frac{2}{X_{i,n} - X_{i-1,n}}\int_{1 - \frac{t_i^2}{f_r^2}}^{1 - \frac{t_{i-1}^2}{f_r^2}} \frac{\mu' t \, dt}{f_r^2}$$

Gaussian integration formulae were used to evaluate the integrals and hence the coefficients given in equations (7.19) were calculated for the ordinary ray. Equations (7.18) were then used to determine the real heights.

The standard ionograms given by Herbert[62] were used to test the program. The real heights calculated for the Cosine Layer Model, the Parabolic Layer Model and the Complicated Monotonic Model are compared with the

actual/...

TABLE 40

TITHERIDGE'S METHOD

COSINE LAYER

ACTUAL	CALCULATED	Δ h
115.00	122.6	7.6
120.01	125.6	5.6
125.01	129.2	4.2
129.99	133.3	3.3
135.01	137.7	2.7
140.00	142.2	2.2
145.01	146.8	1.8
150.00	151.5	1.5
155.00	156.3	1.3
160.00	161.1	1.1
165.01	166.0	1.0
170.00	170.9	0.9
174.99	175.8	0.8
180.01	180.7	0.7
185.01	185.7	0.7
190.01	190.6	0.6
195.01	195.6	0.6
200.01	200.5	0.5
205.00	205.5	0.5
209.99	210.4	0.4
215.00	215.4	0.4
220.00	220.4	0.4
225.01	225.3	0.3
230.01	230.3	0.3
235.00	235.3	0.3
240.00	240.2	0.2
245.01	245.2	0.2
249.98	250.2	0.2
254.99	255.2	0.2
259.98	260.1	0.1
265.02	265.2	0.2
269.98	270.2	0.2
275.03	275.3	0.3
279.98	280.3	0.3
284.93	285.4	0.4
289.86	290.5	0.5

COMPLICATED MONOTONIC LAYER

ACTUAL	CALCULATED	Δ h
81.49	81.5	0.0
82.98	83.0	0.0
84.47	84.5	0.0
85.95	86.0	0.1
87.44	87.5	0.1
88.93	89.0	0.1
90.41	90.5	0.1
91.89	92.0	0.1
93.37	93.5	0.1
94.85	95.0	0.2
96.32	96.5	0.2
97.79	98.0	0.2
99.25	99.5	0.3
100.70	101.0	0.3
102.13	102.4	0.3
103.52	103.8	0.3
104.89	105.2	0.3
106.12	106.5	0.4
111.90	112.2	0.3
115.65	115.9	0.3
118.46	118.6	0.1
121.89	122.0	0.1
125.98	126.0	0.0
130.50	130.4	-0.1
135.33	135.2	-0.1
140.42	140.2	-0.2
145.47	145.2	-0.3
152.78	152.3	-0.5
159.49	159.2	-0.3
166.17	166.1	-0.1
172.88	172.9	0.0
179.57	179.7	0.1
186.28	186.6	0.3
192.97	193.4	0.4
199.65	200.2	0.6
206.37	207.0	0.6
212.98	213.7	0.7
219.64	220.6	1.0
226.38	227.6	1.2

TABLE 41 TITHERIDGE's METHOD

PARABOLIC LAYER

ACTUAL HEIGHT	CALCULATED HEIGHT	△h
101.00	101.0	0.0
102.00	102.0	0.0
103.00	103.0	0.0
104.00	104.0	0.0
105.00	105.0	0.0
107.00	107.0	0.0
109.00	109.0	0.0
111.00	111.0	0.0
113.00	113.0	0.0
115.00	115.0	0.0
119.99	120.0	0.0
125.00	125.1	0.1
130.01	130.1	0.1
135.00	135.1	0.1
140.00	140.1	0.1
145.01	145.1	0.1
150.01	150.2	0.2
154.98	155.1	0.1
160.00	160.2	0.2
165.00	165.2	0.2
170.02	170.2	0.2
175.01	175.2	0.2
180.00	180.2	0.2
185.00	185.2	0.2
190.00	190.2	0.2
195.02	195.2	0.2
199.99	200.2	0.2
205.01	205.1	0.1
209.99	210.1	0.1
214.99	215.1	0.1
219.99	220.0	0.0
224.99	225.0	0.0
229.96	229.9	-0.1
234.97	234.9	-0.1
240.04	239.9	-0.1
245.04	244.9	-0.1
249.94	249.7	-0.2
254.98	254.7	-0.3
260.04	259.8	-0.2
264.92	264.6	-0.3
269.97	269.7	-0.3
275.02	274.8	-0.2
280.02	279.8	-0.2

SIMPLE DEEP VALLEY

ACTUAL HEIGHT	CALCULATED HEIGHT	△h
91.00	91.0	0.0
92.00	92.0	0.0
93.00	93.0	0.0
94.00	94.0	0.0
95.00	95.1	0.1
96.00	96.1	0.1
97.00	97.1	0.1
98.00	98.1	0.1
99.00	99.1	0.1
100.00	100.1	0.1
101.00	101.1	0.1
102.00	102.1	0.1
103.00	103.2	0.2
104.00	104.2	0.2
105.00	105.2	0.2
106.00	106.2	0.2
107.01	107.3	0.3
108.00	108.3	0.3
162.46	116.2	-46.3
163.65	119.9	-43.8
164.65	122.5	-42.2
166.02	125.7	-40.3
167.84	129.6	-38.2
170.13	134.0	-36.1
172.90	139.0	-33.9
176.22	144.4	-31.8
179.98	150.2	-29.8
186.33	159.1	-27.2
192.70	167.5	-25.2
199.04	175.4	-23.6
205.41	183.1	-22.3
211.75	190.5	-21.3
218.12	197.7	-20.4
224.46	204.8	-19.7
230.80	211.7	-19.1
237.18	218.6	-18.6
243.45	225.4	-18.1
249.77	232.1	-17.7
256.17	239.0	-17.2

actual real heights in Tables 40 and 41.

To check for the presence of a valley the extraordinary ray trace is used. Points on the extraordinary ray trace may be scaled and read in by the program. The program then uses the calculated real heights (determined from the ordinary ray virtual heights) to determine the retardation which an extraordinary ray corresponding to an observed frequency should have undergone. If the extraordinary ray virtual heights calculated in this way agree with the observed virtual heights to within some specified tolerance, the program assumes that the calculated N(h) profile is a good approximation to the actual electron density distribution. If not, it assumes that either low-lying ionization or a valley is present (or possibly both). Examples of the program output for the case of Herbert's Complicated Monotonic Layer, the Simple Deep Valley and the Complicated Deep Valley models are shown in Figs. 57, 58 and 59.

7.4 CORRECTING FOR A VALLEY

If a valley is suspected in the actual electron density distribution, some correction for this must be included in the calculated N(h) profile so that the extraordinary ray virtual heights determined from the latter profile agree with the observed virtual heights. The simplest form of correction is the inclusion of a block of ionization immediately above the last point before the critical frequency. One way of doing this if a valley is suspected, is as follows: from the first observed extraordinary ray virtual height above the

valley/...

POINT NUMBER	CALCULATED EXT VIRTUAL HT	OBSERVED EXT VIRTUAL HT	DIFFERENCE
0	87.839	88.140	-0.301
1	91.347	91.680	-0.333
2	94.910	95.270	-0.360
3	98.544	98.940	-0.396
4	102.290	102.710	-0.420
5	106.169	106.600	-0.431
6	110.184	110.630	-0.446
7	114.381	114.870	-0.489
8	118.822	119.310	-0.488
9	123.503	124.040	-0.537
10	128.557	129.120	-0.563
11	134.042	134.640	-0.598
12	140.090	140.740	-0.650
13	146.803	147.540	-0.737
14	154.535	155.290	-0.755
15	163.547	164.490	-0.943
16	174.021	175.000	-0.979
17	213.890	217.140	-3.250
18	225.363	228.030	-2.667
19	231.460	234.020	-2.560
20	237.160	239.920	-2.760
21	242.529	245.710	-3.181
22	247.771	251.190	-3.419
23	252.851	256.460	-3.609
24	258.065	261.690	-3.625
25	263.137	266.760	-3.623
26	269.880	274.090	-4.210
27	283.537	287.040	-3.503
28	300.462	303.700	-3.238
29	319.515	322.720	-3.205
30	340.523	343.680	-3.157
31	363.474	366.880	-3.406
32	388.893	392.540	-3.647
33	417.154	421.340	-4.186
34	449.986	454.580	-4.594
35	487.685	493.100	-5.415
36	534.922	540.970	-6.048

FIG. 57. Example of program output comparing calculated extraordinary virtual heights with observed virtual heights for the Complicated Monotonic Profile (see sec. 7.3.2)

POINT NUMBER	CALCULATED EXT VIRTUAL HT	OBSERVED EXT VIRTUAL HT	DIFFERENCE
0	95.271	95.470	-0.199
1	100.020	100.260	-0.240
2	102.467	102.730	-0.263
3	104.998	105.280	-0.282
4	107.614	107.900	-0.286
5	110.334	110.640	-0.306
6	113.184	113.520	-0.336
7	116.208	116.540	-0.332
8	119.419	119.780	-0.361
9	122.898	123.280	-0.382
10	126.717	127.120	-0.403
11	130.992	131.440	-0.448
12	135.857	136.350	-0.493
13	141.682	142.200	-0.518
14	149.026	149.690	-0.664
15	159.119	159.870	-0.751
16	232.186	312.420	-80.234
17	230.999	296.010	-65.011
18	233.463	289.010	-55.547
19	237.225	283.620	-46.395
20	242.300	280.160	-37.860
21	248.627	279.010	-30.383
22	256.032	280.210	-24.178
23	264.775	283.820	-19.045
24	274.544	289.650	-15.106
25	290.662	302.170	-11.508
26	308.167	317.010	-8.843
27	326.496	333.560	-7.064
28	345.948	351.860	-5.912
29	366.791	371.810	-5.019
30	389.157	393.820	-4.663
31	413.695	418.110	-4.415
32	440.791	445.390	-4.599
33	472.139	476.870	-4.731
34	508.025	513.370	-5.345
35	552.910	558.750	-5.840
36	612.942	619.590	-6.648

FIG. 58. Example of program output comparing calculated extraordinary virtual heights with observed virtual heights for the Simple DeepValley Model.

POINT NUMBER	CALCULATED EXT VIRTUAL HT	OBSERVED EXT VIRTUAL HT	DIFFERENCE
0	95.271	95.470	-0.199
1	97.622	97.840	-0.218
2	100.020	100.260	-0.240
3	102.467	102.730	-0.263
4	104.998	105.280	-0.282
5	107.614	107.900	-0.286
6	110.334	110.640	-0.306
7	113.184	113.520	-0.336
8	116.208	116.540	-0.332
9	119.419	119.780	-0.361
10	122.898	123.280	-0.382
11	126.717	127.120	-0.403
12	130.992	131.440	-0.448
13	135.857	136.350	-0.493
14	141.682	142.200	-0.518
15	149.026	149.690	-0.664
16	159.119	159.870	-0.751
17	270.444	366.020	-95.576
18	267.022	343.970	-76.948
19	267.199	332.650	-65.451
20	267.470	321.940	-54.470
21	267.795	312.060	-44.265
22	268.266	303.610	-35.344
23	270.890	298.710	-27.820
24	275.961	297.650	-21.689
25	282.496	299.520	-17.024
26	294.082	306.770	-12.688
27	307.612	317.180	-9.568
28	322.190	329.700	-7.510
29	337.938	344.090	-6.152
30	355.010	360.150	-5.140
31	373.437	378.130	-4.693
32	393.744	398.190	-4.446
33	416.288	420.870	-4.582
34	442.481	447.200	-4.719
35	472.585	477.840	-5.255
36	510.356	516.050	-5.694

FIG. 59. Example of program output comparing calculated extraordinary virtual heights with observed virtual heights for the Complicated Deep Valley Model.

valley calculate the width of a block of ionization with plasma frequency, f_p, which is 0.9 times the critical frequency and which will give agreement between the calculated and observed virtual height for the extraordinary point in question. The next extraordinary point is then used to determine the frequency of the block to be inserted. If another extraordinary ray point is encountered for which $|\Delta h'_x|$ exceeds the error tolerance, this block is then subdivided into 2 blocks of equal width but different plasma frequencies and so on (see Appendix 8 for detailed exposition).

One snag with this method is that each time a change is made to the valley parameters, the real heights obtained from the ordinary ray trace have to be re-calculated and hence a new value of $h'_{x_{calc}}$ determined. This in turn affects the valley parameters which must be readjusted for this new value of $h'_{x_{calc}}$. The more valley parameters (blocks of ionization) one includes, the more complex this becomes, and even for a simple 2-block valley very many iterations are required to determine the three parameters. An improvement on this method can be obtained by using several extraordinary ray frequencies above the valley simultaneously to solve for the parameters of the valley. At the same time the change in calculated real heights above the valley can be taken into account. A method based on this idea is described in Appendix 8. This method was programmed and has been incorporated into the basic Titheridge method program.

The results obtained using this method on Herbert's data for the Simple Deep Valley, Deep Valley and Complicated Deep Valley Models are given in

Tables/...

Tables 42, 43 and 44. In each case successive pairs of extraordinary points above the valley were used to obtain several estimates of the width and plasma frequency of a single block of ionization in the valley. The means of these estimates were taken and the real heights recalculated accordingly. The real heights after correction for a valley are fairly close to the actual real heights (standard deviations are 4.8, 2.9 and 5.0 km respectively compared with 21.8, 22.8 and 24.1 km respectively before correction) as can be seen from Fig. 60 whch shows the actual profile and the calculated proffles for the Deep Valley Model.

However, when three extraordinary ray frequencies above the valley were used to solve for two blocks of ionization in the valley, the method did not always converge. When four extraordinary ray frequencies were used (3 blocks of ionization in the valley), the method did not converge at all. The results obtained when solving for two blocks of ionization for the Simple Deep Valley Model, are shown in Table 45. The improvement in accuracy over the one-block valley is noticeable.

7.5 SUMMARY AND CONCLUSIONS

Two basic methods of ionogram reduction have been programmed for computer solution. Both methods produce satisfactory results for monotonic N(h) profiles.

The advantage of the Least Squares method is the accuracy of the resulting N(h) profile if a valley is not present. The chief advantage of Titheridge's method is that valleys and low-lying ionization are easily

detected/...

Figure 60

An illustration of Herbert's[62] Deep Valley Model. Curve (a) represents the N(h) profile obtained from Titheridge's method when no valley correction is included; curve (b) the N(h) profile obtained when a single block of ionization is included in the valley and curve (c) shows the actual N(h) distribution for this model.

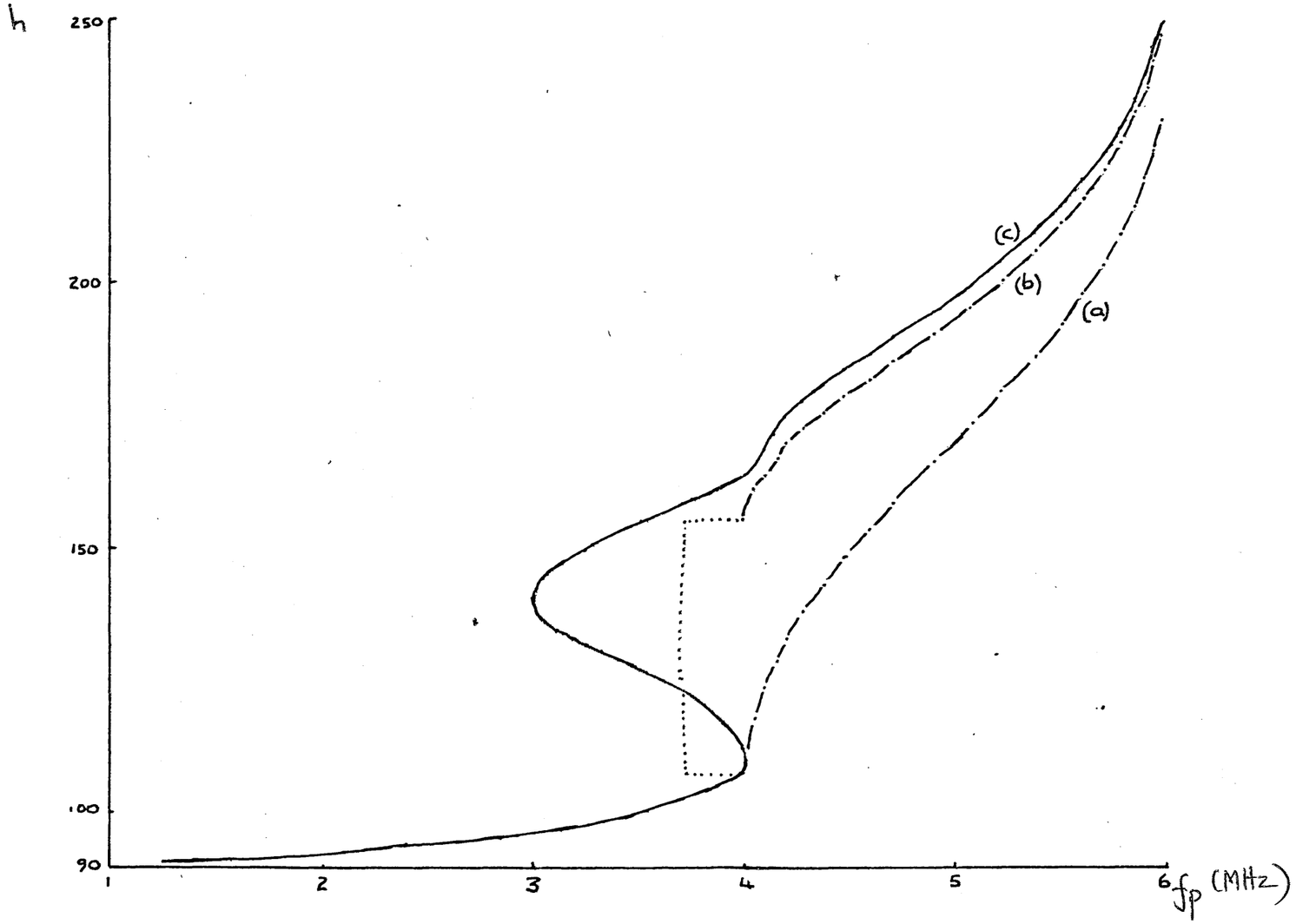
h
250
200
150
100
90
1
2
3
4
5
6
fp (MHz)
(c)
(b)
(a)

detected and can be corrected for. The least squares method will operate efficiently when the number of scaled ordinary ray frequencies is less than about 30 and the number of extraordinary ray frequencies less than about 15. When the number of scaled points exceeds these limits, much use is made of the backing store for the matrix operations and the execution time is drastically increased. Titheridge's method, on the other hand, is a step-by-step method which does not require much use of the backing store and the number of ordinary and extraordinary ray frequencies to which the program is limited has arbitrarily been set at 100 in each case.

The execution time for an ionogram with about 30 scaled ordinary ray frequencies and about 15 scaled extraordinary ray frequencies is approximately 2 minutes in each case. Correction for the presence of a valley requires a further 2 minutes.

CHAPTER 8

AN ANALYSIS OF SANAE IONOGRAMS

8.1 INTRODUCTION

To help understand the processes at work in the F-region of the ionosphere over Antarctica during summer, a series of SANAE ionograms taken at selected times during the day for 2 quiet days during summer were analyzed using the computer programs outlined in the previous chapter.

Although the original aim of this section (as outlined in Section 7.1) could not be achieved for lack of time, the results obtained are presented in order to give a more complete picture of the anomalous F2-region behaviour over SANAE.

8.2 THE ANALYSIS

Two geomagnetically quiet days during summer were selected for which good quality ionograms had been obtained throughout the day at SANAE. The two days selected were 22nd and 25th January 1968. For the 25th January, ionograms obtained every quarter hour of the day were scaled and for the 22nd January, ionograms taken at hourly intervals were used. These ionograms were then converted to N(h) profiles using the programs outlined in Chapter 7. Low-lying ionization was found to be present in the early morning (before 0400 LMT) and in the late evening (after about 1800 LMT), but no obvious valleys were detected during the two days.

Individual/...

Figure 61

N(h) distributions at selected hours of the day for 25th January, 1968, at SANAE.

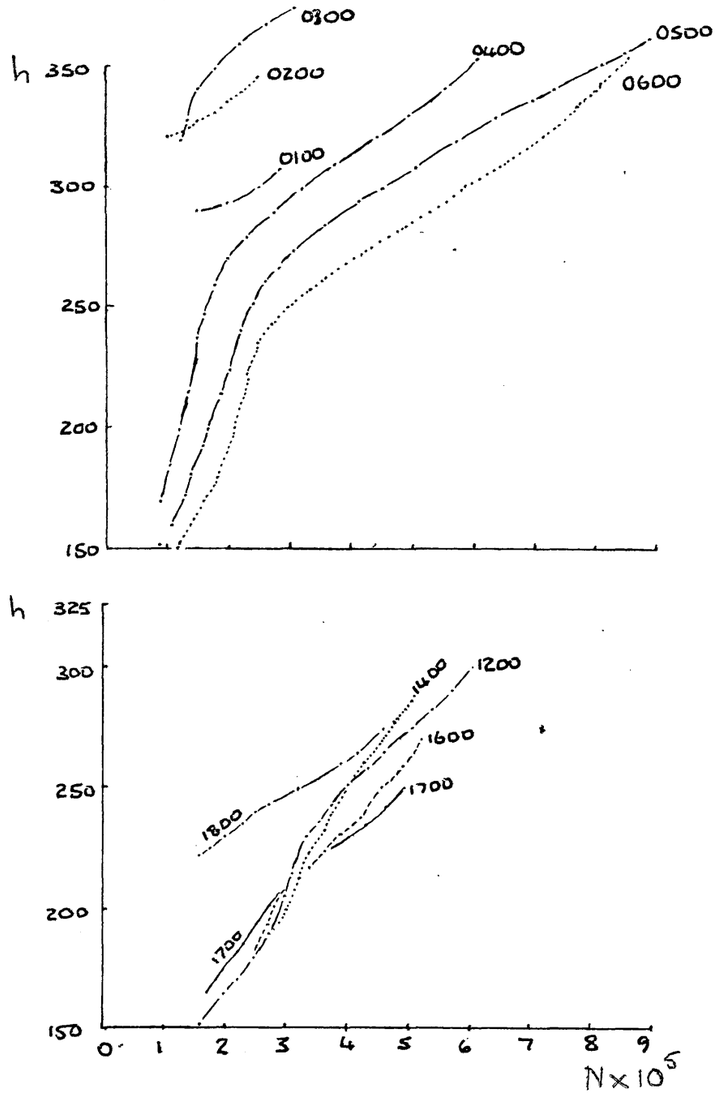
h
350
300
250
200
150
0300
0200
0400
0500
0100
0600
0
1
2
3
4
5
6
7
8
9
N×10⁵

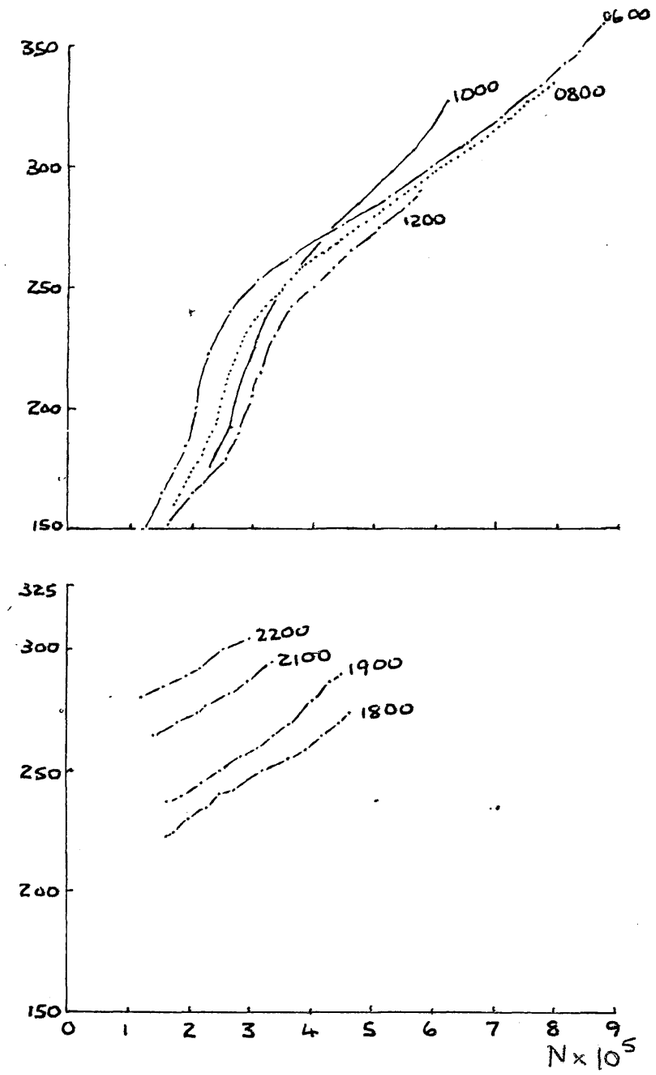
350
300
250
200
150
0600
1000
0800
1200
0
1
2
3
4
5
6
7
8
9
N×10⁵

h
325
300
250
200
150
1400
1200
1600
1800
1700
1700
0
1
2
3
4
5
6
7
8
9
N×10⁵

325
300
250
200
150
2200
2100
1900
1800
0
1
2
3
4
5
6
7
8
9
N×10⁵

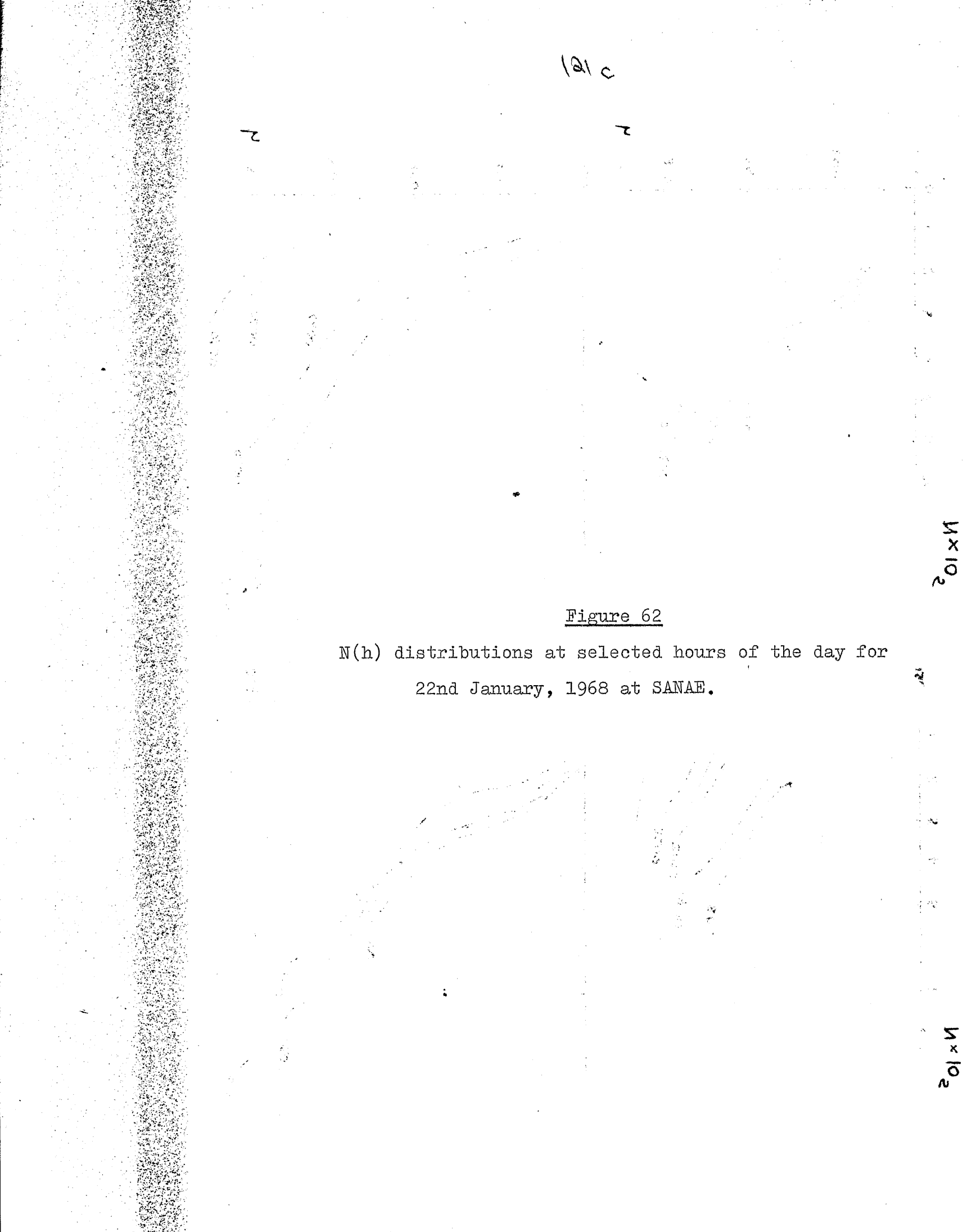

Figure 62

N(h) distributions at selected hours of the day for 22nd January, 1968 at SANAE.

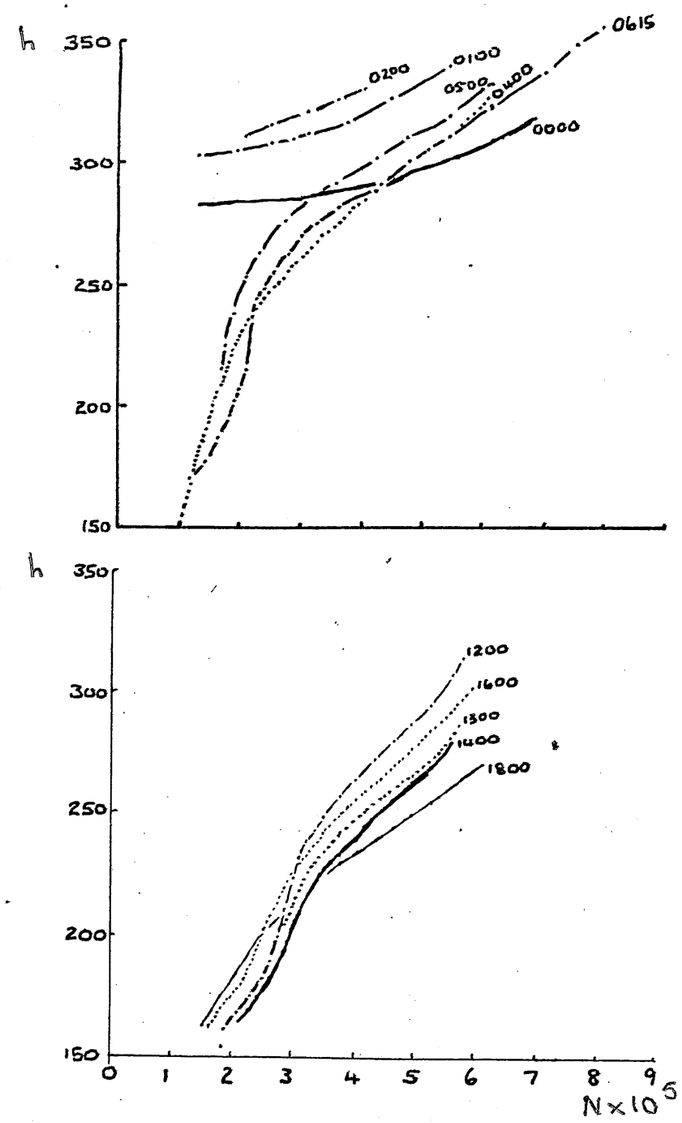
h
350
300
250
200
150
0200
0100
0500
0400
0615
0000
1200
1600
1300
1400
1800
0
1
2
3
4
5
6
7
8
9
N×10^5

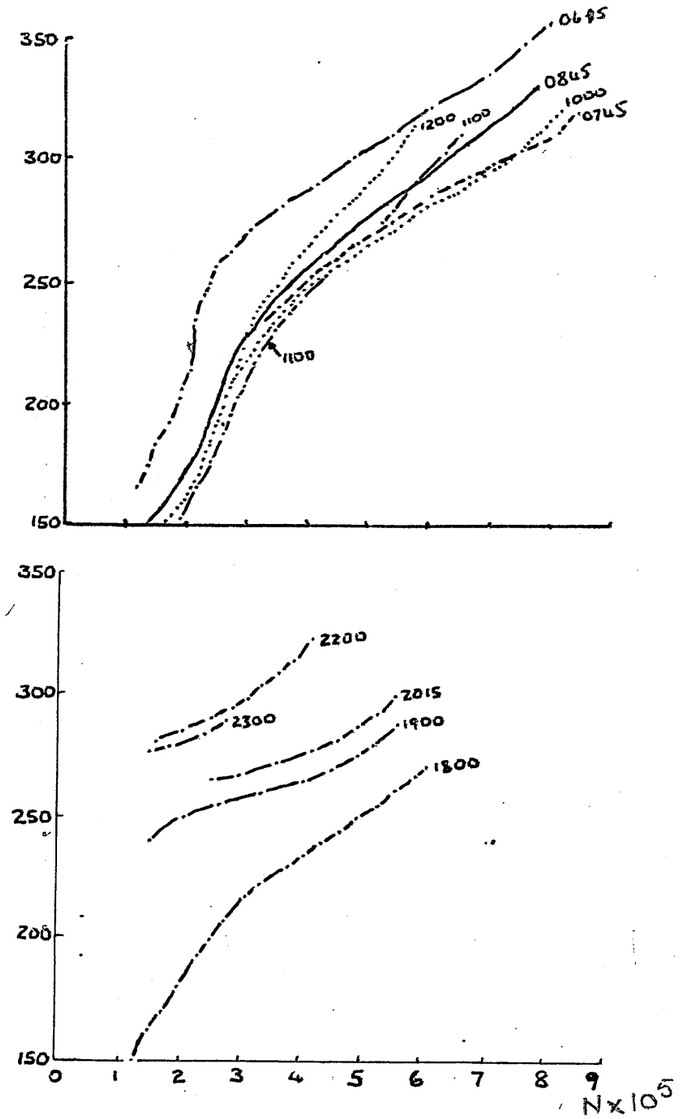
350
300
250
200
150
0645
0845
1200
1100
1000
0745
1100
2200
2300
2015
1900
1800
0
1
2
3
4
5
6
7
8
9
N×10^5

Figure 63

The variation of N with time at fixed heights above SANAE during the day for 25th January, 1968.

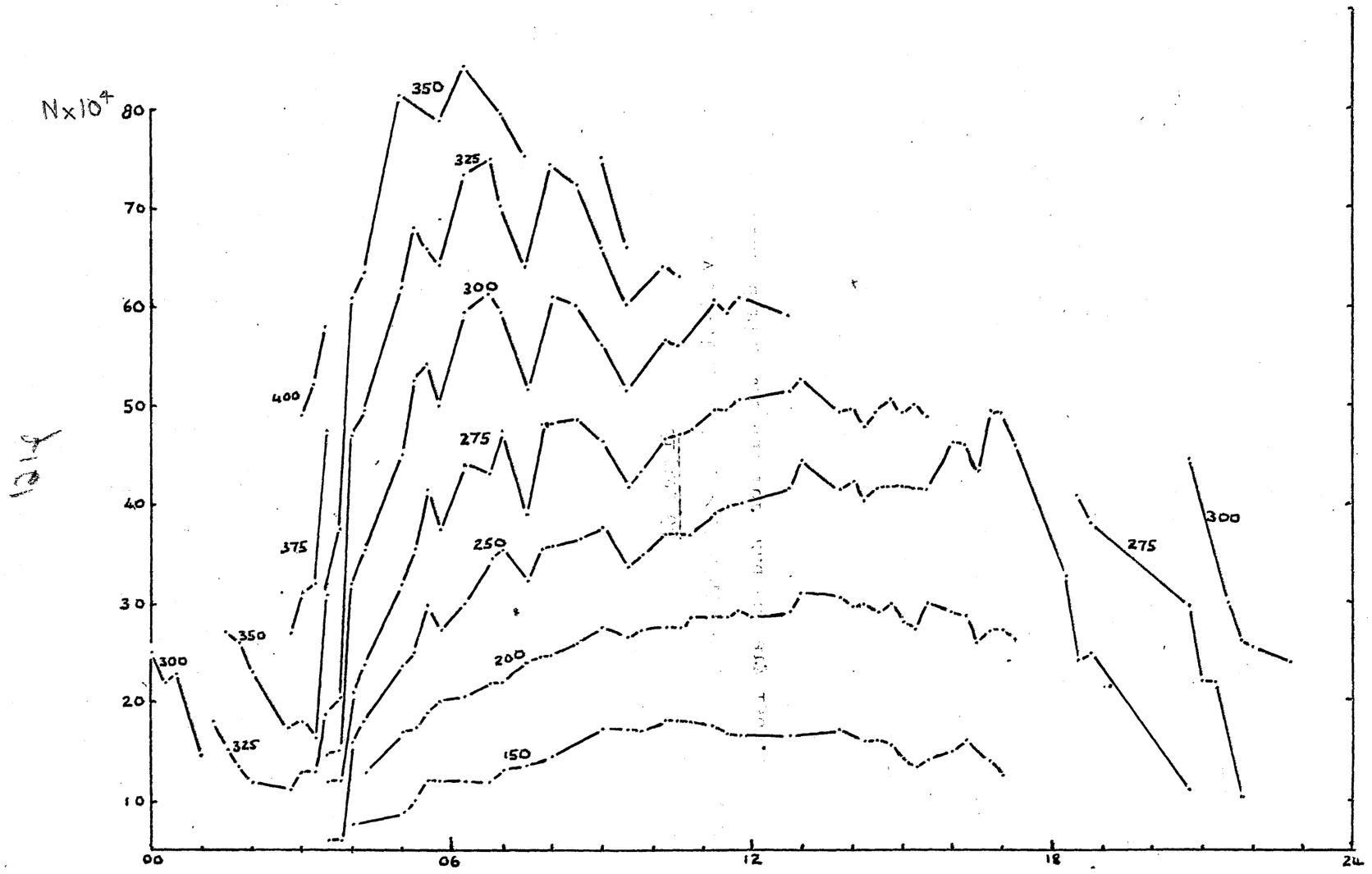
Nx10⁴
80
70
60
50
40
30
20
10
00
06
12
18
24
350
325
300
400
375
275
250
200
150
350
325
300
275
300

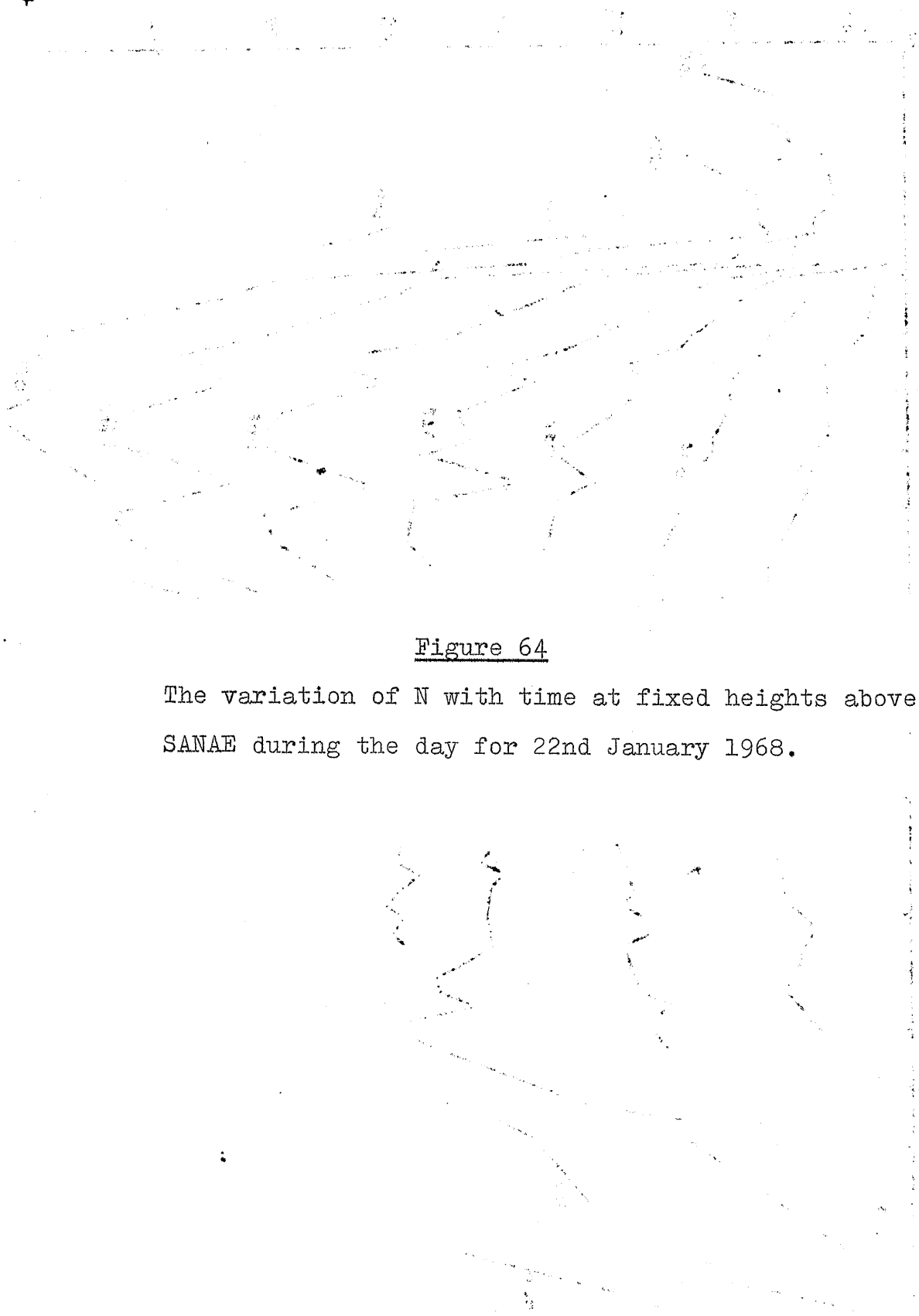

Figure 64

The variation of N with time at fixed heights above SANAE during the day for 22nd January 1968.

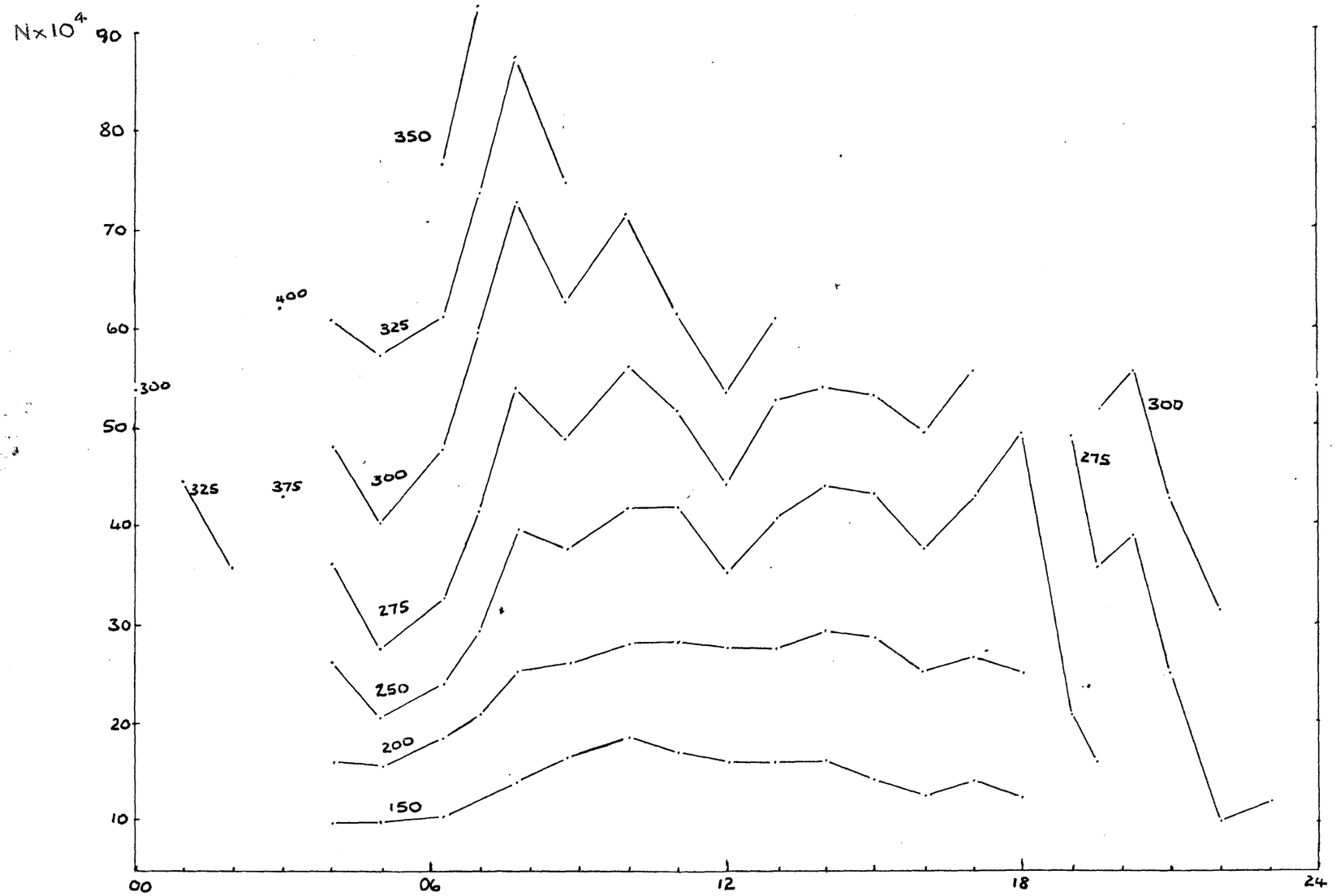
N×10⁴
90
80
70
60
50
40
30
20
10
00
06
12
18
24
350
325
400
300
325
375
300
275
250
200
150
300
275

TABLE 42

TITHERIDGE'S METHOD

SIMPLE DEEP VALLEY

ACTUAL HEIGHT	BEFORE VALLEY CORRECTION REAL HEIGHT	Δ h	AFTER VALLEY CORRECTION REAL HEIGHT	Δh
91.0	91.0	0.0	91.0	0.0
92.0	92.0	0.0	92.0	0.0
93.0	93.0	0.0	93.0	0.0
94.0	94.0	0.0	94.0	0.0
95.0	95.1	0.1	95.1	0.1
96.0	96.1	0.1	96.1	0.1
97.0	97.1	0.1	97.1	0.1
98.0	98.1	0.1	98.1	0.1
99.0	99.1	0.1	99.1	0.1
100.0	100.1	0.1	100.1	0.1
101.0	101.1	0.1	101.1	0.1
102.0	102.1	0.1	102.1	0.1
103.0	103.2	0.2	103.2	0.2
104.0	104.2	0.2	104.2	0.2
105.0	105.2	0.2	105.2	0.2
106.0	106.2	0.2	106.2	0.2
107.0	107.3	0.3	107.3	0.3
108.0	108.3	0.3	108.3	0.3
162.5	116.2	-46.3	153.2	-9.3
163.7	119.9	-43.8	154.8	-8.9
164.7	122.5	-42.2	156.0	-8.7
166.0	125.7	-40.3	157.6	-8.4
167.8	129.6	-38.2	159.6	-8.2
170.1	134.0	-36.1	162.2	-7.9
172.9	139.0	-33.9	165.3	-7.6
176.2	144.4	-31.8	168.9	-7.3
180.0	150.2	-29.8	173.0	-7.0
186.3	159.1	-27.2	179.9	-6.4
192.7	167.5	-25.2	186.7	-6.0
199.0	175.4	-23.6	193.4	-5.6
205.4	183.1	-22.3	200.1	-5.3
211.8	190.5	-21.3	206.7	-5.1
218.1	197.7	-20.4	213.4	-4.7
224.5	204.8	-19.7	219.9	-4.6
230.8	211.7	-19.1	226.5	-4.3
237.2	218.6	-18.6	233.1	-4.1
243.5	225.4	-18.1	239.6	-3.9
249.8	232.1	-17.7	246.1	-3.7
256.2	239.0	-17.2	252.9	-3.3

TABLE 43 TITHERIDGE'S METHOD

DEEP VALLEY MODEL

ACTUAL HEIGHT	BEFORE VALLEY CORRECTION REAL HEIGHT	Δh	AFTER VALLEY CORRECTION REAL HEIGHT	Δh
91.0	91.0	0.0	91.0	0.0
92.0	92.0	0.0	92.0	0.0
93.0	93.0	0.0	93.0	0.0
94.0	94.0	0.0	94.0	0.0
95.0	95.1	0.1	95.1	0.1
96.0	96.1	0.1	96.1	0.1
97.0	97.1	0.1	97.1	0.1
98.0	98.1	0.1	98.1	0.1
99.0	99.1	0.1	99.1	0.1
100.0	100.1	0.1	100.1	0.1
101.0	101.1	0.1	101.1	0.1
102.0	102.1	0.1	102.1	0.1
103.0	103.2	0.2	103.2	0.2
104.0	104.2	0.2	104.2	0.2
105.0	105.2	0.2	105.2	0.2
106.0	106.2	0.2	106.2	0.2
107.0	107.3	0.3	107.3	0.3
108.0	108.3	0.3	108.3	0.3
166.0	118.2	-47.8	160.7	-5.3
169.0	123.9	-45.1	164.2	-4.8
172.0	128.4	-43.6	167.2	-4.8
175.0	133.2	-41.8	170.1	-4.9
178.0	138.2	-39.8	173.1	-4.9
181.0	143.4	-37.6	176.2	-4.8
184.0	148.5	-35.5	179.2	-4.8
187.0	153.7	-33.3	182.3	-4.7
190.0	158.7	-31.3	185.5	-4.5
195.0	166.5	-28.5	190.8	-4.2
200.0	173.6	-26.4	196.1	-3.9
205.0	180.2	-24.8	201.3	-3.7
210.0	186.6	-23.4	206.6	-3.4
215.0	192.7	-22.3	211.8	-3.2
220.0	198.6	-21.4	216.9	-3.1
225.0	204.3	-20.7	222.1	-2.9
230.0	209.9	-20.1	227.2	-2.8
235.0	215.4	-19.6	232.4	-2.6
240.0	220.7	-19.3	237.4	-2.6
245.0	226.1	-18.9	242.6	-2.4
250.0	231.5	-18.5	247.9	-2.1

TABLE 44

TITHERIDGE'S METHOD

COMPLICATED DEEP VALLEY

ACTUAL HEIGHT	BEFORE VALLEY CORRECTION REAL HEIGHT	Δh	AFTER VALLEY CORRECTION REAL HEIGHT	Δh
91.0	91.0	0.0	91.0	0.0
92.0	92.0	0.0	92.0	0.0
93.0	93.0	0.0	93.0	0.0
94.0	94.0	0.0	94.0	0.0
95.0	95.1	0.1	95.1	0.1
96.0	96.1	0.1	96.1	0.1
97.0	97.1	0.1	97.1	0.1
98.0	98.1	0.1	98.1	0.1
99.0	99.1	0.1	99.1	0.1
100.0	100.1	0.1	100.1	0.1
101.0	101.1	0.1	101.1	0.1
102.0	102.1	0.1	102.1	0.1
103.0	103.2	0.2	103.2	0.2
104.0	104.2	0.2	104.2	0.2
105.0	105.2	0.2	105.2	0.2
106.0	106.2	0.2	106.2	0.2
107.0	107.3	0.3	107.3	0.3
108.0	108.3	0.3	108.3	0.3
170.4	119.4	-51.0	161.0	-9.4
172.5	124.2	-48.3	163.4	-9.1
174.0	127.5	-46.5	165.1	-8.9
175.7	131.3	-44.4	167.0	-8.7
177.6	135.5	-42.1	169.1	-8.5
179.8	140.0	-39.8	171.5	-8.3
182.1	144.8	-37.3	174.1	-8.0
184.9	150.0	-34.9	177.3	-7.6
188.1	155.3	-32.8	180.8	-7.3
193.5	163.6	-29.9	186.7	-6.8
198.9	171.2	-27.7	192.6	-6.3
204.2	178.3	-25.9	198.3	-5.9
209.6	185.1	-24.5	204.0	-5.6
215.0	191.6	-23.4	209.6	-5.4
220.4	197.9	-22.5	215.3	-5.1
225.7	204.0	-21.7	220.8	-4.9
231.1	210.0	-21.1	226.4	-4.7
236.5	216.0	-20.5	232.0	-4.5
241.8	221.7	-20.1	237.5	-4.3
247.1	227.5	-19.6	243.0	-4.1
252.6	233.3	-19.3	248.7	-3.9

TABLE 45

TITHERIDGE'S METHOD

SIMPLE DEEP VALLEY

ACTUAL HEIGHT	1-BLOCK VALLEY APPROX. REAL HEIGHT	1-BLOCK VALLEY APPROX. Δh	2-BLOCK VALLEY APPROX. REAL HEIGHT	2-BLOCK VALLEY APPROX. Δh
91.0	91.0	0.0	91.0	0.0
92.0	92.0	0.0	92.0	0.0
93.0	93.0	0.0	93.0	0.0
94.0	94.0	0.0	94.0	0.0
95.0	95.1	0.1	95.1	0.1
96.0	96.1	0.1	96.1	0.1
97.0	97.1	0.1	97.1	0.1
98.0	98.1	0.1	98.1	0.1
99.0	99.1	0.1	99.1	0.1
100.0	100.1	0.1	100.1	0.1
101.0	101.1	0.1	101.1	0.1
102.0	102.1	0.1	102.1	0.1
103.0	103.2	0.2	103.2	0.2
104.0	104.2	0.2	104.2	0.2
105.0	105.2	0.2	105.2	0.2
106.0	106.2	0.2	106.2	0.2
107.0	107.3	0.3	107.3	0.3
108.0	108.3	0.3	108.3	0.3
162.5	153.2	-9.3	156.6	-5.9
163.7	154.8	-8.9	158.0	-5.7
164.7	156.0	-8.7	159.1	-5.6
166.0	157.6	-8.4	160.6	-5.4
167.8	159.6	-8.2	162.5	-5.3
170.1	162.2	-7.9	165.0	-5.1
172.9	165.3	-7.6	167.9	-5.0
176.2	168.9	-7.3	171.5	-4.7
180.0	173.0	-7.0	175.5	-4.5
186.3	179.9	-6.4	182.2	-4.1
192.7	186.7	-6.0	188.9	-3.8
199.0	193.4	-5.6	195.5	-3.5
205.4	200.1	-5.3	202.1	-3.3
211.8	206.7	-5.1	208.7	-3.1
218.1	213.4	-4.7	215.2	-2.9
224.5	219.9	-4.6	221.8	-2.7
230.8	226.5	-4.3	228.3	-2.5
237.2	233.1	-4.1	234.8	-2.4
243.5	239.6	-3.9	241.3	-2.2
249.8	246.1	-3.7	247.9	-1.9
256.2	252.9	-3.3	254.6	-1.6

Individual N(h) distributions are plotted for every one or two hours of the day in Figs. 61 and 62, while the variation of electron density at fixed heights is shown in Figs. 63 and 64.

From these figures the electron densities at low heights (below 250 km) appear to be solar-controlled, i.e. during the morning the densities increase, reach a maximum at about noon and decrease again during the afternoon. The densities from about 250 km upwards exhibit a pronounced enhancement between about 0500 LMT and 0930 LMT. It is not clear whether a corresponding decrease is present at heights above about 250 km between 1700 and 2130 LMT since there is a general decrease in ionization at all heights at about 1700 to 1800 LMT. One striking feature of Figs. 63 and 64 is the rapidity with which N increases at all heights between about 0300 LMT and 0500 LMT and the equally rapid decrease after 1700 - 1800 LMT. These changes seem to be a lot more sudden than might be expected from the gradual variation of vertical drift caused by horizontal neutral winds (see results of King et al[82]).

Besides this rapid enhancement and decrease, the increased electron densities at heights above about 250 km between 0500 and 0930 LMT might be caused either by winds blowing ionization up the magnetic field lines or by precipitation of particles at heights just above the normal F2 peak (Rothwell[129], Stuart and Titheridge[142]).

Two geomagnetically quiet days during winter would have been scaled as well. However, the ionograms obtained during winter at SANAE are generally of poor quality and reflections are usually only visible for several hours of the day.

8.3 CONCLUSIONS/...

8.3 CONCLUSIONS

This brief analysis shows the variation of electron density with height and time for 2 geomagnetically quiet days during summer at SANAE. Although lack of time prevented further investigation, it would have been interesting to obtain N(h) profiles in a similar way for Port Lockroy, Halley Bay, Cape Hallett, Scott and Terre Adelie (the stations used in the analysis of section 2.7) and to compare the variation of N with height and time at stations at the same geographic latitude. However, I leave this as a suggestion to future researchers working on this problem.

"Only those who brave its dangers
Comprehend its mystery"

(Longfellow)

Sunset in Antarctica

APPENDICES

APPENDIX 1

LEAST SQUARES FIT AND STANDARD DEVIATIONS FOR FITTING

(a) EQUATION (1.2)

AND

(b) EQUATION (1.3)

TO THE A_0 DATA

APPENDIX 1

THE LEAST SQUARES FIT

Of two methods that were tried (MARGENAU and MURPHY,[100] 1943; BUCKINGHAM,[16] 1957), the following is the simpler and more accurate.

The first function to be fitted to the observed data y_i was

$$G = A + BS + Cf(\cos\chi) + DSf(\cos\chi)$$

The normal equations for this function are :

$$NA + B\sum_{i=1}^{N} R_i + C\sum_{i=1}^{N} \cos\chi_i + D\sum_{i=1}^{N} R_i\cos\chi_i = \sum_{i=1}^{N} y_i$$

$$A\Sigma R_i + B\Sigma R_i^2 + C\Sigma R_i\cos\chi_i + D\Sigma R_i^2\cos\chi_i = \Sigma y_i R_i$$

$$A\Sigma\cos\chi_i + B\Sigma R_i\cos\chi_i + C\Sigma\cos^2\chi_i + D\Sigma R_i\cos^2\chi_i = \Sigma y_i\cos\chi_i$$

$$A\Sigma R_i\cos\chi_i + B\Sigma R_i^2\cos\chi_i + C\Sigma R_i\cos^2\chi_i + D\Sigma R_i^2\cos^2\chi_i = \Sigma y_i R_i\cos\chi_i$$

Hence if one writes

$$\begin{pmatrix} N & \Sigma R_i & \Sigma\cos\chi_i & \Sigma R_i\cos\chi_i \\ \Sigma R_i & \Sigma R_i^2 & \Sigma R_i\cos\chi_i & \Sigma R_i^2\cos\chi i \\ \Sigma\cos\chi_i & \Sigma R_i\cos\chi_i & \Sigma\cos^2\chi_i & \Sigma R_i\cos^2\chi_i \\ \Sigma R_i\cos\chi_i & \Sigma R_i^2\cos\chi_i & \Sigma R_i\cos^2\chi_i & \Sigma R_i^2\cos^2\chi_i \end{pmatrix} = \overline{A}$$

$$\begin{pmatrix} A \\ B \\ C \\ D \end{pmatrix} = \overline{X} \quad \text{and} \quad \begin{pmatrix} \Sigma y_i \\ \Sigma y_i R_i \\ \Sigma y_i\cos\chi_i \\ \Sigma y_i R_i\cos\chi_i \end{pmatrix} = \overline{B}$$

the normal equations become

$$\overline{A}\,\overline{X} = \overline{B}$$

By setting up these matrices and using the EMA matrix manipulating functions, the solution

$$\overline{X} = \overline{A}^{-1}\overline{B}$$

was easily obtained.

The second equation to be fitted,

$G = A + BS + Cf(\cos\chi) + DSf(\cos\chi) + Eg(\cos\delta) + FSg(\cos\delta)$,

was solved in the same way. In this case

$$\overline{A} = \begin{pmatrix} N & \Sigma a & \Sigma b & \Sigma ab & \Sigma c & \Sigma ac \\ \Sigma a & \Sigma a^2 & \Sigma ab & \Sigma a^2 b & \Sigma ac & \Sigma a^2 c \\ \Sigma b & \Sigma ab & \Sigma b^2 & \Sigma ab^2 & \Sigma bc & \Sigma abc \\ \Sigma ab & \Sigma a^2 b & \Sigma ab^2 & \Sigma a^2 b^2 & \Sigma abc & \Sigma a^2 bc \\ \Sigma c & \Sigma ac & \Sigma bc & \Sigma abc & \Sigma c^2 & \Sigma ac^2 \\ \Sigma ac & \Sigma a^2 c & \Sigma abc & \Sigma a^2 bc & \Sigma ac^2 & \Sigma a^2 c^2 \end{pmatrix}$$

where $a = R_i$

$b = \cos\chi_i$

$c = \cos\delta_i$

$$\overline{B} = \begin{pmatrix} \Sigma y_i \\ \Sigma y_i R_i \\ \Sigma y_i \cos\chi_i \\ \Sigma y_i R_i \cos\chi_i \\ \Sigma y_i \cos\chi_i \\ \Sigma y_i R_i \cos\delta_i \end{pmatrix} \quad \text{and} \quad \overline{X} = \begin{pmatrix} A \\ B \\ C \\ D \\ E \\ F \end{pmatrix}$$

THE STANDARD DEVIATIONS OF THE COEFFICIENTS

In order to derive formulae for the standard deviations of the coefficients A, B, C and D for the function

$$G = A + BS + C\cos\chi + DS\cos\chi \qquad (1)$$

it is necessary to introduce new variables

$$\underline{g}_i = G_i - \overline{G}$$

$$\underline{s}_i = S_i - \overline{S}$$

$$(\underline{\cos\chi}_i) = \cos\chi_i - \overline{\cos\chi}$$

$$(\underline{s_i\cos\chi}_i) = S_i\cos\chi_i - \overline{S\cos\chi}$$

where

$$\overline{S} = \frac{1}{N}\Sigma S_i$$

$$\overline{\cos\chi} = \frac{1}{N}\Sigma\cos\chi_i$$

$$\overline{S\cos\chi} = \frac{1}{N}\Sigma S_i\cos\chi_i$$

and

$$\overline{G} = \frac{1}{N}\Sigma G_i = \frac{1}{N}\Sigma(A + BS_i + C\cos\chi_i + DS_i\cos\chi_i)$$

$$= \frac{1}{N}\Sigma A + \frac{1}{N}\Sigma BS_i + \frac{1}{N}\Sigma C\cos\chi_i + \frac{1}{N}\Sigma DS_i\cos\chi_i$$

$$= A + B\overline{S} + C\overline{\cos\chi} + D\overline{S\cos\chi} \qquad (2)$$

Thus obviously the new variables satisfy the conditions

$$\Sigma\underline{g}_i = 0$$

$$\Sigma\underline{s}_i = 0$$

$$\Sigma(\underline{\cos\chi}_i) = 0$$

$$\Sigma(\underline{s_i\cos\chi}_i) = 0$$

The equation to be fitted then becomes

$$G - \overline{G} = A + BS + C\cos\chi + DS\cos\chi - (A + B\overline{S} + C\overline{\cos\chi} + D\overline{S\cos\chi})$$

or $$\underline{g} = B\underline{s} + C(\underline{\cos\chi}) + D(\underline{s\cos\chi})$$

and the normal equations are

$$B\Sigma\underline{s}_i^2 + C\Sigma\underline{s}_i(\underline{\cos\chi}_i) + D\Sigma\underline{s}_i(\underline{s}_i\underline{\cos\chi}_i) = \Sigma y_i\underline{s}_i$$

$$B\Sigma\underline{s}_i(\underline{\cos\chi}_i) + C\Sigma(\underline{\cos\chi}_i)^2 + D\Sigma(\underline{\cos\chi}_i)(\underline{s}_i\underline{\cos\chi}_i) = \Sigma y_i(\underline{\cos\chi}_i)$$

$$B\Sigma\underline{s}_i(\underline{s}_i\underline{\cos\chi}_i) + C\Sigma(\underline{\cos\chi}_i)(\underline{s}_i\underline{\cos\chi}_i) + D\Sigma(\underline{s}_i\underline{\cos\chi}_i)^2 = \Sigma y_i(\underline{s}_i\underline{\cos\chi}_i)$$

These can be written as

$$\begin{aligned} B\mu_{11} + C\mu_{12} + D\mu_{13} &= \eta_1 \\ B\mu_{21} + C\mu_{22} + D\mu_{23} &= \eta_2 \\ B\mu_{31} + C\mu_{32} + D\mu_{33} &= \eta_3 \end{aligned} \qquad (3)$$

where

$$\begin{aligned} \mu_{11} &= \Sigma\underline{s}_i^2 = \Sigma(S_i - \bar{S})^2 \\ &= \Sigma(S_i^2 - 2S_i\bar{S} + \bar{S}^2) \\ &= \Sigma S_i^2 - 2\bar{S}\Sigma S_i + N\bar{S}^2 \\ &= \Sigma S_i^2 - 2(\tfrac{1}{N}\Sigma S_i)(\Sigma S_i) + N(\tfrac{1}{N}\Sigma S_i)^2 \\ &= \Sigma S_i^2 - \tfrac{2}{N}(\Sigma S_i)^2 + \tfrac{1}{N}(\Sigma S_i)^2 \\ &= \Sigma S_i^2 - \tfrac{1}{N}(\Sigma S_i)^2 \end{aligned}$$

$$\begin{aligned} \mu_{12} &= \Sigma(\underline{s}_i)(\underline{\cos\chi}_i) \\ &= \Sigma(S_i - \bar{S})(\cos\chi_i - \overline{\cos\chi}_i) \\ &= \Sigma(S_i\cos\chi_i - \bar{S}\cos\chi_i - S_i\overline{\cos\chi} + \bar{S}\overline{\cos\chi}) \\ &= \Sigma S_i\cos\chi_i - \bar{S}\Sigma\cos\chi_i - \overline{\cos\chi}\Sigma S_i + N\bar{S}\overline{\cos\chi} \\ &= \Sigma S_i\cos\chi_i - (\tfrac{1}{N}\Sigma S_i)\Sigma\cos\chi_i - (\tfrac{1}{N}\Sigma\cos\chi_i)\Sigma S_i \\ &\qquad + N(\tfrac{1}{N}\Sigma S_i)(\tfrac{1}{N}\Sigma\cos\chi_i) \\ &= \Sigma S_i\cos\chi_i - \tfrac{1}{N}(\Sigma S_i)(\Sigma\cos\chi_i) \end{aligned}$$

$$\begin{aligned}
\mu_{13} &= \Sigma(\underline{s}_i)(\underline{s}_i\underline{\cos\chi}_i) \\
&= \Sigma(S_i - \bar{S})(S_i\cos\chi_i - \overline{S\cos\chi}) \\
&= \Sigma(S_i^2\cos\chi_i - \bar{S}S_i\cos\chi_i - S_i\overline{S\cos\chi} + \bar{S}\,\overline{S\cos\chi}) \\
&= \Sigma S_i^2\cos\chi_i - (\tfrac{1}{N}\Sigma S_i)(\Sigma S_i\cos\chi_i) - (\tfrac{1}{N}\Sigma S_i\cos\chi_i)(\Sigma S_i) + \\
&\qquad\qquad N(\tfrac{1}{N}\Sigma S_i)(\tfrac{1}{N}\Sigma S_i\cos\chi_i) \\
&= \Sigma S_i^2\cos\chi_i - \tfrac{1}{N}(\Sigma S_i)(\Sigma S_i\cos\chi_i)
\end{aligned}$$

$$\begin{aligned}
\mu_{21} &= \mu_{12} \\
\mu_{22} &= \Sigma(\underline{\cos\chi}_i)^2 = \Sigma\cos^2\chi_i - \tfrac{1}{N}(\Sigma\cos\chi_i)^2 \\
\mu_{23} &= \Sigma(\underline{\cos\chi}_i)(\underline{s}_i\underline{\cos\chi}_i) = \Sigma S_i\cos^2\chi_i - \tfrac{1}{N}(\Sigma S_i\cos\chi_i)(\Sigma\cos\chi_i) \\
\mu_{31} &= \mu_{13} \\
\mu_{32} &= \mu_{23} \\
\mu_{33} &= \Sigma(\underline{s}_i\underline{\cos\chi}_i)^2 = \Sigma S_i^2\cos^2\chi_i - \tfrac{1}{N}(\Sigma S_i\cos\chi_i)^2
\end{aligned}$$

$$\begin{aligned}
\eta_1 &= \Sigma y_i\underline{s}_i \\
\eta_2 &= \Sigma y_i(\underline{\cos\chi}_i) \\
\eta_3 &= \Sigma y_i(\underline{s}_i\underline{\cos\chi}_i)
\end{aligned}$$

Writing $\Delta = \begin{vmatrix} \mu_{11} & \mu_{12} & \mu_{13} \\ \mu_{21} & \mu_{22} & \mu_{23} \\ \mu_{31} & \mu_{32} & \mu_{33} \end{vmatrix}$ (4)

From Kendall's (1951)[80] equation (22.49), we have that

$$\text{Var } B = \frac{\begin{vmatrix} 1 & \mu_{12} & \mu_{13} \\ 0 & \mu_{22} & \mu_{23} \\ 0 & \mu_{32} & \mu_{33} \end{vmatrix}}{\Delta}\left(\frac{\text{var } y}{N-p-1}\right) = \frac{(\mu_{22}\mu_{33} - \mu_{23}\mu_{32})\text{var } y}{(N-p-1)\Delta} \qquad (5)$$

$$\text{Var } C = \frac{\begin{vmatrix} \mu_{11} & 0 & \mu_{13} \\ \mu_{21} & 1 & \mu_{23} \\ \mu_{31} & 0 & \mu_{33} \end{vmatrix}}{\Delta} \left(\frac{\text{var } y}{N-p-1}\right) = \frac{(\mu_{11}\mu_{33} - \mu_{13}\mu_{31})\ \text{var } y}{(N-p-1)\Delta} \qquad (6)$$

$$\text{Var } D = \frac{\begin{vmatrix} \mu_{11} & \mu_{12} & 0 \\ \mu_{21} & \mu_{22} & 0 \\ \mu_{31} & \mu_{32} & 1 \end{vmatrix}}{\Delta} \left(\frac{\text{var } y}{N-p-1}\right) = \frac{(\mu_{11}\mu_{22} - \mu_{12}\mu_{21})\text{var } y}{(N-p-1)\Delta} \qquad (7)$$

In this case p = number of coefficients = 3

$\text{var } y = \Sigma(y_i - G_i)^2$ (y_i = observed values)

and standard deviation = $\sqrt{\text{var}}$

From equation (2)

$$A = \overline{F} - B\overline{S} - C\overline{\cos\chi} - D\overline{S\cos\chi}$$

and hence var A is obtained from

$$\text{var } A = \left(\frac{\partial A}{\partial B}\right)^2 \text{var } B + \left(\frac{\partial A}{\partial C}\right)^2 \text{var } C + \left(\frac{\partial A}{\partial D}\right)^2 \text{var } D$$

$$= (\overline{S})^2 \text{var } B + (\overline{\cos\chi})^2 \text{var } C + (\overline{S\cos\chi})^2 \text{var } D$$

Thus the standard deviations are:

$$\sigma_B = \sqrt{\frac{(\mu_{22}\mu_{33} - \mu_{23}\mu_{32})\ \Sigma(y_i - G_i)^2}{(N-4)\Delta}}$$

$$\sigma_C = \sqrt{\frac{(\mu_{11}\mu_{33} - \mu_{13}\mu_{31})\ \Sigma(y_i - G_i)^2}{(N-4)\ \Delta}}$$

$$\sigma_D = \sqrt{\frac{(\mu_{11}\mu_{22} - \mu_{12}\mu_{21})\,\Sigma(y_i - G_i)^2}{(N-4)\Delta}}$$

$$\sigma_A = (\tfrac{1}{N}\Sigma S_i)^2\sigma_B + (\tfrac{1}{N}\Sigma\cos\chi_i)^2\sigma_C + (\tfrac{1}{N}\Sigma S_i\cos\chi_i)^2\sigma_D$$

For the function

$$G = A + BS + C\cos\chi + DS\cos\chi + E\cos\delta + FS\cos\delta$$

equation (3) becomes

$$\begin{aligned}
B\mu_{11} + C\mu_{12} + D\mu_{13} + E\mu_{14} + F\mu_{15} &= \eta_1\\
B\mu_{21} + C\mu_{22} + D\mu_{23} + E\mu_{24} + F\mu_{25} &= \eta_2\\
B\mu_{31} + C\mu_{32} + D\mu_{33} + E\mu_{34} + F\mu_{35} &= \eta_3\\
B\mu_{41} + C\mu_{42} + D\mu_{43} + E\mu_{44} + F\mu_{45} &= \eta_4\\
B\mu_{51} + C\mu_{52} + D\mu_{53} + E\mu_{54} + F\mu_{55} &= \eta_5
\end{aligned}$$

Here

$$\mu_{14} = \Sigma\underline{s}_i(\underline{\cos\delta}_i) = \Sigma S_i\cos\delta_i - \tfrac{1}{N}(\Sigma S_i)(\Sigma\cos\delta_i)$$

$$\mu_{15} = \Sigma\underline{s}_i(\underline{s_i\cos\delta}_i) = \Sigma S_i^2\cos\delta_i - \tfrac{1}{N}(\Sigma S_i)(\Sigma S_i\cos\delta_i)$$

$$\mu_{24} = \Sigma(\underline{\cos\chi}_i)(\underline{\cos\delta}_i) = \Sigma\cos\chi_i\cos\delta_i - \tfrac{1}{N}(\Sigma\cos\chi_i)(\Sigma\cos\delta_i)$$

$$\mu_{25} = \Sigma(\underline{\cos\chi}_i)(\underline{s_i\cos\delta}_i) = \Sigma S_i\cos\chi_i\cos\delta_i - \tfrac{1}{N}(\Sigma\cos\chi_i)(\Sigma S_i\cos\delta_i)$$

$$\mu_{34} = \Sigma(\underline{s_i\cos\chi}_i)(\underline{\cos\delta}_i) = \Sigma S_i\cos\chi_i\cos\delta_i - \tfrac{1}{N}(\Sigma S_i\cos\chi_i)(\Sigma\cos\delta_i)$$

$$\mu_{35} = \Sigma(\underline{s_i\cos\chi}_i)(\underline{s_i\cos\delta}_i) = \Sigma S_i^2\cos\chi_i\cos\delta_i - \tfrac{1}{N}(\Sigma S_i\cos\chi_i)(\Sigma S_i\cos\delta_i)$$

$$\mu_{41} = \mu_{14}$$

$$\mu_{42} = \mu_{24}$$

$$\mu_{43} = \mu_{34}$$

$$\mu_{44} = \Sigma(\underline{\cos\delta_i})(\underline{\cos\delta_i}) = \Sigma\cos^2\delta_i - \frac{1}{N}(\Sigma\cos\delta_i)^2$$

$$\mu_{45} = \Sigma(\underline{\cos\delta_i})(\underline{s_i\cos\delta_i}) = \Sigma S_i\cos^2\delta_i - \frac{1}{N}(\Sigma\cos\delta_i)(\Sigma S_i\cos\delta_i)$$

$$\mu_{51} = \mu_{15}$$

$$\mu_{52} = \mu_{25}$$

$$\mu_{53} = \mu_{35}$$

$$\mu_{54} = \mu_{45}$$

$$\mu_{55} = \Sigma(\underline{s_i\cos\delta_i})(\underline{s_i\cos\delta_i}) = \Sigma S_i^2\cos^2\delta_i - \frac{1}{N}(\Sigma S_i\cos\delta_i)^2$$

Hence in place of equations (4) - (7), one obtains

$$\Delta = \begin{vmatrix} \mu_{11} & \mu_{12} & \mu_{13} & \mu_{14} & \mu_{15} \\ \mu_{21} & \mu_{22} & \mu_{23} & \mu_{24} & \mu_{25} \\ \mu_{31} & \mu_{32} & \mu_{33} & \mu_{34} & \mu_{35} \\ \mu_{41} & \mu_{42} & \mu_{43} & \mu_{44} & \mu_{45} \\ \mu_{51} & \mu_{52} & \mu_{53} & \mu_{54} & \mu_{55} \end{vmatrix}$$

$$\text{Var } B = \frac{\begin{vmatrix} \mu_{22} & \mu_{23} & \mu_{24} & \mu_{25} \\ \mu_{32} & \mu_{33} & \mu_{34} & \mu_{35} \\ \mu_{42} & \mu_{43} & \mu_{44} & \mu_{45} \\ \mu_{52} & \mu_{53} & \mu_{54} & \mu_{55} \end{vmatrix}}{\Delta} \frac{\text{var } y}{N-p-1}$$

$$= \frac{\Delta_{11}\,\text{var } y}{\Delta(N-p-1)}$$

$$\text{Var } C = \frac{\Delta_{22}\,\text{var } y}{\Delta(N-p-1)}$$

$$\text{Var } D = \frac{\Delta_{33}\,\text{var } y}{\Delta(N-p-1)}$$

$$\text{Var } E = \frac{\Delta_{44}\,\text{var } y}{\Delta(N-p-1)}$$

$$\text{Var } F = \frac{\Delta_{55}\,\text{var } y}{\Delta(N-p-1)}$$

where $p = 5$

$$\text{var } y = \Sigma(y_i - G_i)^2$$

and Δ_{jj} is the minor of the item in the j^{th} row and j^{th} column.

Thus the standard deviations are :

$$\sigma_B = \sqrt{\frac{[\mu_{22}\mu_{33}\mu_{44}\mu_{55} + \mu_{23}\mu_{45}(2\mu_{34}\mu_{25} - \mu_{23}\mu_{45}) + \mu_{35}^2(\mu_{24}^2 - \mu_{22}\mu_{44}) - \mu_{25}^2\mu_{34}^2 - \mu_{24}^2\mu_{33}\mu_{55}]\,\Sigma(y_i - G_i)^2}{(N-6)\Delta}}$$

$$\sigma_C = \sqrt{\frac{[\mu_{11}\mu_{33}\mu_{44}\mu_{55} + \mu_{13}\mu_{45}(2\mu_{15}\mu_{34} - \mu_{13}\mu_{45}) + \mu_{35}^2(\mu_{14}^2 - \mu_{11}\mu_{44}) - \mu_{14}^2\mu_{33}\mu_{55} - \mu_{15}^2\mu_{34}^2]\,\Sigma(y_i - G_i)^2}{(N-6)\Delta}}$$

$$\sigma_D = \sqrt{\frac{[\mu_{11}\mu_{22}\mu_{44}\mu_{55} + \mu_{12}\mu_{45}(2\mu_{15}\mu_{24} - \mu_{12}\mu_{45}) + \mu_{25}^2(\mu_{14}^2 - \mu_{11}\mu_{44}) - \mu^2\mu_{15}^2\mu_{24}^2 - \mu^2\mu_{14}^2\mu_{22}\mu_{55}]\Sigma(y_i - G_i)^2}{(N-6)\Delta}}$$

$$\sigma_E = \sqrt{\frac{[\mu_{11}\mu_{22}\mu_{33}\mu_{55} + \mu_{12}\mu_{35}(2\mu_{15}\mu_{23} - \mu_{12}\mu_{35}) + \mu_{25}^2(\mu_{13}^2 - \mu_{33}\mu_{11}) - \mu_{23}^2\mu_{15}^2 - \mu_{13}^2\mu_{22}\mu_{55}]\Sigma(y_i - G_i)^2}{(N-6)\Delta}}$$

$$\sigma_F = \sqrt{\frac{[\mu_{11}\mu_{22}\mu_{33}\mu_{44} + \mu_{12}\mu_{34}(2\mu_{23}\mu_{14} - \mu_{12}\mu_{34}) + \mu_{24}^2(\mu_{13}^2 - \mu_{33}\mu_{11}) - \mu_{23}^2\mu_{14}^2 - \mu_{13}^2\mu_{44}\mu_{22}]\Sigma(y_i - G_i)^2}{(N-6)\Delta}}$$

and

$$\sigma_A = \sqrt{\frac{(\Sigma S_i)^2 \text{var } B + (\Sigma \cos\chi_i)^2 \text{var } C + (\Sigma S_i \cos\chi_i)^2 \text{var } D + (\Sigma \cos\delta_i)^2 \text{var } E + (\Sigma S_i \cos\delta_i)^2 \text{var } F}{N^2}}$$

APPENDIX 2

LISTING OF THE LEAST SQUARES PROGRAM

APPENDIX 2

```
LIST
SEND TO(ED,ICLA-DEFAULT.ELSFIT)
PROGRAM(ELSFITANTFC)
!THIS  PROGRAM  DOES  A  LEAST  SQUARES  FIT  TO  THE  ANTARCTIC
!  COEFFICIENTS
INPUT1=CR0
OUTPUT1=LP0
AUXILIARY(0,2000)
CHAPTER1
A->150
B->150
C->12
F->12
G->50
110)JUMP113,S'#1
K=0(1)149
AK=0                                    ! ZEROIZES  FOURIER  COEFF
REPEAT                                  !LOCATIONS  AK
I=0
1)JUMPDOWN(R0/1)
J'=I'
JUMP23,J'=999
JUMPDOWN(R0/1)
J=I'
JUMPDOWN(R0/1)
K=I'
L=12K+J-23491
JUMP91,AL#0
JUMPDOWN(R0/2)
AL=£'
JUMP1,AL=0
I=I+1
JUMP101
91)JUMPDOWN(R0/2)
AL=£'
JUMP101,AL#0
I=I-1                                   ! IF  INSUFFICIENT  DATA,
JUMP1
101)M=0(1)5
JUMPDOWN(R0/2)
REPEAT
JUMP1
23)N=I
113)JUMP13,S'=9
K=1(1)12
READ(CK)                                ! READS  COS  CHI  VALUES
REPEAT
13)A=0
B=0
C=0
D=0
E=0
F=0
G=0
H=0
U=0
V=0
W=0
X=0
Y=0
Z=0
W'=0
X'=0
```

```
Y'=0
Z'=0
A'=0
B'=0
C'=0
D'=0
£'=0
J=6
I=0(1)149
J=J+1
JUMP77,13>J
J=1
77)JUMP17,AI=0
A=A+BI                  !R
B=B+CJ                  ! COSX
C=C+BICJ                ! RCOSX
D=D+BIBI                !RR
E=E+BIBICJ            ! RRCOSX
F=F+CJCJ                ! COSXCOSX
G=G+BICJCJ              ! RCOSXCOSX
H=H+BIBICJCJ            ! RCOSXRCOSX
U=U+AI                  ! F
V=V+BIAI                ! FR
W=W+AICJ                ! FCOSX
X=X+AIBICJ              ! FRCOSX
Y=Y+AIFJ                ! F%
Z=Z+AIFJBI              ! FR%
W'=W'+FJ                ! %
X'=X'+FJBI              ! R%
Y'=Y'+FJBIBI            ! RR%
Z'=Z'+FJCJ              ! %COSX
A'=A'+FJCJBI            ! %RCOSX
B'=B'+FJCJBIBI          ! %RRCOSX
C'=C'+FJFJ              ! %%
D'=D'+FJFJBI            ! %%R
£'=£'+FJFJBIBI          ! %%RR
17)REPEAT
J=0
G0=N
G1=A
G2=B
G3=C
G4=W'
G5=X'
G6=A
G7=D
G8=C
G9=E
G10=X'
G11=Y'
G12=B
G13=C
G14=F
G15=G
G16=Z'
G17=A'
G18=C
G19=E
G20=G
G21=H
G22=A'
G23=B'
G24=W'
```

```
G25=X'
G26=Z'
G27=A'
G28=C'
G29=D'
G30=X'
G31=Y'
G32=A'
G33=B'
G34=D'
G35=£'
%7(301)G0,36
%7(360)U,6
360=%28(301,6,1)
%6(360)E',4
%6(364)G36,2
47)£=0
V'=0
J=6
J'=1957
I=0(1)149
J=J+1
JUMP88,13>J
J'=J'+1
J=1
88)JUMP80,AI=0
NEWLINE
SPACE20
PRINT(J)2,0
PRINT(J')4,0
SPACE8
PRINT(AI)2,4
SPACE20
U'=E'+F'BI+G'CJ+H'BICJ+G36FJ+G37BIFJ
PRINT(U')2,4
SPACE20
U'=AI-U'
PRINT(U')2,4
V'=V'+U'
£=£+U'U'
80)REPEAT
NEWLINE
SPACE20
PRINT('SIGMA DELTA  ')
PRINT(V')2,4
PRINT('   SIGMA DELTA SQUARED   ')
PRINT(£)2,4
V'=£
PRINT('     MEAN  SQ.  RESIDUAL  ')
PRINT(£/N)1,4
NEWLINE2
SPACE8
PRINT('A ')
PRINT(E')2,4
SPACE8
PRINT('B ')
PRINT(F')2,4
SPACE8
PRINT('C ')
PRINT(G')2,4
SPACE8
PRINT('D ')
PRINT(H')2,4
```

```
SPACE8
PRINT('E ')
PRINT(G36)2,4
SPACE8
PRINT('F ')
PRINT(G37)2,4
NEWLINE2
PRINT('STD. DEVS ')
G0=C'-W'W'/N
G1=D'-W'X'/N
£'=£'-X'X'/N
G2=X'-AW'/N
G3=Y'-AX'/N
G4=Z'-W'B/N
G5=A'-BX'/N
G6=B'-CX'/N
A'=D-AA/N
B'=C-AB/N
C'=E-AC/N
D'=F-BB/N
U'=G-CB/N
V=H-CC/N
G16=A'-CW'/N
G7=G1G1
G8=G2G2
G9=G3G3
G10=G4G4
G11=G5G5
G12=G6G6
G13=C'C'
G17=G16G16
M=N-6
P=NN
U=V'/M
G14=W'
G15=X'
V'=D'VG0£'+G5G16(2U'G1-G5G16)+G12(G10-G0D')-G7U'U'-G10£'V
W'=A'VG0£'+C'G1(2G3G5-C'G1)+G12(G8-G0A')-G9G17-G8£'V
X'=A'D'G0£'+B'G1(2G3G4-B'G1)+G11(G8-G0A')-G9G10-G8£'D'
Y'=A'D'V£'+B'G6(2G3U'-B'G6)+G11(G13-VA')-U'U'G9-G13£'D'
Z'=A'D'VG0+B'G16(2U'G2-B'G16)+G10(G13-VA')-U'U'G8-G13D'G0
U'=2B'U'G16G1G3+2C'G2G4G5G6-VG9G10-A'G11G17-B'B'G0G12-D'G7G13-£'G8U'U'
U'=U'+A'D'VG0£'
U=U/U'
V=V'U
W=W'U
X=X'U
Y=Y'U
Z=Z'U
U=(AAV+BBW+CCX+G14G14Y+G15G15Z)/P
PRINT(%SQRT(U))2,4
SPACE10
PRINT(%SQRT(V))2,4
SPACE10
W=%SQRT(W)
PRINT(W)2,4
SPACE10
X=%SQRT(X)
PRINT(X)2,4
SPACE10
PRINT(%SQRT(Y))2,4
SPACE10
PRINT(%SQRT(Z))2,4
```

```
RUNOUT
JUMP25,S'=9
S'=9
%6(150)B0,150
ACROSS4/0
25)READ(S')
%6(0)B0,150
ACROSS1/0
CLOSE
CHAPTER0
VARIABLES1
I=0(1)1
K=0(1)149
READ(BK)                                    ! READS  SUNSPOT  NOS.
REPEAT
%7(150I)B0,150
REPEAT
I=1(1)12
READ(FI)
REPEAT
S'=1
%6(0)B0,150
1)SPACE50
PRINT('LEAST SQUARES ANALYSIS')
READ DATA TITLE
NEWLINE
4)SPACE50
JUMP2,S'=9
PRINT('AGAINST  SUNSPOT  NO.  R')
JUMP3
2)PRINT('AGAINST  SOLAR  FLUX  S')
3)NEWLINE2
SPACE20
PRINT('MONTH')
SPACE18
PRINT('F OBS                              F CALC
NEWLINE
K=0
I=0
ACROSS110/1
CLOSE
****
```

APPENDIX 3

ADDITIONAL WIND VELOCITY TABLES

Table A1. Hourly values of V_y (averaged for 2-3 antennas) measured at Halley Bay during February 1965.

	00	01	02	03	04	...	19	20	21	22	23
10		10.9	-29.5		-61.7						
11		-23.0									
12	2.8		-13.6								
13	-8.1										
14				7.7	3.1					25.5	
15				3.6					6.7	6.4	6.0
16				14.6						17.7	-23.7
17	2.7	-16.0	-6.9	1.8	-4.0						-0.3
18		1.2	--20.5								
19									-4.6	-8.9	14.7
20		11.5						-11.8			
21							-0.5				29.2
24				-4.2							
25			-10.5	4.1	-14.2		7.8	-111.2			-14.7
26									-0.4		10.1
27				-5.5					32.8	0.1	
28	29.7				-12.7						

Table A2. Hourly values of V_y (averaged for 2-3 antennas) measured at Halley Bay during March 1965.

	00	01	02	03	04	05	06	07	08	...	19	20	21	22	23
1	85.8	-37.5	-14.6		42.2	-189.8									
4															2.5
5	152.3	-10.7	8.4	14.6	-2.7								1.1	6.1	-1.6
6	31.3												-4.8	4.4	5.2
7														24.3	7.2
8						-5.6									
9					-13.1	20.8									
10					16.9										
12					6.9										
13							3.2					1.6	-0.3	8.3	-9.0
16						-19.1	-7.7	-0.4					-20.1		
17								-5.7	7.5						
20							-12.9						47.1		
21												-0.6	1.9		
22															-9.8
25													-0.1		
26							-23.1				-0.5				
27													6.1		
28							-36.9	-16.1							
29												10.8			
30														-5.9	
31													-17.3		

TABLE A3. HOURLY VALUES OF V_y (AVERAGED FOR 2-3 ANTENNAS) MEASURED AT HALLEY BAY DURING OCTOBER 1965.

	00	01	02	03	04	05	06	07	08	09	10	11	12	13	14	15	16	17	18	19	20	21	22	23
1	-7.1	3.4	-17.2																					9.6
4				4.0		-12.2	-16.5	0.7		-3.8		0.1								-2.4			-5.2	
6				-2.3																	-22.0	3.9		
9										-6.3													0.8	
10				19.5		-11.6							-0.8		1.2	-4.6	-7.6			-7.0	-2.8			2.3
11	-16.1				-10.3										-1.3			15.8	4.5	2.6		-1.6	-1.3	
12										1.9													-15.4	-1.8
13		-0.1						29.3	5.5					2.1		-2.6	-1.4						5.7	22.7
14					-26.0													14.4	9.3				-7.0	
15	-34.6												-10.4			3.0	-1.6				5.7	7.2		
16	-1.7	-6.5		-26.3	-10.0																12.9		-0.5	
18				-17.2											-14.8	0.0		12.8						
19	-20.3				-9.4									-4.5	2.3	7.2	-0.6			1.7		-0.1	-1.9	
20					-11.0					1.1				-1.7				1.8				-3.5	-16.8	
21		-1.7	13.4									-4.9												
22		1.2								-45.6		-15.8	-0.8	-3.2	16.1	-3.8		-0.8			53.3			
24										0.0			-10.3								-21.1	7.2	-10.6	
26						-0.7														-0.4			-8.7	6.7
27	2.3	-3.1	6.7	-4.8		-0.3										-0.8								
28																1.2	-12.6	-7.9		-7.5				
29			-0.7	-17.1												-1.4		8.0						-4.2
30	-4.4		-0.6	26.8			-1.0																	10.2
31					3.8					4.7				-16.9	-1.6	-1.5	-5.0	-6.0	-15.6			6.4	2.2	-0.8

Table A4. Hourly values of v_y (averaged for 2-3 antennas) measured at Halley Bay during November 1965.

	00	01	02	03	...	11	12	13	14	15	16	17	18	19	20	21	22	23
1	-15.1	-8.5														1.0		
3											2.8	4.1	3.3	0.4	13.3		17.4	7.4
4		4.0	-20.8				4.9		2.5			4.4	2.6	-7.4	-0.5			
6															-14.3	22.8		
7	2.8						1.0	2.3									-0.5	3.6
8														0.8		-1.2	-7.6	
9	-10.6	-15.7	-7.0						3.2								-4.1	
10	8.4	3.8								4.3		-1.4	-26.5					
11		5.4							12.6									-38.7
14											25.5	-2.9				-12.2	1.9	-3.0
15	-0.3	4.5	1.2															
16	0.2	-0.5	0.2						-0.1	0.9								
18		-1.4	4.9	-13.1						16.1	25.9			3.1	-22.1	8.9	6.5	
19						14.7	12.9							-3.3	-5.4			
22									10.7						-2.7			
23	-37.6	-6.5						-3.6									-10.7	-15.0
25		-3.2								5.8	17.8	3.3			-25.2	-0.6		
26								-4.2	3.3	-28.6						-7.1		
27			9.0											-22.0	-7.6	-31.7	2.1	
28										14.7	-3.5	-5.9	-4.6	2.7		14.9	2.6	
29	3.7	4.7	-31.5												-0.4	1.5		

TABLE A5

Hourly values of v_y (averaged for 2-3 antennas) measured at Halley Bay during December 1965.

	00	01	02	18	19	20	21	22	23
2	-0.1	7.5	-2.3						
4							0.8		5.5
5		4.4							
6							-5.4		5.8
7		-40.9					-5.3		-4.6
8	-18.5								
9				-11.1					
10	-25.3		-0.6	14.5					
12									13.7
13	12.7								
15					-13.7				
20									-12.1
21	-20.9								
22		-0.6	-16.7						
23									0.3
24	-4.8	-2.5							

TABLE A6

Hourly values of v_y (for a single antenna, IKL) measured at Halley Bay during February 1965.

	00	01	02	03	04	05	06		23
10		8.7	-35.4		-92.2				
11		-16.4		-19.1	3.3	4.0			
12	1.5		-0.8						
13		9.7							2.4
14	-0.8			9.7	6.0				
15			-5.1	-1.0	-10.7				-4.0
16	-1.0			-2.9		-44.1			-7.8
17	-3.5	-27.5	-12.9	-2.9	-13.0	-5.7			-8.0
18		-4.2	-12.5		-7.1				
19	-2.4		8.3		-19.1				8.5
20		-0.2							
25			-8.8	-0.7	-3.1				-6.4
26	-2.6					8.5			-1.4
27	-13.4		-10.8	-9.1		-3.8			
28	-2.9		-46.4		-3.5				

Table A7 Hourly values of v_y (for a single antenna, IKL) measured at Halley Bay during March 1965.

	00	01	02	03	04	05	19	20	21	22	23
1	156.6	- 51.6			4.4	- 249.7					
2							3.1		22.6	4.2	
3	17.3			93.6	31.4	9.3				78.1	
4											3.5
5	275.8	- 5.2	6.6	20.4	- 5.6				6.9	1.8	- 3.1
6	67.6	- 51.6		- 18.8					- 9.6	9.4	- 22.9
7										- 4.5	- 3.0
8	- 4.5	3.8		- 2.4	- 1.8	- 4.0		- 0.6	1.0		
9			31.9		- 19.1	- 1.4				- 10.2	
10		- 10.4	10.9		7.8					2.1	
11		70.4						- 18.8		- 6.3	
12					- 1.7						
13				- 1.6	23.3			3.8	0.6	12.9	- 5.8
18	26.2				17.2						
20							92.7	- 3.0	83.8		
21							124.7	- 3.2	- 2.3	- 12.8	10.3
22										- 11.5	- 12.2

TABLE A8

Hourly values of v_y (for a single antenna, IKL) measured at Halley Bay during October 1965.

	00	01	02	03	04	05	06		22	23
1	-11.8	4.4	-12.4							6.1
4				0.0		-4.3				-0.8
10				23.3		-9.2	1.2			-2.3
11	-8.7			-4.9	-7.9				-0.6	
12		-1.8	-14.1						-15.9	-1.4
13		0.4							3.3	23.3
14				-7.5	-9.6				-4.4	-1.6
15	-7.4									
16	-0.8	-3.1		-67.5	-5.0				-0.5	
18				-47.1						
19	1.1				-9.8				-2.6	
20					-1.8				-5.1	
21	0.3	-0.6	-1.7							
22		0.4								
24					-11.4				-12.3	
25									-10.5	-2.0
26										
27	-5.0	-4.3	-2.0	-2.2		-0.3				
28										
29										-3.8
30	-5.6		-1.8	-11.8						-2.6
31	-2.3	-4.4			5.3				-4.0	-0.6

TABLE A9

Hourly values of v_y (for a single antenna, IKL) measured at Halley Bay during November 1965.

	00	01	02	03	04	----	22	23
3							24.1	-3.2
4		24.3	-4.1					
7	5.1		-0.1				-0.4	1.3
9	-4.7	-4.7	-3.8				-2.6	
10								
11		2.3						-11.9
13	1.1	-3.5		-31.3				
14							-1.5	-4.1
15	-1.6	-1.2	0.0					
16	-0.4	-0.3	-1.6					
18		0.2	0.6	-4.9	5.5		4.8	
19								
23	-24.1	-9.9					-9.4	-3.5
25		-3.5						
26		-3.0					-2.7	
27							-3.2	
28							-0.1	
29	2.9	11.9	-65.7					

TABLE A10

Hourly values of v_y (for a single antenna, NRP) measured at Halley Bay during December 1965.

	00	01	02	21	22	23
4				1.6		9.6
5		1.9	4.6			
6				-6.1		5.6
7		-88.9		-6.8		1.6
8	-9.6	3.2				
10	-61.1		0.2			
20						-23.2
21	-26.2					
22		-0.1	-15.6			
23						3.7
24	1.4	-0.2	-1.4			

Table A11. Hourly values of v_y at heights between 200 and 250 km (averaged for 2.3 antennas) measured at Halley Bay during March 1965.

	06	07	08	09	10	15	16	17	18	19	20	21	22
2									- 1.0	9.0		20.7	8.1
3							- 5.6						
5												1.1	
6												- 4.8	4.4
7		- 18.7											
8			- 6.9							6.1	- 0.6	0.6	
9	- 3.2												
10													5.9
11											- 10.4		- 5.6
16	- 7.7	- 0.4											
17			7.5										
18	3.5						8.6	22.0					
19							16.3	31.3					
20								-34.5		79.7	11.3	47.1	
21						20.2	- 57.9		12.3	4.3			
26										- 0.5			
27							28.5	21.0	22.7				
28		- 16.1	- 19.3										
29				0.5					29.6				
30					2.1			1.0	9.3				
31		- 5.9	6.5		0.1			14.3	8.5				

Table A12 Hourly values of v_y at heights between 200 and 250 km (averaged for 2.3 antennas) measured at Halley Bay during October 1965.

	08	09	10	11	12	13	14	15	16	17	18	19	22
1							- 1.2	- 1.1		- 10.2	- 2.3	- 16.4	
2										1.2			
3	- 2.3		0.8							2.1		1.5	
4			- 7.7	0.1		- 2.2	0.6	1.5			5.3	5.6	
5	5.1	3.9											
9										- 3.7			
10							1.2	- 4.6	- 7.6	- 16.8	- 9.2		
11							- 1.3			15.8	4.5	2.6	- 1.3
12													- 15.4
15								3.0	- 1.6				
16													- 0.5
17										2.2			
18								- 14.8	0.0		12.8		
19							2.3	7.2	- 0.6				
20										1.8			
22					- 0.8					- 0.8			
27									- 0.5			1.1	
29								- 1.4					

APPENDIX 4

LISTING OF THE CONTINUITY EQUATION PROGRAM

```
LIST
SEND TO(ED,ICLA-DEFAULT.IONOSPHERE)
DUMPON(ED,PROGRAM TEST)
PROGRAM(CONTINUITY EQ)
INPUT1=CR0
OUTPUT1=LP0
MAIN3426
AUXILIARY(0,7100)
USEAUX(500)=ED(PROGRAM FREE)
OVERLAY(1,1)C1                          ! READ-IN
OVERLAY(1,10)C30                        ! SECOND READ-IN CHAPTER
OVERLAY(1,3)C8                          ! PRINT-OUT TABLE
OVERLAY(1,4)C10                         ! PRINT-OUT GRAPH
OVERLAY(1,5)C11
OVERLAY(1,9)C31                         ! PERCENTAGE PLOT
OVERLAY(1,13)C5                         ! CALCULATION
OVERLAY(1,12)C4                         ! CALCULATION
OVERLAY(1,11)C3                         ! CALCULATION
OVERLAY(1,2)C2                          ! CALCULATION
OVERLAY(1,15)C40
OVERLAY(1,14)C6
OVERLAY(1,6)C20                         ! FINAL SUMMARY TABLE
OVERLAY(1,7)C33                         ! FINAL HMF2 GRAPH
OVERLAY(1,8)C34                         ! FINAL FOF2 GRAPH
OVERLAY(1,17)C50                        ! CALCULATION
OMIT COMMENTS
CHAPTER15
A->479
B->239
C->239
D->239
E->239
F->239
G->239                                          !
H->239
U->239
V->239
W->239
X->239
Y->239
£->65
CLOSE
CHAPTER1                                ! READ  IN
VARIABLES15
1)READ(I')          ! MODE  =0  PRINTOUT EVERY 15 MINS,  =1  PRI
!  =2  ABORT ,  =3  PRINTOUT EVERY HOUR
JUMP2,I'#99
ACROSS1/20
2)K=K
READ(V)
READ(J')            ! STEP LENGTH
J=0(1)14
READ(£(J+21))       !
READ(£(J+36))       !
REPEAT
J=0(1)4
READ(£(J+51))       ! I INFINITY
£(J+51)=£(J+51)V
REPEAT
J=0(1)2
READ(£(J+12))       ! NIO
REPEAT
£8=17.54
```

```
£9=35.06
£10=30.66
£11=32.87
READ(E)                 ! DIFFUSION COEFFICIENT DO
READ(V)                 ! ANGLE OF DIP IN DEGREES
V=£V/180
F=%COS(V)
V=%SIN(V)
J=0(1)2
READ(B(240J))
I=5(5)235
READ(B(I+240J))         ! % ION CONCN AT 10 KM INTERVALS
K=1(1)4
B(I+240J-K)=B(I+240J)-[B(I+240J)-B(I+240J-5)]K/5                    ! INTER
REPEAT
REPEAT
K=236(1)239
READ(B(240J+K))
REPEAT
REPEAT
ACROSS1/30
CLOSE
CHAPTER30
VARIABLES15
1)K=K
READ(F0)
I=5(5)235
READ(FI)                ! ACTUAL ION CONCENTRATION AT 10 KM INTERVALS
K=1(1)4
F(I-K)=FI-0.2[FI-F(I-5)]K                   ! INTERPOLATE
REPEAT
REPEAT
K=236(1)239
READ(FK)
REPEAT
I=0(1)239
BI=BIFI                 ! CALCULATE ACTUAL O+
CI=CIFI                 ! O2+ ,
EI=DIFI                 ! NO+ ,
DI=0                    ! AND N2+ CONCENTRATIONS
REPEAT
%7(0)B0,960             ! STORE INITIAL ION CONCENTRATIONS
%7(4032)G0,1200                         ! INITIAL NEWU DN/DT . . .
READ(Z')                ! HOUR ANGLE  = 0 AT MIDDAY
READ(X')                ! LATITUDE IN DEGREES
READ(Y')                ! DECLINATION IN DEGREES
X'=£X'/180
Y'=£Y'/180
K=0(1)23
READ(A0)
READ(A3)
X=(A3-A0)/3
A1=A0+X
A2=A1+X
I=8(5)48
READ(AI)
X=0.2(AI-A(I-5))
J=1(1)4
A(I-J)=AI-JX
REPEAT
REPEAT
%7(5232+49K)A0,49
REPEAT
```

```
6408=%15(5232,49)
I=0(1)66
READ(AI)
REPEAT
%7(6457)A0,67
D=%COS(%MOD(0.5(X'-Y')))                    ! COSINE ETA
D=D%SQRT(%SQRT(D))
A=%SIN(%MOD(0.5(X'+Y')))                    ! SINE THETA
A=A%SQRT(%SQRT(A))
READ(I)                                     ! DAY NUMBER
READ(B)                                     ! F10.8
READ(C)                                     ! BAR F 10.8
B=418+1.8B+1.8C+[0.37+0.14%SIN(2(I-151)£/365)]C%SIN(4(I-59)£/365)
B=B?
£0=B+0.28BA
£1=0.28B(D-A)
D=%COS(%MOD(0.5(X'-Y'+0.01745)))            ! COSINE ETA AT LATITUDE 2
D=D%SQRT(%SQRT(D))
A=%SIN(%MOD(0.5(X'+Y'+0.01745)))            ! SINE THETA AT LATITUDE 2
A=A%SQRT(%SQRT(A))
£2=B+0.28BA
£3=0.28B(D-A)
ACROSS1/2
CLOSE
CHAPTER2                                    ! CALCULATIONS
VARIABLES15
1)S=0                                       ! DAY COUNTER
T=144                                       ! 5-MINUTE COUNTER, STARTS
2)A=%COS(0.5[Z'+0.2094%SIN(Z'+0.7854)-0.7854])          ! JACCHIA'S
A=A?
JUMP3,A>=0
Z'=Z'-2£
JUMP2
3)K=K
A=AA%SQRT(A)
A=A?
£4=£2+£3A                                   ! T INF AT LATITUDE 2
A=£0+£1A                                    ! T INF AT CORRECT LAT.
A=A?
£4=£4?
B=A-800
B=B/(750+0.0001722BB)
B=0.0291%EXP(-0.5BB)                        ! B FOR LATITUDE 1
C=(A-355)%EXP(120B)                         ! C FOR LATITUDE 1
£5=£4-800
£5=£5/(750+0.0001722£5£5)
£5=0.0291%EXP(-0.5£5£5)                     ! B FOR LATITUDE 2
£6=(£4-355)%EXP(120£5)                      ! C FOR LATITUDE 2
J=0(1)3
£(J+59)=£(J+8)/A                            ! SCALE HEIGHT H I INFINI'
REPEAT
D=%SIN(X')%SIN(Y')+%COS(X')%COS(Y')%COS(Z')                  ! COS
X=180%ARCCOS(D)/£                           ! CHI IN DEGREES
M=%INTPT(X)                                 ! M=DEGREES
X=%FRPT(X)                                  ! X= FRACTION OF A DEGREE
JUMP30,M<30
JUMP31,M>95
%6(6427+M)A',2
D=1/[A'+X(B'-A')]                           ! INTERPOLATE
JUMP30
31)D=0.0001
30)K=K
P=%INTPT(T/12)
```

```
Y=(T+R/300-12P)/12
%6(5232+49P)A382,98
A240=A382+Y(A431-A382)                    ! INTERPOLATE VALUE AT 120
I=1(1)48
A(I+431)=A(I+382)+Y[A(I+431)-A(I+382)]
REPEAT
I=1(1)48
A(240+5I)=A(I+431)                                ! INTERPOLATE AT
K=1(1)4
A(240+5I-K)=A(240+5I)-0.2[A(240+5I)-A(235+5I)]K! INTERPOLATE INTE
REPEAT
REPEAT
%7(6600)A240,240
ACROSS1/3
CLOSE
CHAPTER3
VARIABLES15
1)K=K
!                    STAGE1      INITIAL  CALCULATIONS
! ALPHA1  ALPHA3  QO+  QO2+  QN2+  K2  W  DW/DH  NM  NO  NO2  NN2
I=0(1)239
H=120+2I
G=%EXP(-BH)
A'=A-CG                                   ! T
B'=BCG                                    ! DT/DH
C'=-BB'                                   ! D2T/DH2
£7=£4-£6%EXP(-£5H)                        ! TEMP AT LATITUDE 2
Y=120-H-%LOG(A'/355)/B
J=0(1)2
£(J+15)=A'/£(J+8)                         ! SCALE HEIGHT HI
£(J+18)=355£(J+12)%EXP(Y£(J+59))/A'       ! NI
£(J+63)=100000£(J+15)£(J+18)/D            !
REPEAT
CI=1.08&-5%EXP(-0.7%LOG(A'(A(I+240)-1)))  ! ALPHA 1
DI=1000/(A'(A(I+240)-1))                  !ALPHA 3
DI=4.7&-8DI%SQRT(DI)                      !
XI=A(I+240)
AI=0
A(I+240)=0
A(I+480)=0
JUMP3,M>95                                ! IF SUN IS BELOW HORIZON
K=0(1)4
Y=0
L=0(1)2
Y=Y+£(K+5L+21)£(L+63)
REPEAT
J=0(1)2
A(I+240J)=A(I+240J)+£(K+51)£(K+36+5J)£(J+18)%EXP(-Y)
REPEAT
REPEAT
3)K=K
EI=3.4&-10/%SQRT(A')                      ! K2
YI=£18
FI=£18                                    ! NO
GI=£19                                    ! NO2
HI=£20                                    !NN2
UI=0.4%EXP(-3700/A')£19+0.0000005£18      ! NNO
VI=E%SQRT(A')/(£18+£19+£20)               ! DIFFUSION COEFF
REPEAT
%7(1872)A240,2160
%6(6600)A240,240
ACROSS1/4
CLOSE
```

```
CHAPTER4
VARIABLES15
1)K=K
!                    STAGE 2    CALCULATION  OF  F1 - F5,  G1 - G5
I=1(1)239
G=%EXP(-(120+2I)B)
A'=A-CG                                          ! T
B'=0.00001BCG
C'=-0.00001BB'                                   ! D2T/DH2 IN DEG/CM SQUARED
W=0                                              ! DW/DH
UI=AI                                            ! G4
AI=3.34&-6%EXP(0.71%LOG(A'))/YI                  ! F1
X=1.37&-16A'/YI                                  ! KT/NM
V'=VI                                            ! DIFFUSION COEFFICIENT
F'=100000A'/£8                                   ! SCALE HEIGHT HO+
BI=-XVV/V'
CI=XVF[XI/V'-(B'/A')A(I+240)-1/F']
DI=XVFA(I+240)                                   ! F4
FI=2V'VV                                         ! G1
JUMP2,I<59
JUMP3,I#59
£59=EIGI+5&-13HI
3)K=K
HI=EIGI+5&-13HI
HI=VVV'[(1-100000B'/£8)/(F'F')+2C'/A'+3.5B'/(F'A')+(B'B')/(A'A')]-HI
GI=VVV'(3/F'+5B'/A')
JUMP4
2)GI=EIGI+5&-13HI
4)K=K
XI=0                                             ! VERTICAL WIND VEL
EI=-WI/YI
REPEAT
ACROSS1/40
CLOSE
CHAPTER40
VARIABLES15
!                              INITIAL  VALUES
1)K=K
G0=E0G0+5&-13H0
U0=A0
L=0
JUMP25,S#0
JUMP25,T#144
JUMP25,R#0
L=99
I=0(1)58
W=UI/GI
A(I+240)=W
REPEAT
I=59
W=UI/£59
A(I+240)=W
£60=£59
D'=[11A(I+240)/6+1.5A(I+238)-A(I+237)/3-3A(I+239)]/200000
I=61(2)239
£20=400000D'
£59=-400000[U(I-2)+G(I-2)D'+H(I-2)W]/F(I-2)
£65=400000[D'+0.5£59]
H'=-400000[U(I-1)+G(I-1)(D'+0.5£59)+H(I-1)(W+0.5£20)]/F(I-1)
E'=400000[D'+0.5H']
G'=-400000[U(I-1)+G(I-1)(D'+0.5H')+H(I-1)(W+0.5£65)]/F(I-1)
Y=W
W=W+[£20+2£65+2E'+400000[D'+G']]/6
```

```
D'=D'+[£59+2H'+2G'-400000[UI+GI(D'+G')+HI(Y+E')]/FI]/6
A(I+240)=W
A(I+239)=0.5[W+Y]
REPEAT
£59=£60
%7(0)A240,240
25)%6(0)A240,240
%6(4032)V0,960                          ! CALL NEWU DN/DT DU/DT DU
ACROSS1/50
CLOSE
CHAPTER50
VARIABLES15
1)K=K                  !          SOLUTION  OF  EQNS FOR  O+
I=0(1)58
W=[A(I+240)+J'UI]/[1+J'GI]
A(I+240)=W
REPEAT
J=0(1)15
100)X=£59
I=59
W=[A(I+240)+J'UI]/[1+J'£59]
A(I+240)=W
D'=[11A(I+240)/6+1.5A(I+238)-A(I+237)/3-3A(I+239)]/200000
I=61(2)239
Y=W
72)K=K
£20=400000D'
£59=-400000[U(I-2)+G(I-2)D'+H(I-2)W-WI]/F(I-2)
£65=400000[D'+0.5£59]
H'=-400000[U(I-1)+G(I-1)(D'+0.5£59)+H(I-1)(W+0.5£20)-WI]/F(I-1)
E'=400000[D'+0.5H']
G'=-400000[U(I-1)+G(I-1)(D'+0.5H')+H(I-1)(W+0.5£65)-WI]/F(I-1)
W=W+[£20+2£65+2E'+400000[D'+G']]/6
E'=[W-A(I+240)]/J'
CHECK(WI,E',0.001,73)
WI=E'
W=Y
JUMP72
73)K=K
D'=D'+[£59+2H'+2G'-400000[UI+GI(D'+G')+HI(Y+E')-WI]/FI]/6
A(I+240)=W
A(I+239)=0.5[W+Y]
REPEAT
£59=X
JUMP102,L#99
REPEAT
102)K=K
L=0
ACROSS1/5
CLOSE
CHAPTER5
VARIABLES15
1)K=K
!                      STAGE 4    SOLUTION OF EQUATIONS FOR O2+, N2+
%7(0)A240,240                           ! STORE NEWN
%6(240)A0,720          ! CALL ION CONCENTRATIONS
%6(1152)C0,720         ! CALL D/DT[ION CONCN.]
%6(1872)F0,960         ! CALL QO2+  QN2+  ALPHA1  ALPHA3
%7(4032)V0,960         ! STORE NEWU  DN/DT  DU/DT  DU/DH
%6(0)V0,240                             ! CALL NEWN
%6(3072)W0,720                          ! CALL NO NO2 NN2
I=0(1)239
A'=AI+A(I+240)+BI+VI
```

```
B'=[A(I+240)+J'GI]/[1+J'(2&-10WI+1&-10XI+3&-7A')]
C'=B'-A(I+240)
22)DI=C'/J'
A(I+240)=B'
REPEAT
%6(2832)G0,240
I=0(1)239
FI=FI+GIVI+1&-10XIA(I+240)                    ! GO2+ + GAMMA2(NO2)(NO+) +
YI=5&-13YIVI+2&-10WIA(I+240)
REPEAT
%6(3792)G0,240                                ! CALL NNO
ACROSS5/6
CLOSE
CHAPTER6
VARIABLES15
5)Y=0
I=0(1)239
A'=AI+A(I+240)+BI+VI
B'=[AI+J'FI]/[1+J'(8&-10GI+HIA')]
C'=[BI+J'(YI+8&-10GIAI)]/[1+J'UIA']
X=B'-AI
D'=C'-BI
24)CI=X/J'
EI=D'/J'
25)K=K
AI=B'
BI=C'
WI=A'                                         ! STORE TOTAL ELECTRON DEN
REPEAT
%7(240)A0,720
%7(1152)C0,720                                ! STORE D/DT[ION CONCN.]
JUMP20,%FRPT((300T+R)/900)#0
I=%INTPT(T/3)
J=%MAX(W0,0,239)
A'=J                                          ! I VALUE OF MAX
B'=WJ                                         ! NMF2
%7(960+I)A',1                                 ! STORE IMAX
%7(1056+I)B',1                                ! NMAX
20)K=K
JUMP101,I'=2
JUMP6,I'=1
JUMP6,%FRPT((300T+R)/900)#0
JUMP101,I'#3
JUMP6,%FRPT((300T+R)/3600)#0
101)K=K
ACROSS1/8
6)JUMP9,S=2
JUMP9,I'=2
R=R+J'
Z'=Z'+J'£/43200
JUMP7,R#300
R=0
T=T+1
7)JUMP8,T#288
T=0
S=S+1
JUMP9,S=2
JUMP8,S#1
6840=%15(960,192)
8)ACROSS2/2
9)I'=99
ACROSS1/20
CLOSE
```

```
CHAPTER8
VARIABLES15
1)SPACE45
PRINT('N-H  PROFILE  AT  TIME')
PRINT(%INTPT(T/12)+.6%FRPT(T/12+R/3600))2,2
PRINT('  HOURS')
SPACE15
PRINT('TEMP')
PRINT(A)4,2
NEWLINE
SPACE45
I=1(1)37
PRINT('-')
REPEAT
SPACE15
PRINT('------------')
NEWLINE2
I=1(1)107
PRINT('-')
REPEAT
NEWLINE
3)PRINT('I   HT    I        O+         OO+         NN+         NO+   I')
PRINT('   TOTAL   I ')
PRINT('     %O+    %OO+    %NN+    %NO+   I')
NEWLINE
I=1(1)107
PRINT('-')
REPEAT
NEWLINE
K=0(2)238
PRINT('I  ')
PRINT(120+2K)3,0
PRINT(' I')
SPACE2
PRINT(VK)6,1
PRINT(AK)6,1
PRINT(A(K+240))6,1
PRINT(BK)6,1
X=VK+AK+A(K+240)+BK
PRINT('I')
PRINT(X)6,1
4)PRINT('I')
->120,X=0
PRINT(100VK/X)3,1
I=0(1)2
PRINT(100A(K+240I)/X)3,1
REPEAT
SPACE4
PRINT('I')
120)NEWLINE
REPEAT
I=1(1)107
PRINT('-')
REPEAT
NEWLINE8
ACROSS1/10                              ! TO GRAPH PRINTING S/R
6)JUMP111,I'=2                          ! ABORT RUN
112)ACROSS6/6
111)I'=99
ACROSS1/20
CLOSE
CHAPTER10                               ! GRAPH OF N AND O+ VERSUS HE
VARIABLES15
```

```
1)M'=600
Q'=1
I=23(-1)0
J=4
JUMP119,M'=600
JUMP2,M'>500
JUMP2,200>M'
20)R')=Q'+30)
JUMP(R')
31)PRINT('H')
->47
32)PRINT('E')
->47
33)PRINT('I')
->47
34)PRINT('G')
->47
35)PRINT('H')
->47
36)PRINT('T')
->47
37)PRINT(' ')
->47
38)PRINT(' ')
->47
39)PRINT(' ')
->47
40)PRINT('I')
->47
41)PRINT('N')
->47
42)PRINT(' ')
->47
43)PRINT(' ')
->47
44)PRINT(' ')
->47
45)PRINT('K')
->47
46)PRINT('M')
47)SPACE5
Q'=Q'+1
->3
2)SPACE6
3)PRINT(M')3,0
PRINTCH(%CODE(VB))
J=5(-1)1
119)K=10I+2J
H=VK+AK+A(K+240)+BK
JUMP7,H>=100000
N=0.0005H-6
JUMP71
7)N=0.00005H+39
71)H=VK
JUMP72,H>=100000
0'=0.0005H-6
JUMP8
72)0'=0.00005H+39
8)K=K
JUMP5,0'>90
JUMP84,0'<=0
JUMP50,0'>N
SPACE(0')
```

```
JUMP15,O'#N
PRINT('*')
JUMP5
50)SPACE(N)
PRINT('X')
SPACE(O'-N-1)
PRINT('O')
->5
15)PRINT('O')
SPACE(N-O'-1)
PRINT('X')
->5
84)->5,N<=0
6)SPACE(N)
PRINT('X')
5)NEWLINE
JUMP10,J=1
SPACE12
PRINTCH(%CODE(VB))
REPEAT
10)M'=M'-20
REPEAT
ACROSS1/11
CLOSE
CHAPTER11
VARIABLES15
1)K=K
PRINT('         120 ')
I=1(1)18
PRINT('----+')
REPEAT
NEWLINE
SPACE10
PRINT('1/4  ')
I=2(1)9
PRINT(I)1,0
SPACE1
REPEAT
PRINT('1/5  ')
I=2(1)9
PRINT(I)1,0
SPACE1
REPEAT
PRINT('1/6')
NEWLINE2
SPACE40
PRINT('ELECTRON  DENSITY  IN  ELECTRONS/CC.')
NEWLINE2
PRINT('O  DENOTES  O+  ION CONCENTRATION')
NEWLINE
PRINT('X  DENOTES  TOTAL  ION  CONCENTRATION')
NEWLINE
PRINT('*IS USED WHERE O AND X ARE THE SAME')
NEWLINE5
SPACE25
PRINT('TABLE II : THE RELATIVE CONCENTRATIONS OF ')
PRINT('THE IONS  O+ , OO+ , NO+')
NEWLINE
SPACE25
I=1(1)68
PRINT('-')
REPEAT
NEWLINE4
```

```
ACROSS1/31
CLOSE
CHAPTER31                                   ! PERCENTAGE PLOT
VARIABLES15
1)K=K
I=120(-2)0
SPACE2
X=VI+AI+A(I+240)+BI
PRINT(120+2I)3,0                            ! HEIGHT
M=%INTPT(100VI/X)                           ! % 0+
N=%INTPT(100AI/X)                           ! % 02+
->95,M=0
M=M-1
->83,N=0
PRINTCH(%CODE(VB))
N=N-1
SPACE(M)
PRINT('0')
SPACE(N)
PRINT('X')
N=100-M-N-3
JUMP22,N<=0
SPACE(N)
->4
83)PRINTCH(%CODE(VB))
SPACE(M)
PRINT('*')
N=98-M
JUMP22,N<=0
SPACE(N)
->4
123)K=K
PRINT('-')
SPACE99
->4
95)->123,N=0
N=N-1
SPACE(N)
PRINT('X')
N=98-N
->4,N<=0
SPACE(N)
4)PRINTCH(%CODE(VB))
22)NEWLINE
SPACE8
PRINTCH(%CODE(VB))
SPACE99
PRINTCH(%CODE(VB))
NEWLINE
REPEAT
86)SPACE8
J=0(1)9
PRINT('+---------')
REPEAT
PRINT('+')
NEWLINE
SPACE5
I=0(10)100
PRINT(I)3,0
SPACE4
REPEAT
NEWLINE3
ACROSS6/8
```

```
CLOSE
CHAPTER20                                   ! FINAL SUMMARY TABLE
VARIABLES15
1)SPACE30
PRINT('-------------------------------------------------------')
NEWLINE
SPACE30
PRINT('I     TIME     I  HT OF MAX I F2 EL DENS I     FOF2     I')
NEWLINE
SPACE30
PRINT('-------------------------------------------------------')
%6(960)A0,96
%6(1056)B0,96
NEWLINE
I=0(1)95
SPACE30
PRINT('I')
PRINT(%INTPT(I/4)+0.6%FRPT(0.25I))4,2
PRINT('  I     ')
PRINT(120+2AI)3,0
PRINT('  I')
PRINT(BI)7,1
PRINT('I  ')
BI=%SQRT(BI/12400)
PRINT(BI)2,2
PRINT('  I')
NEWLINE
REPEAT
SPACE30
PRINT('-------------------------------------------------------')
NEWLINE2
ACROSS1/33
CLOSE
CHAPTER33                                   ! FINAL HMF2 GRAPH
VARIABLES15
1)K=K
I=238(-2)0
JUMP20,%FRPT(0.2(I+2))#0
PRINT(120+2I)3,0
JUMP21
20)SPACE6
21)K=K
PRINT('I')
JUMP25,I=0
Q'=0
J=0(1)95
JUMP2,AJ=I
JUMP2,AJ=I+1
Q'=Q'+1
4)REPEAT
SPACE(Q')
JUMP3
2)SPACE(Q')
PRINTCH(%CODE(*))
Q'=0
JUMP4
25)SPACE96
3)PRINT('I')
NEWLINE
REPEAT
SPACE6
PRINT('-+')
M=1(1)24
```

```
PRINT('---+')
REPEAT
NEWLINE
SPACE7
PRINT('0   1   2   3   4   5   6   7   8   9  10  11  12  13  14')
PRINT('  15  16  17  18  19  20  21  22  23')
NEWLINE5
ACROSS1/34
CLOSE
CHAPTER34                                   ! FINAL FOF2 GRAPH
VARIABLES15
1)K=K
SPACE45
PRINT('GRAPH  OF  FOF2  AGAINST  TIME')
NEWLINE
SPACE45
PRINT('------------------------------')
NEWLINE
J=150(-2)0
JUMP8,%FRPT(0.1J)#0
PRINT(0.1J)2,0
JUMP9
8)SPACE5
9)PRINT('I')
JUMP22,J=0
Q'=0
K'=0(1)95
JUMP10,%MOD(BK'-0.1J)<=0.1
Q'=Q'+1
12)REPEAT
SPACE(Q')
JUMP11
10)SPACE(Q')
PRINTCH(%CODE(*))
Q'=0
JUMP12
22)SPACE96
11)PRINT('I')
NEWLINE
REPEAT
SPACE5
PRINT('-+')
M=1(1)24
PRINT('---+')
REPEAT
NEWLINE
SPACE6
PRINT('0   1   2   3   4   5   6   7   8   9  10  11  12  13  14')
PRINT('  15  16  17  18  19  20  21  22  23  ')
NEWLINE10
JUMP101,I'#99
960=%15(6840,192)
I'=0
ACROSS1/20
101)K=K
END
CLOSE
CHAPTER0
ACROSS1/1
CLOSE
****
```

APPENDIX 5

THEORY OF LEAST SQUARES METHOD OF IONOGRAM REDUCTION

APPENDIX 5

THEORY OF LEAST SQUARES METHOD OF IONOGRAM REDUCTION

The set of equations (7.6) in Chapter 7

$$
\begin{aligned}
h'_o(f_1) &= a_o D_{1,1} + b_o D_{1,2} + 0 + \cdots + 0 + h_o D_{1,M+2} \\
h'_o(f_2) &= a_o D_{2,1} + b_o D_{2,2} + b_1 D_{2,3} + 0 + \cdots + 0 + h_o D_{2,M+2} \\
&\text{---------- } \\
&\text{---------- } \\
h'_o(f_M) &= a_o D_{M,1} + b_o D_{M,2} + b_1 D_{M,3} + \cdots + b_{M-1} D_{M,M+1} + h_o D_{M,M+2} \\
h'_x(f_{x_1}) &= a_o D_{M+1,1} + b_o D_{M+1,2} + \cdots + b_{j-1} D_{M+1,j+1} + 0 + \cdots \\
&\qquad + 0 + h_o D_{M+1,M+2} \\
&\text{---------- } \\
&\text{---------- } \\
h'_x(f_{x_{N'}}) &= a_o D_{M+N',1} + b_o D_{M+N',2} + \cdots + b_{k-1} D_{M+N',k+1} + 0 + \cdots \\
&\qquad + 0 + h_o D_{M+N',M+2}
\end{aligned}
\tag{1}
$$

have coefficients $D_{j,k}$ defined as follows.[36] The coefficients of the h_o terms are

$$D_{j,M+2} = 1 \qquad \text{for } j=1(1)M+N' \tag{2}$$

The coefficients of the a_o terms are

$$D_{j,1} = \sum_{k=0}^{j-1} \int_{f_{N_k}}^{f_{N_{k+1}}} \mu'(f_j)\,df_N \qquad \text{for } j=1(1)M+N' \tag{3}$$

The coefficients of the b_i terms are

$$
\begin{aligned}
D_{j,k} = &\int_{f_{N_{j-1}}}^{f_{N_j}} (f_N - f_{N_{j-1}})\mu'(f_j)\,df_N \\
&+ 2(f_{N_k} - f_{N_{k-1}}) \sum_{l=0}^{j-1} \int_{f_{N_l}}^{f_{N_{l+1}}} \mu'(f_j)\,df_N
\end{aligned}
\tag{4}
$$

for $j=2(1)M+N'$, $k=2(1)M+N'-1$ and $k<j+1$

$$D_{j,j+1} = 2\int_{f_{N_{j-1}}}^{f_{N_j}} (f_N - f_{N_{j-1}})\mu'(f_j)df_N \quad \text{for} \quad j=1(1)M \qquad (5)$$

These equations can be written more simply using matrix notation, i.e.

$$DX_h = H' \qquad (6)$$

Here D is an M+N' by M+2 array of coefficients,

X_h is an M+2 column vector of unknowns,

and H' is an M+N' column vector of virtual height data.

Thus we have M+N' linearly independent equations in M+2 unknowns. To obtain a least squares solution to these equations, one requires that

$$\sum_{j=1}^{M+N'} \left\{ \left(\sum_{k=1}^{M+2} D_{jk}X_k \right) - H'_j \right\}^2$$

be a minimum. Alternatively

$$\frac{\partial}{\partial X_i} \sum_{j=1}^{M+N'} \left\{ \left(\sum_{k=1}^{M+2} D_{jk}X_k \right) - H'_j \right\}^2 = 0 \quad \text{for } i=1(1)M+2$$

$$\therefore \quad \sum_{j=1}^{M+N'} 2D_{ji} \left\{ \left(\sum_{k=1}^{M+2} D_{jk}X_k \right) - H'_j \right\} = 0 \qquad (7)$$

Now consider

$$D^t DX_h = D^t H' \qquad (8)$$

Here

$$(D^t DX_h)_i = \sum_{k=1}^{M+2} \sum_{j=1}^{M+N'} D_{ji}D_{jk}X_k = \sum_{j=1}^{M+N'} D_{ji} \sum_{k=1}^{M+2} D_{jk}X_k$$

and

$$(D^t H')_i = \sum_{j=1}^{M+N'} D_{ji}H'_j$$

Hence equation (8) can be written as

$$\sum_{j=1}^{M+N'} D_{ji} \sum_{k=1}^{M+2} D_{jk}X_k - \sum_{j=1}^{M+N'} D_{ji}H'_j = 0 \qquad i=1(1)M+2$$

or

$$\sum_{j=1}^{M+N'} D_{ji} \left\{ \left(\sum_{k=1}^{M+2} D_{jk}X_k \right) - H'_j \right\} = 0$$

which is the same as equation (7). Hence the least squares solution of equation (6) is

$$D^t D X_k = D^t H'$$

APPENDIX 6

REFRACTIVE INDEX FORMULAE

APPENDIX 6

REFRACTIVE INDEX FORMULAE

BECKER'S FORMULAE[9,10]

ORDINARY RAY REFRACTIVE INDEX

$$\left(\frac{\mu_o}{t}\right)^2 = \frac{1 + \dfrac{2\tan^2 I}{1 + \sqrt{1+\gamma t^4}}}{1 + t^2\dfrac{2\tan^2 I}{1 + \sqrt{1+\gamma t^4}}}$$

$$\gamma = \frac{4\tan^2 I}{Y^2\cos^2 I}$$

$$\mu_o' t = \frac{t}{\mu_o}\left\{1 + \frac{X\tan^2 I}{M^2}\left[\frac{1+X}{\sqrt{1+\gamma t^4}} - \frac{2}{1 + \sqrt{1+\gamma t^4}}\right]\right\}$$

$$M = 1 + t^2\frac{2\tan^2 I}{1 + \sqrt{1+\gamma t^4}}$$

$$X = 1 - t^2$$

where I = angle of inclination of Earth's magnetic field

$Y = f_h/f$

f_h = gyrofrequency

f = wave frequency

$t^2 = 1 - f_p^2/f_r^2$

and f_p = plasma frequency under consideration

f_r = plasma frequency of reflection of wave.

EXTRAORDINARY RAY REFRACTIVE INDEX

$$\left(\frac{\mu_x}{t}\right)^2 = (1-Y)(2+\Delta)\,\frac{1 - \dfrac{\beta}{1 + \sqrt{1+\alpha\xi}}}{1 - Y + \Delta - \dfrac{\beta Y\xi}{1 + \sqrt{1+\alpha\xi}}}$$

$$\alpha = \frac{4\sin^2 I}{(1+\sin^2 I)^2} \qquad \beta = \frac{2\sin^2 I}{1+\sin^2 I} \qquad \Delta = t^2\frac{1-Y}{Y} \qquad \xi = 2\Delta+\Delta^2$$

$$\mu_x' t = \left(\frac{t}{\mu_x}\right)\left\{1 + \frac{X(1-Y)}{N^2}\left[1 + \frac{\beta}{2}\left\{\frac{2\xi}{1 + \sqrt{1+\alpha\xi}} - \frac{(1+\xi)(1+X)}{\sqrt{1+\alpha\xi}}\right\}\right]\right\}$$

$$N = 1 - Y + \Delta - \frac{\beta Y\xi}{1 + \sqrt{1+\alpha\xi}}$$

APPLETON - HARTREE FORMULAE (see also Appendix 12)

$$\mu' = \mu + f\frac{\partial\mu}{\partial f}$$

where $$\frac{\partial\mu}{\partial f} = -\frac{\frac{\partial\alpha}{\partial f}\mu^4 + \frac{\partial\gamma}{\partial f}\mu^2 + \frac{\partial\epsilon}{\partial f}}{(4\alpha\mu^3 + 2\gamma\mu)}$$

Hence $$\mu' = \mu - \frac{\left(f\frac{\partial\alpha}{\partial f}\right)\mu^4 + \left(f\frac{\partial\gamma}{\partial f}\right)\mu^2 + \left(f\frac{\partial\epsilon}{\partial f}\right)}{2\mu(2\alpha\mu^2 + \gamma)}$$

where $$\alpha = 1 - X - Y^2 + XY^2\cos^2\theta$$

$$\gamma = -2(1-X)^2 + 2Y^2(1-X) + XY^2\sin^2\theta$$

$$f\frac{\partial\alpha}{\partial f} = 2[X + Y^2 - 2XY^2\cos^2\theta]$$

$$f\frac{\partial\gamma}{\partial f} = -4\{(1-X)(X+Y^2) + X(1-X-Y^2) + XY^2\sin^2\theta\}$$

$$f\frac{\partial\epsilon}{\partial f} = 2\{(1-X)^2X + (1-X)[2X(1-X) + Y^2] - XY^2\}$$

and $$\mu_{X_0}^2 = \frac{-\gamma \pm \sqrt{\gamma^2 - 4\alpha\epsilon}}{2\alpha}$$

$$= \frac{-\gamma \pm \sqrt{X^2Y^4\sin^4\theta + 4(1-X)^2X^2Y^2\cos^2\theta}}{2\alpha}$$

DOUPNIK AND SCHMERLING'S FORMULAE

$$\mu_o' = \frac{1}{\mu_o}\left\{1 - \frac{XY\sin^2\theta}{S^2[Y\cos^2\theta + R]}\left[(1-X) - \frac{Y(1+X)\cos^2\theta}{R}\right]\right\}$$

$$\mu_o = \sqrt{1-X}\left\{\frac{Y(1+\sin^2\theta) + R}{Y(1+\sin^2\theta) - 2XY\sin^2\theta + R}\right\}^{\frac{1}{2}}$$

$$S = \frac{Y[1 + (1-2X)\sin^2\theta] + R}{R + Y\cos^2\theta}$$

$$R = \sqrt{Y^2\cos^4\theta + 4(1-X)^2\sin^2\theta}$$

$$\mu_X' = \frac{1}{\mu_X}\left\{1 + \frac{X(1-T)}{2T^2}\left[1 + \frac{Y^2\cos^2\theta}{R}\left(\frac{1+X}{1-X}\right)\right]\right\}$$

$$\mu_X = \sqrt{1-X-Y}\left\{\frac{(1+Y-X)(1-X)}{Y^2\left[\frac{(1-X)}{Y} - 1 + X\sin^2\theta\right]} \times \left[\frac{2(1-X) - Y^2\cos^2\theta + YR}{2(1-X)^2 - Y^2\cos^2\theta + YR}\right]\right\}^{\frac{1}{2}}$$

$$T = 2\left[\frac{(1-X) + Y^2(X\sin^2\theta - 1)}{2(1-X) - Y\cos^2\theta + YR}\right]$$

APPENDIX 7

LISTING OF COMPUTER PROGRAM DESCRIBED IN SECTION 7.2

FOR CONVERTING IONOGRAMS TO N(h) PROFILES

```
LIST
SEND TO(ED,ICLA-DEFAULT.IONO)
DUMPON(ED,PROGRAM TEST)
PROGRAM(DOUPNIK)
INPUT1=CR0
OUTPUT1=LP0
AUXILIARY(0,10200)
USE AUX(1900)=ED(ICLA-DEFAULT)
OMIT COMMENTS
MAIN700
CHAPTER1
B->50                                   ! ORDINARY FREQUENCIES
C->100                                  ! ORD AND EXT HEIGHTS
D->50                                   ! ETRAORDINARY WAVE FREQUENCIE
X->50
E->50                                   ! EXTRAORDINARY PLASMA FREQUEN
G->50
H->51
U->50
V->1
W->1
Y->50
Z->51
F->0
A->24
£->50                                ! STORES COEFFICIENTS AI FOR ORD MO
CLOSE
CHAPTER2
VARIABLES1
1)A=0                                   ! CALCULATES ORDINARY INTEGRAL
O=0
JUMP111,S'#3
I=%MIN(C0,2,M)
JUMP112,I=2
PRINT('THE REAL HEIGHTS CALCULATED FOR THIS SET OF DATA MAY BE UNREL'
PRINT('IABLE SINCE SCALED POINTS AT LOW FREQUENCIES ARE MISSING')
NEWLINE2
112)£'=CI
£'=£'-1
111)K=K
J=2(1)M
6)K=0(1)M
H(K+1)=0
G(K+1)=0
U(K+1)=0
REPEAT
I=2(1)J
B'=BI
C'=B(I-1)
G'=0
U'=0
A2=%SQRT(BJBJ-C'C')
A3=%SQRT(BJBJ-B'B')
JUMP88,I>J-1
R=0(1)1
A4=0.5(A2+A3)+VR(A2-A3)
T)=2)
JUMP4
2)G0=GI
```

```
U0=UI
A4=0.5(A2+A3)-VR(A2-A3)
T)=3)
JUMP4
3)G'=WRG0+WRGI+G'
U'=WRU0+WRUI+U'
REPEAT
JUMP89
88)R=0(1)3
A4=0.5(A2+A3)+(A2-A3)A(R+16)
T)=80)
JUMP4
80)G0=GI
U0=UI
A4=0.5(A2+A3)-(A2-A3)A(R+16)
T)=81)
JUMP4
81)G'=A(R+20)(G0+GI)+G'
U'=A(R+20)(U0+UI)+U'
REPEAT
89)K=K
GI=G'(A2-A3)                    ! INTEGRAL FROM FN(I-1) TO FN(I) OF MU'(F
UI=U'(A2-A3)                    ! 2 X INTEG FROM F(I-1) TO FN(I) OF MU'(F
REPEAT
JUMP99,S'=3
H(M+1)=1                                ! DN,M+1
H1=0
I=2(1)J
H1=H1+GI                                ! DN,1
REPEAT
K=2(1)J
F0=0
10)JUMP92;J=K
E0=2(BKBK-B(K-1)B(K-1))
L=K+1
I=L(1)J
F0=F0+GI
REPEAT
F0=F0E0
92)HK=UK+F0
REPEAT
JUMP93,A=0
P=J
J=M+0
93)T=M+1
%7(JT-2T)H1,T
JUMP94,A#0
12)REPEAT
JUMP13,S'=3
A=99
O=1(1)N
J=1(1)M
JUMP5,BJ>=E0
REPEAT
101)PRINT('EXTRAORDINARY PLASMA FREQUENCY ENCOUNTERED WHICH IS GREATE')
PRINT('R THAN ALL THE ORDINARY FREQUENCIES')
NEWLINE2
PRINT('OFFENDING FREQUENCY IS')
PRINT(0.000001D0)2,2
PRINT('MHZ')
NEWLINE2
PRINT('PLEASE REMOVE THIS FREQUENCY OR SCALE ADDITIONAL ORD ')
PRINT('FREQUENCIES')
```

```
NEWLINE10
HALT
JUMP101
5)B0=BJ
BJ=E0
JUMP6
94)BP=B0
REPEAT
ACROSS2/6
13)ACROSS1/4
4)DOWN2/8
JUMP(T)
99)JUMP40,J=4                          ! CALCULATES ORD MODE COEFF
JUMP43,J>4
JUMP41,J=3
X2=G2
Y2=U2
JUMP12
41)Z2=[(G2+G3)(C2-95)-X2(C3-95)]/[(G2+G3)Y2-(U2+U3)X2-2G3X2B2B2]
£2=(C2-95-Y2Z2)/X2                                                  ! A1
X=[(G2+G3)(C2-£')-X2(C3-£')]/[(G2+G3)Y2-(U2+U3)X2-2G3X2B2B2]
Y2=(C2-£'-Y2X)/X2                                                   ! A1
X2=X
JUMP12
40)£3=£2+2Z2B3B3                       ! A2
Y3=Y2+2X2B3B3                          ! A2
X=0
Y=0
JUMP44
43)X'=B(J-1)B(J-1)-B(J-2)B(J-2)
£(J-1)=£(J-2)+2Z(J-2)X'                ! A(J-2)
Y(J-1)=Y(J-2)+2X(J-2)X'                ! A(J-2)
X=0
Y=0
I=J-2
K=3(1)I
X=X+ZKU(K+1)
Y=Y+XKU(K+1)
REPEAT
44)X=X+£2(G2+G3)+Z2(U2+U3)+2Z2G3B2B2
Y=Y+Y2(G2+G3)+X2(U2+U3)+2X2G3B2B2
I=J-1
K=3(1)I
X=X+£KG(K+1)
Y=Y+YKG(K+1)
REPEAT
Z(J-1)=(CJ-95-X)/UJ
X(J-1)=(CJ-£'-Y)/UJ
JUMP12
CLOSE
CHAPTER8
VARIABLES1
2)K=K
JUMP3,A#0
X'=A4A4/(BJBJ)
X=1-X'
Y=A'/BJ
JUMP7
3)X=(BJBJ-A4A4)/(DODO)
X'=1-X
Y=A'/DO
U=XYYDD-X-YY+1
G=YYCCCC+4DD-8XDD+4XXDD
```

```
Y'=%SQRT(G)
H=%SQRT(-X-0.5XYY'/U-0.5XYY/U-0.5XYYDD/U+XXYYDD/U+1)
F'=4HHH-4H+4YYH-4YYHHH+8XH+2XYYCCH-4YYXH-4XHHH+4YYXDDHHH-4XXH
Z'=6XXX-12XX+8XXHH+8XYYHH-4XYYDDHHHH-8XHH+2XHHHH+6X-4XYYCCHH-4XYY-4YYH
Z'=Z'+2YYHHHH+2YY
G=2A4
X'=HG-Z'G/F'
JUMP12
7)G=YYCCCC
H=4DD/G
F'=%SQRT(1+HX'X')
H'=1+F'
V=CC
V'=DD/V
Y'=1+2V'X'/H'
U=1+2V'/H'
W=Y'/U
U=%SQRT(W)
G=%SQRT(X')
H=(1+X)/F'-2/H'
F'=Y'Y'
V=XV'H/F'
X'=U+UV
X'=2X'BJ
12)K=K
V=0
GI=X'
UI=BJBJ-A4A4-C'C'
UI=2UIX'
UP
CLOSE
CHAPTER4
VARIABLES1
1)SPACE50
PRINT('N-H PROFILE FOR ')
I=0(1)P'
U NPACK(A8,I,K)
PRINTCH(K)
REPEAT
NEWLINE
SPACE50
PRINT('----------------')
I=0(1)P'
PRINT('-')
REPEAT
NEWLINE
PRINT('TIME ')
PRINT(A1)2,2
SPACE25
PRINT('DATE ')
PRINT(A6)2,0
PRINT(A7)2,0
PRINT(A5)2,0
SPACE25
PRINT('METHOD ')
JUMP4,S'=3
PRINT('LEAST SQUARES ')
JUMP5,S'#2
NEWLINE
SPACE90
PRINT('FOLLOWED BY ')
4)PRINT('ORD MODE ')
5)NEWLINE5
```

```
SPACE9
PRINT('PLASMA FREQ ')
SPACE3
PRINT('VIRTUAL HT')
SPACE5
PRINT('EL DENS ')
SPACE7
PRINT('REAL HT ')
JUMP101,S'#3
SPACE7
PRINT('REAL HT ')
101)SPACE12
PRINT('A ')
SPACE15
PRINT('B ')
NEWLINE
SPACE11
PRINT('IN MHZ')
SPACE9
PRINT('IN KM')
SPACE7
PRINT('IN ELS/CC')
SPACE8
PRINT('IN KM')
JUMP102,S'#3
SPACE10
PRINT('IN KM')
102)K=K
JUMP103,S'#3
NEWLINE
SPACE53
PRINT('FLAT BASE')
SPACE4
PRINT('BASE = 95 KM')
103)K=K
NEWLINE3
JUMP111,S'=3
I=2(1)P
YI=Y(I-1)+2X(I-1)BIBI-2X(I-1)B(I-1)B(I-1)
REPEAT
I=2(1)M
X'=(BIBI-B(I-1)B(I-1))
ZI=Z(I-1)+Y(I-1)X'+X(I-1)X'X'
REPEAT
JUMP112
111)£1=95
Z1=£'
X'=£2
Y'=Z2
X1=X2
Y1=Y2
I=2(1)M
G=£I
H=ZI
X=BIBI-B(I-1)B(I-1)
£I=£(I-1)+X'X+Y'XX
ZI=Z(I-1)+Y(I-1)X+X(I-1)XX
X'=G
Y'=H
XI=XI                                   ! FLAT BASE BI
YI=YI                                   ! FLAT BASE AI
REPEAT
112)K=K
```

```
I=1(1)M
SPACE5
PRINT(I)2,0
PRINT(0.000001BI)1,4
SPACE5
PRINT(CI)3,2
SPACE5
PRINT(0.0000000124BIBI)7,0
SPACE5
PRINT(ZI)3,3
SPACE5
JUMP104,S'#3
PRINT(£I)3,3
SPACE5
104)K=K
PRINT(YI)0,8
PRINT(XI)0,8
NEWLINE2
REPEAT
Q=M-1
R=Q-1
S=R(1)Q
F'=ZS-Z(S-1)
G'=B(S-1)/Y(S-1)-BS/YS
GS=ZS+F'BS/(G'YS)
REPEAT
S=R(1)Q
F'=BSBS-B(S-1)B(S-1)
U=GS-ZS
V=GS-Z(S-1)
W=VV-UU
US=BSBS+F'UU/W
US=%SQRT(US)
REPEAT
NEWLINE5
SPACE18
PRINT('POSITION OF MAXIMUM ')
PRINT(G(M-1))3,0
SPACE6
PRINT('EL DENS AT MAXIMUM ')
PRINT(U(M-1))7,0
NEWLINE
SPACE37
PRINT(G(M-2))3,0
SPACE25
PRINT(U(M-2))7,0
RUNOUT
JUMP15,S'#2
S'=3
ACROSS1/2
15)K=K
ACROSS5/0
CLOSE
CHAPTER6
VARIABLES1
2)K=K
A=MM+MN+N-1
P=M+N-1
J=A
J=%16(0,M+N-1,M+1)                    ! DT
0=%26(J,0,M+1,M+1,M+N-1)              ! DT*D
%7(2J)C2,P
J=%26(J,2J,M+1,1,M+N-1)               ! DT*H'
```

```
J=%28(0,M+1,1)
P=M+1
%6(J)X0,P
Y1=X0
Z1=XM
XM=0
YM=0
P=M-1
Q=2
ACROSS1/4
CLOSE
CHAPTER0
VARIABLES1
14)K=K
I=0(1)3
READ(VI)                                    ! GAUSS COEFFICIENTS
REPEAT
I=0(1)7
READ(A(I+16))
REPEAT
32)READCH(I)
JUMP32,I#3994
I=0(1)31
READCH(J)
PACK(A8,I,J)
REPEAT
I=31(-1)0
UNPACK(A8,I,J)
JUMP33,J#16
REPEAT
33)P'=I
READ(A')
READ(C)                                     ! ANGLE OF DIP
C=£C/180
D=%SIN(C)
C=%COS(C)
5)K=K
READ(A1)
JUMP6,A1<=24
NEWLINE20
END
6)READ(A6)
READ(A7)
READ(A5)
READ(S')
READ(M)
C1=0
B1=0
M=M+1
I=2(1)M
READ(A)
BI=1000000A
READ(CI)
REPEAT
JUMP98,U>50
JUMP7,S'=3
READ(N)
I=1(1)N
READ(A)
A=1000000A
DI=A
EI=%SQRT(AA-AA')
READ(C(I+M))
                                            REPEAT
                                            JUMP7,MM+MN+N<1500
                                            98)K=K
                                            PRINT('TOO MANY SCALED POINTS')
                                            NEWLINE
                                            END
                                            7)K=K
                                            ACROSS1/2
                                            CLOSE
```

APPENDIX 8

A METHOD FOR CORRECTING FOR THE PRESENCE OF A SUSPECTED VALLEY IN AN N(h) PROFILE

APPENDIX 8

A METHOD FOR CORRECTING FOR THE PRESENCE OF A SUSPECTED VALLEY IN AN N(h) PROFILE

In order to correct for the presence of a valley, information from both the ordinary and the extraordinary ray traces must be used. In this method the ordinary ray trace is used to calculate a monotonic N(h) profile using straightforward ionogram reduction techniques (Titheridge's method). This profile is then used to determine the retardation of the extraordinary ray for each of the scaled extraordinary frequencies.

Let the difference between the observed extraordinary virtual height for the i^{th} frequency $\left(f_{x_i}\right)$ and the calculated virtual height for the same frequency be $\Delta h'_x\left(f_{x_i}\right)$, i.e.

$$\Delta h'_x\left(f_{x_i}\right) = h'_x\left(f_{x_i}\right)_{obs} - h'_x\left(f_{x_i}\right)_{calc} \qquad (1)$$

If the calculated N(h) profile is a good approximation to the actual N(h) distribution then the absolute values of $\Delta h'_x\left(f_{x_i}\right)$ should be relatively small. However, if a valley is present, $\left|\Delta h'_x\left(f_{x_i}\right)\right|$ will be large for frequencies which are reflected at heights just above the valley, decreasing gradually to smaller values for higher frequencies (compare results for the Complicated Monotonic Layer model with those for the Simple Deep Valley model - Figs 57, 58).

If a valley is detected in this manner, a correction may be introduced in the form of k slabs of ionization ($k \geq 1$). It will be assumed that the slabs are of equal thickness Δh and have plasma frequencies $f_{p_{v_i}}$ ($i = 1(1)k$). To derive the basic equations, consider the following situation:

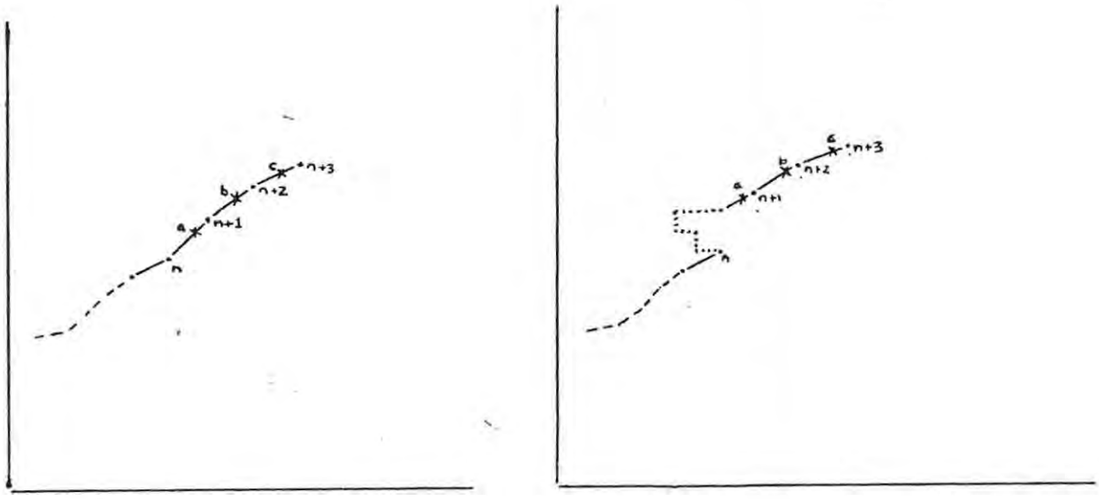

MONOTONIC PROFILE BEFORE VALLEY CORRECTION

N(h) PROFILE AFTER VALLEY CORRECTION

Dots (·) mark the positions of the ordinary plasma frequencies
Crosses (×) mark the positions of the extraordinary plasma frequencies.

In the accompanying diagrams f_{o_n} represents the last scaled ordinary ray frequency which is reflected below the valley, $f_{o_{n+1}}$, $f_{o_{n+2}}$, $f_{o_{n+3}}$, etc., represent scaled ordinary ray frequencies which are reflected above the valley. Assume that the frequencies f_{p_a}, f_{p_b}, f_{p_c}, etc., represent plasma frequencies falling within the $(n+1)^{th}$, $(n+2)^{th}$, $(n+3)^{th}$, etc., frequency intervals of our calculated profile respectively

and that these correspond to scaled extraordinary wave frequencies (f_{x_a}, f_{x_b}, f_{x_c}, etc.) reflected at heights above the suspected valley.

The addition of k slabs of ionization will affect the retardation of the extraordinary ray and these slabs can be adjusted to reduce the absolute value of $\Delta h'_x \left(f_{x_i} \right)$ for points above the valley. However, the introduction of this additional ionization will also affect the real heights above the valley as calculated from the scaled ordinary ray frequencies. These real heights (the monotonic profile) are initially calculated using Titheridge's method in which the ordinary ray virtual heights are given by

$$
\begin{aligned}
h'_o &= h_o \\
h'_1 &= h_o + \bar{\mu}'_o(1,1)\,\Delta h_1 \\
&\text{---------} \\
&\text{---------} \\
h'_n &= h_o + \sum_{r=1}^{n} \bar{\mu}'_o(r,n)\,\Delta h_r \\
h'_{n+1} &= h_o + \sum_{r=1}^{n+1} \bar{\mu}'_o(r,n+1)\,\Delta h_r \\
&\text{---------} \\
&\text{---------}
\end{aligned}
\qquad (2)
$$

If additional slabs of ionization are to be inserted, the retardation of the ordinary ray will be changed and the above set of equations can be rewritten as:

$$h'_0 = h_0$$

$$h'_1 = h_0 + \bar{\mu}'_0(1,1)\,\Delta h_1$$

$$h'_n = h_0 + \sum_{r=1}^{n} \bar{\mu}'_0(r,n)\,\Delta h_r$$

$$h'_{n+1} = h_0 + \sum_{r=1}^{n} \bar{\mu}'_0(r,n+1)\,\Delta h_r + \bar{\mu}'_0(v,n+1)\,\Delta h_v + \bar{\mu}'_0(n+1,n+1)\,\Delta h_{n+1} \qquad (3)$$

$$h'_{n+2} = h_0 + \sum_{r=1}^{n} \bar{\mu}'_0(r,n+2)\,\Delta h_r + \bar{\mu}'_0(v,n+2)\,\Delta h_v + \sum_{r=n+1}^{n+2} \bar{\mu}'_0(r,n+2)\,\Delta h_r$$

---

where $\bar{\mu}'_0(v,i)\,\Delta h_v$ is the retardation of the ordinary ray of frequency f_{o_i} in passing through the valley. For example, for a two-slab valley approximation

$$\bar{\mu}'_0(v,i) = \bar{\mu}'_0(f_{p_{v_1}}, f_{o_i}) + \bar{\mu}'_0(f_{p_{v_2}}, f_{o_i}) \qquad (4)$$

and Δh_v is the thickness of each slab. Hence

$$\Delta h_1' = \bar{\mu}'_o(1,1)\,\Delta h_1$$

$$\Delta h'_n = \bar{\mu}'_o(n,n)\,\Delta h_n - \sum_{r=1}^{n-1} (\bar{\mu}'_o(r,n-1) - \bar{\mu}'_o(r,n))\,\Delta h_r$$

$$\Delta h'_{n+1} = \bar{\mu}'_o(n+1,n+1)\,\Delta h_{n+1} - \sum_{r=1}^{n} (\bar{\mu}'_o(r,n) - \bar{\mu}'_o(r,n+1))\,\Delta h_r$$

$$+\bar{\mu}'_o(v,n+1)\,\Delta h_v \qquad (5)$$

$$\Delta h'_{n+2} = \bar{\mu}'_o(n+2,n+2)\,\Delta h_{n+2} - \sum_{r=1}^{n} (\bar{\mu}'_o(r,n+1) - \bar{\mu}'_o(r,n+2))\,\Delta h_r$$

$$-(\bar{\mu}'_o(v,n+1) - \bar{\mu}'_o(v,n+2))\,\Delta h_v - (\bar{\mu}'_o(n+1,n+1) - \bar{\mu}'_o(n+1,n+2))\,\Delta h_{n+1}$$

. .

---

and so the correct formulae for real height after inserting k slabs of ionization should be:

$$\Delta h^c_1 = \frac{1}{\bar{\mu}'_o(1,1)}\,\Delta h'_1$$

$$\Delta h^c_n = \frac{1}{\bar{\mu}'_o(n,n)}\left[\Delta h'_n + \sum_{r=1}^{n-1} (\bar{\mu}'_o(r,n-1) - \bar{\mu}'_o(r,n))\,\Delta h_r\right]$$

$$\Delta h^c_{n+1} = \frac{1}{\bar{\mu}'_o(n+1,n+1)}\left[\Delta h'_{n+1} + \sum_{r=1}^{n} (\bar{\mu}'_o(r,n) - \bar{\mu}'_o(r,n+1))\,\Delta h_r\right.$$

$$\left. -\mu_o(v,n+1)\,\Delta h_v\right] \qquad (6)$$

$$h^c_{n+2} = \frac{1}{\bar{\mu}'_o(n+2,n+2)}\Big[\Delta h'_{n+2} + \sum_{r=1}^{n}(\bar{\mu}'_o(r,n+1)-\bar{\mu}'_o(r,n+2))\Delta h_r$$

$$+(\bar{\mu}'_o(v,n+1)-\bar{\mu}'_o(v,n+2))\Delta h_v$$

$$+(\bar{\mu}'_o(n+1,n+1)-\bar{\mu}'_o(n+1,n+2))\Delta h_{n+1}\Big]$$

where Δh^c_i represents the corrected real height thickness of the i^{th} lamination of the monotonic N(h) profile .

Thus when calculating the extraordinary virtual heights after additional slabs of ionization have been inserted, the above equations for real height must be used. Hence for extraordinary ray frequencies having the same plasma frequencies as the ordinary ray frequencies,

$$h'_{x_1} = h_o + \bar{\mu}'_x(1,1)\,\Delta h^c_1$$

$$h'_{x_n} = h_o + \sum_{r=1}^{n}\bar{\mu}'_x(r,n)\,\Delta h^c_r \qquad (7)$$

$$h'_{x_{n+1}} = h_o + \sum_{r=1}^{n}\bar{\mu}'_x(r,n+1)\Delta h^c_r + \bar{\mu}'_x(n+1,n+1)\Delta h^c_{n+1}$$

$$+\bar{\mu}'_x(v,n+1)\Delta h_v$$

$$h'_{x_{n+2}} = h_o + \sum_{r=1}^{n}\bar{\mu}'_x(r,n+2)\Delta h^c_r + \sum_{r=n+1}^{n+2}\bar{\mu}'_x(r,n+2)\Delta h^c_r$$

$$+\bar{\mu}'_x(v,n+2)\,\Delta h_v$$

This is equivalent to

$$h'_{x_1} = h_o + \bar{\mu}'_x(1,1)\Delta h_1$$

$$h'_{x_n} = h_o + \sum_{r=1}^{n} \bar{\mu}'_x(r,n)\,\Delta h_r$$

$$h'_{x_{n+1}} = h_o + \sum_{r=1}^{n+1} \bar{\mu}'_x(r,n+1)\Delta h_r - \frac{\bar{\mu}'_x(n+1,n+1)}{\bar{\mu}'_o(n+1,n+1)}\,\bar{\mu}'_o(v,n+1)\Delta h_v + \bar{\mu}'_x(v,n+1)\Delta h_v \qquad (8)$$

$$h'_{x_{n+2}} = h_o + \sum_{r=1}^{n+2} \bar{\mu}'_x(r,n+2)\,\Delta h_r - \frac{\bar{\mu}'_x(n+1,n+2)}{\bar{\mu}'_o(n+1,n+1)}\,\bar{\mu}'_o(v,n+1)\Delta h_v + \frac{\bar{\mu}'_x(n+2,n+2)}{\bar{\mu}'_o(n+2,n+2)}\,(\bar{\mu}'_o(v,n+1) - \bar{\mu}'_o(v,n+2))\,\Delta h_v - \frac{\bar{\mu}'_x(n+2,n+2)}{\bar{\mu}'_o(n+2,n+2)}\left(\frac{\bar{\mu}'_o(n+1,n+1) - \bar{\mu}'_o(n+1,n+2)}{\bar{\mu}'_o(n+1,n+1)}\right)\mu_o(v,n+1)\Delta h_v + \bar{\mu}'_x(v,n+2)\Delta h_v$$

---

where the Δh_i are the original real height differences calculated for the monotonic profile.

The virtual heights calculated from the monotonic profile for the same extraordinary frequencies would be:

$$h'_{x_1} = h_o + \bar{\mu}'_x(1,1)\Delta h_1$$

$$h'_{x_n} = h_o + \sum_{r=1}^{n} \bar{\mu}'_x(r,n)\Delta h_r \qquad (9)$$

$$h'_{x_{n+1}} = h_o + \sum_{r=1}^{n+1} \bar{\mu}'_x(r,n+1)\Delta h_r$$

$$h'_{x_{n+2}} = h_o + \sum_{r=1}^{n+2} \bar{\mu}'_x(r,n+2)\Delta h_r$$

Hence the difference in the virtual height of the extraordinary ray caused by the introduction of additional slabs of ionization will be:

$$\Delta h'_{x_{n+1}} = h'_{x_{n+1}}\text{(with valley)} - h'_{x_{n+1}}\text{(without valley)}$$

$$= \bar{\mu}'_x(v,n+1)\Delta h_v - \frac{\bar{\mu}'_x(n+1,n+1)}{\bar{\mu}'_o(n+1,n+1)}\bar{\mu}'_o(v,n+1)\Delta h_v$$

$$\Delta h'_{x_{n+2}} = \bar{\mu}'_x(v,n+2)\Delta h_v - \frac{\bar{\mu}'_x(n+1,n+2)}{\bar{\mu}'_o(n+1,n+1)}\bar{\mu}'_o(v,n+1)\Delta h_v$$

$$+ \frac{\bar{\mu}'_x(n+2,n+2)}{\bar{\mu}'_o(n+2,n+2)}\left[\bar{\mu}'_o(v,n+1)\,\frac{\bar{\mu}'_o(n+1,n+2)}{\bar{\mu}'_o(n+1,n+1)}\right. \qquad (10)$$

$$\left. - \bar{\mu}'_o(v,n+2)\right]\Delta h_v$$

Since this holds only for extraordinary ray frequencies with the same plasma frequencies as the scaled ordinary ray frequencies, consider now the arbitrarily chosen extraordinary ray frequencies f_{x_a}, f_{x_b}, f_{x_c}, etc. which have been chosen to lie within the $(n+1)^{th}$, $(n+2)^{th}$, $(n+3)^{th}$, etc. frequency interval respectively. In this case, the virtual heights calculated from the monotonic profile will be:

$$
\begin{aligned}
h'_{x_a} &= h_o + \sum_{r=1}^{n} \bar{\mu}'_x(f_r, f_{x_a})\Delta h_r + \left\{ \frac{f_{p_a}^2 - f_n^2}{f_{n+1}^2 - f_n^2} \right\} \bar{\mu}'_x(f_{p_a}, f_{x_a})\Delta h_{n+1} \\
h'_{x_b} &= h_o + \sum_{r=1}^{n+1} \bar{\mu}'_x(f_r, f_{x_b})\Delta h_r + \left\{ \frac{f_{p_b}^2 - f_{n+1}^2}{f_{n+2}^2 - f_{n+1}^2} \right\} \bar{\mu}'_x(f_{p_b}, f_{x_b})\Delta h_{n+2} \\
h'_{x_c} &= h_o + \sum_{r=1}^{n+2} \bar{\mu}'_x(f_r, f_{x_c})\Delta h_r + \left\{ \frac{f_{p_c}^2 - f_{n+2}^2}{f_{n+3}^2 - f_{n+2}^2} \right\} \bar{\mu}'_x(f_{p_c}, f_{x_c})\Delta h_{n+3}
\end{aligned}
\tag{11}
$$

Writing $\left\{ \frac{f_{p_a}^2 - f_n^2}{f_{n+1}^2 - f_n^2} \right\}$ as F_a, $\left\{ \frac{f_{p_b}^2 - f_{n+1}^2}{f_{n+2}^2 - f_{n+1}^2} \right\}$ as F_b,

$\left\{ \frac{f_{p_c}^2 - f_{n+2}^2}{f_{n+3}^2 - f_{n+2}^2} \right\}$ as F_c, etc., (12)

equations (11) become:

$$
\begin{aligned}
h'_{x_a} &= h_o + \sum_{r=1}^{n} \bar{\mu}'_x(f_r, f_{x_a})\,\Delta h_r + F_a\,\bar{\mu}'_x(f_{p_a}, f_{x_a})\,\Delta h_{n+1} \\
h'_{x_b} &= h_o + \sum_{r=1}^{n+1} \bar{\mu}'_x(f_r, f_{x_b})\,\Delta h_r + F_b\,\bar{\mu}'_x(f_{p_b}, f_{x_b})\,\Delta h_{n+2} \\
h'_{x_c} &= h_o + \sum_{r=1}^{n+2} \bar{\mu}'_x(f_r, f_{x_c})\,\Delta h_r + F_c\,\bar{\mu}'_x(f_{p_c}, f_{x_c})\,\Delta h_{n+3}
\end{aligned}
$$

In this case the calculated virtual heights after additional slabs of ionization have been inserted will be:

$$h'_{x_a} = h_o + \sum_{r=1}^{n} \bar{\mu}'_x(f_r, f_{x_a})\Delta h_r + F_a \bar{\mu}'_x(f_{p_a}, f_{x_a})\Delta h_{n+1} - F_a \frac{\bar{\mu}'_x(f_{p_a}, f_{x_a})}{\bar{\mu}_{o(n+1,n+1)}} \bar{\mu}'_o(v,n+1)\Delta h_v + \bar{\mu}'_x(v, f_{x_a})\Delta h_v$$

$$h'_{x_b} = h_o + \sum_{r=1}^{n+1} \bar{\mu}'_x(f_r, f_{x_b})\Delta h_r + F_b \bar{\mu}'_x(f_{p_b}, f_{x_b})\Delta h_{n+2} - \frac{\bar{\mu}'_x(f_{n+1}, f_{x_b})}{\bar{\mu}_{o(n+1,n+1)}} \bar{\mu}'_o(v,n+1)\Delta h_v + \bar{\mu}'_x(v, f_{x_b})\Delta h_v + \frac{F_b \bar{\mu}'_x(f_{p_b}, f_{x_b})}{\bar{\mu}_{o(n+2,n+2)}} \left[\frac{\bar{\mu}'_{o(n+1,n+2)}}{\bar{\mu}_{o(n+1,n+1)}} \bar{\mu}_o(v,n+1)\Delta h_v - \bar{\mu}'_o(v,n+2)\Delta h_v \right]$$

$$h'_{x_c} = h_o + \sum_{r=1}^{n+2} \bar{\mu}'_x(f_r, f_{x_c})\Delta h_r + F_c \bar{\mu}'_x(f_{p_c}, f_{x_c})\Delta h_{n+3} - \frac{\bar{\mu}'_x(f_{n+1}, f_{x_c})}{\bar{\mu}_{o(n+1,n+1)}} \bar{\mu}'_o(v,n+1)\Delta h_v + \bar{\mu}'_x(v, f_{x_c})\Delta h_v + \frac{\bar{\mu}'_x(f_{n+2}, f_{x_c})}{\bar{\mu}_{o(n+2,n+2)}} \left[\frac{\bar{\mu}'_{o(n+1,n+2)}}{\bar{\mu}_{o(n+1,n+1)}} \bar{\mu}'_o(v,n+1)\Delta h_v - \bar{\mu}'_o(v,n+2)\Delta h_v \right] + \frac{F_c \bar{\mu}'_x(f_{p_c}, f_{x_c})}{\bar{\mu}_{o(n+3,n+3)}} \left[\frac{\bar{\mu}'_o(n+1,n+3)}{\bar{\mu}_{o(n+1,n+1)}} \bar{\mu}'_o(v,n+1)\Delta h_v - \frac{\bar{\mu}'_o(n+2,n+3)}{\bar{\mu}_{o(n+2,n+2)}} \left\{ \frac{\bar{\mu}'_o(n+1,n+2)}{\bar{\mu}_{o(n+1,n+1)}} \bar{\mu}'_o(v,n+1) - \bar{\mu}'_o(v,n+2) \right\} \Delta h_v - \bar{\mu}'_o(v,n+3)\Delta h_v \right]$$

(13)

Subtracting equations (12) from (13) will once again give the difference in calculated extraordinary virtual height caused by the introduction of additional slabs of ionization. Since one would like this difference to account for the difference between the observed virtual height and the virtual height calculated for that frequency from the monotonic profile, we write:

$$\Delta h'_x(f_{x_a}) = \bar{\mu}'_x(v,f_{x_a})\,\Delta h_v - F_a \frac{\bar{\mu}'_x(f_{p_a},f_{x_a})}{\bar{\mu}'_o(n+1,n+1)}\,\bar{\mu}'_o(v,n+1)\Delta h_v$$

$$\Delta h'_x(f_{x_b}) = \bar{\mu}'_x(v,f_{x_b})\,\Delta h_v - \frac{\bar{\mu}'_x(f_{n+1},f_{x_b})}{\bar{\mu}'_o(n+1,n+1)}\,\bar{\mu}'_o(v,n+1)\,\Delta h_v$$

$$+ \frac{F_b\,\bar{\mu}'_x(f_{p_b},f_{x_b})}{\bar{\mu}'_o(n+2,n+2)}\left[\frac{\bar{\mu}'_o(n+1,n+2)}{\bar{\mu}'_o(n+1,n+1)}\,\bar{\mu}'_o(v,n+1)\Delta h_v - \bar{\mu}'_o(v,n+2)\,\Delta h_v\right]$$

$$\Delta h'_x(f_{x_c}) = \bar{\mu}'_x(v,f_{x_c})\,\Delta h_v - \frac{\bar{\mu}'_x(f_{n+1},f_{x_c})}{\bar{\mu}'_o(n+1,n+1)}\,\bar{\mu}'_o(v,n+1)\Delta h_v$$

$$+ \frac{\bar{\mu}'_x(f_{n+2},f_{x_c})}{\bar{\mu}'_o(n+2,n+2)}\left[\frac{\bar{\mu}'_o(n+1,n+2)}{\bar{\mu}'_o(n+1,n+1)}\,\bar{\mu}'_o(v,n+1)\Delta h_v - \bar{\mu}'_o(v,n+2)\Delta h_v\right]$$

$$+ \frac{F_c\,\bar{\mu}'_x(f_{p_c},f_{x_c})}{\bar{\mu}'_o(n+3,n+3)}\left[\frac{\bar{\mu}'_o(n+1,n+3)}{\bar{\mu}'_o(n+1,n+1)}\,\bar{\mu}'_o(v,n+1)\Delta h_v - \bar{\mu}'_o(v,n+3)\,\Delta h_v\right.$$

$$\left. - \frac{\bar{\mu}'_o(n+2,n+3)}{\bar{\mu}'_o(n+2,n+2)}\left\{\frac{\bar{\mu}'_o(n+1,n+2)}{\bar{\mu}'_o(n+1,n+1)}\,\bar{\mu}'_o(v,n+1) - \bar{\mu}'_o(v,n+2)\right\}\Delta h_v\right] \qquad (14)$$

Dividing equations (14) by Δh_v gives:

$$\bar{\mu}'_x(v,f_{x_a}) - F_a \frac{\bar{\mu}'_x(f_{p_a}, f_{x_a})}{\bar{\mu}'_o(n+1,n+1)} \bar{\mu}'_o(v,n+1) - \frac{\Delta h'_x(f_{x_a})}{\Delta h_v} = 0$$

$$\bar{\mu}'_x(v,f_{x_b}) - \frac{\bar{\mu}'_x(f_{n+1}, f_{x_b})}{\bar{\mu}'_o(n+1,n+1)} \bar{\mu}'_o(v,n+1)$$

$$+ \frac{F_b \bar{\mu}'_x(f_{p_b}, f_{x_b})}{\bar{\mu}'_o(n+2,n+2)} \left[\frac{\bar{\mu}'_o(n+1,n+2)}{\bar{\mu}'_o(n+1,n+1)} \bar{\mu}'_o(v,n+1) \right.$$

$$\left. - \bar{\mu}'_o(v,n+2) \right] - \frac{\Delta h'_x(f_{x_b})}{\Delta h_v} = 0 \qquad (15)$$

Thus one has a set of $k + 1$ equations in $k + 1$ variables. These can be represented by the vector function of a vector variable:

$$\bar{F}(\bar{x}) = \bar{0} \qquad (16)$$

where $\bar{x} = \begin{pmatrix} f_{p_{v_1}} \\ f_{p_{v_2}} \\ \vdots \\ f_{p_{v_k}} \\ \Delta h_v \end{pmatrix}$ and $\bar{F}(\bar{x}) = \begin{pmatrix} F_1(\bar{x}) \\ F_2(\bar{x}) \\ \vdots \\ F_{k+1}(\bar{x}) \end{pmatrix}$. Since these equations are non-linear, there is no simple way of finding a solution. One way of finding a solution is by means of a Newton-Raphson technique (Margenau and Murphy p. 493). This is an iterative process in which

$$\bar{x}_{n+1} = \bar{x}_n - (\bar{F}'(\bar{x}_n))^{-1} \bar{F}(\bar{x}_n) \qquad (17)$$

where $\overline{F}'(\overline{x}) = \begin{pmatrix} \frac{\partial F_1}{\partial f_{p_{v_1}}} & \frac{\partial F_1}{\partial f_{p_{v_2}}} & \cdots & \frac{\partial F_1}{\partial f_{p_{v_k}}} & \frac{\partial F_1}{\partial \Delta h_v} \\ \vdots & & & & \vdots \\ \frac{\partial F_{k+1}}{\partial f_{p_{v_1}}} & & \cdots & & \frac{\partial F_{k+1}}{\partial \Delta h_v} \end{pmatrix}$ (18)

For example, for the case of a one slab valley approximation using the extraordinary points a and b above the valley, equation (17) becomes

$$\overline{x}_i = \overline{x}_{i-1} - \frac{\begin{pmatrix} f_1(\overline{x}_{i-1}) \\ f_2(\overline{x}_{i-1}) \end{pmatrix}}{\begin{pmatrix} f_{11}(\overline{x}_{i-1}) & f_{12}(\overline{x}_{i-1}) \\ f_{21}(\overline{x}_{i-1}) & f_{22}(\overline{x}_{i-1}) \end{pmatrix}} \qquad (19)$$

where $f_1 = \overline{\mu}_x'(v, f_{x_a}) - F_a \frac{\overline{\mu}_x'(f_{p_a}, f_{x_a})}{\overline{\mu}_o'(n+1, n+1)} \overline{\mu}_o'(v, n+1) - \frac{\Delta h_x'(f_{x_a})}{\Delta h_v}$

$$f_2 = \overline{\mu}_x'(v, f_{x_b}) - F_b \frac{\overline{\mu}_x'(f_{p_b}, f_{x_b})}{\overline{\mu}_o'(n+2, n+2)} \overline{\mu}_o'(v, n+2) + A_1 \overline{\mu}_o'(v, n+1) - \frac{\Delta h_x'(f_{x_b})}{\Delta h_v}$$

$$f_{11} = \frac{\partial \overline{\mu}_x'(v, f_{x_a})}{\partial f_{p_v}} - F_a \frac{\overline{\mu}_x'(f_{p_a}, f_{x_a})}{\overline{\mu}_o'(n+1, n+1)} \frac{\partial \overline{\mu}_o'}{\partial f_{p_v}}(v, n+1)$$

$$f_{12} = \frac{\Delta h_x'(f_{x_a})}{(\Delta h_v)^2}$$

$$f_{21} = \frac{\partial \overline{\mu}_x'(v, f_{x_b})}{\partial f_{p_v}} - F_b \frac{\overline{\mu}_x'(f_{p_b}, f_{x_b})}{\overline{\mu}_o'(n+2, n+2)} \frac{\partial \overline{\mu}_o'}{\partial f_{p_v}}(v, n+2) + A_1 \frac{\partial \overline{\mu}_o'}{\partial f_{p_v}}(v, n+1)$$

$$f_{22} = \frac{\Delta h_x'(f_{x_b})}{(\Delta h_v)^2}$$

$$A_i = F_b \frac{\bar{\mu}'_x(f_{p_b}, f_{x_b})}{\bar{\mu}'_o(n+2, n+2)} \times \frac{\bar{\mu}'_o(n+1, n+2)}{\bar{\mu}'_o(n+1, n+1)} - \frac{\bar{\mu}'_x(n+1, f_{x_b})}{\bar{\mu}'_o(n+1, n+1)}$$

and $\bar{x}_i = \begin{pmatrix} f_{p_v} \\ \Delta h_v \end{pmatrix}$

APPENDIX 9

LISTING OF COMPUTER PROGRAM TO CONVERT IONOGRAMS

TO N(h) PROFILES USING TITHERIDGE'S METHOD

```
LIST
SEND TO(ED,ICLA-DEFAULT.TITH)
DUMPON(ED,PROGRAM TEST)
PROGRAM(TITH  ION  RED  P)
INPUT1=CR0
OUTPUT1=LP0
MAIN899
AUXILIARY(0,13200)
NO PAGING
CREATE AUX(1000)=ED(ICLA-DEFAULT)
OMIT COMMENTS
OVERLAY(1,2)C2,C3                          ! CALCULATES  TITH  COEF
OVERLAY(1,7)C30                            ! MAIN  READ  ROUTINE
OVERLAY(1,6)C4,C6,C7
OVERLAY(1,5)C8,C9,C10                      ! OUTPUT ROUTINES
OVERLAY(1,12)C29,C26,C24,C5,C16,C15,C22,C23
CHAPTER1
A->149
H->149
B->99
G->99
X->149
C->49
D->149
Z->7
E->15
INDEX STORES 5
CLOSE
CHAPTER30                                  ! MAIN  READ  ROUTINE
VARIABLES1
122)K=K
JUMP124,0'#999
ACROSS126/15
124)K=K
I=0(1)873
AI=0
REPEAT
K'=1
L'=0
M'=0
READ(N')
M=0(1)199
AM=0
REPEAT
M=0(1)65
%7(200M)A0,200
REPEAT
J=0
X=0
Y=0
W=0
K=1
READ(I)                                    ! METHOD OF INPUT
READ(M)
READ(N)
JUMP83,I=1
J=M-1
I=0(1)J
READ(A)
READ(B)
AI=1000000A
JUMP5,X>=AI
HI=B-Y
```

```
X=AI
Y=B
REPEAT
JUMP3,N=0
J=N-1
I=0(1)J
READ(A)
READ(GI)
BI=1000000A
JUMP7,W>=BI
W=BI
REPEAT
JUMP3
83)K=K
I=0
S=M+N
1)T=I+J
JUMP3,T=S
102)K=K
READ CH(I')
JUMP102,I'=%CODE(SP)
JUMP102,I'=%CODE(NL)
READ(A)
READ(B)
JUMP2,I'=%CODE(X)
JUMP60,I'#%CODE(O)
AI=1000000A          ! AI CONTAINS ORD FREQUENCIES FO,        I=0(1)M-1
JUMP5,X>=AI
HI=B-Y               ! HI CONTAINS DELTA H'(FO)
X=AI
Y=B
I=I+1
JUMP1,I#150
65)PRINT('TOO  MANY  ORDINARY  FREQUENCIES  READ  IN . LIMIT  IS  150')
PRINT('POINTS')
RUNOUT
HALT
2)BJ=1000000A        ! BJ CONTAINS EXT FREQUENCIES FX ,       J=0(1)5-1
JUMP7,W>=BJ
GJ=B                 ! GJ CONTAINS H'(FX)
W=BJ
J=J+1
JUMP1,J#100
66)PRINT('TOO  MANY  EXTRAORDINARY  FREQUENCIES  READ  IN . LIMIT  IS'
PRINT('  100  POINTS')
RUNOUT
HALT
3)K=K
READ(W)                                  ! GYROFREQUENCY
READ(P)                                  ! NO. OF CRITICAL FREQUENCIES
CO=P
I=1(1)P
READ(A)
CI=1000000A
C(P+I)=0
J=1(1)M
JUMP27,A(J-1)>=CI
REPEAT
27)C(2P+I)=J-1
JUMP28,N=0
J=1(1)N
A=B(J-1)
JUMP28,%SQRT(AA-WA)>=CI
```

```
REPEAT
28)T=3P+I
CT=J
REPEAT
CT=CT+1
J=T+P
%7(700)C0,J
READ(C)
C=£C/180
D=%SIN(C)
C=%COS(C)
I=0(1)3
READ(CI)
REPEAT
SPACE30
PRINT('N-H  PROFILE  FOR')
SPACE53
4)PRINT('TIME ')
PRINT(C0)2,2
READ DATA TITLE
SPACE15
PRINT('DATE  ')
PRINT(C1)2,0
PRINT(C2)1,0
PRINT(C3)4,0
I=0(1)7
READ(ZI)                                    ! GAUSS COEFFICIENTS
REPEAT
READ(E)
I=0(1)3
EI=0
REPEAT
%7(1000)H0,1
ACROSS91/2
7)NEWLINE2
PRINT('EXTRAORDINARY  FREQUENCY  ENCOUNTERED  WHICH  IS  LESS  THAN')
PRINT('OR  EQUAL  TO  THE  PREVIOUS  EXTRAORDINARY  FREQUENCY')
Q=999
JUMP10
5)NEWLINE2
PRINT('ORDINARY  FREQUENCY  ENCOUNTERED  WHICH  IS  LESS  THAN  OR')
PRINT('EQUAL  TO  THE  PREVIOUS  ORDINARY  FREQUENCY')
10)NEWLINE2
PRINT('TROUBLESOME  FREQUENCY  IS  THE  ')
PRINT(T)1,0
A=%FRPT(0.1T)
JUMP71,%FRPT(0.01T)-0.1A=1
JUMP11,A=0.1
JUMP12,A=0.2
JUMP13,A=0.3
71)PRINT('TH')
JUMP14
11)PRINT('ST')
JUMP14
12)PRINT('ND')
JUMP14
13)PRINT('RD')
14)PRINT('  FREQUENCY  WHOSE  VALUE  IS ')
JUMP8,Q=999
PRINT(0.000001AI)1,2
JUMP9
8)PRINT(0.000001BJ)1,2
9)PRINT('MHZ  .  THIS  STOP  IS  NOT  RECOVERABLE')
```

```
NEWLINE5
55)HALT
JUMP55
60)PRINT('LETTER  PRECEDING  A  FREQUENCY  IS  EITHER  MISSING  OR  '
PRINT('INCORRECT')
NEWLINE2
PRINT('THE  TROUBLESOME  VALUE  IS  THE')
PRINT(T)1,0
PRINT('TH')
PRINT('FREQUENCY  READ  IN')
RUNOUT
HALT
CLOSE
CHAPTER2                                    ! REAL HEIGHT CALCULATING ROUT
VARIABLES1
91)K=K
M=M-1
K=M
D0=0
X0=H0
I=1(1)K
      DI=0                                  ! CALCULATE
      O=I-1                                 !AND
      A=AI                                  ! STORE
      DOWN9/3                               ! TITHERIDGE
      JUMP5,I=1                             ! COEFFICIENTS
R=O-J
5)K=K
H=HI
JUMP33,I=1
R=I-R+1
J=I(-1)R.
H=H+C(J-2)X(J-1)
REPEAT
JUMP33,O'=0
JUMP33,I<=K'
JUMP36,I>K'+1
A=AI
JUMPDOWN26
H=H-ZX100
JUMP33
36)A=A(I-1)
JUMPDOWN26
X101=Z
A=AI
JUMPDOWN26
H=H+(X101-Z)X100
JUMP33
33)XI=H/CO                                  ! DELTA H - REAL HEIGHT
REPEAT
I=0(1)K
DI=XI
REPEAT
S=1
M=M+1
A=S
%7(954)A,1
L=1
JUMP25,O'=999
ACROSS110/7
25)O'=0
I=M-1
J=I(-1)K'
```

```
A(J+1)=AJ
H(J+1)=HJ
D(J+1)=DJ
X(J+1)=XJ
REPEAT
M=M+1
K=M-1
A(K'+1)=£'
H(K'+1)=999
D(K'+1)=X100
X(K'+1)=X100
%7(1001)D1,M
ACROSS33/9
26)Z=£'/A
G'=H
X=ZZ
X'=1-X
Y=W/A
Q'=999999
DOWN4/3
H=G'
Q'=0
RETURN
CLOSE
CHAPTER3                                    ! ORDINARY INTEGRALS
VARIABLES1
9)J=0(-1)0
G'=0
G=AJ
H=A(J+1)
2)Y=W/A
B=H/A
B=BB
F=G/A
F=FF
E'=%SQRT(1-B)
W'=%SQRT(1-F)
G=0.5E'
H=0.5W'
E'=G-H
W'=G+H
R=0(1)3
X'=E'ZR+W'
T)=51)
JUMP1
51)U'=Z
X'=-E'ZR+W'
T)=50)
JUMP1
50)G'=Z(R+4)U'+Z(R+4)Z+G'
REPEAT
U'=B-F
G'=G'/U'
JUMP29,E0=55
CJ=DJ+E'G'
DJ=-E'G'
R=0-J
JUMP21,R>=49
JUMP21,0.001>%MOD(CJ/DO)
REPEAT
21)C0=-C0
T=0
JUMP29
```

```
1)X'=X'X'
X=1-X'
4)K=K
Z=YY
F'=DD
H=XF'
G=CC
U=X'-Z+HZ
Y'=%SQRT(ZGG+4X'X'F')
G=H
H=YCC+Y'
H=X'-Z+2X'YG/H
Z'=X'H/U
H=%SQRT(Z')
F'=Z'H
V=X'H-F'+GF'
F'=4[X'F'+ZV-X'X'H]+2XZCCH
V=X+Z
U=XV-X
V=2V-4GZ
Y'=2-4X-4Z'-4XCCZ'
Z'=6XX'X'+8Z'U+VZ'Z'+ZY'
Z=H-Z'/F'
JUMP29,Q'=999999
H'=%SQRT(X')
Z=2ZH'
JUMP(T)
29)UP
CLOSE
CHAPTER4                                    ! EXTRAORDINARY INTEGRALS
VARIABLES1
11)W'=G+H
R=0(1)3
X'=E'ZR+W'
T)=12)
JUMP14
12)U'=Z
X'=-E'ZR+W'
T)=13)
JUMP14
13)G'=Z(R+4)U'+Z(R+4)Z+G'
REPEAT
U'=B-F
G'=G'/U'
UP
14)H'=X'
X'=X'X'
X=1-X'
JUMP10
4)X=ZZ
X'=1-X
22)H'=%SQRT(X')
10)Y=W/A
Z=YY
F'=DD
H=XF'
G=CC
U=X'-Z+HZ
Y'=%SQRT(ZGG+4X'X'F')
G=H
H=XYY'+XZ+HZ
H=GXZ-0.5H
Z'=X'+H/U
```

```
H=%SQRT(Z')
F'=Z'H
V=H-F'-XH+GF'
F'=F'-H+ZV-XF'-XXH
F'=4F'+8XH+2XZCCH
V=X+Z
U=XV-X
V=2V-4GZ
Y'=2-4X-4Z'-4XCCZ'
Z'=6XX'X'+8Z'U+VZ'Z'+ZY'
Z=H-Z'/F'
JUMP5,T#999
UP
5)Z=2ZH'
JUMP6,T#99
UP
6)JUMP(T)
CLOSE
CHAPTER5
VARIABLES1
9)J=0(-1)0
S=J-L
G'=0
G=AJ
2)Y=W/A
B=H/A
B=BB
F=G/A
F=FF
E'=%SQRT(1-B)
W'=%SQRT(1-F)
G=0.5E'
H=0.5W'
E'=G-H
W'=G+H
R=0(1)3
X'=E'ZR+W'
T)=51)
JUMP1
51)U'=Z
X'=-E'ZR+W'
T)=50)
JUMP1
50)G'=Z(R+4)U'+Z(R+4)Z+G'
REPEAT
U'=B-F
G'=G'/U'
JUMP29,Q'=55
AS=BS+E'G'
BS=-E'G'
R=0-J
JUMP21,R>=50
JUMP21,0.001>%MOD(AS/BO)
REPEAT
21)AO=-AO
T=0
29)UP
1)X'=X'X'
X=1-X'
4)V=CC
G=YV
G=DX'/G
F'=%SQRT(1+4GG)
```

```
H'=1+F'
V'=DD/V
G=2V'/H'
Y'=1+GX'
U=1+G
U=%SQRT(Y'/U)
H=1+X
H=H/F'-2/H'
F'=Y'Y'
Z=U+UXV'H/F'
JUMP29,Q'=999999
Z=2Z
JUMP(T)
CLOSE
CHAPTER6
VARIABLES1
96)K=K
%6(700+P+I)A,1
A=A+1
%7(700+P+I)A,1
98)K=K
%6(701+2P)B0,P
J=1(1)P
B(J-1)=B(J-1)+1
REPEAT
%7(701+2P)B0,P
M=M+1
UP
7)B=H/A
B=BB
F=G/A
F=FF
E'=%SQRT(1-B)
W'=%SQRT(1-F)
G=0.5E'
H=0.5W'
E'=G-H
DOWN11/4
Z=-E'G'
UP
18)Z=E2/A
A'=0
ACROSS54/5
CLOSE
CHAPTER7
VARIABLES1
110)JUMP20,N#0
K=M-1
%7(1001)D1,M
ACROSS5/9
20)B=B(L-1)                          ! IF N#0, LOOK FOR EXT HTS
B=%SQRT(BB-BW)
I=M-1
J=0(1)I
JUMP29,AJ>=B
REPEAT
122)K=M-1                           ! EXTRAORDINARY  >  ORDINARY
L=N
JUMP13
29)A=B-A(J-1)
JUMP30,A>1000
J=J-1
30)K=J
```

```
13)I=0
111)F=HI
JUMP113,K'=1
%7(1000+I)F,1
DI=HI
JUMP112,HI#999
I=I+1
JUMP111
112)I=I+1
JUMP101
113)P=K-1
I=1(1)P
F=F+DI
REPEAT
JUMP35
101)K=K
JUMP34,I#1
1)I=1(1)149
34)H=HI
JUMP90,H>996
JUMP90,Z>996
JUMP33,I=1
%6(1400+50I)C0,50
R=I-%INTPT(C0)+1
P=1
J=I(-1)R
H=H+CPD(J-1)
P=P+1
REPEAT
31)R=%INTPT(CP)
JUMP33,R=0
JUMP33,P>=50
T=%INTPT(C(P+1))
R=T-R+1
P=P+2
J=T(-1)R
JUMP33,0>J
H=H+CPDJ
P=P+1
REPEAT
JUMP33,P=50
JUMP31
33)%6(1249+I)A,1
DI=H/A
JUMP91
90)%6(1000+I)DI,1
91)T=I
Z=H
JUMP35,K=T
F=F+DI
REPEAT
35)K=K
T=M-1
JUMP36,K#T
JUMP36,N>=L
ACROSS1/9                                   ! IF  LAST  POINT,
36)Z=[BB-A(K-1)A(K-1)]/[AKAK-A(K-1)A(K-1)]
F=F+ZDK                                     ! REAL HT OF EXT POI
H'=0
I=0
T=99
V'=F
A=B(L-1)
```

```
75)K=K
A'=DK
J=K(-1)1
G'=0
G=A(J-1)
H=AJ
B'=D(J-1)
JUMP2,J#K
H=B
A'=ZA'
2)K=K
JUMP79,H(J-1)=999                          ! IF POINT WITHIN VALLEY, GO T
DOWN7/6                                    ! CALCULATE RETARDATION IN J'TH
Z=(Z-1)A'                                  ! Z = (INTEG MU' - 1 )(DELTA H
JUMP102
79)Z=A(J-1)/A                              ! POINT IN VALLEY
T=999
DOWN4/4                                    ! CALCULATE RETARDATION
Z=(Z-1)B'
B'=A'
A(J-1)=AJ
102)K=K
JUMP17,Z>=0.005
H'=AJ
17)V'=V'+Z
A'=B'
18)REPEAT
F=G(L-1)
X(L-1)=V'                                  ! STORE CALCULATED VIRTUAL HT
JUMP7,K'=1
9)F=F-V'?
F'=%MOD(F)
JUMP14,E3=199
JUMP14,F'>E
7)L=L+1
A'=E3
JUMP80,L>N
JUMP20
80)K=M-1
JUMP13
14)%6(700)A20,1
CLOSE
CHAPTER15
VARIABLES1
1)K=K
PRINT('IF  AN  ERROR  OCCURS  IN  CALCULATING  THE  VALLEY,  TYPE  GO')
PRINT('  20  AND  THE  PROGRAM  WILL  AUTOMATICALLY  RECOVER')
NEWLINE10
SPACE40
PRINT('ESTIMATES  OF  VALLEY  PARAMETERS')
NEWLINE
SPACE40
PRINT('--------------------------------')
NEWLINE2
SPACE30
PRINT('PLASMA  FREQUENCY  FV')
SPACE15
PRINT('VALLEY  WIDTH  DELTA H')
NEWLINE2
%6(950)A,1
K'=A
X130=0
X131=0
```

```
X132=0
0'=999
L'=1(1)4
M'=L'+1
N'=0
!          TEST  TO  CHECK  WHETHER  SUFFICIENT  EXTRAORDINARY
P=2
£'=0.95AK'
Q=P-1
N=P
X100=0.5(GL-XL)
107)I=1(1)M'
C(I+10)=0
CI=0
A=B(I+L-1)
G=A(I+K'-1)
H=%SQRT(AA-AW)
C37=G
C38=H
PRESERVE INDICES(Q,5)
G'=0
DOWN7/26
RESTORE INDICES(Q,5)
G=C37
H=C38
A=A(I+K')
F=Z[H-G]/[A-G]
H=A
C37=F
PRESERVE INDICES(Q,5)
G'=0
Q'=55
DOWN2/5
Z=-E'G'
RESTORE INDICES(Q,5)
F=C37
X(I+100)=F/Z
A=B(I+L-1)
Z=£'/A
T=999
DOWN4/24
C(I+10)=C(I+10)+Z
G=£'
DOWN10/22
T=IP-I-P+111
XT=Z
A=A(I+K')
Z=£'/A
X=ZZ
X'=1-X
Y=W/A
Q'=999999
DOWN4/5
C40=Z/%SQRT(X')
DOWN4/23
Z=C40
Q'=0
CI=CI+Z
G=£'
Q'=3333
DOWN10/22
T=IP-I-P+121
XT=Z
```

```
T=T-10
XT=XT-X(I+100)Z
Q'=0
C(I+10)=C(I+10)-CIX(I+100)
REPEAT
R=I
111)K=K
ACROSS111/16
126)REPEAT
ACROSS1/17
CLOSE
CHAPTER16
VARIABLES1
111)K=K
PRESERVEINDICES(I,3)
PRESERVE INDICES(M,4)
PRESERVE INDICES(Q,5)
J'=L
DOWN1/29
RESTORE INDICES(I,3)
RESTORE INDICES(M,4)
RESTORE INDICES(Q,5)
R=R-1
K=1(1)R
C(R+11)=C(R+11)+C(K+40)CK
REPEAT
T=N-1
I=1(1)T
J=109+NR-R+I
K=1(1)R
XJ=XJ+C(K+40)X(120+NK-K+I-N)
REPEAT
REPEAT
R=R+1
JUMP112,R#N'
R=M'
JUMP111
112)JUMP113,R#M'
R=L'
JUMP111,R>=2
113)K=K
I=L'
K=1
72)K=K
J=P-1
%7(1500+PK-P)X(110+JI-J),J
Y=G(I+L-1)-X(I+L-1)
X=Y/[X100X100]
%7(1500+PK-1)X,1
C(K+10)=C(I+10)-Y/X100
K=K+1
JUMP73,I#L'
I=M'
JUMP72
73)JUMP74,I#M'
I=N'
JUMP72,I#0
74)K=K
%7(1756)C11,P
1756=%28(1500,P,1)
%6(1756)X144,P
X=£'-X144
JUMP31,X<A(K'+1)-1000
```

```
X=A(K'+1)-1000
31)£'=X
X100=X100-X145
R=P
N=P
JUMP2,%MOD(X145)<0.00001
ACROSS107/15
2)K=K
PRINT('POINTS')
PRINT(L')1,0
PRINT('AND')
PRINT(M')1,0
SPACE18
PRINT(0.000001£')2,3
SPACE30
PRINT(X100)2,2
NEWLINE2
X130=X130+£'
X131=X131+X100
X132=X132+1
ACROSS126/15
CLOSE
CHAPTER17
VARIABLES1
1)K=K
NEWLINE3
SPACE37
PRINT('-----')
SPACE33
PRINT('-----')
NEWLINE
JUMP20,X132=0
£'=X130/X132
X100=X131/X132
PRINT('AVERAGE  VALUES :')
SPACE18
PRINT(0.000001£')2,3
SPACE30
PRINT(X100)2,2
NEWLINE2
PRINT('USING  THESE  AVERAGE  ESTIMATES  FOR  THE  VALLEY,  THE  ')
PRINT('PROFILE  WITH  VALLEY  BECOMES :')
NEWLINE
RUNOUT
%7(1001+K')X100,1
HALT
ACROSS91/2
20)PRINT('NO  VALLEY  ESTIMATES  ARE  POSSIBLE  BECAUSE  SCALING  '
PRINT('ERRORS  ARE  TOO  LARGE')
END
CLOSE
CHAPTER29
VARIABLES1
35)K=K
C37=F
PRESERVE INDICES(1,0)
PRESERVE INDICES(Q,2)
A=A(L+K')
G=A(I+K'-1)
H=A(I+K')
G'=0
Q'=55
DOWN2/5
```

```
Z=-E'G'
RESTORE INDICES(I,0)
RESTORE INDICES(Q,2)
F=C37
RETURN
1)K=K
B=0
R=R-1
J=1(1)R
C(J+40)=0
K=1(1)J
JUMP51
2)I=K+R-J
L=R+1
JUMPDOWN35
F=Z
F=FX(R+101)
I=K+R-J
L=R+1
C37=F
PRESERVE INDICES(I,0)
PRESERVE INDICES(Q,2)
A=B(L+J'-1)
G=A(I+K'-1)
H=A(I+K')
G'=0
DOWN7/26
F=C37
RESTORE INDICES(I,0)
RESTORE INDICES(Q,2)
F=F-Z
I=K+R-J
L=I
JUMPDOWN35
F=F/Z
I=K
L=K
JUMPDOWN35
F=F/Z
C(K+40)=C(K+40)-FE
REPEAT
REPEAT
R=R+1
UP
51)JUMP71,J#R
I=K
L=K
JUMPDOWN35
E=-Z
JUMP2
71)S=R-J
I=K
L=K+S
JUMPDOWN35
E=Z
JUMP2,S=1
Q=S-1
P=1(1)Q
I=K
L=K+P
JUMPDOWN35
F=Z
I=K+P
```

```
L=I
JUMPDOWN35
F=F/Z
I=K+P
L=K+S
JUMPDOWN35
E=E-FZ
REPEAT
JUMP2,S=2
P=2(1)Q
O=P(1)Q
I=K
L=K+P-1
JUMPDOWN35
F=Z
I=K+P-1
L=I
JUMPDOWN35
F=F/Z
 I=K+P-1
L=K+O
JUMPDOWN35
F=FZ
I=K+O
L=I
JUMPDOWN35
F=F/Z
I=K+O
L=K+S
JUMPDOWN35
E=E+FZ
REPEAT
REPEAT
JUMP2,S=3
T=Q-1
P=2(1)T
O=P(1)T
M=O(1)Q
I=K
L=K+P-1
JUMPDOWN35
F=Z
I=K+P-1
L=I
JUMPDOWN35
F=F/Z
I=K+P-1
L=K+O
JUMPDOWN35
F=FZ
I=K+O
L=I
JUMPDOWN35
F=F/Z
I=K+O
L=K+M
JUMPDOWN35
F=FZ
I=K+M
L=I
JUMPDOWN35
F=F/Z
I=K+M
```

```
L=K+S
JUMPDOWN35
E=E-FZ
REPEAT
REPEAT
REPEAT
JUMP2,S=4
I=K
L=K+1
JUMPDOWN35
F=Z
I=K+1
L=I
JUMPDOWN35
F=F/Z
I=K+1
L=K+2
JUMPDOWN35
F=FZ
I=K+2
L=I
JUMPDOWN35
F=F/Z
I=K+2
L=K+3
JUMPDOWN35
F=FZ
I=K+3
L=I
JUMPDOWN35
F=F/Z
I=K+3
L=K+4
JUMPDOWN35
F=FZ
I=K+4
L=I
JUMPDOWN35
F=F/Z
I=K+4
L=K+5
JUMPDOWN35
E=E+FZ
JUMP2
CLOSE
CHAPTER26
VARIABLES1
7)B=H/A
B=BB
F=G/A
F=FF
E'=%SQRT(1-B)
W'=%SQRT(1-F)
G=0.5E'
H=0.5W'
E'=G-H
DOWN11/24
Z=-E'G'
UP
CLOSE
CHAPTER22
VARIABLES1
10)V=YY
```

```
V'=DD
Z'=XV'
U=X'-V+Z'V
G=2X/G
Y'=1-3X
Y'=2Y'X'-2Y'VCC+VVCC
Y'=2GY'
H'=1-4X
H'=-VVCC+2VCC-2XV-6XVCC+6XXV-4XXZ'V-2X'X'H'
H'=2GH'
Y'=Y'HH+H'
H'=-2X'X'+2VX'+XCCV
F'=H'+2UHH
F'=2HF'
Z'=4X'-2V+VCC
Z'=Z'G
V'=-1+VV'
V'=V'G
G'=1-2X
G'=4X'G'DD+VCCCC
G'=XVGG'
V=X'X'X'-VX'
V=%SQRT(H'H'-4UV)
JUMP1,Q'#3333
V=-V
1)V=0.5Z'+V'HH+0.5G'/V
V=-0.5V/(UH)
V'=UHH(8V'H+12UV)+2[V'H'H+U(Z'H+H'V)]
Z=Z-H
Y'=Y'-ZV'
Z=X+YY-2XYYDD
V'=2X'X+YYX'-XYY+XYYCC
Z=2H'Z+4UV'
Z=2ZVH+Y'
Z=Z/(F'U)+V
UP
CLOSE
CHAPTER23
VARIABLES1
29)UP
4)K=K
Z=YY
F'=DD
H=XF'
G=CC
U=X'-Z+HZ
Y'=%SQRT(ZGG+4X'X'F')
G=H
H=YCC+Y'
H=X'-Z+2X'YG/H
Z'=X'H/U
H=%SQRT(Z')
F'=Z'H
V=X'H-F'+GF'
F'=4[X'F'+ZV-X'X'H]+2XZCCH
V=X+Z
U=XV-X
V=2V-4GZ
Y'=2-4X-4Z'-4XCCZ'
Z'=6XX'X'+8Z'U+VZ'Z'+ZY'
Z=H-Z'/F'
JUMP29,Q'=999999
H'=%SQRT(X')
```

```
Z=2ZH'
JUMP(T)
CLOSE
CHAPTER24
VARIABLES1
11)W'=G+H
R=0(1)3
X'=E'ZR+W'
T)=12)
JUMP14
12)U'=Z
X'=-E'ZR+W'
T)=13)
JUMP14
13)G'=Z(R+4)U'+Z(R+4)Z+G'
REPEAT
U'=B-F
G'=G'/U'
UP
14)H'=X'
X'=X'X'
X=1-X'
JUMP10
4)X=ZZ
X'=1-X
22)H'=%SQRT(X')
10)Y=W/A
Z=YY
F'=DD
H=XF'
G=CC
U=X'-Z+HZ
Y'=%SQRT(ZGG+4X'X'F')
G=H
H=XYY'+XZ+HZ
H=GXZ-0.5H
Z'=X'+H/U
H=%SQRT(Z')
F'=Z'H
V=X'H-F'+GF'
F'=4[X'F'+ZV-X'X'H]+2XZCCH
V=X+Z
U=XV-X
V=2V-4GZ
Y'=2-4X-4Z'-4XCCZ'
Z'=6XX'X'+8Z'U+VZ'Z'+ZY'
Z=H-Z'/F'
JUMP5,T#999
UP
5)Z=2ZH'
JUMP6,T#99
UP
6)JUMP(T)
CLOSE
CHAPTER8                                  ! MAIN  PRINT-OUT  ROUTINE
VARIABLES1
2)SPACE15
PRINT('I')
SPACE12
PRINT('I')
SPACE13
PRINT('I')
SPACE21
```

```
PRINT('I')
SPACE19
PRINT('I')
SPACE19
PRINT('I')
NEWLINE
SPACE15
PRINT('I    ')
JUMP4,Q#4321
SPACE6
JUMP5
4)PRINT(Q)3,0
5)PRINT('    I    ')
PRINT(0.000001A)2,2
PRINT('  I      ')
PRINT(0.0000000124AA)8,0
PRINT('      I       ')
JUMP9,Q#4321
SPACE8
JUMP10
9)PRINT(H')3,1
10)PRINT('      I       ')
PRINT(H)3,1
PRINT('      I')
NEWLINE
R=R+2
JUMP7,62>=R
SPACE15
P=0(1)14
PRINT('------')
REPEAT
NEWLINE(68-R)
R=2
DOWN8/8
7)UP
1)NEWLINE2
R=3
8)SPACE15
P=0(1)2
PRINT('-------------------------------')
REPEAT
NEWLINE
SPACE15
PRINT('I  ORDINARY  I  FREQUENCY  I  ELECTRON  DENSITY  I  VIRTUAL
PRINT('HEIGHT  I    REAL  HEIGHT   I')
NEWLINE
SPACE15
PRINT('I    POINT   I   IN  MHZ   I      IN  ELS/CC     I')
SPACE7
PRINT('IN  KM       I')
SPACE7
PRINT('IN  KM       I')
NEWLINE
SPACE15
P=0(1)14
PRINT('------')
REPEAT
NEWLINE
R=R+4
UP
CLOSE
CHAPTER9                                  ! MAIN  PRINT-OUT  ROUTINE
VARIABLES1
```

```
33)SPACE50
PRINT('TABLE  3')
NEWLINE
SPACE50
PRINT('--------')
NEWLINE
SPACE39
PRINT('THE  CORRECTED  N-H  PROFILE')
NEWLINE
R=5
JUMP59
1)K=K
%7(1001)D1,M                              ! STORE REMAINING REAL HEIGHTS
JUMP6,K'=1
JUMP7,M'=1
%7(12300)X0,L                             ! STORE CALCULATED EXT VIRTUAL
JUMP4
7)%7(12200)X0,L
JUMP4
6)%7(12400)X0,L
4)K=K
R=2
NEWLINE5
SPACE27
PRINT('ACCORDING  TO  THE  ERROR  TOLERANCE  WHICH  YOU  HAVE  SPECIF'
PRINT('IED,')
NEWLINE2
SPACE54
PRINT('E=')
PRINT(E)1,1
PRINT('KM')
NEWLINE2
J=0
R=0
I=0(1)2
JUMP50,%MOD(XI-GI)>E      ! IF MOD( CALCULATED EXT VIRT HT - OBSERVED )
REPEAT
52)%6(700)X,1
I=X
P=I-2
JUMP53,P<=0
%6(702+3I)C0,P
%6(702+2I)C10,P
I=1(1)P
T=C(I-1)-1
S=C(I+9)-1
R=0(1)2
JUMP51,%MOD(X(T+R)-G(T+R))>E
REPEAT
REPEAT
JUMP53
50)J=999
JUMP52
51)R=999
53)SPACE34
PRINT('THERE  IS:  (1)  ')
JUMP55,J=999
PRINT('NO  ')
55)PRINT('LOW-LYING  IONIZATION  PRESENT')
NEWLINE2
SPACE40
PRINT('AND  (2)  ')
JUMP56,R=999
```

```
PRINT('NO  ')
JUMP57
56)PRINT('AT  LEAST  ONE  ')
57)PRINT('VALLEY  PRESENT')
I'=0
NEWLINE10
JUMP77,R#999
PRINT('VALLEY  CORRECTIONS  WILL  BE  MADE  BY  INSERTING  A  BLOCK'
PRINT('  OF  IONIZATION  BETWEEN  EXTRAORDINARY  FREQUENCY')
NEWLINE
PRINT(0.000001B(T-1))1,2
PRINT('MHZ  AND  FREQUENCY')
PRINT(0.000001BT)2,2
PRINT('MHZ')
A=T
%7(998)A,1
I'=999
A=S
%7(950)A,1
77)K=K
RUNOUT
58)SPACE50
PRINT('TABLE  1')
NEWLINE
SPACE50
PRINT('--------')
PRINTLINE
THE  FOLLOWING  TABLE  COMPARES  THE  CALCULATED  EXTRAORDINARY  VIR
PRINT('  HEIGHTS  WITH  THE  OBSERVED  VALUES')
NEWLINE2
!  THIS  SECTION  PRINTS  OUT  THE  FIRST  TABLE  -  THE  DIFFERENCE
SPACE22
J=0(1)14
PRINT('-----')
REPEAT
NEWLINE
SPACE22
PRINT('I          I                    I                    I')
SPACE20
PRINT('I')
NEWLINE
SPACE22
PRINT('I  POINT   I     CALCULATED     I      OBSERVED      I')
SPACE20
PRINT('I')
NEWLINE
SPACE22
PRINT('I  NUMBER  I  EXT  VIRTUAL  HT  I  EXT  VIRTUAL  HT  I     D');
PRINT('IFFERENCE     I')
NEWLINE
SPACE22
PRINT('I          I                    I                    I')
SPACE20
PRINT('I')
NEWLINE
SPACE22
J=0(1)24
PRINT('---')
REPEAT
NEWLINE
R=10
N=N-1
I=0(1)N
```

```
SPACE22
PRINT('I   ')
PRINT(I)3,0
PRINT('  I       ')
PRINT(XI)3,3
PRINT('     I       ')
PRINT(GI)3,3
PRINT('     1       ')
A=XI-GI
PRINT(A)3,3
PRINT('     1')
9)NEWLINE
R=R+1
JUMP8,R#64
SPACE22
PRINT('-----------------------------------------------------------------'
PRINT('---------------')
NEWLINE4
R=3
SPACE22
PRINT('-----------------------------------------------------------------'
PRINT('---------------')
NEWLINE
8)REPEAT
SPACE22
J=0(1)14
PRINT('-----')
REPEAT
RUNOUT
5)SPACE50
PRINT('TABLE  2')
NEWLINE
SPACE50
PRINT('--------')
NEWLINE
SPACE39
PRINT('THE  UNCORRECTED  N-H  PROFILE')
NEWLINE
R=5
59)K=K
20)DOWN8/8
T=0
I=0
S=1
O=0
H'=0
H=0
%6(700)U,1
P=%INTPT(U)
J=2P
%6(701)C1,J
J=P+S
J=%INTPT(CJ)
J=J-1
13)JUMP3,T>J
I=T(1)J
Q=4321
A=AI
X=HI
%6(1000+I)Y,1
H=H+Y
DOWN2/8
REPEAT
```

```
I=I+1
3)Q=0
S=S+1
10)A=AI
JUMP12,I>K
X=HI
JUMP67,X=999
%6(1000+I)Y,1
Q=Q+1
I=I+1
H'=H'+X
H=H+Y
DOWN2/8
JUMP10
67)O=Q
P=%INTPT(U)
J=P+S
J=%INTPT(CJ)
T=I
J=I+J
JUMP13
12)SPACE15
I=0(1)14
PRINT('------')
REPEAT
NEWLINE(66-R)
60)HALT
JUMP75,I'#999
%6(998)A,1
L=%INTPT(A)
ACROSS1/15
75)K=K
ACROSS20/7
CLOSE
CHAPTER10
VARIABLES1
14)NEWLINE5
SPACE26
PRINT('INSUFFICIENT  DATA  OR  DATA  INSUFFICIENTLY  ACCURATE  TO  '
PRINT('CONTINUE')
NEWLINE3
SPACE18
PRINT('ANALYSIS  THUS  FAR  .....')
NEWLINE2
R=11
Z'=999
ACROSS20/9
2)NEWLINE2
SPACE10
PRINT(L)3,0
A=%FRPT(0.1L)
JUMP71,%FRPT(0.01L)-0.1A=1
JUMP11,A=0.1
JUMP12,A=0.2
JUMP13,A=0.3
71)PRINT('TH')
JUMP10
11)PRINT('ST')
JUMP10
12)PRINT('ND')
JUMP10
13)PRINT('RD')
10)PRINT('  EXTRAORDINARY  POINT    F=')
```

```
%6(499+L)X,1
%6(749+L)Y,1
PRINT(0.000001X)2,2
PRINT('MHZ       H=')
PRINT(Y)3,0
PRINT('KM    CAUSING  DIFFICULTY')
R=R+4
NEWLINE2
JUMP15,65>R
NEWLINE(68-R)
R=2
15)PRINT('IF  YOU  TYPE  "GO"  ON  THE  CONSOLE  TYPEWRITER  I  WILL'
PRINT('  REPEAT  THE  ANALYSIS  WITHOUT  THIS  POINT')
NEWLINE(67-R)
58)HALT
Z'=0
L=L+1
JUMP100,L>N
ACROSS20/7
100)K=M-1
ACROSS13/7
1)K=K
A34=0
Q=0(1)7
G'=0
H=A18-QA5
G=H-A5
DOWN7/6
A34=A34+Z
Z=Z?
JUMP17,A46#39
%6(1402+50K+Q)A47,1
JUMP18
17)JUMP16,A46#19
%6(K-1)A,1
G'=0
H=A18-QA5
G=H-A5
A6=55
DOWN2/3
A47=-E'G'
%6(K)A,1
G'=0
H=A18-QA5
G=H-A5
DOWN2/3
A47=A47+E'G'
A=A7
18)A34=A34+A45A47
PRINT(A47)0,8
A34=A34?
16)A6=0
REPEAT
Z=0.125A34
A46=0
CLOSE
CHAPTER0
VARIABLES1
ACROSS122/30
CLOSE
****
```

APPENDIX 10

THE TRANSPORT TERM OF THE CONTINUITY EQUATION

APPENDIX 10

THE TRANSPORT TERM OF THE CONTINUITY EQUATION

From Dougherty[35], the equation of motion of the neutral air is:

$$\frac{d\overline{U}}{dt} = -\frac{1}{\rho}\nabla p + \overline{g} + \zeta\nabla^2\overline{U} + \frac{Nm_i\nu_i}{N_n m_n}(\overline{u}_i - \overline{U}) \qquad (1)$$

where $\overline{U} = (U,V,W)$ = velocity of neutral air,

$\overline{u}_i = (u_i, v_i, w_i)$ = velocity of ions,

$\overline{g} = -(0,0,g)$ = acceleration due to gravity,

p = pressure,

m_n = average particle mass of neutral air,

N_n = no. density of neutral particles,

m_i = ion mass,

N = ion density = electron density,

$\rho = N_n m_n$ = mass density,

ζ = kinematic viscosity,

and ν_i = collision frequency of ions with neutral molecules.

(Axes are chosen such that U is the component of the wind velocity in the N - S direction — South positive — V is the component in the E-W direction — East positive — and W the component in the vertical direction — upwards is positive.)

The momentum equations for ions and electrons (without acceleration terms) are:

$$m_i\nu_i(\overline{u}_i - \overline{U}) + m_e\nu_{ei}(\overline{u}_i - \overline{u}_e) = e(\overline{E} + \overline{u}_i \times \overline{B}) - \frac{k}{N}\nabla(T_i N) + m_i\overline{g} \qquad (2)$$

$$m_e\nu_e(\overline{u}_e - \overline{U}) + m_e\nu_{ei}(\overline{u}_e - \overline{u}_i) = -e(\overline{E} + \overline{u}_e \times \overline{B}) - \frac{k}{N}\nabla(T_e N) + m_e\overline{g} \qquad (3)$$

where $\overline{u}_e = (u_e, v_e, w_e)$ = velocity of electrons,

ν_e = collision frequency of electrons with neutral molecules,

ν_{ei} = collision frequency of electrons with ions,

$\overline{E} = (E_x, E_y, E_z)$ = electric field strength,

$\overline{B} = (-B\cos I, 0, -B\sin I)$ = magnetic field,

I = inclination of Earth's magnetic field,

and k = Boltzmann's constant.

Acceleration terms can justifiably be omitted (Dougherty[35], Stubbe[144]) as can terms which take account of the friction between ions and electrons and between electrons and neutral particles. The gravitational term in equation (3) can be omitted on account of the low electron mass. Thus one obtains:

$$m_i \nu_i (\overline{u}_i - \overline{U}) = e(\overline{E} + \overline{u}_i \times \overline{B}) - \frac{k}{N}\nabla(T_i N) + m_i \overline{g} \qquad (4)$$

$$0 = -e(\overline{E} + \overline{u}_e \times \overline{B}) - \frac{k}{N}\nabla(T_e N) \qquad (5)$$

Taking components of equations (4) and (5), we get

$$\left.\begin{aligned}
m_i \nu_i (u_i - U) &= e(E_x - v_i B\sin I) - \frac{k}{N}\frac{\partial (T_i N)}{\partial x} \\
m_i \nu_i (v_i - V) &= e(E_y + u_i B\sin I - w_i B\cos I) - \frac{k}{N}\frac{\partial (T_i N)}{\partial y} \\
m_i \nu_i (w_i - W) &= e(E_z + v_i B\cos I) - \frac{k}{N}\frac{\partial (T_i N)}{\partial z} - m_i g \\
0 &= -e(E_x - v_e B\sin I) - \frac{k}{N}\frac{\partial (T_e N)}{\partial x} \\
0 &= -e(E_y + u_e B\sin I - w_e B\cos I) - \frac{k}{N}\frac{\partial (T_e N)}{\partial y} \\
0 &= -e(E_z + v_e B\cos I) - \frac{k}{N}\frac{\partial (T_e N)}{\partial z}
\end{aligned}\right\} \qquad (6)$$

Assume that no charge separation occurs, i.e. that the vertical velocity of the ions equals the vertical velocity of the electrons. Then

$$w_i = w_e = w \qquad (7)$$

Assuming that the horizontal components of $\nabla(T_i N)$ and $\nabla(T_e N)$ are small compared with other terms in the corresponding equations, and writing h in place of z (vertical height) to conform with the notation used throughout this thesis, equations (6) become

$$m_i\nu_i(u_i - U) = e(E_x - v_i B\sin I) \quad (8)$$

$$m_i\nu_i(v_i - V) = e(E_y + u_i B\sin I - wB\cos I) \quad (9)$$

$$m_i\nu_i(w - W) = e(E_z + v_i B\cos I) - \frac{k}{N}\frac{\partial(T_i N)}{\partial h} - m_i g \quad (10)$$

$$0 = e(E_x - v_e B\sin I) \quad (11)$$

$$0 = e(E_y + u_e B\sin I - wB\cos I) \quad (12)$$

$$0 = e(E_z + v_e B\cos I) + \frac{k}{N}\frac{\partial(T_e N)}{\partial h} \quad (13)$$

Subtracting equation (13) from equation (10), one obtains

$$m_i\nu_i(w - W) = e(v_i B\cos I - v_e B\cos I) - \frac{k}{N}\frac{\partial(T_i N)}{\partial h} - \frac{k}{N}\frac{\partial(T_e N)}{\partial h} - m_i g \quad (14)$$

For the sake of simplicity, it is convenient to define

$$eE_p = \frac{k}{N}\frac{\partial(T_i N)}{\partial h} + \frac{k}{N}\frac{\partial(T_e N)}{\partial h} + m_i g \quad (15)$$

Equation (14) then becomes

$$m_i\nu_i(w - W) = e(v_i - v_e)B\cos I - eE_p \quad (16)$$

Equation (11) is subtracted from equation (8) to give

$$m_i\nu_i(u_i - U) = e(v_e B\sin I - v_i B\sin I) \quad (17)$$

Equation (17)$\times\cos I$ + equation (16)$\times\sin I$ gives

$$m_i\nu_i\sin I(w - W) + m_i\nu_i\cos I(u_i - U) = -eE_p\sin I$$

$$u_i - U = -(w-W)\tan I - \frac{e}{m_i\nu_i}E_p\tan I \quad (18)$$

To eliminate w, multiply equation (18) by $\cos^2 I$ and subtract equation (9)$\times\frac{\sin I}{Be}$:

$$(u_i - U)\cos^2 I + u_i\sin^2 I = W\cos I\sin I + \frac{m_i\nu_i(v_i - V)}{Be}\sin I - \frac{E_y}{B}\sin I - \frac{e}{m_i\nu_i}E_p\cos I\sin I$$

$$u_i = U\cos^2 I + W\cos I\sin I + \frac{m_i\nu_i}{Be}(v_i - V)\sin I - \frac{E_y}{B}\sin I - \frac{e}{m_i\nu_i}E_p\cos I\sin I \quad (19)$$

To eliminate v_i from this equation, add $\frac{m_i \nu_i}{B^2 e^2} \times$ equation (8) to equation (19) :

$$u_i\left(1 + \frac{m_i^2 \nu_i^2}{B^2 e^2}\right) = U\left(\cos^2 I + \frac{m_i^2 \nu_i^2}{B^2 e^2}\right) + W\cos I \sin I - \frac{m_i \nu_i}{Be} V \sin I + \frac{m_i \nu_i}{Be} \frac{E_x}{B} - \frac{E_y}{B} \sin I - \frac{e}{m_i \nu_i} E_p \cos I \sin I$$

Substituting $\omega_i = \frac{Be}{m_i}$ = ion gyrofrequency

and $\alpha = 1 + \frac{\nu_i^2}{\omega_i^2}$, yields

$$\alpha u_i = U\left(\cos^2 I + \frac{\nu_i^2}{\omega_i^2}\right) + W\cos I \sin I - \frac{\nu_i}{\omega_i} V \sin I + \frac{\nu_i}{\omega_i} \frac{E_x}{B} - \frac{E_y}{B} \sin I - \frac{e}{m_i \nu_i} E_p \cos I \sin I \qquad (20)$$

To solve for u_e, consider equation (12) :

$$u_e \sin I = w\cos I - \frac{E_y}{B}$$

w can be eliminated from this equation by adding $\frac{\cos I}{m_i \nu_i} \times$ equation (16) ,

$$u_e \sin I = W\cos I + \frac{eB\cos^2 I}{m_i \nu_i} (v_i - v_e) - \frac{e}{m_i \nu_i} E_p \cos I - \frac{E_y}{B}$$

Multiply this by $\frac{\nu_i^2}{\omega_i^2}$ and divide by sinI

$$\frac{\nu_i^2}{\omega_i^2} u_e = \frac{\nu_i^2}{\omega_i^2} W\cot I + \frac{\nu_i}{\omega_i} \frac{\cos^2 I}{\sin I} (v_i - v_e) - \frac{\nu_i^2}{\omega_i^2} \frac{e}{m_i \nu_i} E_p \cot I - \frac{\nu_i^2}{\omega_i^2} \frac{E_y}{B \sin I} \qquad (21)$$

Subtracting equation (12) from equation (9) gives

$$m_i \nu_i (v_i - V) = eB \sin I (u_i - u_e) \qquad (22)$$

$$\therefore u_i - u_e = \frac{\nu_i}{\omega_i} (v_i - V)\sin I + \frac{\nu_i}{\omega_i} (v_i - V)\cos I \cot I \qquad (23)$$

If equation (23) is subtracted from equation (21), one obtains

$$u_e\left(1 + \frac{\nu_i^2}{\omega_i^2}\right) - u_i = \frac{\nu_i^2}{\omega_i^2} W\cot I - \frac{\nu_i}{\omega_i} (v_i - V)\sin I + \frac{\nu_i}{\omega_i} \frac{\cos^2 I}{\sin I} (V - v_e) - \frac{\nu_i^2}{\omega_i^2} \frac{e}{m_i \nu_i} E_p \cot I - \frac{\nu_i^2}{\omega_i^2} \frac{E_y}{B \sin I}$$

Adding equation (19) to this produces

$$\alpha u_e = U\cos^2 I + W(\cos I \sin I + \frac{\nu_i^2}{\omega_i^2}\cot I) + \frac{\nu_i}{\omega_i}\frac{\cos^2 I}{\sin I}(V - v_e)$$
$$- \frac{\beta E_y}{B}\sin I - \frac{\beta e}{m_i \nu_i} E_p \cos I \sin I \qquad (24)$$

where $\beta = 1 + \frac{\nu_i^2}{\omega_i^2 \sin^2 I}$

From equation (11),

$$v_e = \frac{E_x}{B\sin I}$$

Substituting this into equation (24) gives

$$\alpha u_e = U\cos^2 I + W(\cos I \sin I + \frac{\nu_i^2}{\omega_i^2}\cot I) - \frac{\beta E_y}{B}\sin I$$
$$- \frac{\beta e}{m_i \nu_i} E_p \cos I \sin I + \frac{\nu_i}{\omega_i} V \cos I \cot I - \frac{\nu_i}{\omega_i}\frac{E_x}{B}\cot^2 I \qquad (25)$$

From equations (20) and (25),

$$\alpha u_i - \alpha u_e = U\frac{\nu_i^2}{\omega_i^2} - W\frac{\nu_i^2}{\omega_i^2}\cot I + \frac{\nu_i^2}{\omega_i^2}\frac{E_y}{B\sin I} + \frac{\nu_i^2}{\omega_i^2}\frac{e}{m_i \nu_i} E_p \cot I$$
$$- \frac{\nu_i}{\omega_i} V \cos I \cot I + \frac{\nu_i}{\omega_i}\frac{E_x}{B}\cot^2 I - \frac{\nu_i}{\omega_i} V \sin I + \frac{\nu_i}{\omega_i}\frac{E_x}{B}$$

Hence from equation (22) :

$$\alpha(v_i - V) = \frac{\omega_i}{\nu_i}(\alpha u_i - \alpha u_e)\sin I$$
$$= U\frac{\nu_i}{\omega_i}\sin I - W\frac{\nu_i}{\omega_i}\cos I + \frac{\nu_i}{\omega_i}\frac{E_y}{B} + \frac{\nu_i}{\omega_i}\frac{e}{m_i \nu_i} E_p \cos I$$
$$- V\cos^2 I + \frac{E_x}{B}\cos I \cot I - V\sin^2 I + \frac{E_x}{B}\sin I$$

$$\therefore \alpha v_i = U\frac{\nu_i}{\omega_i}\sin I - W\frac{\nu_i}{\omega_i}\cos I + \frac{\nu_i}{\omega_i}\frac{E_y}{B} + \frac{\nu_i^2}{\omega_i^2} V + \frac{E_x}{B}\operatorname{cosec} I$$
$$+ \frac{E_p}{B}\cos I \qquad (26)$$

v_e is obtained from equation (11)

$$v_e = \frac{E_x}{B}\operatorname{cosec} I \qquad (27)$$

Finally w is obtained from equation (16)

$$w - W = \frac{\omega_i}{\nu_i}(v_i - v_e)\cos I - \frac{e}{m_i \nu_i} E_p$$

Multiplying this by α and substituting from equations (26) and (27)

$$\alpha w = \alpha W + U\sin I\cos I - W\cos^2 I + \frac{E_y}{B}\cos I + \frac{\nu_i}{\omega_i} V\cos I$$
$$+ \frac{\omega_i}{\nu_i}\frac{E_x}{B}\cot I + \frac{\omega_i}{\nu_i}\frac{E_p}{B}\cos^2 I - \frac{\omega_i}{\nu_i}\frac{E_x}{B}\cot I$$
$$- \frac{\nu_i}{\omega_i}\frac{E_x}{B}\cot I - \frac{\alpha e}{m_i \nu_i} E_p$$

$$= W\sin^2 I + \frac{\nu_i^2}{\omega_i^2} W + U\sin I\cos I + \frac{E_y}{B}\cos I + \frac{\nu_i}{\omega_i} V\cos I$$
$$- \frac{\nu_i}{\omega_i}\frac{E_x}{B}\cot I + \frac{eE_p}{m_i \nu_i}\cos^2 I - \frac{\alpha e E_p}{m_i \nu_i}$$

$$\therefore \alpha w = W\sin^2 I + \frac{\nu_i^2}{\omega_i^2} W + U\sin I\cos I + \frac{E_y}{B}\cos I + \frac{\nu_i}{\omega_i} V\cos I$$
$$- \frac{\nu_i}{\omega_i}\frac{E_x}{B}\cot I - \frac{\beta e}{m_i \nu_i} E_p \sin^2 I \qquad (28)$$

To simplify these equations, the assumption

$$\frac{\nu_i}{\omega_i} \ll \sin I$$

is made. This assumption is generally true in the F-region except at very low magnetic latitudes. In the polar regions, therefore, this assumption is certainly satisfied. From this it follows that

$$\frac{\nu_i}{\omega_i} \ll 1$$

Hence $\alpha = \beta = 1$. Thus omitting terms of order $\frac{\nu_i}{\omega_i}$, equations (20), (25), (26), (27) and (28) become

$$u_i = u_e = U\cos^2 I + W\cos I\sin I - \frac{E_y}{B}\sin I - \frac{e}{m_i \nu_i} E_p \sin I\cos I \qquad (29)$$

$$v_i = v_e = \frac{E_x}{B}\operatorname{cosec} I \qquad (30)$$

$$w = W\sin^2 I + U\sin I\cos I + \frac{E_y}{B}\cos I - \frac{e}{m_i \nu_i} E_p \sin^2 I \qquad (31)$$

where $eE_p = \frac{k}{N}\frac{\partial(T_i N)}{\partial h} + \frac{k}{N}\frac{\partial(T_e N)}{\partial h} + m_i g$

$$= \frac{k}{N}\frac{\partial}{\partial h}\left[T_i\left(1 + \frac{T_e}{T_i}\right) N\right] + m_i g$$

and writing

$$\tau = \frac{T_e}{T_i} ,$$

$$eE_p = kT_i\left[\frac{(1+\tau)}{N}\frac{\partial N}{\partial h} + \frac{(1+\tau)}{T_i}\frac{\partial T_i}{\partial h} + \frac{\partial \tau}{\partial h}\right] + m_i g \qquad (32)$$

Since the scale height H_i is defined as

$$H_i = \frac{kT_i}{m_i g}$$

one can write

$$eE_p = kT_i(1+\tau)\left[\frac{1}{N}\frac{\partial N}{\partial h} + \frac{1}{T_i}\frac{\partial T_i}{\partial h} + \frac{1}{(1+\tau)}\frac{\partial \tau}{\partial h} + \frac{1}{H_i(1+\tau)}\right]$$

Thus the final term in equation (31) becomes

$$-\frac{eE_p}{m_i \nu_i}\sin^2 I = -\frac{kT_i}{m_i \nu_i}(1+\tau)\sin^2 I\left[\frac{1}{N}\frac{\partial N}{\partial h} + \frac{1}{T_i}\frac{\partial T_i}{\partial h} + \frac{1}{(1+\tau)}\frac{\partial \tau}{\partial h} + \frac{1}{H_i(1+\tau)}\right]$$

$$= -D(1+\tau)\sin^2 I\left[\frac{1}{N}\frac{\partial N}{\partial h} + \frac{1}{T_i}\frac{\partial T_i}{\partial h} + \frac{1}{(1+\tau)}\frac{\partial \tau}{\partial h} + \frac{1}{H_i(1+\tau)}\right] \qquad (33)$$

where $D = \frac{kT_i}{m_i \nu_i}$ = ambipolar diffusion coefficient.

This is the component of velocity due to ambipolar diffusion. Thus writing

$$v_D = -D(1+\tau)\sin^2 I\left[\frac{1}{N}\frac{\partial N}{\partial h} + \frac{1}{T_i}\frac{\partial T_i}{\partial h} + \frac{1}{(1+\tau)}\frac{\partial \tau}{\partial h} + \frac{1}{H_i(1+\tau)}\right] \qquad (34)$$

$$v_W = W\sin^2 I + U\sin I\cos I \qquad (35)$$

$$v_E = \frac{E_y}{B}\cos I , \qquad (36)$$

the transport term in the continuity equation becomes

$$- \operatorname{div}(N\bar{v}) = - \frac{\partial}{\partial h} (Nw)$$

$$= - \frac{\partial}{\partial h} [N(v_D + v_w + v_E)]$$

$$= - \frac{\partial}{\partial h} (Nv_D) - \frac{\partial}{\partial h} (Nv_w) - \frac{\partial}{\partial h} (Nv_E) \qquad (37)$$

where v_D = ion velocity due to ambipolar diffusion,
v_w = ion velocity due to neutral atmospheric winds,
and v_E = ion velocity due to an electric field in the East-West direction.

The first term of equation (37) is thus

$$- \frac{\partial}{\partial h}(Nv_D) = \frac{\partial}{\partial h} \left\{ ND(1+\tau)\sin^2 I \left[\frac{1}{N} \frac{\partial N}{\partial h} + \frac{1}{T_i} \frac{\partial T_i}{\partial h} + \frac{1}{(1+\tau)} \frac{\partial \tau}{\partial h} + \frac{1}{H_i (1+\tau)} \right] \right\}$$

$$= \sin^2 I \left\{ \frac{\partial D}{\partial h} (1+\tau) \frac{\partial N}{\partial h} + D \frac{\partial \tau}{\partial h} \frac{\partial N}{\partial h} + D(1+\tau) \frac{\partial^2 N}{\partial h^2} \right.$$

$$+ \frac{\partial D}{\partial h} (1+\tau) \frac{N}{T_i} \frac{\partial T_i}{\partial h} + D \frac{\partial \tau}{\partial h} \frac{N}{T_i} \frac{\partial T_i}{\partial h}$$

$$+ D(1+\tau) \frac{\partial N}{\partial h} \frac{1}{T_i} \frac{\partial T_i}{\partial h} + D(1+\tau) \frac{N}{T_i} \frac{\partial^2 T_i}{\partial h^2}$$

$$- D(1+\tau) \frac{N}{T_i^2} \left(\frac{\partial T_i}{\partial h} \right)^2 + \frac{\partial D}{\partial h} N \frac{\partial \tau}{\partial h} + D \frac{\partial N}{\partial h} \frac{\partial \tau}{\partial h}$$

$$\left. + DN \frac{\partial^2 \tau}{\partial h^2} + \frac{\partial N}{\partial h} \frac{D}{H_i} + \frac{N}{H_i} \frac{\partial D}{\partial h} - \frac{ND}{H_i^2} \frac{\partial H_i}{\partial h} \right\} \qquad (38)$$

From Chapman and Cowling[23], the diffusion coefficient for O^+ diffusing through O is to a first approximation given by

$$D = \frac{3}{8\sigma^2 n} \left(\frac{kT}{\pi m(O)} \right)^{\frac{1}{2}}$$

This can be written as

$$D = \frac{b T^{\frac{1}{2}}}{n}$$

where $$b = \frac{3}{8\sigma^2} \left(\frac{k}{\pi m(O)} \right)^{\frac{1}{2}}$$

Hence $$\frac{\partial D}{\partial h} = \frac{b}{n}\frac{1}{2T^{\frac{1}{2}}}\frac{\partial T}{\partial h} - \frac{bT^{\frac{1}{2}}}{n^2}\left(\frac{\partial n}{\partial h}\right) \qquad (39)$$

From equation 4.3, n is given by

$$n = n_o\frac{T_o}{T}\exp\left(-\int_{h_o}^{h}\frac{dh}{H}\right)$$

Thus

$$\frac{\partial n}{\partial h} = n_o T_o\left[-\frac{1}{T^2}\frac{\partial T}{\partial h}e^{-\int_{h_o}^{h}\frac{dh}{H}} - \frac{1}{T}\frac{1}{H}e^{-\int_{h_o}^{h}\frac{dh}{H}}\right] = -n\left[\frac{1}{T}\frac{\partial T}{\partial h} + \frac{1}{H}\right]$$

Substituting into equation (39) gives

$$\frac{\partial D}{\partial h} = \frac{bT^{\frac{1}{2}}}{n}\frac{1}{2T}\frac{\partial T}{\partial h} + \frac{bT^{\frac{1}{2}}}{n}\left[\frac{1}{T}\frac{\partial T}{\partial h} + \frac{1}{H}\right]$$

$$= D\left[\frac{3}{2T}\frac{\partial T}{\partial h} + \frac{1}{H}\right]$$

Substituting this into equation (38) yields

$$-\frac{\partial}{\partial h}(Nv_D) = D\sin^2 I\left\{(1+\tau)\frac{\partial^2 N}{\partial h^2} + \left[(1+\tau)\left(\frac{5}{2T}\frac{\partial T}{\partial h} + \frac{1}{H}\right) + \left(2\frac{\partial \tau}{\partial h} + \frac{1}{H_i}\right)\right]\frac{\partial N}{\partial h} + \left[\frac{(1+\tau)}{T}\left\{\frac{1}{2T}\left(\frac{\partial T}{\partial h}\right)^2 + \frac{1}{H}\frac{\partial T}{\partial h} + \frac{\partial^2 T}{\partial h^2}\right\} + \frac{\partial T}{\partial h}\frac{1}{2T}\left(\frac{3}{H_i} + 5\frac{\partial \tau}{\partial h}\right) + \frac{1}{H}\left(\frac{\partial \tau}{\partial h} + \frac{1}{H_i}\right) - \frac{1}{H_i^2}\frac{\partial H_i}{\partial h} + \frac{\partial^2 \tau}{\partial h^2}\right] N\right\} \qquad (40)$$

This is the most general form of the diffusion term for O^+ ions and electrons diffusing together through a neutral gas consisting of atomic oxygen. Here

$$H_i = \frac{kT_i}{m(O^+)g} \quad , \quad H = \frac{kT}{m(O)g} .$$

and one can write $H = H_i$. Torr and Torr[161] use this equation with $H = H_i$ and $\frac{\partial^2 \tau}{\partial h^2} = 0$, ie

$$-\frac{\partial}{\partial h}(Nv_D) = D\sin^2 I\left\{(1+\tau)\frac{\partial^2 N}{\partial h^2} + \left[(1+\tau)\left(\frac{5}{2T}\frac{\partial T}{\partial h} + \frac{1}{H}\right) + \left(2\frac{\partial \tau}{\partial h} + \frac{1}{H}\right)\right]\frac{\partial N}{\partial h} + \left[\frac{(1+\tau)}{T}\left\{\frac{1}{2T}\left(\frac{\partial T}{\partial h}\right)^2 + \frac{1}{H}\frac{\partial T}{\partial h} + \frac{\partial^2 T}{\partial h^2}\right\} + \frac{\partial T}{\partial h}\frac{1}{2T}\left(\frac{3}{H} + 5\frac{\partial \tau}{\partial h}\right) + \frac{1}{H}\left(\frac{\partial \tau}{\partial h} + \frac{1}{H}\right) - \frac{1}{H^2}\frac{\partial H}{\partial h}\right] N\right\}$$

Torr[159] (Case 1) uses equation (40) with $\frac{\partial^2\tau}{\partial h^2} = 0$, $\frac{\partial\tau}{\partial h} = 0$, $\tau = 1$ and $D' = 2D$, i.e.

$$-\frac{\partial}{\partial h}(Nv_D) = D'\sin^2 I \left\{ \frac{\partial^2 N}{\partial h^2} + \left[\frac{5}{2T}\frac{\partial T}{\partial h} + \frac{3}{2H} \right] \frac{\partial N}{\partial h} + N\left[\frac{1}{2T^2}\left(\frac{\partial T}{\partial h}\right)^2 + \frac{7}{4HT}\frac{\partial T}{\partial h} + \frac{1}{T}\frac{\partial^2 T}{\partial h^2} + \frac{1}{2H^2} - \frac{1}{2H^2}\frac{\partial H}{\partial h} \right] \right\} \qquad (41)$$

One further simplification is obtained from

$$H_i = \frac{kT_i}{m_i g}$$

$$\therefore \quad \frac{\partial H_i}{\partial h} = \frac{k}{m_i g}\frac{\partial T_i}{\partial h} - \frac{kT_i}{m_i g^2}\frac{\partial g}{\partial h}$$

But $$g = \frac{g_o(h_o + R_E)^2}{(h + R_E)^2}$$

$$\therefore \quad \frac{\partial g}{\partial h} = \frac{-2g_o(h_o + R_E)^2}{(h + R_E)^3} = -\frac{2g}{(h + R_E)}$$

Thus $$-\frac{1}{H_i^2}\frac{\partial H_i}{\partial h} = -\frac{1}{H_i T_i}\frac{\partial T_i}{\partial h} - \frac{2}{H_i(h + R_E)}$$

Substituting this into equation (40) and neglecting terms in $\frac{\partial\tau}{\partial h}$ and $\frac{\partial^2\tau}{\partial h^2}$, one obtains

$$-\frac{\partial}{\partial h}(Nv_D) = D\sin^2 I \left\{ (1+\tau)\frac{\partial^2 N}{\partial h^2} + \left[(1+\tau)\left(\frac{5}{2T}\frac{\partial T}{\partial h} + \frac{1}{H}\right) + \frac{1}{H_i} \right] \frac{\partial N}{\partial h} + \left[\frac{(1+\tau)}{T}\left(\frac{1}{2T}\left(\frac{\partial T}{\partial h}\right)^2 + \frac{1}{H}\frac{\partial T}{\partial h} + \frac{\partial^2 T}{\partial h^2} \right) + \frac{\partial T}{\partial h}\frac{1}{2TH} + \frac{1}{H^2} - \frac{2}{H(h + R_E)} \right] N \right\} \qquad (42)$$

For ambipolar diffusion in an atmosphere consisting of two gases (O and N_2) , the diffusion coefficient becomes (Chapman and Cowling[23]) :

$$D = \frac{3}{8\sigma_{12}^2 n}\left[\frac{kT(m_1 + m_2)}{2\pi m_1 m_2} \right]^{\frac{1}{2}} \qquad (43)$$

where $n = n_1 + n_2$, $\sigma_{12} = \frac{1}{2}(\sigma_1 + \sigma_2)$

However, this can still be written in the form

$$D = \frac{bT^{\frac{1}{2}}}{n}$$

where $b = \frac{3}{8\sigma_{i2}^2}\left[\frac{k(m_1 + m_2)}{2\pi m_1 m_2}\right]^{\frac{1}{2}}$

Neglecting the term in $\frac{\partial\tau}{\partial h}$, the diffusion velocity becomes

$$v_D = -D(1+\tau)\sin^2 I\left[\frac{1}{N}\frac{\partial N}{\partial h} + \frac{1}{T}\frac{\partial T}{\partial h} + \frac{\mu}{(1+\tau)H_i}\right] \qquad (44)$$

and the ambipolar diffusion term is

$$\begin{aligned} -\frac{\partial}{\partial h}(Nv_D) = D\sin^2 I\Bigg\{ & (1+\tau)\frac{\partial^2 N}{\partial h^2} + \frac{\partial N}{\partial h}\left[\frac{1}{D}\frac{\partial D}{\partial h}(1+\tau)\right. \\ & \left. + \frac{1}{T}\frac{\partial T}{\partial h}(1+\tau) + \frac{\partial\tau}{\partial h} + \frac{\mu}{H_i}\right] + N\Bigg[\left(\frac{1}{D}\frac{\partial D}{\partial h}\frac{1}{T}\frac{\partial T}{\partial h}\right. \\ & \left. - \frac{1}{T^2}\left(\frac{\partial T}{\partial h}\right)^2 + \frac{1}{T}\frac{\partial^2 T}{\partial h^2}\right)(1+\tau) + \frac{\partial\tau}{\partial h}\frac{1}{T}\frac{\partial T}{\partial h} \\ & \left. - \frac{\mu}{H_i^2}\frac{\partial H_i}{\partial h} + \frac{1}{H_i}\frac{\partial\mu}{\partial h} + \frac{1}{D}\frac{\partial D}{\partial h}\frac{\mu}{H_i}\Bigg]\right\} \end{aligned}$$

Again neglecting terms in $\frac{\partial\tau}{\partial h}$, one finds

$$\begin{aligned} -\frac{\partial}{\partial h}(Nv_D) = D\sin^2 I\Bigg\{ & (1+\tau)\frac{\partial^2 N}{\partial h^2} + \frac{\partial N}{\partial h}\left[\frac{1}{D}\frac{\partial D}{\partial h}(1+\tau)\right. \\ & \left. + \frac{1}{T}\frac{\partial T}{\partial h}(1+\tau) + \frac{\mu}{H_i}\right] + N\Bigg[\left(\frac{1}{D}\frac{\partial D}{\partial h}\frac{1}{T}\frac{\partial T}{\partial h}\right. \\ & \left. - \frac{1}{T^2}\left(\frac{\partial T}{\partial h}\right)^2 + \frac{1}{T}\frac{\partial^2 T}{\partial h^2}\right)(1+\tau) + \frac{1}{D}\frac{\partial D}{\partial h}\frac{\mu}{H_i} \\ & \left. - \frac{\mu}{H_i^2}\frac{\partial H_i}{\partial h} + \frac{1}{H_i}\frac{\partial\mu}{\partial h}\right]\Bigg\} \qquad (45) \end{aligned}$$

If $\tau = \frac{T_e}{T_i} = 1$, $D' = 2D$ and $H' = 2H_i$ (since $(1+\tau)H_i = 2H_i$), one obtains the form used by Torr[159] (Case 2), viz.

$$\begin{aligned} -\frac{\partial}{\partial h}(Nv_D) = D'\sin^2 I\Bigg\{ & \frac{\partial^2 N}{\partial h^2} + \frac{\partial N}{\partial h}\left[\frac{1}{T}\frac{\partial T}{\partial h} + \frac{1}{D}\frac{\partial D}{\partial h} + \frac{\mu}{H'}\right] \\ & + N\left[\frac{1}{D}\frac{\partial D}{\partial h}\left(\frac{1}{T}\frac{\partial T}{\partial h} + \frac{\mu}{H'}\right) + \frac{1}{T}\frac{\partial^2 T}{\partial h^2}\right. \\ & \left. - \frac{1}{T^2}\left(\frac{\partial T}{\partial h}\right)^2 - \frac{\mu}{H'^2}\frac{\partial H'}{\partial h} + \frac{1}{H'}\frac{\partial\mu}{\partial h}\right]\Bigg\} \qquad (46) \end{aligned}$$

Torr considers a system of four gases. However, since the contribution of molecular oxygen is fairly small (about 5% of the neutral atmosphere at 200km and less than 1% at 300km, for $T_\infty = 800K$), this component can be neglected. If the contribution of helium is also neglected, one is left with a system of two gases, atomic oxygen and molecular nitrogen, for which equation (43) holds. Thus

$$\frac{\partial D}{\partial h} = \frac{b}{n}\frac{1}{2T^{\frac{1}{2}}}\frac{\partial T}{\partial h} - bT^{\frac{1}{2}}\frac{\partial}{\partial h}\left(\frac{1}{n_1 + n_2}\right)$$

$$= \frac{bT^{\frac{1}{2}}}{n}\frac{1}{2T}\frac{\partial T}{\partial h} - \frac{bT^{\frac{1}{2}}}{n^2}\left(\frac{\partial n_1}{\partial h} + \frac{\partial n_2}{\partial h}\right)$$

$$= D\left[\frac{3}{2T}\frac{\partial T}{\partial h} + \frac{1}{n}\left(\frac{n_1}{H_1} + \frac{n_2}{H_2}\right)\right]$$

Thus equation (45) becomes

$$-\frac{\partial}{\partial h}(Nv_D) = D\sin^2 I\left\{(1+\tau)\frac{\partial^2 N}{\partial h^2} + \frac{\partial N}{\partial h}\left(\left[\frac{5}{2T}\frac{\partial T}{\partial h} + \frac{1}{n}\left(\frac{n_1}{H_1} + \frac{n_2}{H_2}\right)\right](1+\tau) + \frac{\mu}{H_i}\right) + N\left(\left[\frac{1}{2T^2}\left(\frac{\partial T}{\partial h}\right)^2 + \frac{1}{T}\frac{\partial^2 T}{\partial h^2} + \frac{1}{nT}\left(\frac{n_1}{H_1} + \frac{n_2}{H_2}\right)\frac{\partial T}{\partial h}\right](1+\tau) + \frac{1}{2H_i T}\frac{\partial T}{\partial h} + \frac{\mu}{nH_i}\left(\frac{n_1}{H_1} + \frac{n_2}{H_2}\right) - \frac{2\mu}{H_i(h + R_E)} + \frac{1}{H_i}\frac{\partial \mu}{\partial h}\right)\right] \quad (47)$$

where $\mu = \dfrac{m(O^+)}{2\left(\dfrac{m(O)n(O) + m(N_2)n(N_2)}{n(O) + n(N_2)}\right)}$

The diffusion coefficient used by Stubbe[144] is

$$D = \frac{kT_i}{2\nu_{in}\mu_{in}}$$

Substituting the collision frequencies $0.82\times10^{-9}n(O)s^{-1}$ for collisions between O^+ and O and $0.97\times10^{-9}n(N_2)s^{-1}$ for collisions between O^+ and N_2, Stubbe obtains

$$D = \frac{D_o T_i}{n(O) + 1.426 n(N_2)}$$

Hence

$$\frac{\partial D}{\partial h} = \frac{D_o}{n(O) + 1.426 n(N_2)} \frac{\partial T_i}{\partial h} - \frac{D_o T_i}{(n(O) + 1.426 n(N_2))^2} \times$$

$$\left(\frac{\partial n(O)}{\partial h} + 1.426 \frac{\partial n(N_2)}{\partial h} \right)$$

$$= D \frac{1}{T_i} \frac{\partial T_i}{\partial h} + \frac{D_o T_i}{(n(O) + 1.426 n(N_2))^2} \times$$

$$\left[n(O) \left(\frac{1}{T} \frac{\partial T}{\partial h} + \frac{1}{H(O)} \right) + 1.426 n(N_2) \left(\frac{1}{T} \frac{\partial T}{\partial h} + \frac{1}{H(N_2)} \right) \right]$$

$$= D \frac{1}{T_i} \frac{\partial T_i}{\partial h} + D \frac{1}{T} \frac{\partial T}{\partial h} + \frac{D \left(\frac{n(O)}{H(O)} + 1.426 \frac{n(N_2)}{H(N_2)} \right)}{n(O) + 1.426 n(N_2)}$$

Since $T_i = T$, this becomes

$$\frac{\partial D}{\partial h} = D \left[\frac{2}{T} \frac{\partial T}{\partial h} + \frac{n(O) + 1.426 \frac{H(O)}{H(N_2)} n(N_2)}{H(O)(n(O) + 1.426 n(N_2))} \right] \qquad (48)$$

where $\frac{H(O)}{H(N_2)} = \frac{\frac{kT_i}{m(O)g}}{\frac{kT_i}{m(N_2)g}} = \frac{m(N_2)}{m(O)} = 1.875$

Thus writing

$$p = \frac{n(O) + 1.426 \frac{H(O)}{H(N_2)} n(N_2)}{n(O) + 1.426 n(N_2)}$$

$$= \frac{n(O) + 2.496 n(N_2)}{n(O) + 1.426 n(N_2)} \quad ,$$

equation (48) becomes

$$\frac{\partial D}{\partial h} = D \left(\frac{2}{T} \frac{\partial T}{\partial h} + \frac{p}{H_i} \right)$$

Substituting this into equation (45) with $\mu = 1$, $\frac{\partial \mu}{\partial h} = 0$ and ignoring terms in $\frac{\partial^2 T}{\partial h^2}$ yields

$$-\frac{\partial}{\partial h}(Nv_D) = D\sin^2 I\left\{(1+\tau)\frac{\partial^2 N}{\partial h^2} + \frac{\partial N}{\partial h}\left[\frac{1}{H_i} + (1+\tau)\left(\frac{p}{H_i} + \frac{3}{T_i}\frac{\partial T_i}{\partial h}\right)\right]\right.$$
$$+ N\left[\frac{p}{H_i^2} + \frac{1}{H_i T_i}\frac{\partial T_i}{\partial h} - \frac{2}{(R_E+h)H_i}\right.$$
$$\left.\left. + (1+\tau)\left(\frac{p}{H_i T_i}\frac{\partial T_i}{\partial h} + \frac{1}{T^2}\left(\frac{\partial T}{\partial h}\right)^2\right)\right]\right\} \qquad (49)$$

and if the term in $\left(\frac{\partial T}{\partial h}\right)^2$ is ignored, the form of the diffusion term used by Stubbe[144] is obtained, viz.

$$-\frac{\partial}{\partial h}(Nv_D) = D\sin^2 I\left\{(1+\tau)\frac{\partial^2 N}{\partial h^2} + \frac{\partial N}{\partial h}\left[\frac{1}{H_i} + (1+\tau)\left(\frac{p}{H_i} + \frac{3}{T_i}\frac{\partial T_i}{\partial h}\right)\right]\right.$$
$$+ N\left[\frac{p}{H_i^2} + \frac{1}{H_i T_i}\frac{\partial T_i}{\partial h} - \frac{2}{(R_E+h)H_i}\right.$$
$$\left.\left. + (1+\tau)\frac{p}{H_i T_i}\frac{\partial T_i}{\partial h}\right]\right\} \qquad (50)$$

If the assumptions $\tau = 1$, $\frac{\partial \tau}{\partial h} = 0$, $\frac{\partial^2 \tau}{\partial h^2} = 0$ and $D' = 2D$ are made, equation (50) reduces to

$$-\frac{\partial}{\partial h}(Nv_D) = D'\sin^2 I\left\{\frac{\partial^2 N}{\partial h^2} + \frac{\partial N}{\partial h}\left[\frac{3}{T}\frac{\partial T}{\partial h} + \frac{p}{H_i} + \frac{1}{2H_i}\right]\right.$$
$$\left. + N\left[\frac{p}{2H_i^2} + \frac{1}{2H_i T}\frac{\partial T}{\partial h} - \frac{1}{H_i(R_E+h)} + \frac{P}{H_i T_i}\frac{\partial T_i}{\partial h}\right]\right\} \qquad (51)$$

whereas equation (47) (ambipolar diffusion of O^+ in a mixture of O and N_2) becomes

$$-\frac{\partial}{\partial h}(Nv_D) = D'\sin^2 I\left\{\frac{\partial^2 N}{\partial h^2} + \frac{\partial N}{\partial h}\left[\frac{5}{2T}\frac{\partial T}{\partial h} + \frac{1}{n}\left(\frac{n_1}{H_1} + \frac{n_2}{H_2}\right) + \frac{\mu}{2H_i}\right.\right.$$
$$+ N\left[\frac{1}{2T^2}\left(\frac{\partial T}{\partial h}\right)^2 + \frac{1}{T}\frac{\partial^2 T}{\partial h^2} + \frac{1}{nT}\left(\frac{n_1}{H_1} + \frac{n_2}{H_2}\right)\frac{\partial T}{\partial h}\right.$$
$$\left.\left. + \frac{1}{4H_i T_i}\frac{\partial T}{\partial h} - \frac{1}{H_i(h+R_E)} + \frac{1}{2nH_i}\left(\frac{n_1}{H_1} + \frac{n_2}{H_2}\right)\right]\right\} \qquad (52)$$

and equation (40) yields

$$-\frac{\partial}{\partial h}(Nv_D) = D'\sin^2 I\left\{\frac{\partial^2 N}{\partial h^2} + \frac{\partial N}{\partial h}\left[\frac{5}{2T}\frac{\partial T}{\partial h} + \frac{1}{H} + \frac{1}{2H_i}\right]\right.$$
$$+ N\left[\frac{1}{2T^2}\left(\frac{\partial T}{\partial h}\right)^2 + \frac{5}{4HT}\frac{\partial T}{\partial h} + \frac{1}{T}\frac{\partial^2 T}{\partial h^2} + \frac{1}{2HH_i}\right.$$
$$\left.\left. - \frac{1}{H_i(h+R_E)}\right]\right\} \qquad (53)$$

If the variation of g with height is neglected and an isothermal atmosphere consisting only of O^+ and O is assumed, then

$$p = 1$$

$$\frac{1}{n}\left(\frac{n_1}{H_1} + \frac{n_2}{H_2}\right) = \frac{1}{H(O)}$$

$$\mu = 1$$

and equations (51), (52) and (53) all reduce to

$$-\frac{\partial}{\partial h}(Nv_D) = D'\sin^2 I\left\{\frac{\partial^2 N}{\partial h^2} + \frac{3}{2H}\frac{\partial N}{\partial h} + \frac{\partial N}{2H^2}\right\} \qquad (54)$$

SUMMARY :

The diffusion term of the continuity equation is

$$-\operatorname{div}(N\bar{v}) = -\frac{\partial}{\partial h}(Nv_D) - \frac{\partial}{\partial h}(Nv_W) - \frac{\partial}{\partial h}(Nv_E)$$

where $-\frac{\partial}{\partial h}(Nv_D)$ = ambipolar diffusion term (given by any of equations (40), (42), (46), (47), (50), (51), (52), (53) or (54)).

$$-\frac{\partial}{\partial h}(Nv_W) = -\frac{\partial N}{\partial h}(W\sin^2 I + U\sin I\cos I) - N\left(\frac{\partial W}{\partial h}\sin^2 I + \frac{\partial U}{\partial h}\sin I\cos I\right)$$

$$-\frac{\partial}{\partial h}(Nv_E) = -\frac{\partial N}{\partial h}\frac{E_y}{B}\cos I - \frac{N}{B}\frac{\partial E_y}{\partial h}\cos I$$

The N-S component of the horizontal neutral wind velocity, U , is obtained by solving equation (1)

$$\frac{\partial U}{\partial t} = -\frac{1}{\rho}\frac{dp}{dx} + \zeta\frac{\partial^2 U}{\partial x^2} + \frac{Nm_i\nu_i}{N_n m_n}(u_i - U)$$

where u_i is given by equation (29) :

$$u_i = U\cos^2 I + W\cos I\sin I - \frac{E_y}{B}\sin I + \frac{e}{m_i\nu_i}E_p\sin I\cos I$$

The vertical component of the neutral wind velocity, W, used here was derived from the "breathing atmosphere" model proposed by Harris and Priester[181]. This form has been adopted by Torr and Torr[161] and Stubbe[144,146]. From this model

$$W(h) = W(h_o) + T \int_{h_o}^{h} \frac{1}{\bar{T}^2} \frac{\partial T}{\partial t} \, dh'$$

(Stubbe [144]). If W = 0 is assumed for $h \leq 120$km,

$$W(h) = T \int_{120}^{h} \frac{1}{\bar{T}^2} \frac{\partial T}{\partial t} \, dh' \qquad (55)$$

APPENDIX 11

FINAL FORM OF THE COUPLED IONOSPHERIC DIFFERENTIAL EQUATIONS

APPENDIX 11

FINAL FORM OF THE COUPLED IONOSPHERIC DIFFERENTIAL EQUATIONS

The equation of motion of the neutral atmosphere and the wind velocity equation (equation (29) of Appendix 10) are

$$\frac{\partial U}{\partial t} = -\frac{1}{\rho}\frac{\partial p}{\partial x} + \zeta\frac{\partial^2 U}{\partial x^2} + \frac{Nm_i\nu_i}{N_n m_n}(u_i - U) \qquad (1)$$

and

$$u_i = U\cos^2 I + W\cos I\sin I - \frac{e}{m_i\nu_i}E_p\cos I\sin I \qquad (2)$$

where (ignoring the term in $\frac{\partial\tau}{\partial h}$)

$$eE_p = kT_i(1+\tau)\left[\frac{1}{N}\frac{\partial N}{\partial h} + \frac{1}{T}\frac{\partial T}{\partial h} + \frac{1}{H_i(1+\tau)}\right] \qquad (3)$$

Substituting equations (2) and (3) into equation (1), one obtains

$$\frac{\partial U}{\partial t} = -\frac{1}{\rho}\frac{\partial p}{\partial x} + \zeta\frac{\partial^2 U}{\partial x^2} + \frac{Nm_i\nu_i}{N_n m_n}\left\{\cos I\sin I\left[W - D(1+\tau)\left(\frac{1}{N}\frac{\partial N}{\partial h} + \frac{1}{T}\frac{\partial T}{\partial h} + \frac{1}{H_i(1+\tau)}\right)\right] - U\sin^2 I\right\} \qquad (4)$$

This can be written in the form

$$\frac{\partial U}{\partial t} = f_1\frac{\partial^2 U}{\partial x^2} + f_2 UN + f_3 N - f_4\frac{\partial N}{\partial h} + f_5$$

where $f_1 = \zeta$

$$f_2 = -\frac{m_i\nu_i\sin^2 I}{N_n m_n}$$

$$f_3 = \frac{m_i\nu_i\sin I\cos I}{N_n m_n}\left\{W - D(1+\tau)\left(\frac{1}{T}\frac{\partial T}{\partial h} + \frac{1}{H_i(1+\tau)}\right)\right\}$$

$$f_4 = \frac{kT_i(1+\tau)\sin I\cos I}{N_n m_n}$$

$$f_5 = -\frac{1}{\rho}\frac{\partial p}{\partial x}$$

Similarly the continuity equations can be written in the form

$$\frac{\partial n(O^+)}{\partial t} = g_1\frac{\partial^2 n(O^+)}{\partial h^2} + g_2\frac{\partial n(O^+)}{\partial h} + g_3 n(O^+) + g_4$$

$$-U\sin I\cos I\,\frac{\partial n(O^+)}{\partial h} - \frac{\partial U}{\partial h}\sin I\cos I n(O^+)$$

$$\frac{\partial n(O_2^+)}{\partial t} = g_5 n(O_2^+) + g_6 n(O^+) + g_7 n(N_2^+) + g_8$$

$$\frac{\partial n(N_2^+)}{\partial t} = g_9 n(N_2^+) + g_{10}$$

$$\frac{\partial n(NO^+)}{\partial t} = g_{11} n(NO^+) + g_{12} n(O^+) + g_{13} n(N_2^+) + g_{14} n(O_2^+)$$

where
$$g_4 = q_{O^+}$$
$$g_5 = -\gamma_4 n(NO) - \alpha_1 N_e$$
$$g_6 = +\gamma_2 n(O_2)$$
$$g_7 = +\gamma_5 n(O_2)$$
$$g_8 = q_{O_2^+}$$
$$g_9 = -\gamma_3 n(O) - \gamma_5 n(O_2) - \alpha_2 N_e$$
$$g_{10} = q_{N_2^+}$$
$$g_{11} = -\alpha_3 N_e$$
$$g_{12} = +\gamma_1 n(N_2)$$
$$g_{13} = +\gamma_3 n(O)$$
$$g_{14} = +\gamma_4 n(NO)$$

The functions g_1, g_2 and g_3 depend on the form of the ambipolar diffusion term which is used. Four different forms where tried.

(a) THE SIMPLE DIFFUSION TERM (A10-54)

$$g_1 = D'\sin^2 I$$

$$g_2 = \frac{3}{2H} D'\sin^2 I - W\sin^2 I$$

$$g_3 = \frac{1}{2H^2} D'\sin^2 I - \frac{\partial W}{\partial h}\sin^2 I - \gamma_1 n(N_2) - \gamma_2 n(O_2)$$

(b) DIFFUSION TERM FOR O^+ IN ATOMIC OXYGEN ($T_e = T_i$) (A10-41)

$$g_1 = D'\sin^2 I$$

$$g_2 = D'\sin^2 I \left[\frac{5}{2T}\frac{\partial T}{\partial h} + \frac{3}{2H}\right] - W\sin^2 I$$

$$g_3 = D'\sin^2 I \left[\frac{1}{2T^2}\left(\frac{\partial T}{\partial h}\right)^2 + \frac{7}{4HT}\frac{\partial T}{\partial h} + \frac{1}{T}\frac{\partial^2 T}{\partial h^2} + \frac{1}{2H^2} - \frac{1}{2H^2}\frac{\partial H}{\partial h}\right] - \frac{\partial W}{\partial h}\sin^2 I - \gamma_1 n(N_2) - \gamma_2 n(O_2)$$

(c) DIFFUSION TERM FOR O^+ IN ATOMIC OXYGEN ($T_e \neq T_i$) (A10-40)

$$g_1 = D(1+\tau)\sin^2 I$$

$$g_2 = D\sin^2 I \left\{(1+\tau)\left[\frac{5}{2T}\frac{\partial T}{\partial h} + \frac{1}{H}\right] + \frac{1}{H}\right\} - W\sin^2 I$$

$$g_3 = D\sin^2 I \left\{\frac{(1+\tau)}{T}\left[\frac{1}{2T}\left(\frac{\partial T}{\partial h}\right)^2 + \frac{1}{H}\frac{\partial T}{\partial h} + \frac{\partial^2 T}{\partial h^2}\right] + \frac{\partial T}{\partial h}\frac{3}{2TH} + \frac{1}{H^2} - \frac{1}{H^2}\frac{\partial H}{\partial h}\right\} - \frac{\partial W}{\partial h}\sin^2 I - \gamma_1 n(N_2) - \gamma_2 n(O_2)$$

(Here $\frac{\partial \tau}{\partial h}$ and $\frac{\partial^2 \tau}{\partial h^2}$ have been assumed to be negligible.)

(d) STUBBE'S DIFFUSION TERM FOR TWO-COMPONENT ATMOSPHERE (A10-50)

$$g_1 = D(1+\tau)\sin^2 I$$

$$g_2 = D\sin^2 I \left[\frac{1}{H_i} + (1+\tau)\left(\frac{p}{H_i} + \frac{3}{T}\frac{\partial T}{\partial h}\right)\right] - W\sin^2 I$$

$$g_3 = D\sin^2 I \left[\frac{p}{H_i^2} + \frac{1}{H_i T}\frac{\partial T}{\partial h} - \frac{2}{(R_E + h)H_i} + (1+\tau)\frac{p}{H_i T}\frac{\partial T}{\partial h}\right] - \frac{\partial W}{\partial h}\sin^2 I - \gamma_1 n(N_2) - \gamma_2 n(O_2)$$

APPENDIX 12

DERIVATION OF μ' AND $\frac{\partial \mu'}{\partial f_P}$

APPENDIX 12

DERIVATION OF μ' AND $\frac{\partial \mu'}{\partial f}_p$

The phase refractive index, μ, can be written (Ratcliffe[119]) in the form:

$$F(\mu) = \alpha\mu^4 + \gamma\mu^2 + \epsilon = 0 \tag{1}$$

where
$$\begin{aligned} \alpha &= (1-X) - Y^2(1-X\cos^2\theta) \\ \gamma &= -2(1-X)^2 + 2Y^2(1-X) + XY^2\sin^2\theta \\ \epsilon &= (1-X)^3 - Y^2(1-X) \end{aligned} \tag{2}$$

The two solutions of equation (1) are:

$$\mu^2 = \frac{-\gamma \pm \sqrt{\gamma^2 - 4\alpha\epsilon}}{2\alpha} \tag{3}$$

corresponding to the ordinary and extraordinary modes.

The group refractive index, μ', is derived from the phase refractive index as follows:

$$\mu' = \mu + f\frac{\partial \mu}{\partial f} \tag{4}$$

To obtain $\frac{\partial \mu}{\partial f}$, we must differentiate equation (1):

$$\frac{\partial F}{\partial f} = (4\alpha\mu^3 + 2\gamma\mu)\frac{\partial \mu}{\partial f} + \frac{\partial \alpha}{\partial f}\mu^4 + \frac{\partial \gamma}{\partial f}\mu^2 + \frac{\partial \epsilon}{\partial f} = 0$$

Then
$$f\frac{\partial \mu}{\partial f} = -f\,\frac{\frac{\partial \alpha}{\partial f}\mu^4 + \frac{\partial \gamma}{\partial f}\mu^2 + \frac{\partial \epsilon}{\partial f}}{(4\alpha\mu^2 + 2\gamma)\mu} \tag{5}$$

and putting $\alpha\mu^4 = -\gamma\mu^2 - \epsilon$ from equation (1), this becomes:

$$f\frac{\partial \mu}{\partial f} = f\,\frac{\left(\gamma\frac{\partial \alpha}{\partial f} - \alpha\frac{\partial \gamma}{\partial f}\right)\mu^2 + \epsilon\frac{\partial \alpha}{\partial f} - \alpha\frac{\partial \epsilon}{\partial f}}{2\alpha\mu(2\alpha\mu^2 + \gamma)} \tag{6}$$

$$\therefore\ \mu' = \mu + \frac{\left[\gamma\left(f\frac{\partial \alpha}{\partial f}\right) - \alpha\left(f\frac{\partial \gamma}{\partial f}\right)\right]\mu^2 + \epsilon\left(f\frac{\partial \alpha}{\partial f}\right) - \alpha\left(f\frac{\partial \epsilon}{\partial f}\right)}{2\alpha\mu(2\alpha\mu^2 + \gamma)} \tag{7}$$

where:

$$\left.\begin{aligned} f\frac{\partial \alpha}{\partial f} &= 2[X + Y^2 - 2XY^2\cos^2\theta] \\ f\frac{\partial \gamma}{\partial f} &= -4[(1-X)(X+Y^2) + X(1-X-Y^2) + XY^2\sin^2\theta] \\ f\frac{\partial \epsilon}{\partial f} &= 2\{(1-X)^2X + (1-X)[2X(1-X)+Y^2] - XY^2\} \end{aligned}\right\} \tag{8}$$

From equation (1) the rate of change of μ' with plasma frequency, $\frac{\partial \mu'}{\partial f_p}$, is:

$$\frac{\partial \mu'}{\partial f_p} = \frac{\partial \mu}{\partial f_p} + f_r \frac{\partial^2 \mu}{\partial f_p \partial f_r}$$

$$= \frac{\partial \mu}{\partial f_p} + f_r \frac{\partial}{\partial f_p}\left[\frac{\left(\gamma\frac{\partial \alpha}{\partial f_r} - \alpha\frac{\partial \gamma}{\partial f_r}\right)\mu^2 + \epsilon\frac{\partial \alpha}{\partial f_r} - \alpha\frac{\partial \epsilon}{\partial f_r}}{2\alpha\mu(2\alpha\mu^2 + \gamma)}\right]$$

From the quotient rule:

$$= \frac{\partial \mu}{\partial f_p} + f_r \frac{\frac{\partial}{\partial f_p}\left[\left(\gamma\frac{\partial \alpha}{\partial f_r} - \alpha\frac{\partial \gamma}{\partial f_r}\right)\mu^2 + \epsilon\frac{\partial \alpha}{\partial f_r} - \alpha\frac{\partial \epsilon}{\partial f_r}\right]}{2\alpha\mu(2\alpha\mu^2 + \gamma)}$$

$$- f_r \frac{\left[\left(\gamma\frac{\partial \alpha}{\partial f_r} - \alpha\frac{\partial \gamma}{\partial f_r}\right)\mu^2 + \epsilon\frac{\partial \alpha}{\partial f_r} - \alpha\frac{\partial \epsilon}{\partial f_r}\right]}{2\alpha\mu(2\alpha\mu^2 + \gamma)} \cdot \frac{\left[\frac{\partial}{\partial f_p}(4\alpha^2\mu^3 + 2\alpha\gamma\mu)\right]}{2\alpha\mu(2\alpha\mu^2 + \gamma)}$$

$$= \frac{\partial \mu}{\partial f_p} + \frac{\left[\frac{\partial \gamma}{\partial f_p}\left(f_r \frac{\partial \alpha}{\partial f_r}\right) + \gamma\left(f_r \frac{\partial^2 \alpha}{\partial f_p \partial f_r}\right) - \frac{\partial \alpha}{\partial f_p}\left(f_r \frac{\partial \gamma}{\partial f_r}\right)\right]\mu^2}{2\alpha\mu(2\alpha\mu^2 + \gamma)}$$

$$\frac{-\left[\alpha\left(f_r \frac{\partial^2 \gamma}{\partial f_p \partial f_r}\right)\right]\mu^2 + \frac{\partial \epsilon}{\partial f_p}\left(f_r \frac{\partial \alpha}{\partial f_r}\right)}{2\alpha\mu(2\alpha\mu^2 + \gamma)}$$

$$+ \frac{-\frac{\partial \alpha}{\partial f_p}\left(f_r \frac{\partial \epsilon}{\partial f_r}\right) + \epsilon\left(f_r \frac{\partial^2 \alpha}{\partial f_p \partial f_r}\right) - \alpha\left(f_r \frac{\partial^2 \epsilon}{\partial f_p \partial f_r}\right)}{2\alpha\mu(2\alpha\mu^2 + \gamma)}$$

$$+ \frac{\left[\gamma\left(f_r \frac{\partial \alpha}{\partial f_r}\right) - \alpha\left(f_r \frac{\partial \gamma}{\partial f_r}\right)\right] 2\mu\frac{\partial \mu}{\partial f_p}}{2\alpha\mu(2\alpha\mu^2 + \gamma)}$$

$$- f_r\left[\frac{\left(\gamma\frac{\partial \alpha}{\partial f_r} - \alpha\frac{\partial \gamma}{\partial f_r}\right)\mu^2 + \epsilon\frac{\partial \alpha}{\partial f_r} - \alpha\frac{\partial \epsilon}{\partial f_r}}{2\alpha\mu(2\alpha\mu^2 + \gamma)}\right] \cdot$$

$$\left[\frac{8\alpha\frac{\partial \alpha}{\partial f_p}\mu^3 + 12\alpha^2\mu^2\frac{\partial \mu}{\partial f_p} + 2\frac{\partial \alpha}{\partial f_p}\gamma\mu + 2\alpha\frac{\partial \gamma}{\partial f_p}\mu + 2\alpha\gamma\frac{\partial \mu}{\partial f_p}}{2\alpha\mu(2\alpha\mu^2 + \gamma)}\right]$$

(9)

Writing

$$A = \frac{\partial \alpha}{\partial f_p} = \frac{2X}{f_p}(Y^2\cos^2\theta - 1)$$

$$B = \frac{\partial \gamma}{\partial f_p} = \frac{2X}{f_p}(Y^2\sin^2\theta + 4(1-X) - 2Y^2)$$

$$C = \frac{\partial \epsilon}{\partial f_p} = \frac{2X}{f_p}[Y^2 - 3(1-X)^2]$$

$$D = f_r \frac{\partial \alpha}{\partial f_r} = 2[X + Y^2 - 2XY^2\cos^2\theta]$$

$$E = f_r \frac{\partial \gamma}{\partial f_r} = -4\{(1-X)(2X+Y^2) - XY^2\cos^2\theta\}$$

$$F = f_r \frac{\partial \epsilon}{\partial f_r} = 2\{3X(1-X)^2 + Y^2 - 2XY^2\}$$

$$G = \alpha = 1 - X - Y^2(1 - X\cos^2\theta)$$

$$H = \gamma = -2(1-X)^2 + 2Y^2(1-X) + XY^2\sin^2\theta$$

$$T = \epsilon = (1-X)^3 - Y^2(1-X)$$

$$U = f_r \frac{\partial^2 \alpha}{\partial f_p \partial f_r} = \frac{4X}{f_p}(1 - 2Y^2\cos^2\theta)$$

$$V = f_r \frac{\partial^2 \gamma}{\partial f_p \partial f_r} = -\frac{8X}{f_p}(2 - 4X - Y^2 - Y^2\cos^2\theta)$$

$$W = f_r \frac{\partial^2 \epsilon}{\partial f_p \partial f_r} = \frac{4X}{f_p}(3 - 12X + 9X^2 - 2Y^2)$$

equation (9) becomes

$$\frac{\partial \mu'}{\partial f_p} = \frac{\partial \mu}{\partial f_p} + \frac{[BD+HU-AE-GV]\mu^2 + CD+TU-AF-GW}{2G\mu(2G\mu^2 + H)} + \frac{(HD-GE)2\frac{\partial \mu}{\partial f_p}\mu}{2G\mu(2G\mu^2 + H)}$$

$$-[\mu' - \mu]\left[\frac{8GA\mu^3 + 12G^2\mu^2\frac{\partial \mu}{\partial f_p} + 2AH\mu + 2GB\mu + 2GH\frac{\partial \mu}{\partial f_p}}{2G\mu(2G\mu^2 + H)}\right] \qquad (10)$$

where $\mu_{\substack{X \\ 0}} = \left(\frac{-\gamma \mp \sqrt{\gamma^2 - 4\alpha\epsilon}}{2\alpha}\right)^{\frac{1}{2}}$

$$\text{and } \frac{\partial \mu}{\partial f_p} = \frac{1}{2}\left(\frac{-\gamma \mp \sqrt{\gamma^2-4\alpha\epsilon}}{2\alpha}\right)^{-\frac{1}{2}} \frac{\partial}{\partial f_p}\left(\frac{-\gamma \mp \sqrt{\gamma^2-4\alpha\epsilon}}{2\alpha}\right)$$

$$= \frac{1}{2}\frac{1}{\mu}\left[\frac{2\alpha\left\{-\frac{\partial\gamma}{\partial f_p} \mp \frac{1}{2}(\gamma^2-4\alpha\epsilon)^{-\frac{1}{2}}(2\gamma\frac{\partial\gamma}{\partial f_p} - 4\epsilon\frac{\partial\alpha}{\partial f_p} - 4\alpha\frac{\partial\epsilon}{\partial f_p})\right\}}{4\alpha^2}\right]$$

$$-\frac{1}{2}\frac{1}{\mu}\left[\frac{2\frac{\partial\alpha}{\partial f_p}(-\gamma \mp \sqrt{\gamma^2-4\alpha\epsilon})}{4\alpha^2}\right]$$

$$= \frac{1}{2\alpha\mu}\left[-\frac{1}{2}\frac{\partial\gamma}{\partial f_p} - \frac{\partial\alpha}{\partial f_p}\mu^2 \mp \frac{\gamma\frac{\partial\gamma}{\partial f_p} - 2\frac{\partial\alpha}{\partial f_p}\epsilon - 2\alpha\frac{\partial\epsilon}{\partial f_p}}{2\sqrt{\gamma^2-4\alpha\epsilon}}\right]$$

$$= -\frac{1}{2G\mu}\left[0.5B + A\mu^2 \pm \frac{HB - 2AT - 2GC}{2\sqrt{HH-4GT}}\right] \qquad (11)$$

The term HB-2AT-2GC can be simplified by substituting the values of H,B,A, etc and cancelling where possible. It can be shown that:

$$HB - 2AT - 2GC = \frac{2X^2Y^2}{f_p}[Y^2\sin^4\theta + 4(1-X)(1-2X)\cos^2\theta]$$

Thus

$$\frac{\partial\mu}{\partial f_p} = -\frac{1}{2G\mu}\left[0.5B + A\mu^2 \pm \frac{A'}{2\sqrt{HH-4GT}}\right] \qquad (12)$$

$$\text{where } A' = \frac{2X^2Y^2}{f_p}[Y^2\sin^4\theta + 4(1-X)(1-2X)\cos^2\theta] \qquad (13)$$

Similarly equation (10) can be rewritten and simplified as follows:

$$B' = BD + HU - AE - GV$$

$$= \frac{4X}{f_p}[2(1-3X)(1-X) - 2(1-3X)Y^2\sin^2\theta + Y^4\sin^2\theta] \qquad (14)$$

$$C' = CD + TU - AF - GW$$

$$= \frac{4X}{f_p}[-Y^4\sin^2\theta - 6XY^2\sin^2\theta + 2Y^2\sin^2\theta + 6X^2Y^2$$

$$- 2XY^2 - 4X^3Y^2\cos^2\theta - 2(1-X)^2(1-4X)] \qquad (15)$$

and

$$\frac{\partial \mu'}{\partial f_p} = \frac{\partial \mu}{\partial f_p} + \frac{B'\mu^2 + C'}{2G\mu(2G\mu^2 + H)} + \frac{(HD - GE)2\frac{\partial \mu}{\partial f_p}\mu}{2G\mu(2G\mu^2 + H)}$$

$$-[\mu'-\mu]\left[\frac{8GA\mu^3 + 12G^2\mu^2\frac{\partial \mu}{\partial f_p} + 2AH\mu + 2GB\mu + 2GH\frac{\partial \mu}{\partial f_p}}{2G\mu(2G\mu^2 + H)}\right] \quad (16)$$

REFERENCES

References.

1. Abur-Robb M.F.K. and Windle D.W., On the Day and Night Reversal in $N_m F2$ North-South Asymmetry, 1969, Planet. Space Sci., Vol. 17, pp. 97-106.
2. Allen C.W., World Wide Variations in the F2 Region, 1954, J. Atmosph. Terr. Phys., Vol. 4, pp. 53-67.
3. Andrews M.K. and Thomas J.O., Electron Density Distribution Above the Winter Pole, 1969, Nature, Vol. 221, pp. 223-227.
4. Bailey G.J., Moffett R.J. and Rishbeth H., Solution of the Coupled Ion and Neutral Air Equations of the Mid-Latitude Ionospheric F2-Layer, 1969, J. Atmosph. Terr. Phys., Vol. 31, pp. 253-270.
5. Barish F.D., Conjugate Intersects to Selected Geophysical Stations, May 1969, STP Notes Inter-Union Commission on Solar-Terrestrial Physics, No. 4, pp. 91-109.
6. Bartels J., Terrestrial-magnetic Activity and its Relations to Solar Phenomena, 1932, Terr. Magnetism and Atmosph. Elec., Vol. 37, pp. 1-52.
7. Bartels J., Discussion of Time-variations of Geomagnetic Activity Indices K_p and A_p, 1932-1961, 1963, Ann. Geophys., Vol. 19, pp. 1-20.
8. Batey P.H., Court G.R., and Sayers J., Afterglow Measurements of the Rate Coefficients for the Reactions $O^+ + O_2 \rightarrow O_2^+ + O$ and $O^+ + N_2 \rightarrow NO^+ + N$, 1965, Planet. Space Sci., Vol. 13, pp. 911-917.
9. Becker W., Tables of Ordinary and Extraordinary Refractive Indices, Group-Refractive Indices and $h'_{o,x}(f)$-curves for standard Ionospheric Layer Models, 1960, Proc. Max-Planck-Institut für Aeronomie, Vol. 4, No. 1.

10. Becker W., On the Manual and Digital Computer Methods used at Lindau for the Conversion of Multifrequency Ionograms to Electron Density-Height Profiles, 1967, Radio Sci., Vol. 2, pp. 1205-1232.

11. Bellchambers W.H., Barclay L.W., and Piggott W.R., Ionosphere Observations, 2, Analysis of Results in the Royal Society IGY Antarctic Expedition, Halley Bay 1955-1959, 1962, Vol. 2, p. 179.

12. Biondi M.A., Laboratory Measurements of Electron-Ion Recombination Coefficients, 1967, Space Research VII, Vol. 1, pp. 154-164.

13. Bohme D.K., Ong P.P., Hasted J.B. and Megill L.R., Energy Dependence of Reactions O^+ with N_2, O_2. I. Drift Tube Measurements, 1967, Planet. Space Sci., Vol. 15, pp. 1777-1780.

14. Boller B.R. and Stolov H.L., Kelvin-Helmholtz Instability and the Semi-Annual Variation of Geomagnetic Activity, 1970, J. Geophys. Res., Vol. 75, pp. 6073-6084.

15. Booth A.D., Numerical Methods, 1957, Butterworths Scientific Publications, p. 44.

16. Buckingham R.A., Numerical Methods, 1957, Sir Isaac Pitman and Sons, Ltd., pp. 298-333.

17. Bullen J.M., Ionospheric Recombination and the Polar Stratospheric Warming, 1964, J. Atmosph. Terr. Phys., Vol. 26, pp. 559-568.

18. Burch J.L., Low-Energy Electron Fluxes at Latitudes above the Auroral Zone, 1968, J. Geophys. Res., Vol. 73, pp. 3585-3591.

19. Challinor, R.A., Universal Time Control of the Polar Ionosphere, 1969, Nature, Vol. 221, pp. 941-943.

20. Challinor R.A., and Eccles D., Longitudinal Variations of the Mid-Latitude Ionosphere Produced by Neutral-Air Winds-I. Neutral-Air Winds and Ionospheric Drifts in the Northern and Southern Hemispheres, 1971, J. Atmosph. Terr. Phys., Vol. 33, pp. 363-369.

21. Chan F.T., Electron-Ion and Ion-Ion Dissociative Recombination of Oxygen. I. Electron-Ion Recombination, 1968, J. Chem. Phys., Vol. 49, pp. 2533-2540.

22. Chandra S. and Herman J.R., F-Region Ionization and Heating During Magnetic Storms, 1969, Planet. Space Sci., Vol. 17, pp. 841-851.

23. Chapman S. and Cowling T.G., The Mathematical Theory of Non-Uniform Gases, 1960, Cambridge University Press.

24. C.I.R.A., Cospar International Reference Atmosphere, 1965, compiled by the members of the Cospar Group IV, Amsterdam, North Holland Publishing Co.

25. Cook G.E., Variations in Exospheric Density During 1967-68, as revealed by Echo 2, 1970a, Planet. Space Sci., Vol. 18, pp. 387-394.

26. Cook G.E., The Semi-Annual Variation in the Upper Atmosphere during 1967 and 1968, 1970b, Planet. Space Sci., Vol. 18, pp. 1573-1584.

27. Cook G.E., and Scott D.W., The Semi-Annual Variation in Air Density at a Height of 1100 km From 1964 to 1967, 1969, Planet. Space Sci., Vol. 17, pp. 107-119.

28. Copsey M.J., Smith D. and Sayers J., Laboratory Afterglow Studies of O^+ Ions in Helium-Oxygen and Helium-Oxygen-Nitrogen Mixtures, 1966, Planet. Space Sci., Vol. 14, pp. 1047-1055.

29. Coroniti S.C., and Penndorf R., The Diurnal and Annual Variations of f_0F2 over the Polar Regions, 1959, J. Geophys. Res., Vol. 64, pp. 5-18.

30. Dalgarno A., Ambipolar Diffusion in the F2 Layer, 1958, J. Atmosph. Terr. Phys., Vol. 12, pp. 219-220.

31. Dalgarno A., Ambipolar Diffusion in the F-Region, 1964, J. Atmosph. Terr. Phys., Vol. 26, p. 939.

32. Dalgarno A. and Smith F.J., The Thermal Conductivity and Viscosity of Atomic Oxygen, 1962, Planet. Space Sci., Vol. 9, pp. 1-2.

33. Dickinson P.H.G. and Sayers J., Ion Charge-Exchange Reactions in Oxygen Afterglows, 1960, Proc. Phys. Soc., Vol. 76, pp. 137-148.

34. Donahue T.M., Ionospheric Reaction Rates in the Light of Recent Measurements in the Ionosphere and the Laboratory, 1966, Planet. Space. Sci., Vol. 14, pp. 33-48.

35. Dougherty J.P., On the Influence of Horizontal Motion of the Neutral Air on the Diffusion Equation of the F-Region, 1961, J. Atmosph. Terr. Phys., Vol. 20, pp. 167-176.

36. Doupnik J.R. and Schmerling E.R., The Reduction of Ionograms from the Bottomside and Topside, 1965, Pennsylvania State University Scientific Report No. 230.

37. Duncan R.A., Universal-time Control of the Arctic and Antarctic F-Region, 1962, J. Geophys. Res., Vol. 67, pp. 1823-1830.

38. Duncan R.A., Neutral Winds and Universal-Time Control of the Polar F-Region, 1969, J. Atmosph. Terr. Phys., Vol. 31, pp. 1003-1009.

39. Dunkin D.B., Fehsenfeld F.C., Schmeltekopf A.L. and Ferguson E.E., Ion-Molecule Reaction Studies from 300° to 600°K in a Temperature-Controlled Flowing Afterglow System, 1968, J. Chem. Phys., Vol. 49, pp. 1365-1371.

40. Eccles D., King J.W. and Rothwell P., Longitudinal Variations of the Mid-Latitude Ionosphere Produced by Neutral-Air Winds II. Comparison of the Calculated Variations of Electron Concentration with Data obtained from the Ariel I and Ariel III Satellites, 1971, J. Atmosph. Terr. Phys., vol. 33, pp. 371-377.

Evans, see 180.

41. Faire A.C. and Champion K.S.W., Measurements of Dissociative Recombination and Diffusion in Nitrogen at Low Pressures, 1959, Phys. Rev., vol. 113, pp.1-6.

42. Fehsenfeld F.C., Dunkin D.B. and Ferguson E.E., Rate Constants for the Reaction of CO_2^+ with O, O_2 and NO; N_2^+ with O and NO; and O_2^+ with NO, 1970, Planet. Space Sci. vol. 18, pp. 1267-1269.

43. Fehsenfeld F.C., Goldan P.D., Schmeltekopf A.L. and Ferguson E.E., Laboratory Measurement of the Rate of the Reaction $O^+ + O_2 \rightarrow O_2^+ + O$ at Thermal Energy, 1965, Planet.Space Sci., vol. 13, pp. 579-582.

44. Fehsenfeld F.C., Schmeltekopf A.L. and Ferguson E.E., Some Measured Rates for Oxygen and Nitrogen Ion-Molecule Reactions of Atmospheric Importance including $O^+ + N_2 \rightarrow NO^+ + N$, 1965a, Planet.Space Sci., vol. 13, pp. 219-223.

45. Fehsenfeld F.C., Schmeltekopf A.L. and Ferguson E.E., Correction in the Laboratory Measurement of the Rate Constant for $N_2^+ + O_2 \rightarrow N_2 + O_2^+$ at 300°K, 1965b, Planet. Space Sci., vol. 13, pp. 919-920.

46. Ferguson E.E., Ionospheric Ion-Molecule Reaction Rates, 1967, Rev. Geophys., vol. 5, pp. 305-327.

47. Ferguson E.E., Fehsenfeld F.C., Goldan P.D., Schmeltekopf A.L. and Schiff H.I., Laboratory Measurement of the Rate of the Reaction $N_2^+ + O \rightarrow NO^+ + N$ at Thermal Energy, 1965a, Planet. Space Sci., vol. 13, pp. 823-827.

48. Ferguson E.E., Fehsenfeld F.C., Goldan P.D., and Schmeltekopf A.L., Positive Ion-Neutral Reactions in the Ionosphere, 1965b, J. Geophys. Res., vol. 70, pp. 4323-4329.

49. Ferraro V.C.A., The Coefficient of Diffusion of Ions in the F2 Region, 1957, J. Atmosph. Terr. Phys., vol. 11, pp. 296-298.

50. Fite W.L., Rutherford J.A., Snow W.R. and van Lint V.A.J., Ion-Neutral Collisions in Afterglows, 1962, Discussions Faraday Soc., vol. 33, pp. 264-272.

Geisler, see 182, 183.

51. Geisler J.E. and Bowhill S.A., Ionospheric Temperatures at Sunspot Minimum, 1965, J. Atmosph. Terr. Phys., vol. 27, pp. 457-474.

52. Ghosh S.N., Distributions and Lifetimes of N and NO between 100 and 280 Kilometres, 1968, J. Geophys. Res., vol. 73, pp. 309-318.

53. Gledhill J.A., Torr D.G. and Torr M.R., Ionospheric Disturbance and Electron Precipitation from the Outer Radiation Belt, 1967, J. Geophys. Res., vol. 72, pp. 208-214.

54. Gledhill J.A. and Williams M.H., Harmonic Analysis of the F2 Critical Frequencies at Several Antarctic Stations, 1971, J. Atmosph. Terr. Phys., vol. 33, pp. 1055-1066.

55. Gliddon J.E.C. and Kendall P.C., Theoretical World Curves of Maximum Ion Density in a Quiet F-Region, 1960, J. Atmosph. Terr. Phys., vol 18, pp. 48-60.

56. Goldan P.D., Schmeltekopf A.L., Fehsenfeld F.C., Schiff H.I. and Ferguson E.E., Thermal Energy Ion-Neutral Reaction Rates. II. Some Reactions of Ionospheric Interest, 1966, J. Chem. Phys., vol. 44, pp. 4095-4103.

57. Golden D.E., Sinnott G. and Varney R.N., Charge-Transfer Cross Sections for the Reaction $N_2^+ + O_2 \rightarrow O_2^+ + N_2$ at very Low Energies, 1968, Phys. Rev. Letters, 20, pp. 239-241.

58. Gunton R.C. and Shaw T.M., Electron-Ion Recombination in Nitric Oxide in the Temperature Range 196 to 358^{o}K, 1965, Phys. Rev., vol. 140A, pp. 756-763.

59. Hackam R., Temperature Dependence of Electron-Ion Recombination and Ion Mobilities in Nitrogen Afterglows, 1965, Planet. Space Sci., vol. 13, pp. 667-674.

60. Hall L.A., Schweizer W. and Hinteregger H.E., Improved Extreme Ultraviolet Absorption Measurements in the Upper Atmosphere, 1965, J. Geophys. Res., vol. 70, pp. 105-111.

61. Hansen C.F., Temperature Dependence of the $NO^+ + e$ Dissociative-Recombination-Rate Coefficient, 1968, Phys. of Fluids, vol. 11, pp. 904-906.

Harris and Priester, see 181.

62. Herbert Th., Tables of Virtual Heights for Models of Monotonic and Non-monotonic Ionospheric Layers, 1967, Radio Science, vol. 2, pp. 1269-1277.

63. Herman J.R. and Chandra S., The Influence of Varying Solar Flux on Ionospheric Temperatures and Densities: A Theoretical Study, 1969, Planet. Space Sci., vol. 17, pp. 815-840.

64. Hill, G.E., Anomalous f_0F2 Variations in the Antarctic, 1960, J. Geophys. Res., vol. 65, pp. 2011-2023.

65. Hill G.E., Sudden Enhancements of F-Layer Ionization in Polar Regions, 1963, J. Atmosph. Sci., vol. 20, pp. 492-497.

66. Hinteregger H.E., Hall L.A. and Schmidtke G., Solar XUV Radiation and Neutral Particle Distribution in July 1963 Thermosphere, 1965, Space Research V, pp. 1175-1190.

67. Hinteregger H.E. and Watanabe K., Photoionization Rates in the E and F Regions, 2, 1962, J. Geophys. Res., vol. 67, pp. 3373-3392.

68. Howe H.H. and McKinnis D.E., Ionospheric Electron-Density Profiles with Continuous Gradients and Underlying Ionization Corrections. II. Formulation for a Digital Computer, 1967, Radio Science, vol. 2, pp. 1135-1158.

69. Istomin V.G., Investigation of the Ion Composition of the Earth's Atmosphere on Geophysical Rockets 1957-1959, 1962, Planet. Space Sci., vol. 9, pp. 179-193.

70. Ivanov-Kholodny G.S., Maintenance of the Night Ionosphere and Corpuscular Fluxes in the Upper Atmosphere, 1965, Space Res., vol. 5, pp. 19-42.

71. Jacchia L.G, Static Diffusion Models of the Upper Atmosphere with Empirical Temperature Profiles, 1965, Smithsonian Contributions to Astrophysics, vol. 8, pp. 215-257.

72. Jacchia L.G., Recent Results in the Atmospheric Region above 200 km and Comparisons with CIRA 1965, 1967, Smithson. Astrophys. Obs. Spec. Rep. 245.

73. Jacchia L.G. and Slowey J.W., Diurnal and Seasonal-Latitudinal Variations in the Upper Atmosphere, 1967a, Smithson. Astrophys. Obs. Spec. Rep. 242.

74. Jacchia L.G. and Slowey J.W., The Shape and Location of the Diurnal Bulge in the Upper Atmosphere, 1967b, Space Research VII, vol. 2, pp. 1077-1090.

75. Jackson J.E., A New Method for obtaining Electron-Density Profiles from P'-f Records, 1956, J. Geophys. Res., vol. 61, pp. 107-127.

76. Johnson C.Y., Meadows E.B. and Holmes J.C., Ion Composition of the Arctic Ionosphere, 1958, J. Geophys. Res., vol. 63, pp. 443-444.

77. Kasner W.H., Study of the Temperature Dependence of Electron-Ion Recombination in Nitrogen, 1967, Phys. Rev., vol. 164, pp. 194-200.

78. Kasner W.H. and Biondi M.A., Temperature Dependence of the Electron-O_2^+-ion Recombination Coefficient, 1968, Phys. Rev., vol. 174, pp. 139-144.

79. Keating G.M. and Prior E.J., Latitudinal and Seasonal Variations in Atmospheric Densities obtained during Low Solar Activity by means of the Inflatable Air Density Satellites, 1967, Space Research VII, pp. 1119-1131.

80. Kendall M.G., The Advanced Theory of Statistics, Volume 2, Third Edition, 1951, Charles Griffin and Co., p. 154.

81. King J,W., A Review of the Large-Scale Structure of the Ionospheric F Layer, Annals of the IQSY, Vol. 5, Solar-Terrestrial Physics : Terrestrial Aspects, 1969, M.I.T. Press, pp. 131-165.

82. King J.W., Eccles D. and Kohl H., The Behaviour of the Antarctic Ionosphere, 1971, J. Atmosph. Terr. Phys. vol. 33, pp. 1067-1077.

83. King J.W., Kohl H. and Pratt R., The Effect of Atmospheric Winds on the Height of the F2-Layer Peak at Middle and High Latitudes, 1967, J. Atmosph. Terr. Phys., vol. 29, pp. 1529-1539.

84. King J.W., Kohl H., Preece D.M. and Seabrook C., An Explanation of Phenomena occurring in the High-Latitude Ionosphere at Certain Universal Times, 1968, J. Atmosph. Terr. Phys., vol. 30, pp. 11-23.

85. King-Hele D.G., The Orbit of 1968-59A, and its Use in Upper-Atmosphere Research, 1970, Planet. Space Sci., vol. 18, pp. 1585-1595.

86. King-Hele D.G. and Hingston J., Air Density at Heights near 190 km in 1966-67, From the Orbit of Secor 6, 1968, Planet. Space Sci., vol. 16, pp. 675-671.

87. King-Hele D.G. and Walker D.M.C, Air Density at Heights of 140-180 km, From Analysis of the Orbit of 1968-59A, 1969a, Planet. Space Sci., vol. 17, pp. 1539-1556.

88. King-Hele D.G. and Walker D.M.C., Revised Profiles of Air Density at Heights of 130-180 km, From the Orbits of 1968-59A and B, 1969b, Planet. Space Sci., vol. 17, pp. 2027-2029.

89. King-Hele D.G. and Walker D.M.C., Air Density at Heights near 180 km in 1968 and 1969, From the Orbit of 1967-31A, 1971, Planet Space Sci., vol.19, pp. 297-311.

90. Knecht R.W., Observations of the Ionosphere over the South Geographic Pole, 1959, J. Geophys. Res., vol. 64, pp. 1243-1250.

91. Knof H., Mason E.A. and Vanderslice J.T., Interaction Energies, Charge Exchange Cross-Sections and Diffusion Cross-Sections for N^+-N and O^+-O Collisions, 1964, J. Chem-Phys., vol. 40, pp. 3548-3553.

92. Kohl H. and King J.W., Atmospheric Winds Between 100 and 700 km and their Effects on the Ionosphere, 1967, J. Atmosph. Terr. Phys., vol. 29, pp. 1045-1062.

93. Kohl H., King J.W. and Eccles D., Some Effects of Neutral Air Winds on the Ionospheric F-Layer, 1968, J. Atmosph. Terr. Phys., vol. 30, pp. 1733-1744.

94. Kühn G.J., Riometer Absorption events at L=4 (SANAE, Antarctica) during the Years 1964 to 1966, 1969, Thesis, Potchefstroom University for C.H.E., South Africa.

95. Langstroth G.F.O. and Hasted J.B., General Discussions, 1962, Discussions Faraday Soc., vol. 33, p. 298.

96. Lincoln J.V., Geomagnetic and Solar Data, J. Geophys. Res., relevant issues (1957-1968)
Solar-Geophysical Data, U.S. Dept. of Commerce - relevant issues (1969).

97. Maehlum B.N., On the "Winter Anomaly" in the Mid-Latitude D Region, 1967, J. Geophys. Res., vol. 72, pp. 2287-2299.

98. Maehlum B.N., Universal-time Control of the Low-energy Electron Fluxes in the Polar Regions, 1968, J. Geophys. Res., vol. 73, pp. 3459-3468.

99. Maier E.J. and Rao B.C.N., Observations of the Suprathermal Electron Flux and the Electron Temperature at High Latitudes, 1970, J. Geophys. Res., vol. 75, pp. 7168-7174.

100. Margenau H. and Murphy G.M., The Mathematics of Physics and Chemistry , 1943, van Nostrand Co., pp. 500-502.

101. Mehr F.J. and Biondi M.A., Electron Temperature Dependence of Recombination of O_2^+ and N_2^+ Ions with Electrons, 1969, Phys. Rev., vol. 181, pp. 264-270.

102. Mentzoni M.H., Effective Electron Recombination in Heated Nitrogen, 1963, J. Geophys. Res., vol. 68, pp. 4181-4186.

103. Mentzoni M.H. and Donohoe J., Electron Decay Following d-c. Discharge Ionization in NO and NO-Ne Mixtures, 1967, Can. J. Phys., vol. 45, pp. 1565-1578.

104. Mitra A.P., A Review of D-Region Processes in Non-Polar Latitudes, 1968, J. Atmosph. Terr. Phys. vol. 30, pp. 1065-1114.

105. Monro P.E., The Diurnal Variations of the Concentrations of NO^+, O_2^+, NO and N in the Ionospheric E-Region, 1970, J. Atmosph. Terr. Phys., vol. 32, pp. 373-382.

106. Nakshbandi M.M. and Hasted J.B., Energy Dependence of Reactions of O^+ with N_2,O_2. II. Afterglow Measurements, 1967, Planet. Space Sci., vol. 15, pp. 1781-1786.

107. Nicolet M., Nitrogen Oxides in the Chemosphere, 1965a, J. Geophys. Res., vol. 70, pp. 679-689.

108. Nicolet M., Ionospheric Processes and Nitric Oxide, 1965b, J. Geophys Res., vol. 70, pp. 691-701.

109. Norton R.B., van Zandt T.E. and Denison J.S., A Model of the Atmosphere and Ionosphere in the E and F1 Regions, Proceedings of the International Conference on the Ionosphere 1962, 1963, The Institute of Physics and the Physical Society, pp. 26-34.

110. Oguti T. and Marubashi K., Enhanced Ionization in the Ionospheric F2 Region Around Geomagnetic Noon in High Latitudes, 1967, Rep. Ion. Sp. Res. Japan, vol. 21, pp. 96-100.

111. Paetzold H.K., A Preliminary Model for the Variations of Upper Air Densities, 1961, Nature, vol. 190, pp. 35-36.

112. Paul A.K. and Wright J.W., Some Results of a New Method for Obtaining Ionospheric N(h) Profiles and their Bearing on the Structure of the Lower F Region, 1963, J. Geophys. Res., vol. 68, pp. 5413-5420.

113. Penndorf R., The Average Ionospheric Conditions over the Antarctic, Antarctic Research Series, Vol. 4, Geomagnetism and Aeronomy, 1965, American Geophysical Union, pp. 1-45.

114. Piggott W.R. and Shapley A.H., The Ionosphere over Antarctica, Antarctic Research, Geophysical Monograph No. 7, 1962, American Geophysical Union, pp. 111-126.

115. Pike C.P., Universal Time Control of the South Polar F Layer During the IGY, 1970, J. Geophys. Res., vol. 75, pp. 4871-4876.

116. Rastogi R.G., Abnormal Features of the F2 Region of the Ionosphere at some Southern High-Latitude Stations, 1960a, J. Geophys. Res., vol. 65, pp. 585-592.

117. Rastogi R.G., Asymmetry Between the F2 Region of the Ionosphere in the Northern and Southern Hemispheres, 1960b, J. Geophys. Res., vol. 65 pp. 857-868.

118. Ratcliffe J.A., The Formation of the Ionospheric Layers F-1 and F-2, 1956, J. Atmosph. Terr. Phys. vol. 8, pp. 260-269.

119. Ratcliffe J.A., The Magneto-Ionic Theory and its Applications to the Ionosphere, 1959, Cambridge University Press, pp. 16-20.

120. Ratcliffe J.A., Physics of the Upper Atmosphere, 1960, Academic Press, p. 429.

121. Reber C.A. and Nicolet M., Investigation of the Major Constituents of the April-May 1963 Heterosphere by the Explorer XVII Satellite, 1965, Planet. Space Sci., vol. 13, pp. 617-646.

122. Rishbeth H., A Time-varying Model of the Ionospheric F2-Layer, 1964, J. Atmosph. Terr. Phys., vol. 26, pp. 657-685.

123. Rishbeth H., The Effect of Winds on the Ionospheric F2-Peak, 1967, J. Atmosph. Terr. Phys., vol. 29, pp. 225-238.

124. Rishbeth H., The Effect of Winds on the Ionospheric F2-Peak - II, 1968, J. Atmosph. Terr. Phys., vol. 30, pp. 63-71.

125. Rishbeth H., F-Region Dynamics : Some Topics for Further Study, Progress in Radio Science 1966-1969, Volume 1, 1970, International Union of Radio Science, pp. 3-15.

126. Rishbeth H. and Barron D.W., Equilibrium Electron Distributions in the Ionospheric F2-Layer, 1960, J. Atmosph. Terr. Phys., vol. 18, pp. 234-252.

127. Rishbeth H. and Garriott O.K., Introduction to the Ionosphere and Geomagnetism, 1964, NASA Technical Report No. 8, pp. 55-59.

128. Rishbeth H., Moffett R.J. and Bailey G.J., Continuity of Air Motion in the Mid-Latitude Thermosphere, 1969, J. Atmosph. Terr. Phys., vol. 31, pp. 1035-1047.

129. Rothwell P., Winter Diurnal Variation in the Topside Ionosphere in the Southern Hemisphere, Space Research V, 1964, North Holland Publishing Co., pp. 635-636.

130. Rüster R., Solution of the Coupled Ionospheric Continuity Equations and the Equations of Motion for the Ions, Electrons and Neutral Particles, 1971a, J. Atmosph. Terr. Phys., vol. 33, pp. 137-147.

131. Rüster R., The Relative Effects of Electric Fields and Atmospheric Composition Changes on the Electron Concentration in the Mid-Latitude F-Layer, 1971b, J. Atmosph. Terr. Phys., vol. 33, pp. 275-280.

132. Sato T. and Rourke G.F., F-Region Enhancements in the Antarctic, 1964, J. Geophys. Res., vol. 69, pp. 4591-4607.

133. Schield M.A. and Frank L.A., Electrons Between the Inner Edge of the Plasma Sheet and the Plasmasphere, 1970, J. Geophys. Res., vol. 75, pp. 5401-5414.

134. Schmeltekopf A.L., Fehsenfeld F.C., Gilman G.I. and Ferguson E.E., Reaction of Atomic Oxygen Ions with Vibrationally Excited Nitrogen Molecules, 1967, Planet. Space Sci., vol. 15, pp. 401-406.

135. Schmeltekopf A.L., Ferguson E.E. and Fehsenfeld F.C., Afterglow Studies of the Reactions He^+, $He(2^3S)$, and O^+ with Vibrationally Excited N_2, 1968, J. Chem. Phys., vol. 48, pp. 2966-2973.

136. Shahin M.M., Use of Corona Discharges for the Study of Ion-Molecule Reactions, 1967, J. Chem. Phys., vol. 47, pp. 4392-4398.

137. Sharp R.D., Evans J.E., Imhof W.L., Johnson R.G., Reagan J.B. and Smith R.V., Satellite Measurements of Low-Energy Electrons in the Northern Auroral Zone, 1964, J. Geophys. Res., vol. 69, pp. 2721-2730.

138. Smith D. and Fouracre R.A., The Temperature Dependence of the Reaction Rate Coefficients of O^+ Ions with molecular Oxygen and Nitrogen, 1968, Planet. Space Sci., vol. 16, pp. 243-252.

139. Smith D. and Goodall C.V., The Dissociative Recombination Coefficient of O_2^+ Ions with Electrons in the Temperature Range 180^o-630^o K, 1968, Planet. Space Sci., vol. 16., pp. 1177-1188.

140. Spencer N.W., Brace L.H., Carignan G.R., Taeusch D.R. and Niemann H., Electron and Molecular Nitrogen Temperature and Density in the Thermosphere, 1965, J. Geophys. Res., vol. 70, pp. 2665-2698.

141. Stebbings R.F., Turner B.R. and Rutherford J.A., Low-Energy Collisions Between some Atmospheric Ions and Neutral Particles, 1966, J. Geophys. Res., vol. 71, pp. 771-784.

142. Stuart G.F. and Titheridge J.E., The Distribution of Irregularities in the Antarctic Ionosphere - II. Diurnal, Magnetic and Solar Cycle Effects, 1969, J. Atmosph. Terr. Phys. vol. 31, pp. 905-924.

143. Stubbe P., Temperature Variation at the F-Layer Maximum During a Sunspot Cycle, 1964, J. Atmosph. Terr. Phys., vol. 26, pp. 1055-1068.

144. Stubbe P., Theory of the Night-time F-Layer, 1968, J. Atmosph. Terr. Phys., vol. 30, pp. 243-263.

145. Stubbe P., Temperature Dependence of the Rate Constants for the Reactions $O^+ + O_2 \rightarrow O_2^+ + O$ and $O^+ + N_2 \rightarrow NO^+ + N$, 1969, Planet. Space Sci., vol. 17, pp. 1221-1231.

146. Stubbe P., Simultaneous Solution of the Time Dependent Coupled Continuity Equations, Heat Conduction Equations, and Equations of Motion for a System Consisting of a Neutral Gas, an Electron Gas, and a Four Component Ion Gas, 1970, J. Atmosph. Terr. Phys., vol. 32, pp. 865-903.

147. Swider W., A Study of the Nighttime Ionosphere and its Reaction Rates, 1965, J. Geophys. Res., vol. 70, pp. 4859-4873.

148. Talrose V.L., Markin M.I. and Larin I.K., The Reaction $O^+ + N_2 \rightarrow NO^+ + N$, 1962, Discussions Faraday Soc., vol. 33, pp. 257-263.

149. Taylor H.A., Jr., and Brinton H.C., Atmospheric Ion Composition Measured above Wallops Island, Virginia, 1961, J. Geophys. Res., vol. 66, pp. 2587-2588.

150. Thomas G.R. and Venables F.H., The Effect of Diurnal Temperature Changes on the F2-Layer, 1967, J. Atmosph. Terr. Phys., Vol. 29, pp. 621-640.

151. Thomas J.O., The Electron Density Distribution in the F2 Layer of the Ionosphere in Winter, 1963, J. Geophys. Res., vol. 68, pp. 2707-2718.

152. Thomas J.O., "The Electron Density Distribution in the Fe-Layer of the Ionsphere in Winter" in Electron Density Distribution in Ionosphere and Exosphere, ed. E. Thrane, 1964, North-Holland Publishing Co., pp. 226-242.

153. Thomas J.O. and Andrews M.K., The Trans-Polar Exospheric Plasma, 3, A Unified Picture, 1969, Planet. Space Sci., vol. 17, pp. 433-446.

154. Titheridge J.E., The Calculation of Real and Virtual Heights of Reflection in the Ionosphere, 1959a, J. Atmosph. Terr. Phys., vol. 17, pp. 96-109.

155. Titheridge J.E., The Use of the Extraordinary Ray in the Analysis of Ionospheric Records, 1959b, J. Atmosph. Terr. Phys., vol. 17, pp. 110-125.

156. Titheridge J.E., Ionization Below the Nighttime F-Layer, 1959c, J. Atmosph. Terr. Phys., vol. 17, pp. 126-133.

157. Titheridge J.E., The Analysis of Nighttime h'(f) Records, 1961a, J. Atmosph. Terr. Phys., vol. 20, pp. 209-211.

158. Titheridge J.E., A New Method for the Analysis of Ionospheric h'(f) records, 1961b, J. Atmosph. Terr . Phys., vol. 21, pp. 1-12.

159. Torr D.G., Ionospheric Effects in the Southern Radiation Anomaly, 1966, Thesis, Rhodes University.

160. Torr D.G., and Torr M.R., A Method of Solution of the F1 layer Non-Linear Ionospheric Continuity Equation and the Early Morning and Late Evening Increase in Electron Density Observed at Some Stations. 1969a, Ann. Geophys., vol. 25, pp. 571-575.

161. Torr D.G. and Torr M.R., A Theoretical Investigation of Corpuscular Radiation Effects on the F-Region of the Ionosphere, 1970, J. Atmosph. Terr. Phys. vol. 32, pp. 15-34.

162. Torr M.R., A Theoretical Investigation of the F-Region of the Ionosphere, 1968, Thesis, Rhodes University.

163. Torr M.R. and Torr D.G., The Inclusion of a Particle Source of Ionization in the Ionospheric Continuity Equation, 1969b, J. Atmosph. Terr. Phys. vol. 31, pp. 611-614.

164. Torr M.R. and Torr D.G., A Theoretical Investigation of the F Region of the Ionosphere, 1969c, CSIR Research Report 271.

165. Torr M.R. and Torr D.G., Low Energy Electrons and the Ionosphere, 1969d, Trans. S.A. Inst. Elec. Eng., RT48.

166. Torr M.R. and Torr D.G., OI and N_2^+ Emissions Observed at SANAE, 1971, South African Journal of Antarctic Research, No. 1, pp. 24-26.

167. Volland H., A Theory of Thermospheric Dynamics - I Diurnal and Solar Cycle Variations, 1969a, Planet. Space Sci., Vol. 17, pp. 1581-1597.

168. Volland H., A Theory of Thermospheric Dynamics - II Geomagnetic Activity Effect, 27-Day Variation and Semi-annual Variation, 1969b, Planet Space Sci., vol. 17, pp. 1709-1724.

Walker, see 184.

169. Warneck P., Studies of Ion-Neutral Reactions by a Photoionization-Mass Spectrometer Technique. III. Several Ionospheric Reactions, 1967a, Planet. Space Sci., vol. 15, pp. 1349-1359.

170. Warneck P., Studies of Ion-Neutral Reactions by a Photoionization Mass-Spectrometer Technique. I., 1967b, J. Chem. Phys., vol. 46, pp. 502-512.

171. Warneck P., Laboratory Rate Coefficients for Positive Ion-Neutral Reactions in the Ionosphere, 1967c, J. Geophys. Res., vol. 72, pp. 1651-1653.

172. Watanabe K. and Hinteregger H.E., Photoionization Rates in the E and F Regions, 1962, J. Geophys. Res., vol. 67, pp. 999-1006.

173. Whitten R.C. and Popoff I.G., Reaction Rates Determined from Ionospheric Observations, 1964a, Discussions of the Faraday Soc., vol. 37, pp. 185-191.

174. Whitten R.C. and Popoff I.G., Ion Kinetics in the Lower Ionosphere, 1964b, J. Atmosph. Sci., vol. 21, pp. 117-133.

175. White W.A., Solar X-Rays : A Comparison with Microwave Radiation, 1964, Goddard Space Flight Center Report X-610-64-42.

176. Wolf F.A. and Turner B.R., Energy Dependence of Charge-Transfer Reactions in the Thermal and Low-Electron-Volt Region, 1968, J. Chem. Phys., vol. 48, pp. 4226-4233.

177. Wright J.W., Ionospheric Electron-Density Profiles with Continuous Gradients and Underlying Ionization Corrections. III. Practical Procedures and some Instructive Examples, 1967, Radio Science, vol. 2 pp. 1159-1168.

178. Wright J.W. and Smith G.H., Review of Current Methods for Obtaining Electron-Density Profiles from Ionograms, 1967, Radio Science, vol. 2, pp. 1119-1125.

179. Young R.A. and St. John G., Recombination Coefficient of NO^+ with e, 1966, Phys. Rev., vol. 152, pp. 25-28.

180. Evans J.V., Ionospheric Backscatter Observations at Millstone Hill, 1965, Planet. Space Sci., vol. 13, pp. 1031-1074.

181. Harris I. and Priester W., Theoretical Models for the Solar-Cycle Variation of the Upper Atmosphere, 1962, J. Geophys. Res., vol. 67, pp. 4585-4591.

182. Geisler J.E., Atmospheric Winds in the Middle Latitude F-Region, 1966, J. Atmosph. Terr. Phys., vol. 28, pp. 703-720.

183. Geisler J.E., A Numerical Study of the Wind System in the Middle Thermosphere, 1967, J. Atmosph. Terr. Phys., vol. 29, pp. 1469-1482.

184. Walker A.D.M., A Theoretical Investigation of the Effects of Solar Eclipses on the Ionosphere, 1962, Thesis, Rhodes University.